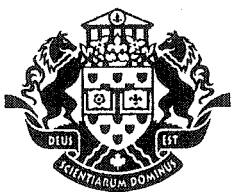

Université d'Ottawa · University of Ottawa

Your file Votre référence
ISBN: 0-612-85383-7
Our file Notre référence
ISBN: 0-612-85383-7

Laughter is the best form of medicine.
For when we laugh, we neither think, grieve, or feel.

-Eugene Lam

Abstract

The work presented in this thesis deals primarily with living free radical polymerization (LFRP). Two main specific areas of this process have been studied; thermal and photochemical reaction sequences. Stoichiometric unimolecular initiators were found to be ideal probes for studying the reactions involved in the LFRP process. The bond dissociation energy (BDE) of the labile C-O bond of the alkoxyamine initiators was found to be ca. 28 kcal/mol and is dependent on the resulting carbon centered radical produced upon thermal decomposition. Lower activation energies were measured for more stable carbon centered radicals. Complementary to the thermal studies, photoacoustic studies (PAC) involving photochemical decomposition of the initiators led to the homolytic N-O and C-O bond cleavages in addition to disproportionation product formation. The BDE for the N-O bond of these initiators is ca. 43 kcal/mol. These studies also provided insight into volume effects, where a strict homologous solvent series is not required for extrapolating true enthalpies of reactions and volume correction factors for PAC. The decomposition quantum yields of a series of ketone based actinometers used for PAC BDE studies were re-evaluated and found to be solvent independent.

The specific kinetics of thermal LFRP were equally investigated through the use of probes which are normally used for thermal initiation. Fast time resolved techniques of laser flash photolysis (LFP) were used to measure the bi-molecular rate constant for the coupling reaction between a carbon centered radical and a nitroxide radical involved in LFRP. Typical values lay in the area of 10^8 M^{-1} s^{-1} and are influenced by the structure of the carbon centered radical and not that of the nitroxide. The rate constants were observed to be slower with more stable carbon centered radicals, similar to the BDE results where weaker dissociation energies were observed.

The formation of minor disproportionation products upon thermal decomposition of the unimolecular initiators was assigned to a concerted four center elimination ultimately responsible for the lack of controlled polymerization with acrylates. The incorporation of steric effects into the monomer or the nitroxide suppressed the formation of these products by increasing the energy barrier necessary for correct orbital alignment required for

the elimination reaction. Living polymerization of acrylate monomers was achieved with a nitroxide containing bulky substituents in its 2 and 6 positions. Moderate success of living polymerization was also achieved with acrylate type monomers through the use of an additional phase not miscible with the bulk phase.

Chromophores producing triplet states upon excitation were found to undergo fast and efficient energy transfer to a covalently linked alkoxyamine subsequently promoting C-O bond homolysis. The orientation of the C-O bond relative to the chromophore in addition to the distance separating the two influences the efficiency of energy transfer and bond cleavage. Using a benzophenone type chromophore with a covalently linked alkoxyamine initiator promoted photoinduced living type polymerization of acrylate.

Acknowledgments

During the course of my four years of studies, I have had the opportunity to meet and interact with many great people. Unfortunately I cannot thank them all, but I would like to thank a few of these people who have made a impact and helped mold many parts of life.

Tout d'abord, j'aimerais remercier Lamine Diop qui est responsable pour m'avoir montré le chemin de la recherche en chimie. Ces encouragements et son assistance ont été bien appréciés et je les ai pris à coeur. I would also like to acknowledge Prof. T. Durst for allowing me the chance to wet my appetite for research early during my studies.

I wish to thank the members of the Scaiano group, past and present, for their friendship and help along the way, in particular, Gonzalo Cosa, Sonia Corrent, and Michelle Chrétien. I truly appreciate the guidance of Alain Berinstain and Dean Weldon for showing me the ropes during the early stages and introducing me to *balance* as well as tolerating the many phone calls during the weekend asking for assistance. I wish to recognize the contagious enthusiasm for chemistry of Drs. Terry Connolly, Gerd Pohlers, and Lydia Martinez. Their tolerance for many brain storming ideas and inciting many thought provoking discussions to put me back on track is greatly appreciated. Veillen dank Gerd für dein gantz Hilfe, reichliche Diskussion Sitzungen, interesant Lektionen Deutche des Würfelzehr und zahlreiche Abendessen an Ihrem legendären Haus 502! André Simard, Gerry Charette, Anita Bowman, and Betty Yakimenko's willingness to always help me out with many problems during the past few years cannot be dismissed. I had the great pleasure of supervising three students (Peter Hahn, Alan Martin, and Ivan Pilectic) during the course of my studies who were very enthusiastic and taught me a lot.

My appreciation is also extended to Prof. Peter Wilson for the many occasions spent at the black board helping me find my way through the synthetic forest. Un beau remerciement au gang des français pour leurs assistances en français puis en synthèse.

I would also like to recognize the help of many people that I had the opportunity to work with at the Max-Planck-Institut für Strahlenchemie and Bayer A.G. for

giving me the great opportunities to do chemistry in Germany. Many thanks to Prof. S.E. Braslavsky, Drs. Uwe Hugger, Ingolf Michler, Réné Williams, Saltuk Saldamli, Simon Belt, and Edith Rau for their friendship and opportunity to learn different things about chemistry, in particular their patience for listening to many photoacoustic problems that occurred and my interesting German phrases.

There are many people without whose help during the course of my work would have made this thesis extremely difficult to complete. A special acknowledgment goes to my parents for their constant support with every decision I made. I immensely appreciate the friendships of Jill Cairns, Sherri Meek, and Mara Bertelsen who found the light and released it! Même si vous n'étiez pas présentes pendant la rédaction de cette thèse, quotidiennement je pense à vous tous. Je pense aux nombreux sourires que vous m'avaient offerts et qui m'ont encouragé à en faire autant.

I thank Andrea Della Valle and Geneviève Brown for their tremendous support and constant reassurance while I was writing. Thanks so much Andrea for the ritual coffee sessions at F&F and H&C and reminding me of important things and to step back and re-evaluate. Thank you Mausi for all the wonderful distractions you provided during this time. A special mention is also extended to the Allen brothers for always bringing a smile to my face and making me laugh.

A special acknowledgment is extended to my supervisor, Tito Scaiano, for the opportunity to work for him in such a nurturing environment. I greatly appreciate his patience and insight while I struggled to find my way on many occasions even when my route took me to Germany a couple of times!

Table of Contents

List of Figures

CHAPTER 3

CHAPTER 4

CHAPTER 5

CHAPTER 6

CHAPTER 7

List of Schemes

List of Tables

List of Equations

List of Abbreviations

α	Thermal compressive parameter
μM	Micromolar
μs	Microsecond
ρ	Density
AIBN	2,2′-Azobisisobutyronitrile
ATRP	Atom transfer radical polymerization
BPO	Benzoylperoxide
BR	Bond rotation
C_p	Heat Capacity
CHD	Cyclohexadiene
CSA	Camphorsulfonic acid
CT	Charge transfer
DCC	1,3-Dicyclohexylcarbodiimide
DMAP	4-Dimethylaminopyridine
DMF	N,N-Dimethylformamide
DNMR	Dynamic nuclear magnetic resonance
DP	Degree of polymerization
E_A	Activation energy
EI	Electron impact
EG	Ethylene glycol
EPR	Electron pair resonance
ESI	Electrospray ionization
ESR	Electron spin resonance
FAB	Fast atom bombardment
GC	Gas chromatograph
GC/MS	Gas chromatography/mass spectrometry
GPC	Gel permeation chromatography
H-Abs	Hydrogen abstraction
HPLC	High pressure liquid chromatography
IC	Internal conversion
IR	Infrared
ISC	Intersystem crossing
Laser	Light amplified stimulation of emitted light
LIOAC	Laser induced optoacoustic calorimetry
MS	Mass spectrometry
OHBP	*o*-Hydroxybenzophenone
M_w	Average weight molecular weight
M_n	Average number molecular weight
MW	Molecular weight
NMR	Nuclear magnetic resonance
NBS	N-bromosuccinimide
Log A	Pre-exponential factor or frequency factor
LFRP	Living free radical polymerization
mmol	Millimoles
M	Molar
MA	Methyl acrylate

mM	Millimolar
MMA	Methyl methacrylate
ms	Millisecond
nBA	*n*-Butyl acrylate
NI	Nitrogen inversion
NMR	Nuclear magnetic resonance
ns	Nanosecond
PAC	Photoacoustic calorimetry
PD	Polydispersity
PDC	Pyridinium dichromate
PTM	Photothermal method
PVF_2	β-Polyvinylidene difluoride
PZT	Piezoelectric transducer
RAFT	Reversible addition fragmentation chain transfer
RI	Refractive index
RI	Ring inversion
SEC	Size exclusion chromatography
TBD	Thermal beam deflection
TEMPO	2,2,6,6-Tetramethylpiperidine-N-oxide
THF	Tetrahydrofurane
TLC	Thin layer chromatography
TRTL	Time-resolved thermal lensing
*p*TsOH	*p*-Toluenesulfonic acid
UV-Vis	Ultraviolet-visible
YAG	Ytterium-argon-garnate

Man errs as long as he strives.

-Goethe

1. LFRP Introduction

1.1 Introduction

Polymerization is an ideal and inexpensive method for creating new materials of long molecular lengths and intriguing architecture. The attractive benefit to this approach is rapid amplification of chain lengths with a limited amount of initiator and effort. From an industrial point of view, free radical polymerization is an attractive means of polymer synthesis because it is robust and inexpensive compared to ionic methods.[1] The general mechanism involves activation of an initiator (R•) either under thermal of photochemical conditions. This is followed by monomer addition to generate the propagating radical which continuously adds to monomers unless terminated by one of three ways. Simple termination can occur with complete monomer consumption, but conventional free radical polymerization terminates by two predominate routes. These are by combination or disproportionation, where the preferred route of termination depends on the monomer polymerized. Styrene typically terminates by combination while the polymerization of acrylates terminates by disproportionation.[2] An alternate termination route is chain transfer in which the propagating radical is transferred to another polymer chain. The general scheme for free radical polymerization is represented in Scheme 1-1.

Initiation

$$I \longrightarrow 2R\bullet$$

Propagation

$$R\bullet + M \longrightarrow RM\bullet$$

$$RM_n\bullet + M \longrightarrow RM_{n+1}\bullet$$

Termination

$$RM_n\bullet + RM_m\bullet \longrightarrow RM_{n+m}R \quad \text{(Combination)}$$

$$RM_n\bullet + RM_n\bullet \longrightarrow RM_nH + RM_n(-H) \quad \text{(Disproportionation)}$$

Chain Transfer

$$RM_n\bullet + RH \longrightarrow RM_nH + R\bullet$$

Scheme 1-1. General reaction scheme for radical polymerization.

Free radical polymerization is a robust technique that promotes the polymerization of many different types of vinyl monomers in the absence of

oxygen.[3] It is also a suitable method for providing an unlimited number of copolymers with a variety of composition and molecular size. The most beneficial aspect of free radical polymerization is its tolerance for many reaction conditions. It can be done in bulk, solution, suspension, and emulsion polymerization, unlike other polymerization methods that require strict conditions. Also, the reaction can endure a wide temperature range from 0 ° to 150 °C.[4]

Even though conventional free radical polymerization may appear as a universal technique for polymer synthesis it suffers from many limitations that hinder its practical use, especially for industrial purposes. Its suffers primarily from a lack of control, that is to say, once the reaction has begun it cycles uncontrollably till terminated by combination, disproportionation, or chain transfer. This results in polymers that are not of uniform length rendering it difficult to predict the properties of the end polymer. Also the molecular weight is difficult to control resulting in polymers of arbitrary length. The amount and occurrence of termination by disproportionation and combination also cannot be controlled leading once again to polymers of inconsistent molecular weight distribution, hence a large polydispersity (*vide infra*). The polymeric architecture by this polymerization method is limited to copolymers and cannot be expanded to include more complicated architectures found with other methods. Modification of the free radical process does lead to various architectures, where the method of polymer control is the focus of this chapter.

There are two primary steps that dictate the outcome of the polymerization process; propagation and initiation. Normally free radical initiators undergo slow decomposition where the polymer chains are initiated at different times. This is compounded with rapid chain elongation resulting in chains of variable length due to different initiation time. Free radical polymerization is characterized by an instantaneous formation of a few polymers of maximum length followed by slow growth of the chains. However, polymers of consistent length are rarely obtained and their conversions are normally quite low, typically < 50 %. Complete initiator decomposition at the onset of the polymerization followed by controlled chain extension would regulate the polymerization techniques leading to polymers of low polydispersity which ultimately have commercial applications. A controlled polymerization would lead to defined molecular weights which could be determined by the number of chains initiated, hence the ratio of monomer to initiator used. Also, complicated polymer

architecture, as shown in Figure 1-7, could also be obtained by this process. Currently there are several methods by which this controlled free radical polymerization can be achieved and they are discussed within. The phrase "controlled" or "living" free radical polymerization (LFRP) is used to describe the polymerization process in which the polymerization steps are regulated leading to well defined polymers of specific structure, polydispersity, and molecular weight.

1.2 Ionic Living Polymerization

The term "living", as applied to polymers, was first coined by Szwarc in his seminal paper on ionic polymerization in 1956.[5,6] Here he described the process by which ionic polymerization occurred in a controlled fashion without undesired termination. A counter ion was used as a temporary terminal cap that was removed with the subsequent addition of a monomer unit. The polymerization proceeded till complete monomer consumption was obtained leading to polymers with low polydispersities. Also, the counter ion was still present at the termination of the polymerization reaction. Control over the polymerization process was achieved by the use of an initiator where each initiator molecule produced one growing chain and the degree of polymerization (*vide infra*) could easily be predicted by the ratio of monomer to initiator used. The controlled aspect of the polymerization only holds true if the rate of initiator addition to the monomer is greater than the rate of monomer addition.

A brief description of anionic and cationic living polymerization is presented for subsequent comparison to radical living polymerization.

1.2.1 Cationic

Cationic living polymerization is more complex than its anionic counterpart due to the presence of side reactions. β-Hydrogens are readily transferred from electron rich monomers by strong protic acids leading to new polymer chains.[7] The results are a lower observed molecular weight and several dead polymers as shown in Scheme 1-2.

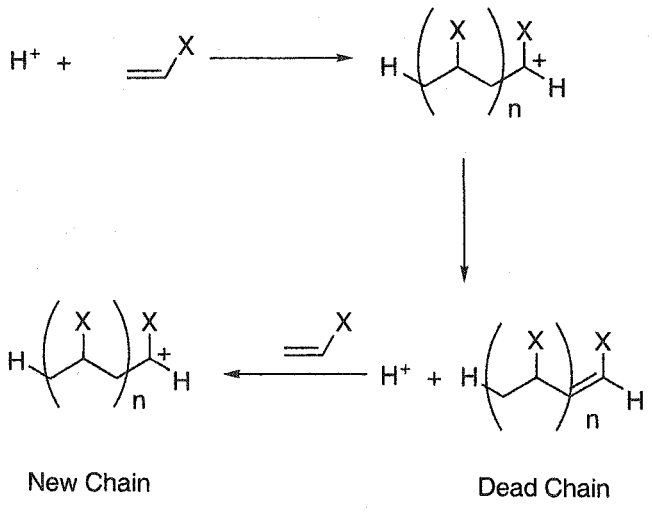

Scheme 1-2. β-Hydrogen transfer leading to dead polymers in living cationic polymerization.

This problem can be circumvented through the use of halides, i.e. iodine, which act as a temporary terminal cap for the polymer. The polymer-iodo bond is then activated with a Lewis acid catalyst to allow insertion of the monomer in a controlled fashion. However, the iodo-polymer terminus is light sensitive and undergoes uncontrolled cleavage upon exposure to light. Currently, other halides, i.e. bromine and chlorine, are used in addition to various Lewis acids to promote living polymerization.[8] The use of Lewis acid during the polymerization has a two fold effect. Firstly it stabilizes the propagating carbonium ion, and secondly it lowers the propagation rate, which are all beneficial for sustaining living polymerization.[9] A generic cationic living polymerization of vinyl acrylates with ethylaluminum dichloride as the Lewis acid is depicted in the following Scheme. Currently, many types of Lewis acids are used to promote cationic living polymerization, however they must be used in at least stoichiometric amounts.

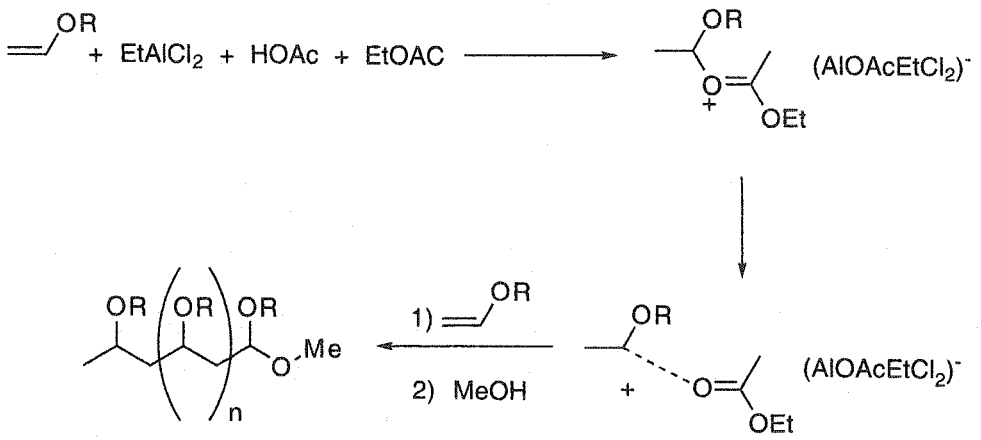

Scheme 1-3. Cationic living polymerization of polyvinylether promoted by ethylaluminum dichloride.

1.2.2 Anionic

Anionic living polymerization is similar to the cation method with the exception that the propagating species is negatively charged instead of positively charged. Polymerization is relatively facile with monomers such as ethylene oxide, hexamethlycyclotrisiloxane, butadienes, styrenes, acrylates, methacrylates, and lactones providing they do not posses sensitive functional groups.[5,10-16] Anionic polymerization is initiated by a powerful reducing agent, such as butyl lithium or metals such as sodium,[17] where the vinyl polymer is reduced generating an anion responsible for the polymer growth. The negatively charged propagating species is balanced by a counter cation. The general anionic polymerization as applied to styrene is shown in Scheme 1-4.

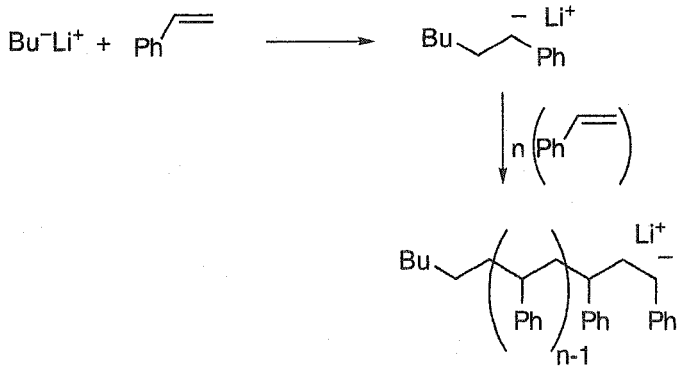

Scheme 1-4. General living anionic polymerization as applied to styrene.

The anionic polymerization may appear as a simple reaction, but it is sensitive to many factors including counter ion size, solvent polarity, solvent coordination factors, and many structural parameters. Also, the reactivity of the monomer is primarily determined by the substituents across the monomer unsaturation. Electron-withdrawing substituents increase the stability of the anion generated and also increase the electrophilic character of the double bond, thereby rendering it more reactive towards the initiator. Since strong reducing agents are used as initiators, only polymers whose functional groups are tolerant to these initiators can be polymerized.

1.2.3 Advantages and Disadvantages

The advantages to ionic polymerization are its versatility to polymerize a wide variety of monomers. In addition to this, complicated architecture of the types shown in Figure 1-7 can be readily obtained by this method depending on the initiator used. However, there are many disadvantages. This method is extremely sensitive to solvent and reagent impurities where they both must be ultra-pure in addition to being void of moisture. The polymerization must be done in solution precluding its use in commercially viable bulk polymerization. A high cost is also associated with ionic polymerization because of the strict requirements and the expensive cost of counter ions used to maintain the polymerization. The Lewis acid required to sustain the controlled cationic polymerization is required in stoichiometric amounts or more. Also, harsh conditions are required to induce polymerization which normally destroy sensitive monomer functional groups. Most importantly, the end-group in the form of a counter-ion is hydrolyzed upon polymer isolation precluding the possibility of further chain extension. This makes copolymerization difficult and must be done in a "one-pot" fashion, which is rather difficult by these means.

1.3 Living Free Radical Polymerization

Living free radical polymerization (LFRP) is the term introduced to denote controlled polymerization promoted by free radicals. Unlike ionic living polymerization, in order for the method to be termed LFRP a large list of criterion must be satisfied. The list to be satisfied is found immediately below.

i) Correlation of chain length with initiator concentration.

ii) High conversion.

iii) Linear conversion of molecular weight with time.

iv) Linear correlation of experimental with theoretical molecular weight.

v) Polydispersity ≤ 1.5. (i.e. Molecular weight control).

vi) Stop-and-grow polymerization properties.

The criterion presented above relate to the controlling capacity during the polymerization reaction. Complete initiator decomposition with fast addition to the monomer implies all polymer chains are initiated simultaneously. This is then followed by propagation of all the chains with the same rate. If this process occurs, the molecular weight of the resulting polymer can be predetermined by the monomer/initiator ratio. Also, the polymers will all be of consistent length leading to polydispersities less than the normal Poisson distribution of 1.5 expected for radical polymerization.

These properties can be obtained similar to the ionic living polymerization with the use of a capping agent. Instead of using an ionic counter ion as a cap, a covalently bound capping agent is used for LFRP. The propagating radical during the course of the reaction is trapped by this agent leading to a "dormant" species represented by R-X in Scheme 1-5. Under the polymerization conditions, the dormant species is reactivated thermally through homolytic bound cleavage generating the propagation radical (R•) which subsequently undergoes monomer addition. Chain elongation can be thought of as a perpetual series of steps involving decapping followed by monomer addition and subsequent capping. Since the radical is trapped after each monomer addition, the probability of it generating a dead chain, i.e. recombination or disproportionation, is quite small. The process continues till all the monomer

has been consumed or the reaction halted by cooling the reaction mixture. High molecular weight polymers are easily obtained by this approach. Upon completion of the polymerization process, all the polymer termini are capped by the trapping agent. This allows for re-polymerization using either the same or a different monomer leading to stop-and-grow properties and ultimately to complicated polymer architecture.

Scheme 1-5. Schematic representation of active (R•) and dormant (R-X) species in LFRP.

The capping and decapping steps leading to the dormant and active species, depicted in Scheme 1-5, are under the influence of an equilibrium. The equilibrium established is in favor of the dormant species with few active radicals present at any time during the course of the polymerization. The radicals that are present undergo monomer addition followed by rapid capping to regenerate the dormant species. The ultimate result is polymers with high molecular weights, low polydispersities, and high conversions. The polymeric architecture that can be achieved with this method is endless and a few examples are represented in Scheme 1-7.

Many methods of LFRP are currently available and undergo controlled free radical polymerization according to Scheme 1-5. They differ only in the type of capping agent used to trap the active radical.

In the following sections, three methods of achieving controlled radical polymerization or LFRP are presented. Major emphasis is placed on nitroxide mediated LFRP in order to thoroughly introduce this topic since the bulk of the work presented in this thesis is based on this concept. The two other methods of achieving polymerization are also described to provide a contrast and comparison to nitroxide mediated LFRP. By no means do the controlled methods depicted here represent the only techniques by which one can achieve LFRP. They are however the most commonly used and successful methods of achieving polymers with living properties.

1.3.1 Nitroxide mediated LFRP

The use of nitroxides (N-O•) in chemistry has been extensive including widespread applications. They have primarily been used as spin trapping agents

in organic solution and biological media for ESR work involving radicals.[18-20] Other applications of nitroxides include the introduction of functionality[21] for synthetic purposes, reducing properties,[22-25] and they may also be used as a protecting group.[26] Apart from these uses, nitroxides have been exploited extensively to trap carbon centered radicals including their use as scavengers to deter polymerization or polymer degradation.[27-33] However, work by the Australian CSIRO group have taken advantage of the carbon centered trapping capabilities of nitroxides to promote LFRP as outlined in their original patent.[34] In short, the nitroxide plays the role as capping agent illustrated in Figure 1-5.

The term nitroxide mediated LFRP is employed to differentiate it from other types of LFRP. The general mechanism of nitroxide mediated radical polymerization does not differ greatly from that of conventional free radical polymerization. The process can either be initiated by typically used initiators such as benzoyl peroxide (BPO) or with unimolecular initiators (*vide infra*). They both generate an initiating radical that undergoes monomer addition leading to a propagating radical (see Equation 2). However, the similarities between the mechanisms ceases there. In nitroxide mediated polymerization, the propagating radical is trapped by the nitroxide creating a new covalent alkoxyamine bond. The new bond (C-O) is relatively labile and is cleaved to regenerated two radicals (R• and N-O•) at the typical polymerization conditions of 120 °C.[35-41] The carbon centered radical adds to the monomer and is subsequently re-trapped regenerating the dormant species. Similar to that mentioned above, an equilibrium between the active and dormant species is present and lays in favor of the dormant species, ~10^{-11} M at 125 °C.[38,41-48] The polymer termini are all temporarily capped with the nitroxide group creating a thermally stable alkoxyamine at room temperature at the completion of the polymerization. Upon exposure to heat, the polymerization can be reinitiated in the presence of the same or different monomers. The general nitroxide mediated LFRP of styrene initiated by benzoyl peroxide and controlled by 2,2,6,6-tetramethylpiperidine (TEMPO) is represented in Scheme 1-6.

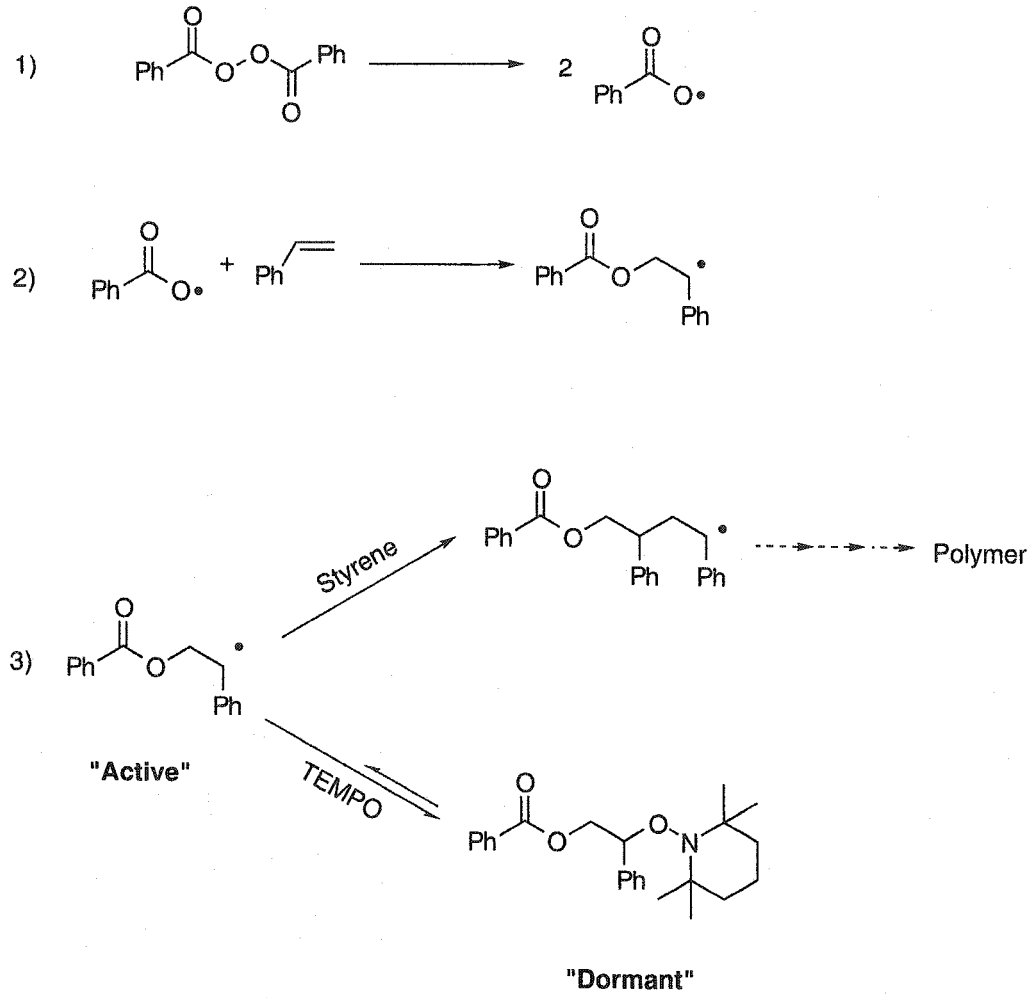

Scheme 1-6. Nitroxide mediated LFRP initiated by benzoyl peroxide.

Two pivotal factors are responsible for the observed controlled LFRP with nitroxides; (i) a labile C-O bond (ii) the Fischer-Ingold persistent radical effect. A labile bond is required otherwise the trap is permanently bound by a covalent bond giving a dead polymer. Nitroxides are known to trap carbon centered radicals with rate constants ~10^7-10^8 M^{-1} s^{-1}, which are well below the diffusion controlled limit satisfying the kinetic criterion listed above.[27-29] The persistent radical refers to exclusive radical trapping by nitroxides, which cannot undergo a self-reaction.[49-51]

Even though the CSIRO group originally patented the nitroxide mediated LFRP,[34] it was the Xerox group of Georges et al. who found that this class of persistent radicals could control the polydispersity during the free radical

polymerization of styrene.[52,53] Previously the lack of adequate molecular weight control was a major drawback. The discovery of living free radical polymerization has drawn great interest recently, as now the free radical method for polymerization is more attractive as less stringent requirements are necessary compared to ionic polymerization.[54] The incorporation of the nitroxide group also renders the polymer "living" as the thermally labile cap can be removed and polymerization resumed with the same or other monomers leading to complicated polymer architecture. The primary benefit to LFRP is the control over the polymerization reactions ultimately leading to defined structures with predictable properties.

1.3.1.1 Nitroxide Structure

Typically the nitroxide structures used for nitroxide mediated polymerization are those which are commercially available and inexpensive. Cyclic nitroxides were found to give better LFRP results than acyclic ones, where the most widely used nitroxide is the 6 membered ring; TEMPO.[55-57] Nitroxides based on a 5 membered ring were shown to give polymerization results of styrene similar to those of 6 membered rings regardless if another heteroatom was including within the ring.[58]

The synthesis of new nitroxides is not trivial and is laborious.[18,22,37,39,59-72] For this reason, computational analyses have focused on calculating the effect of nitroxide structure upon the labile C-O bond strength.[57,73-75] The consensus between these works is that electron-withdrawing groups stabilize the C-O bond rendering it less labile. Conversely, electron-donating groups weaken the C-O bond. A few nitroxide structures used to calculate the influence of nitroxide structure upon the C-O are found in Figure 1-1 and are grouped according to their relative stability.

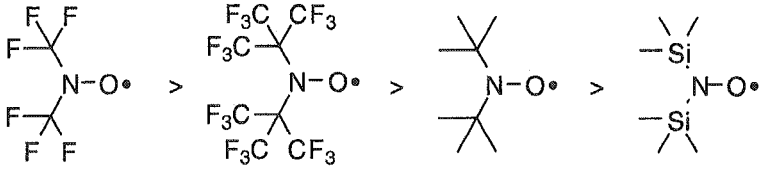

Figure 1-1. General order of C-O bond stability based upon electronic effects on the nitroxide.[56]

1.3.1.2 New Generation of Nitroxides

Traditionally, nitroxides have always been synthesized with substituents other than hydrogen in the 2 and 6 positions. The main reason for this is to increase the persistent nature of the nitroxide. With the incorporation of hydrogen in the α-position to the nitroxide function, a disproportionation reaction results as shown in Figure 1-2.[76,77] This reaction leads to the formation of a hydroxylamine and a nitrone, both of which are not able to sustain LFRP. Therefore, nitroxides containing α-hydrogens are not suitable for promoting nitroxide mediated LFRP.

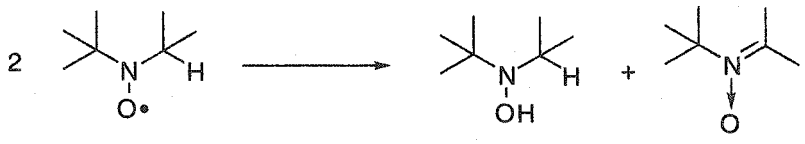

Figure 1-2. Nitroxide disproportionation products.

The new generation of nitroxides used for LFRP contain an α-hydrogen, yet are able to yield polymers with living properties. This strategy has been successfully adopted by two separate and independent groups in California and France.[37,61,66,71,78-84] Since LFRP is attained, the new class of nitroxides must not undergo the disproportionation reaction shown in Figure 1-2. The bulky groups attached to the nitroxide do not allow for proper orbital alignment which is primarily responsible for the formation of disproportionation products. At the polymerization temperatures, there is a slow rotation to the correct geometry, leading to small amounts of disproportionation product formation. A few of the new nitroxides used for the polymerization of monomers other than styrene are represented in Figure 1-3.

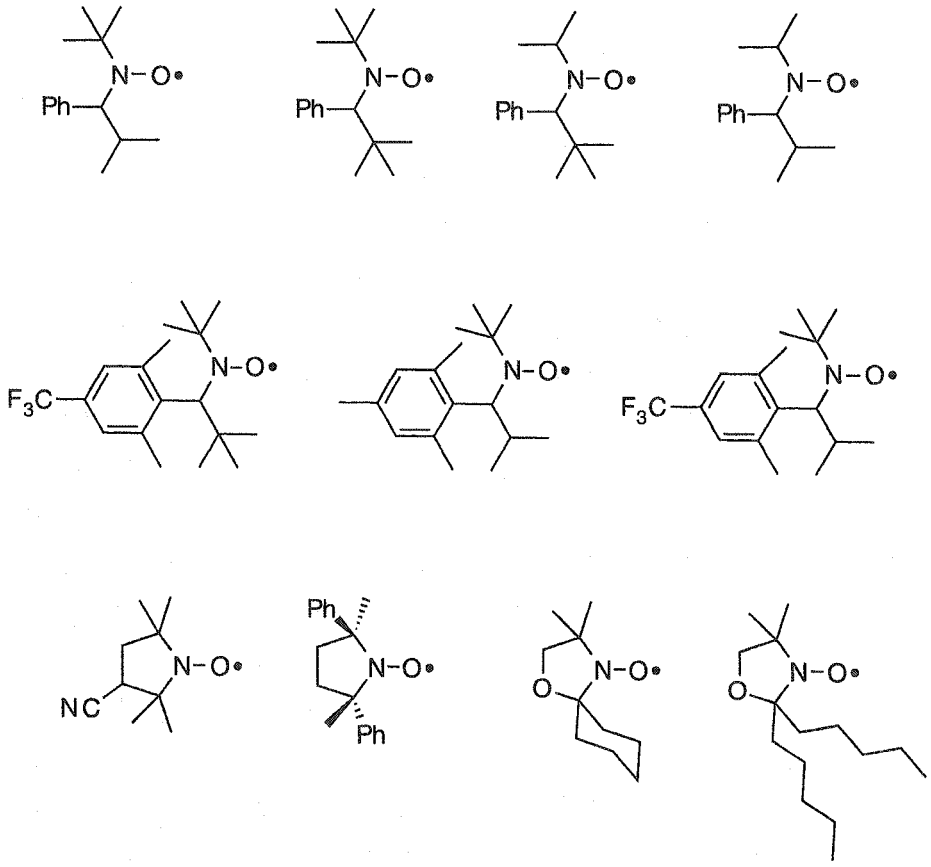

Figure 1-3. New generation of acyclic and cyclic nitroxides.[66]

The French group of Grimaldi has recently synthesized a nitroxide incorporating the electron donating phosphate group shown in Figure 1-4.[37] The addition of this group is expected to decrease the bond dissociation energy of the C-O bond of the alkoxyamine thereby promoting polymerization of new monomers. The preliminary trapping rate constants measured[71,81] are similar to those measured by Ingold et al.[27-29] and would suggest no kinetic benefit with the new nitroxides. However, the new class of nitroxides are able to sustain polymerization of monomers which conventional nitroxides cannot polymerize, including aliphatic monomers. However, these new structures are still not able to induce living polymerization of acrylates or methacrylates.

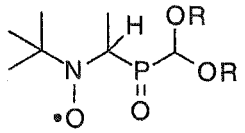

Figure 1-4. New generation of nitroxides containing an electron donating group and α-hydrogen.

1.3.1.3 Unimolecular Initiators

Unimolecular initiators are nitroxide containing compounds that produce two radicals upon thermal decomposition being the carbon centered radical and a nitroxide. The structure of the typically used unimolecular initiator for nitroxide mediated LFRP is found in Figure 1-5.

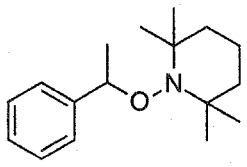

Figure 1-5. 1-Phenylethyl-TEMPO unimolecular initiator.

The advantage of using such initiators is multifold ranging from practical polymerization to their LFRP mimetic character. They are easily synthesized and offer an alternative to using conventional free radical initiators. Yet another attractive aspect to their use is they are shelf-stable and the polymerization can be induced with simple monomer addition and heating. More importantly, the decomposition of these initiators yield a stoichiometric amount of nitroxide relative to the initiating radical. The importance of this is great as each polymer chain initiated will be capped by a nitroxide leading to controlled living polymerization and ultimately polymers with low polydispersities. The amount of initiator added to the polymerization can be accurately weighed, and subsequently, the resulting polymer chain length can be determined by the monomer to initiator ratio. The most attractive benefit to the use of unimolecular initiators is their mimetic character. They have been taken advantage of by many groups to probe the intricacies of the LFRP process.[36-38,41,43,44,46,48,66,71,80-82,85-97] This thesis readily uses these initiators for this purpose in order to examine the kinetics and thermodynamics of nitroxide mediated LFRP.

These initiators are not without their drawbacks. In order to achieve living polymerization, the radical structure of the carbon centered radical formed upon decomposition should resemble the propagating radical. Changes to the radical structures alter the addition kinetics to the monomer subsequently interfering with the living properties of the resulting polymer.[98] A number of theoretical studies have been done in order to propose the ideal unimolecular structure for LFRP initiation.[56,57,75,99] A few of these initiators undergo an additional reaction upon thermal decomposition being the formation of disproportionation products. This decomposition route is thoroughly discussed in a following chapter.

1.3.1.4 Limitations of Nitroxide Mediated LFRP

The advantage of nitroxide mediated LFRP is that no metals are used therefore metal contamination of the synthesized polymer is nonexistent. This is an attractive approach for commercial applications since the polymers are more often being used as materials in the semiconductor industry.[79,80] The lack of metal contamination is also desirable for 'environmentally' friendly products. More importantly, nitroxide mediated LFRP yields polymers with complicated architectures not possible with conventional free radical polymerization. A few representative structures are found in Figure 1-7. The ultimate benefit to nitroxide mediated LFRP is the control over the polymerization process leading to predictable and defined molecular weights, low polydispersities, and high conversions.

Nitroxide mediated polymerization easily yields living polymers with high molecular weights, high conversions, and low polydispersities for polystyrene and its analogues.[19,33,58,72,95,100-109] Copolymerization using styrene or its analogues in combination of other monomers also give living polymers. However, the homopolymerization of alkyl monomers is less successful where the polymers obtained normally have broader molecular weight distributions, lower molecular weights, and poorer conversions, relative to their styrene counterparts. Currently a great deal of research is concerned with understanding the lack of observed living polymerization for acrylates and other alkyl vinyl monomers.[26,46,72,92,93,103,110-114] A portion of this thesis investigates this lack of controlled polymerization with acrylates and a couple of polymerization alternative methods leading to living polymers are proposed. This thesis also examines the fundamental kinetics involving radical trapping by nitroxides and

the energetics of the labile C-O, both encountered in the nitroxide mediated LFRP process. The proposal of new unimolecular initiators is also included. The last section deals with promoting nitroxide mediated LFRP under photochemical conditions including new photoinitiators for this process.

1.3.2 RAFT

An alternative approach to nitroxide mediated polymerization recently introduced by the CSIRO group in Australia is the use of thiocarbonylthio compounds as trapping agents.[105,115-118] This method is presented to bring to light other radical polymerization methods that yield living type polymers. Their approach undergoes reversible addition fragmentation chain transfer (RAFT) and is different than nitroxide mediated polymerization. The trapping agent used is of the general structure shown in Figure 1-6 where varying the R and Z groups leads to polymerization of different polymers.[119]

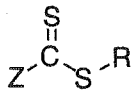

Figure 1-6. General structure of thiocarbonylthio trapping agent used for RAFT polymerization.

Unlike LFRP with unimolecular initiators that produce a stoichiometric amount of trapping agent, RAFT requires the use of standard radical initiating agents to generate the propagating radical ($P_n\bullet$). The propagating radical is trapped by the thiocarbonylthio compound by addition giving a carbon centered radical. Fragmentation leads to the generation of a new radical ($R\bullet$) at the early stage of the polymerization. The new radical acts like an initiator and reacts with the monomer to give a new "active" propagating radical ($P_m\bullet$). The propagating chain radical can subsequently add to the thiocarbonylthio compound containing another "dormant" chain P_n. There is an equal probability of chain growth due to the equilibrium between "dormant" and "active" $P_n\bullet/P_m\bullet$ species. The vast majority of the polymer chains are capped by the thiocarbonylthio compound upon polymerization completion and narrow polydispersities are obtained. The presence of a "dormant" thio portion means polymerization can be re-initiated in the presence of another monomer. The general schematic representation for RAFT polymerization is shown in Scheme 1-7.

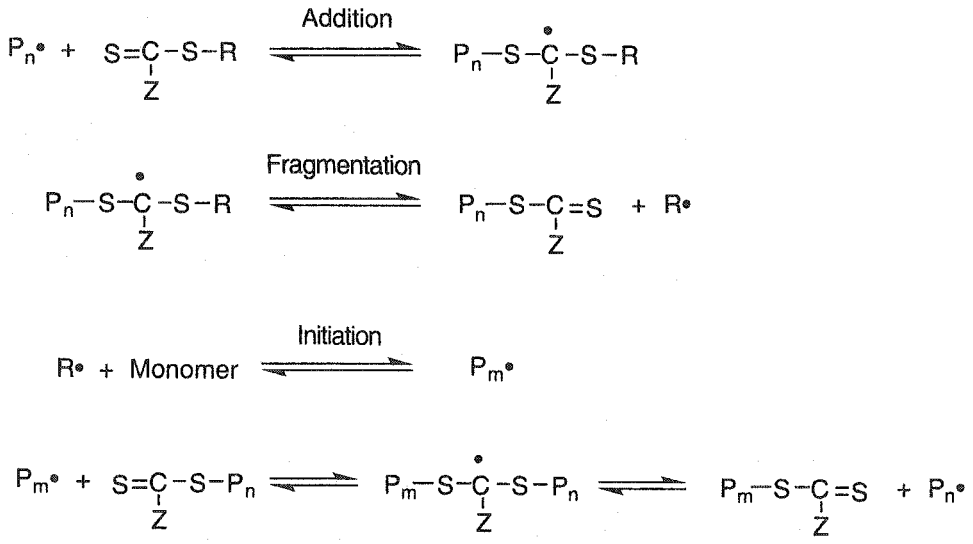

Scheme 1-7. General schematic representation of RAFT polymerization

Normally the polymerization is done with the addition of a chosen amount of thiocarbonylthio compound to the standard free radical polymerization mixture. Similar to nitroxide mediated polymerization, the amount of thiocarbonylthio compound added predetermines the polymer chain length. However contrary to the nitroxide polymerization, RAFT offers similar versatility and reaction conversions to conventional free radical polymerization. Also, complicated structures with narrow polydispersities such as copolymers, gradient, star, and block polymers can easily be synthesized by the RAFT approach.[118] An attractive advantage to using the RAFT trapping agents is the ease with which they are synthesized compared to different nitroxide structures.[120]

The choice of substituent groups Z and R on the thiocarbonylthio trap is crucial for the polymerization of monomers. The R group must be a good homolytic leaving group relative to the attacking radical $P_n\bullet$ in order to sustain the controlled polymerization. Typically R groups are tertiary radicals with one substituent being either Ph, COOR or CN. Ideally, R should be similar in structure to the propagating radical leading to equivalent rates of addition and fragmentation and subsequently controlled polymerization.

The Z group must be carefully selected to coincide with the polymerization of a desired monomer. This group influences the rate of addition of propagating radicals to the C=S bond. Typical Z groups are aryl or alkyl in nature.

RAFT polymerization appears to be an attractive alternative to nitroxide mediated polymerization for achieving LFRP especially with monomers that cannot be polymerized in the presence of nitroxides. However, this method is not without its disadvantages. Not all chains initiated will be capped by the thio trap, hence not all chains are living. The amount of dead polymers is determined by the amount of conventional initiator originally used to initiate the polymerization. A high ratio of dithio compound to initiator gives fewer dead polymers, but the molecular weight is sacrificed as a result. Another disadvantage to RAFT polymerization is the color of the resulting polymers. Since the thiocarbonylthio moiety is colored ranging in color from pale yellow to pink depending on the Z and R groups, the resulting polymer is also colored. However, the color can be eliminated by chemical modification with NaOCl, H_2O_2, or with irradiation.

1.3.3 ATRP

Another alternative approach to achieving LFRP without the use of nitroxides as trapping agents is the method developed by Matyjaszewski et al. at Carnagie Mellon University. This new method involves the use of metals that undergo an oxidation-reduction cycle in the presence of ligands and monomers and is called atom transfer radical polymerization (ATRP).[8,121-131]

The general mechanism of ATRP is shown below in Scheme 1-8. An active compound (R-X) is required as an initiator where X is a halide (Br or Cl) and R is similar in structure to the monomer to be polymerized.[132] The metal promotes reversible cleavage of the initiator's covalent bond resulting in a propagating radical (R•) and an oxidation of the metal center. Addition to the monomer occurs in a similar fashion to the nitroxide mediated path where the radical is trapped after addition. The dormant species is generated upon successful trapping by the halide previously coordinated to the metal center. At the polymerization temperatures, the metal center promotes homolytic cleavage of the organo-halide bond to form the "active" chain carrying species and the catalytic site is completed. There is the possibility that R• may react with another R•, but this reaction is not dominant because the concentration of the two species is quite small. The end result is polymerization in a controlled fashion leading to high conversions and polymers with high molecular weights and low polydispersities.

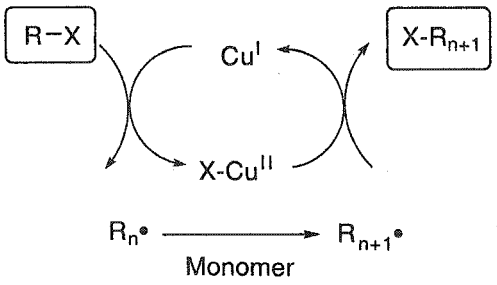

Scheme 1-8. Schematic representation of ATRP involving the regeneration of active Metal species.

Several metals that have been used for ATRP are Cu(I), Ni(II), Ru(II)/$Al(OR)_3$, and Fe(II), which all undergo one electron oxidation with simultaneous abstraction of a halogen from the initiator.[133] There has also been some success with Ni and Pd, yet the Cu metal has been extensively studied and gives the best results for LFRP. Certain criterion for the metal must be satisfied for successful ATRP. It must be able to (i) undergo one electron redox with relative ease, (ii) its coordination number must increase upon oxidation to accommodate the new halogen ligand, (iii) the number of *d* electrons should be paired for lower oxidation metals, providing the configuration is stable, (iv) it must have a low affinity for alkyl radicals and hydrogen atoms in order to promote atom transfer and not β-hydrogen elimination, (v) the metal selected must not be a strong Lewis acid to prevent ionization of the initiator or end-groups, (vi) oxidation should occur within the metal's inner-sphere and not its outer-sphere.

The choice of ligand coordinated to the metal center is also of importance and is normally bidentate and contains nitrogen. The typically used ligand that gives good results is 2,2'-bipyridine and its derivatives. However, living polymerization can also be sustained using other π accepting and nitrogen-based chelating ligands such as 2-iminopyridines or aliphatic polyamines. The typical metal-ligand complex used as a catalyst for ATRP is schematically represented in Scheme 1-9. Prior to the polymerization, the catalyst has a tetrahedral geometry. Oxidation of the metal causes homolytic cleavage of the organo-halide bond giving the propagating radical. The subsequently formed halide is coordinated to the oxidized center generating a trigonal bipyramid new structure. There is an equilibrium between the two forms with preference going to the penta-coordinated species.

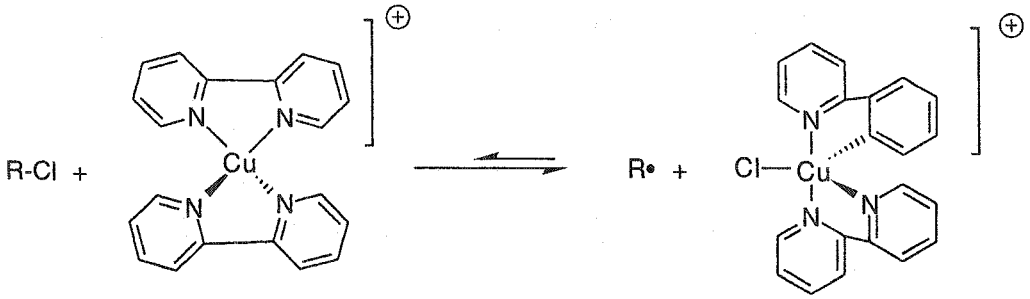

Scheme 1-9. Activation of the copper species through a configurational change from tetrahedral to bipyramidal.

Unlike nitroxide mediated LFRP, ATRP is able to promote the living polymerization of many different type of monomers. A few examples of monomers that have been successfully homopolymerized are styrene and its analogues, methyl methacrylate, methacrylate, acrylamide, acrylonitrile, isoprene, vinylpyrrolidinone, and 2-(dimethylamino)ethyl acrylate.[133] The list of monomers that can be copolymerized with this approach is too extensive to include here. Regardless, the list of polymerizable monomers supersedes that of nitroxide mediated LFRP. Selection of the correct metal and its corresponding chelating agent are important for the polymerization of the various monomers. The choice of different metal centers and ligands change the redox properties of the catalyst thereby promoting or suppressing the homolytic cleavage of the organo-halide initiator bond.

Even though ATRP would appear to be more advantageous than nitroxide based polymerization, it suffers from drawbacks. Original problems with this method are similar to RAFT where the end polymer was discolored due to contaminants. The solubility of the catalyst is an issue for ATRP in certain monomers. Synthetically complicated modifications of the ligand must be done in order to solubilize sufficient catalyst for the polymerization of acrylate monomers. Also, the bipyridine ligand cannot be used to polymerize monomers containing acid functions and therefore limits its applicability. The structure and reactivity are strongly affected by the solvent used, hence the monomer selected for bulk polymerization. The major disadvantage with the ATRP approach is the end polymer is normally contaminated with metals. This precludes its use for the synthesis of polymers used in the semi-conductor industry as any metal contamination would destroy the inert character of the polymer. For this reason, nitroxide mediated LFRP is more attractive as complicated architectures can be

achieved without contamination of the resulting polymers making it an attractive industrially applicable method.

1.3.4 Section Summary

Three methods of achieving of LFRP have been presented including their advantages and disadvantages. Particular emphasis has been placed on nitroxide mediated polymerization to contrast and compare with the other LFRP methods available. The focus of this thesis deals with nitroxide mediated LFRP with particular attention to the kinetics and thermodynamics of this process. Also, the specific reactions occurring during LFRP are investigated in order to propose a living polymerization route for the elusive acrylates.

1.4 Polymer Terminology and Structures

The definitions that follow are standard polymer terminology which are important for characterizing the polymers synthesized. In general, the terms used are all related to the polymer's molecular weight which in turn determines the polymer's physical properties. There are many ways by which molecular weights can be measured in general. However, because of differences in the experimental techniques used, different values of polymer molecular weights are normally obtained. Molecular weight measurements by various methods have been defined in order to maintain a universal nomenclature standard. Measurements done with methods that use the polymer's colligative properties or end-group analysis lead to the number average molecular weight (M_n) expressed in Equation 1-1. Here N represents the number of moles and M is the molecular weight. This value is determined by any method which counts the number of molecules present relative to the mass, i.e. boiling point elevation, osmotic pressure, freezing-point depression, vapor pressure osmometry, end-group analysis, or membrane osmometry. The last three methods are typically used for determining M_n.

$$M_n = \frac{\sum N_i M_i}{N_i M_i}$$

Equation 1-1. Number average molecular weight for polymers.

The value of M_n is extremely sensitive to low molar mass species simply because they contribute more to the number of molecules present than the mass. Measured values of M_n are typically smaller than other molecular weights for the same polymer because of the contribution just mentioned.

The weight average molecular weight (M_w) is yet another type of polymeric molecular weight term. It is defined according to Equation 1-2 and is quadratically dependent upon the molecular weight of the polymer. The desired value is calculated as the summation of the weight fraction for each species as a function of its molecular weight. M_w is normally determined by light scattering methods, ultra-centrifugation, or determination of the mass by species present.

$$M_w = \frac{\sum W_i M_i}{\sum w_i} = \frac{\sum N_i M_i^2}{N_i M_i}$$

Equation 1-2. Weight average molecular weight for polymers.

Contrary to M_n where smaller molecular weights contribute more to the value, M_w is influenced more by higher molecular weights. This is due to the method of analysis. The amount of scattered light is greater for larger molecules than for smaller ones leading to higher values of M_w. However, when the difference between the larger and smaller polymers is relatively small, the difference between M_n and M_w is equally small.

The difference between the measured molecular weight (M_w and M_n) values determined by different methods provides information pertaining to the molecular weight distribution. The polydispersity index (PDI) is the term used to described the molecular weight distribution of the polymer. Here, the terms PDI and polydispersity (PD) are used interchangeably. The PD is expressed in Equation 1-3 and is the ratio of M_w and M_n. The smaller the value of PD, the more uniform are the molecular weights, hence monodisperse.

$$PD = \frac{M_w}{M_n}$$

Equation 1-3. Polydispersity identity.

The degree of polymerization (DP) refers to the number of repeating units in the polymer.

The methods used to measure the molecular weights are complicated when applied to polymers. However, the observed values can be obtained through the use of chromatographic methods. The method of choice is size exclusion chromatography (SEC) or gel permeation chromatography (GPC). This consists of selected size beads packed onto a column. Smaller length polymers can penetrate between the beads and are retained longer on the column than longer length polymers. The different length polymers subsequently elute with different retention times. Polystyrene standards of known molecular weights are used to create a calibration curve of molecular weight versus retention time. The M_w, M_n, and PD of the polymer of study are obtained by comparing the shape, area under the curve, and the retention time relative to the polystyrene

standards. The advantage of this approach is ease of characterization and rapid analysis time.

The calibrated GPC method was exclusively used to characterize the polymers synthesized and discussed in this thesis in terms of M_w, M_n, and PD.

A few interesting polymeric structures possible through LFRP techniques are represented in Figure 1-7.

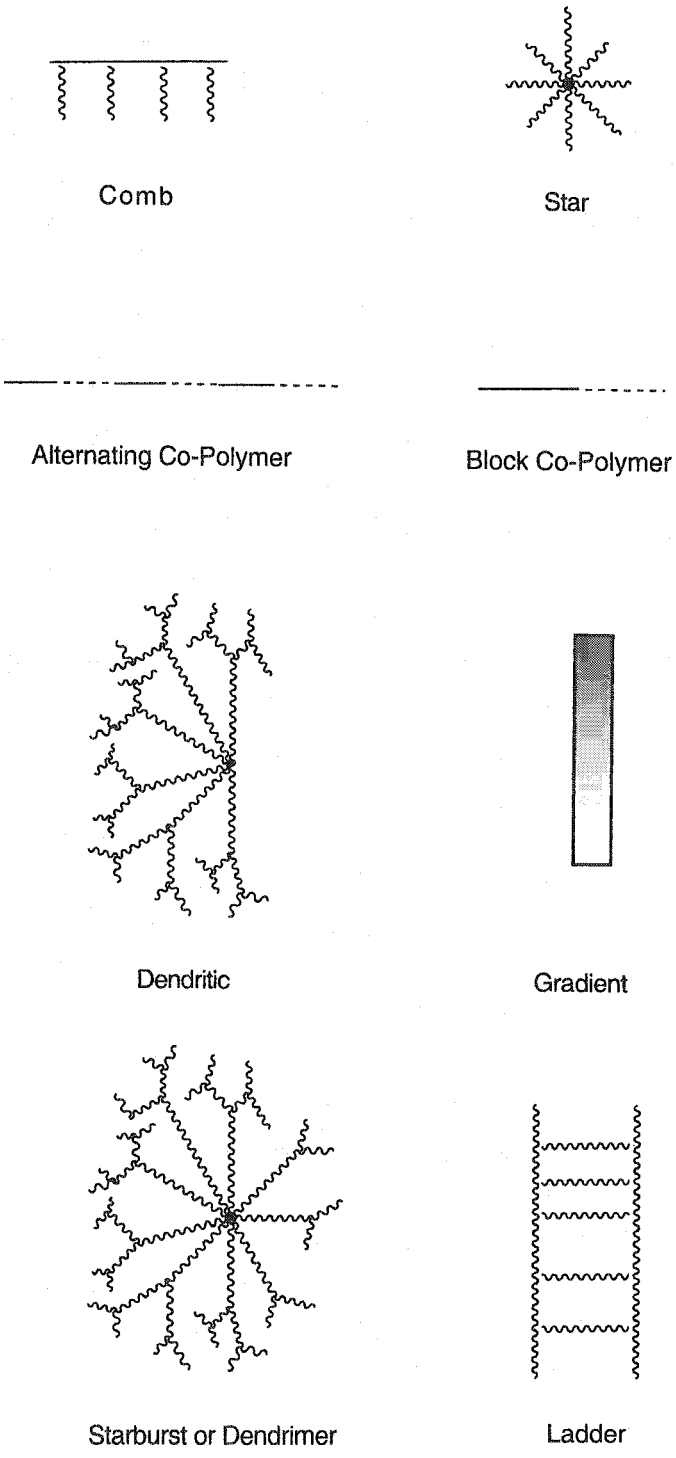

Figure 1-7. Polymer architecture possible by nitroxide mediated LFRP.

1.5 Chapter References

1. Stewart, J. J. P. Semiempirical Molecular Orbital Methods. In *Reviews in Computational Chemistry I*; Lipkowitz, K. B., Boyd, D. B., Eds.; VCH:, 1990; 45-81.
2. Cowie, J. M. G. *Polymers: Chemistry and Physics of Modern Materials*, 2nd ed.; Blackie and Sons Ltd.: Glasgow, 1991, pp 436.
3. Bevington, J. C. Overall Mechanisms. In *Comprehensive Polymer Science. The Synthesis, Characterization, Reaction and Applications of Polymers*; G., A., Bevington, J. C., Booth, C., Ledwith, A., Russo, S., Aggarwar, S. L., Eastmond, G. C., Price, C., Sigwalt, P., Eds.; Pergamon Press: Toronto, 1989; Vol. 3; 65-84.
4. Berger, K. C.; Meyerhoff, G. Propagation and Termination Constants in Free Radical Polymerization. In *Polymer Handbook*; 3rd ed.; Brandrup, J., Immergut, E. H., Eds.; John Wiley & Sons: New York, 1989; .
5. Szwarc, M. *Science* **1970**, *170*, 23-31.
6. Szwarc, M.; Levy, R.; R., M. *J. Am. Chem. Soc.* **1956**, *78*, 2656-2657.
7. Kennedy, J. P.; Marechal, E. *Carbocationic Polymerization*; Wiley: New York, 1982, .
8. Matyjaszewski, K. *New Polym. Mater.* **1990**, *2*, 115-123.
9. Penczek, S.; Kubisa, P. Living Polymer Systems. In *Polymer Handbook*; 4th ed.; Brandrup, J., Immergut, E. H., Grulke, E. A., Abe, A., Bloch, D. R., Eds.; John Wiley & Sons: New York, 1999; 380-435.
10. Szwarc, M. *Carbanions, Living Polymers, and Electron Transfer Processes*; Interscience: New York, 1968, pp 685.
11. Szwarc, M. *Encycl. Polym. Sci. Technol.* **1968**, *8*, 303-325.
12. Szwarc, M. *Polym. Prepr., Am. Chem. Soc., Div. Polym. Chem.* **1967**, *8*, 22-25.

13. Henderson, J. F.; Szwarc, M. *Macromol. Rev.* **1968**, *3*, 317-401.
14. Szwarc, M. *Ann. N. Y. Acad. Sci.* **1969**, *155*, 400-418.
15. De Groof, B.; Mortier, W.; Van Beylen, M.; Szwarc, M. *Macromolecules* **1977**, *10*, 598-602.
16. De Groof, B.; Van Beylen, M.; Szwarc, M. *Macromolecules* **1975**, *8*, 396-400.
17. Fontanille, M. Carbanionic Polymerization: General Aspects and Initiation. In *Polymer Handbook*; 4th ed.; Brandrup, J., Immergut, E. H., Grulke, E. A., Abe, A., Bloch, D. R., Eds.; John Wiley & Sons: New York, 1999; 365-375.
18. Keana, J. F.; Hideg, K.; Birrell, G. B. *Can. J. Chem.* **1982**, *60*, 1439-1447.
19. Zaremskii, M.; Stoyachenko, Y.; Plutalova, A.; Lachinov, M.; Golubev, V. *Vysokomol. Soed. Ser. A & Ser. B* **1999**, *41*, 398-398.
20. Fuchs, J.; Nitschmann, W. H.; Packer, L.; Hankovszky, O. H.; Hideg. *Free Rad. Res. Comms.* **1990**, *10*, 315-328.
21. Nagashima, T.; Curran, D. P. *Synlett.* **1996**, *4*, 330-332.
22. Dagonneau, M.; Kagan, E. S.; Mikhailov, V. I.; Rozantsev, E. G.; Sholle, V. D. *Synthesis* **1984**, *11*, 895-916.
23. Rychnovsky, S. D.; Vaidynanathan, R. *J. Org. Chem.* **1999**, *64*, 310-612.
24. Cella, J. A.; Kelley, J. A.; Kenehan, E. F. *Tetrahedron Lett.* **1975**, *33*, 2869-2872.
25. Limoges, B.; Degrand, C. *J. Electroanal. Chem.* **1997**, *422*, 7-12.
26. Duz, A.; Onen, A.; Yagci, Y. *Angew. Makromol. Chem.* **1998**, *258*, 1-4.
27. Bowry, V. W.; Ingold, K. U. *J. Am. Chem. Soc.* **1992**, *114*, 4992-4996.
28. Chateauneuf, J.; Lusztyk, J.; Ingold, K. U. *J. Org. Chem.* **1988**, *53*, 1629-1632.
29. Beckwith, A. J.; Bowry, V. W.; Ingold, K. U. *J. Am. Chem. Soc.* **1992**, *114*, 4983-4992.
30. Rizzardo, E.; Solomon, D. H. *Polym. Bull.* **1979**, *1*, 529-534.
31. Moad, G.; Rizzardo, E.; Solomon, D. H. *Macromolecules* **1982**, *15*, 909-914.

32. Moad, G.; Rizzardo, E.; Solomon, D. H. *J. Macromol. Sci. Chem.* **1982**, *A17*, 51-59.
33. Moad, G.; Rizzardo, E.; Solomon, D. H. *Polym. Bull.* **1982**, *6*, 589-293.
34. Solomon, D. H.; Rizzardo, E.; Cacioli, P. U.S. Patent 4,581,429, **1986**.
35. Mahoney, L. R.; Mendenhall, G. D.; Ingold, K. U. *J. Am. Chem. Soc.* **1973**, *95*, 8610-8614.
36. Engel, P. S.; Duan, S.; Arhancet, G. G. *J. Org. Chem.* **1997**, *62*, 3537-3541.
37. Grimaldi, S.; Finet, J.-P.; Zeghdaoui, A.; Tordo, P.; Benoit, D.; Gnanou, Y.; Fountanille, M.; Nicol, P.; Pierson, J.-F. *Polym. Prepr.* **1997**, *38*, 651-653.
38. Fukuda, T.; Tsujii, Y.; Miyamoto, T. *Polym. Prepr.* **1997**, *38*, 723-724.
39. Stipa, P.; Greci, L.; Carloni, P.; Damiani, E. *Polymer Degrad. Stab.* **1997**, *55*, 323-327.
40. Ciriano, M. V.; Korth, H.-G.; van Scheppingen, W. B.; Mulder, P. *J. Am. Chem. Soc.* **1999**, *121*, 6375-6381.
41. Fukuda, T.; Goto, A.; Ohno, K. *Macromol. Rapid Commun.* **2000**, *21*, 151-165.
42. Fukuda, T.; Terauchi, T.; Goto, A.; Ohno, K.; Tsujii, Y.; Miyamoto, T. *Macromolecules* **1996**, *29*, 6393-6398.
43. Fukuda, T.; Goto, A. *Macromol. Rapid Commun.* **1997**, *18*, 683-688.
44. Goto, A.; Rerauchi, T.; Fukuda, T.; Miyamoto, T. *Macromol. Rapid Commun.* **1997**, *18*, 373-381.
45. Ide, N.; Fukuda, T. *Macromolecules* **1999**, *32*, 95-99.
46. Goto, A.; Fukuda, T. *Macromolecules* **1999**, *32*, 618-623.
47. Fukuda, T.; Atsushi, G. *Polym. Prepr.* **1999**, *40*, 311-312.
48. Fukuda, T.; Goto, A.; Ohno, K.; Tsujii, Y. "Mechanism and Kinetics of Nitroxide-Controlled Free-Radical Polymerization"; Controlled Radical Polymerization, 1998, San Francisco, CA.
49. Fischer, H. *J. Am. Chem. Soc.* **1986**, *108*, 3925-3927.

50. Fischer, H. *Macromolecules* **1997**, *30*, 5666-5672.
51. Fischer, H. *J. Polym. Sci., Part A: Polym. Chem.* **1999**, *37*, 1885-1901.
52. Georges, M. K.; Veregin, R. P. N.; Kazmaier, P. M.; Hamer, G. K. *Macromolecules* **1993**, *26*, 2987-2988.
53. Georges, M. K.; Veregin, R. P. N.; Kazmaier, P. M.; Hamer, G. K.; Saban, M. *Macromolecules* **1994**, *27*, 7228-7229.
54. Stevens, M. P. *Polymer Chemistry, An Introduction*, 2nd ed.; Oxford University Press: New York, 1990, pp 633.
55. Veregin, R. P. N.; Odell, P. G.; Michalak, L. M.; Georges, M. K. *Macromolecules* **1996**, *29*, 4161-4163.
56. Moad, G.; Rizzardo, E. *Macromolecules* **1995**, *28*, 8722-8728.
57. Kazmaier, P. M.; Moffat, K. M.; Georges, M. K.; Veregin, R. P. N.; Hamer, G. K. *Macromolecules* **1995**, *28*, 1841-1846.
58. Yamada, B.; Miura, Y.; Nobukane, Y.; Aota, M. "Styrene Polymerization Mediated by Five-Membered Cyclic Nitroxides"; Controlled Radical Polymerization, 1998, San Francisco, CA.
59. Stipa, P.; Finet, J.-P.; Le Moigne, F.; Tordo, P. *J. Org. Chem.* **1993**, *58*, 4465-4468.
60. Le Moigne, F.; Mercier, A.; Tordo, P. *Tetrahedron Lett.* **1991**, *32*, 3841-3844.
61. Doa, J.; Benoit, D.; Hawker, C. J. *J. Polym. Sci. A. Polym. Chem.* **1998**, *36*, 2161-2167.
62. Braslau, R.; Chaplinski, V. *J. Org. Chem.* **1998**, *63*, 9857-9864.
63. Naik, N.; Braslau, R. *Tetrahedron* **1998**, *54*, 667-696.
64. Einhorn, J.; Einhorn, C.; Ratajczak, F.; Durif, A.; Averbuch, M.-T.; Pierre, J.-L. *Tetrahedron Lett.* **1998**, *39*, 2565-2568.
65. Murray, R. W.; Singh, M. *Tetrahedron Lett.* **1988**, *29*, 4677-4680.
66. Benoit, D.; Chaplinski, V.; Braslau, R.; Hawker, C. J. *J. Am. Chem. Soc.* **1999**, *121*, 3904-3920.

67. Klemchuk, P. P. Introduction to Hindered Amine Stabilizers. In *Polymer Stabilization and Degradation*; Klemchuk, P. P., Ed.; American Chemical Society: Washington, 1985; Vol. 280; 1-10.

68. Müller, H. K. A Decade of Hindered Amine Light Stabilizers. In *Polymer Stabilization and Degradation*; Klemchuk, P. P., Ed.; American Chemical Society: Washington, 1985; Vol. 280; 1-10.

69. Toda, T.; Kurumada, T.; Marayama, K. Progress in the Light Stabilizataion of Polymers. In *Polymer Stabilization and Degradation*; Klemchuk, P. P., Ed.; American Chemical Society: Washington, 1985; Vol. 280; 1-10.

70. Griffiths, P. G.; Moad, G.; Rizzardo, E.; Solomon, D. H. *Aust. J. Chem.* **1983**, *36*, 397-401.

71. Le Mercier, C.; Bernard-Henriet, C.; de Sainte-Claire, V.; Le Moigne, F.; Tordo, P. *Polym. Prepr.* **1999**, *40*, 403-404.

72. Lokaj, J.; Vlcek, P.; Kriz, J. *Macromolecules* **1997**, *30*, 7644-7646.

73. Cogen, J. M. *Polymer Degrad. Stab.* **1994**, *44*, 49-53.

74. Marsal, P.; Roche, M.; Tordo, P.; de Sainte Claire, P. *J. Phys. Chem. A* **1999**, *103*, 2899-2905.

75. Kysel, O.; Mach, P.; Micov, M. *Polymer Degrad. Stab.* **1993**, *40*, 31-35.

76. Rozantsev, E. G.; Sholle, V. D. *Synthesis* **1971**, 401-414.

77. Rozantsev, E. G.; Kagan, E. S.; Sholle, V. D.; Ivanov, V. B.; Smirnov, V. A. Discovery, Chemistry, and Application of Hindered Amines. In *Polymer Stabilization and Degradation*; Klemchuk, P. P., Ed.; American Chemical Society: Washington, 1985; Vol. 280; 1-10.

78. Hawker, C. J. *Acc. Chem. Res.* **1997**, *30*, 373-382.

79. Harth, E.; Benoit, D.; Helms, B.; Hawker, C. J. *Polym. Prepr.* **2000**, *41*, 42-43.

80. Benoit, D.; Harth, E.; Fox, P.; Waymouth, R. M.; Hawker, C. J. *Macromolecules* **2000**, *33*, 363-370.

81. Le Mercier, C.; A., G.; Siri, D.; Tordo, P.; Marque, S.; Martschke, R.; Fischer, H. *Polym. Prepr.* **1999**, *40*, 313-314.

82. Hawker, C.; Benoit, D.; Rivera, F., Jr.; Piotti, M.; Rees, I.; Hedrick, J. L.; Zech, C.; Maier, G.; Voit, B.; Braslau, R.; Fréchet, J. M. J. *Polym. Prepr.* **1999**, *40*, 315-316.

83. Malmström, E. E.; Miller, R. D.; Hawker, C. J. *Tetrahedron* **1997**, *53*, 15225-15236.

84. Devonport, W.; Michalak, L.; Malmstrom, E.; Mate, M.; Kurdi, B.; Hawker, C. J. *Macromolecules* **1997**, *30*, 1929-1934.

85. Skene, W. G.; Scaiano, J. C. **2000**, Manuscript in preparation.

86. Skene, W. G.; Scaiano, J. C.; Listigovers, N. A.; Kazmaier, P. E.; Georges, M. K. *Macromolecules* **2000**, *33*, 5065-5072.

87. Moffat, K. A.; Hamer, G. K.; Georges, M. K. *Macromolecules* **1999**, *32*, 1004-1012.

88. Fischer, A.; Brembilla, A.; Lochon, P. *Macromolecules* **1999**, *32*, 6069-6072.

89. Bon, S. A. F.; Chambard, G.; German, A. L. *Macromolecules* **1999**, *32*, 8269-8276.

90. Georges, M. K.; Veregin, R. P. N.; Daimon, K. The Stable Free-Radical Polymerization Process: Role of Excess Nitroxide. In *Controlled Radical Polymerization*; Matyjaszewski, K., Ed.; American Chemical Society: Washington, 1998; Vol. 685; 170-179.

91. Scaiano, J. C.; Connolly, T. J.; Mohtat, N.; Pliva, C. N. *Can. J. Chem.* **1997**, *75*, 92-97.

92. Georges, M. K.; Listigovers, N. A.; Odell, P. G.; Hamer, G. K.; Quilan, M. H.; Veregin, R. P. N. *Polym. Prepr.* **1997**, *38*, 454-455.

93. MacLeod, P. J.; Georges, M. K.; Quinlan, M.; Moffat, K. A.; Listigovers, N. A. *Polym. Prepr.* **1997**, *38*, 459-460.

94. Georges, M. K.; Odell, P. G.; Veregin, R. P. N.; Keoshkerian, B. *Polym. Prepr.* **1997**, *38*, 721-722.

95. Connolly, T. J.; Scaiano, J. C. *Tetrahedron Lett.* **1997**, *38*, 1133-1136.

96. Hawker, C. J.; Barclay, G. G.; Dao, J. *J. Am. Chem. Soc.* **1996**, *118*, 11467-11471.

97. Skene, W. G.; Belt, S. T.; Connolly, T. J.; Hahn, P.; Scaiano, J. C. *Macromolecules* **1998**, *31*, 9103-9105.

98. The lifetimes and trapping kinetics of the various carbon centered radicals are discussed in the following chapters.

99. Martinez, L. J.; Scaiano, J. C. *J. Phys. Chem. A* **1999**, *103*, 203-208.

100. Saban, M. D.; Georges, M. K.; Veregin, R. P. N.; Hamer, G. K.; Kazmaier, P. M. *Macromolecules* **1995**, *28*, 7032-7034.

101. Hammouch, S. O.; Catala, J.-M. *Macromol. Rapid. Commun.* **1996**, *17*, 683-691.

102. Barclay, G. G.; Hawker, C. J.; Ito, H.; Orellana, A.; Malenfant, P. R. L.; Sinta, R. F. *Macromolecules* **1998**, *31*, 1024-1031.

103. Rizzardo, E.; Serelis, A. K.; Solomon, D. H. *Aust. J. Chem.* **1982**, *35*, 2013-2024.

104. Kobatake, S.; Harwood, H. J.; Quirk, R. P.; Priddy, D. B. *J. Polym. Sci. A. Polym. Chem.* **1998**, *36*, 2555-2561.

105. Maldonado-Textle, H.; De Leon-Saenz, M. E.; Putaux, J. L.; Ramos-De Valle, L. F.; Guerrero-Santos, R. *Macromolecules* **1998**, *31*, 2697-2698.

106. Marestin, C.; Noel, C.; Guyot, A.; Claverie, J. *Macromolecules* **1998**, *31*, 4041-4044.

107. Yoshida, E.; Sugita, A. *J. Polym. Sci. A. Polym. Chem.* **1998**, *36*, 2059-2068.

108. Lansalot, M.; Charleux, B.; Vairon, J.-P. *Polym. Prepr.* **1999**, *40*, 317-318.

109. Lutz, J.-F.; Lacrois-Desmazes, P.; Boutevin, B. *Polym. Prepr.* **1999**, *40*, 319-320.

110. Odell, P. G.; Rabien, A.; Michalak, L. M.; Vergin, R. P. N.; Quinlan, M. H.; Moffat, K. A.; MacLeod, P. J.; Listigovers, N. A.; Honeyman, C. H.; Georges, M. K. *Polym. Prepr.* **1997**, *38*, 414-415.

111. Keoshkerian, B.; Georges, M.; Quinlan, M.; Veregin, R.; Goodbrand, B. *Macromolecules* **1998**, *31*, 7559-7561.

112. Haddleton, D. M.; Kukulj, D.; Duncalkf, D. J.; Heming, A. M.; Shooter, A. J. *Macromolecules* **1998**, *31*, 5201-5205.

113. Plutalova, A.; Zaremskii, M.; Pavlov, M.; Garina, E.; Lachinov, M.; VB, G. *Vysok. Soed. Ser. A & B* **1999**, *41*, 552-555.

114. Burguière, C.; Dourges, M.-A.; Charleux, B.; Vairon, J.-P. *Macromolecules* **1999**, *32*, 3883-3890.

115. Cao, T.; Weiping, Y.; Webber, S. E. *Macromolecules* **1994**, *27*, 7459-7464.

116. Chiefari, J.; Chong, Y. K.; Ercole, F.; Krstina, J.; Jeffery, J.; Le, T. P. T.; Mayadunne, R. T. A.; Meijs, G. F.; Moad, C. L.; Moad, G.; Rizzardo, E.; Thang, S. H. *Macromolecules* **1998**, *31*, 5559-5562.

117. Li, Y.; Desmone, J. M.; Poon, C.-D.; Samulski, E. T. *J. Appl. Polym. Sci.* **1997**, *64*, 883-889.

118. Rizzardo, E.; Chiefari, J.; Chong, B. Y. K.; Ercole, F.; Krstina, J.; Jeffery, J.; Le, T. P. T.; Mayadunne, R. T. A.; Meijs, G. F.; Moad, C. L.; Moad, G.; Thang, S. H. Tailored polymers by free radical processes. In *Macromolecular Symposia*, 1999; Vol. 143; 291-307.

119. Kristina, J.; Moad, C. L.; Moad, G.; Rizzardo, E. *Macromol. Symp.* **1996**, *111*, 13-23.

120. Thang, S. H.; Chong, Y. K.; Mayadunne, R. T. A.; Moad, G.; Rizzardo, E. *Tetrahedron Lett.* **1999**, *40*, 2435-2438.

121. Patten, T. E.; Xia, J.; Abernathy, T.; Matyjaszewski, K. *Science* **1996**, *272*, 866-868.

122. Miller, P. J.; Matyjaszewski, K. *Macromolecules* **1999**, *32*, 8760-8767.

123. Matyjaszewski, K. *Polym. Prepr.* **1999**, *40*, 309-311.

124. Matyjaszewski, K. "Overview: Fundamentals of Controlled/Living Radical Polymerization"; Controlled Radical Polymerization, 1998, San Francisco, CA.

125. Matyjaszewski, K.; Woodworth, B. E.; Zhang, X.; Gaynor, S. G.; Metzner, Z. *Macromolecules* **1998**, *31*, 5955-5957.

126. Matyjaszewski, K.; Gaynor, S.; Jin-Shan, W. *Macromolecules* **1995**, *28*, 2093-2095.

127. Matyjaszewski, K.; Pugh, C. *Makromol. Chem., Macromol. Symp.* **1993**, *67*, 67-82.

128. Matyjaszewski, K.; Grimaud, T. , 456-457.

129. Mardare, D.; Shigemoto, T.; Matyjaszewski, K. *Polym. Prepr.* **1994**, *35*, 557-558.

130. Li, I.; Howell, L.; Matyjaszewski, K.; Shigemoto, T.; Smith, P. B.; Priddy, D. B. *Macromolecules* **1995**, *28*, 6692-6693.

131. Kajiwara, A.; Matyjaszewski, K.; Kamachi, M. *Polym. Prepr.* **1999**, *40*, 301-303.

132. Poutsma, M. L. Atom-Transfer and Substitution Reaction. In *Free Radicals*; Kochi, J. K., Ed.; John Wiley & Sons: Toronto, 1973; Vol. 2; 113-158.

133. Matyjaszewski, K. "Mechanistic Aspects of Atom Transfer Radical Polymerization"; Controlled Radical Polymerization, 1998, San Francisco, CA.

2. Photoacoustic and Photothermal Methods

2.1 Introduction

The objective of this chapter is to present the photothermal techniques available of the University of Ottawa. These were subsequently used for measurements involving LFRP initiators and the data collected will be discussed in the chapter immediately following. Only the general concept of the photothermal methods including useful equations and volume effects are the focus of this chapter. The technique of laser flash photolysis used for kinetic investigation has been omitted as a thorough description of this method and experimental setup can be found elsewhere.[1-6] The material presented here is intended as a reference for future students concerning the experimental set-up and data treatment for photoacoustic calorimetry and thermal lensing methods at the University of Ottawa. No actual experimental data will be discussed here, only the techniques.

Photoacoustic calorimetry (PAC), also known as laser induced optoacoustic calorimetry (LIAOC), and photothermal methods (PTM) can be categorized as similar techniques. Both of which are capable of resolving the energetics and kinetics[7] of a given process resulting from absorption of radiation. In principle, these techniques mimic laser flash photolysis (LFP) where a short burst of energy is required to produce transients whose decays are subsequently monitored. However, the similarities between the two techniques stop here as the metastable species produced in the thermal methods are not spectroscopically monitored as with LFP. Upon radiation absorption, the reagent studied is excited producing metastable species. Deactivation of the metastable species can occur by many routes and a general schematic is represented in Figure 2-1 along with the detection method associated with the decay. The deactivation process causes local heating in the medium, subsequently forming a pressure wave that propagates through the solution. Photoacoustic calorimetry measures the amplitude of the propagating pressure wave recorded typically with piezoelectric detectors, which act as a microphone. In addition to acoustic waves, localized heating leads to changes in the refractive index within the radiation plume. Photothermal techniques measure the refractive index gradient in order to determine the energetics of the reaction studied. These methods are described more in detail in the appropriate sections that follow. The advantage of these techniques over LFP, is the transients produced need not be optically visible as it is the energy deposited into the medium that is monitored.

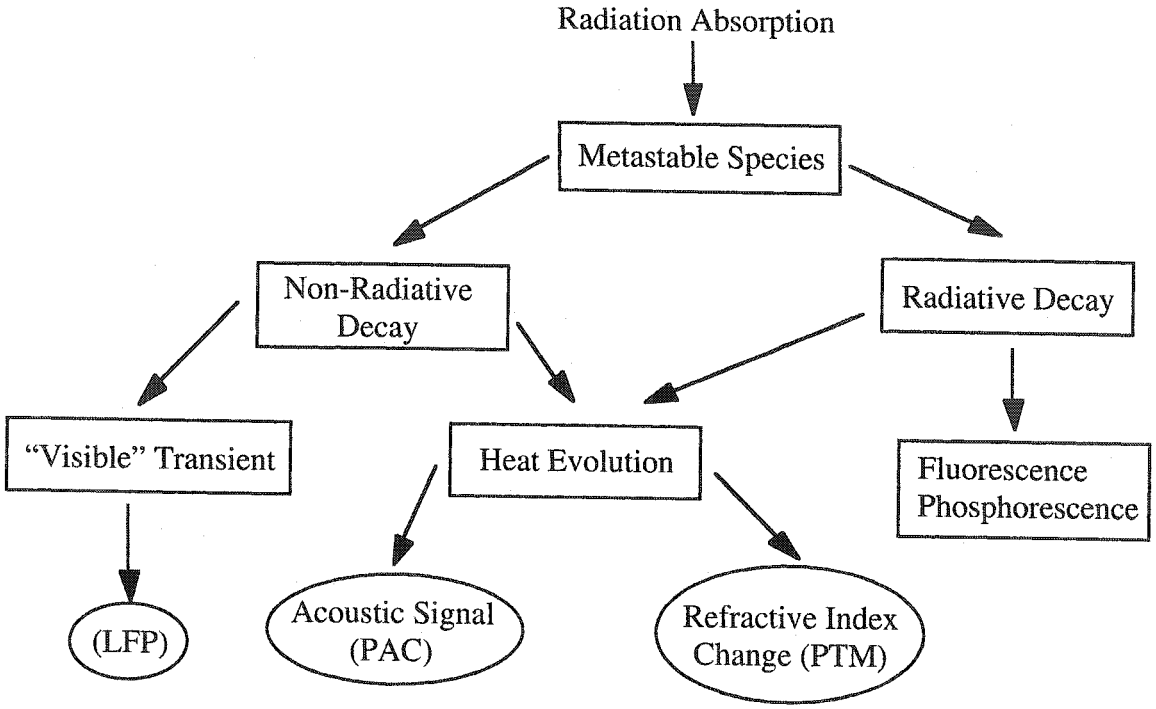

Figure 2-1. General flow chart illustrating the use of different methods for various photoinduced processes.

PAC and PTM are two energy balance techniques and as a result are calorimetric in nature. The energy pumped into the system in the form of light ($E_{h\upsilon}$) is dissipated by the metastable transient and the subsequent changes it induces are detected and accounted for by the right hand term of Equation 2-1. Here E_f is the energy dissipated by fluorescence and the quantum yield of the given process (Φ_f), α is the fraction of energy deposited into the medium as prompt heat, and the last term, the amount of energy stored by longer lived transients. In general, this equation accounts for radiative processes (first term), fast heat release (second term), and slow heat release (third term). Some typical processes associated with the second term are vibrational relaxation and bond cleavage, while the third term accounts for phosphorescence or long lived transients.

$$E_{h\upsilon} = \Phi_f \cdot E_f + \alpha \cdot E_{h\upsilon} + \Phi_{st} \cdot E_{st}$$

Equation 2-1. Energy balance equation for PAC and PTM techniques.

2.2 History

The photoacoustic technique saw its origins with Alexander Bell's preliminary research with the telephone. His original report in 1880 described the detection of sound with a primitive selenium cell connected to a set of headphones. An audible acoustic wave could be detected after a gas sample sealed in a selenium cell was illuminated with a focused beam of sun light.[8] With refinement of the technique and further research, a year later he reported the frequency of an acoustic signal was proportional to the frequency of the absorbed light and the amplitude of the signal was also dependent on the amount of light absorbed by the sample.[9] These observations were limited to gases and not solids or solutions because the acoustic waves produced by the two latter media are several orders of magnitude smaller due to their smaller thermoelastic parameters (*vide infra*). Therefore, Bell was not able to observe any signals with his primitive microphone. It has only been with the advent of more sensitive detectors that acoustic signals in solids and solutions following irradiation can be measured.

The photothermal technique rapidly fell out of fashion due to limitations with detectors and excitation sources. It was not until the invention of the microphone that photoacoustic studies resurfaced, albeit not at the forefront of research. The technique was still outperformed by more sensitive and easier techniques such as ESR, UV-Vis, IR, fluorescence and phosphorescence spectroscopies. With more sensitive detectors, the technique regained popularity, but was confined to detecting long lived transients (~μs or longer) as the limiting factor was the irradiation light source or modulating frequency of choppers. The availability of lasers has re-opened the field of photothermal studies as this light source provides ultra-short energy pulses to generate metastable species and fast decays can then be subsequently monitored either by acoustic wave propagation or refractive index change .

2.3 Photothermal Methods

The purpose of this section is to provide a succinct presentation of the photothermal method available at the University of Ottawa. Only fundamental equations and concepts are given in order for a concise understanding of this technique and to contrast and compare to the photoacoustic method.

2.3.1 General description

The photothermal method is a self-calibrating method where a reference is not needed in order to extract kinetic and/or thermodynamic information. Like LFP, an short excitation pulse is required to induced a chemical reaction. The metastable species produced upon laser excitation can radiatively and nonradiatively decay dependent of the species produced. Radiationless decay produces localized heating within the irradiated area. The heated area then expands to the surrounding area causing a temperature gradient. The refractive index (n) of the medium is changed by dn/dT due to the local warming effect and subsequently causes a divergent thermal lens to form which is monitored by a continuous probe or reference beam.[10,11] The size of the probe beam increases due to the change in refractive index and subsequently causes a pronounced movement in the beam that is measured by a diode detector. The change is monitored as a plume formation, shown in Figure 2-2, where the amplitude of the resulting signal gives the energetics of the process and the kinetics are easily derived from the growth of the signal.

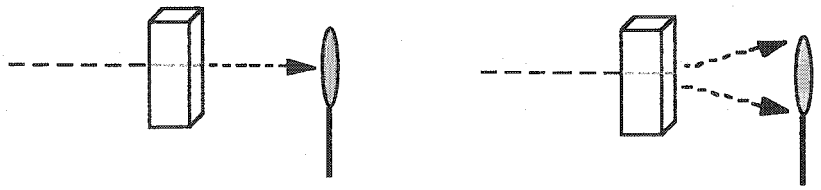

Figure 2-2. General representation of refractive index change resulting from heat deposition with photothermal methods.

The general Equation 2-2 represents the observed signal (U(t)) as being proportional to the probe beam after deflection (E(t)) and its undeflected value (E(t=0)).[11,12]

$$U(t) = \frac{E(t) - E(t=0)}{E(t)}$$

Equation 2-2. General equation for photothermal methods.

The observed signal is also dependent upon the change in refractive index (dn/dp), the amount of energy absorbed (E_{abs}), the fast heat deposit component (ϕ_1) and a slow heat deposit term, which is time dependent component (ϕ_2) shown in Equation 2-3.

$$U(t) \propto (dn/dp) \cdot E_{abs} \cdot \left(\phi_1 - \phi_2(t)\right)$$

Equation 2-3. Signal related to refractive index change with photothermal methods.

The signal measured during the course of one photothermal experiment gives rise to an initial jump followed by a slow growth as seen in Figure 2-3. The slow portion corresponds to ΔU while the difference between final and initial signal amplitude gives U_{total}. The ratio of these two values, according to Equation 2-4, gives the energetics of the process and the kinetics can be determined by fitting the slow portion, ΔU. The parameters in Equation are 2-4 are: Avogadro's number (N_A), Planck's constant (h), frequency of the excitation irradiation (ν_e), fluorescence frequency (ν_f), fraction of energy for the reaction studied ($\Phi\Delta E$). Therefore, the reaction pathway or deactivation pathways of the studied reaction must be accurately known to satisfy the unknown parameters.

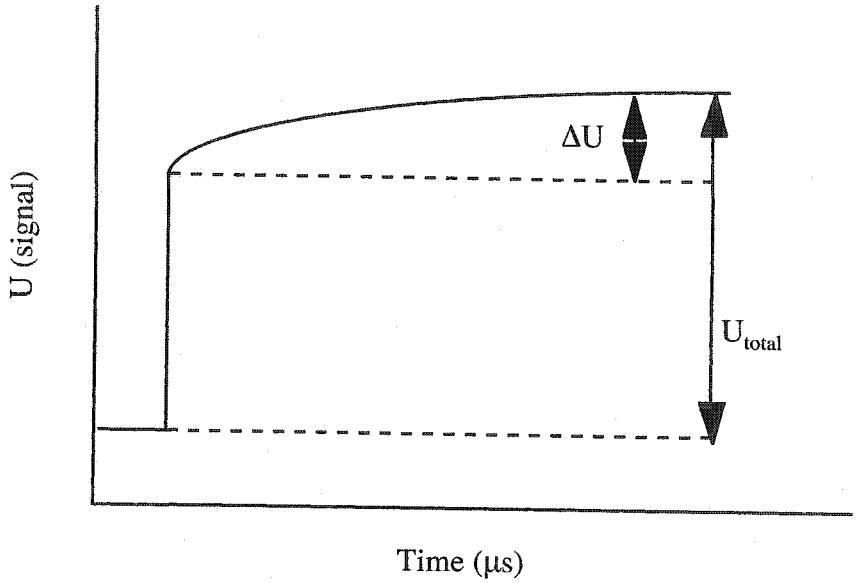

Figure 2-3. Typical signal observed from photothermal method.

$$\frac{\Delta U}{U_{total}} = \frac{\Phi E}{N_A h} \cdot \left(\upsilon_e - \Phi_f \nu_f \right)$$

Equation 2-4. General equation for extrapolating data from photothermal signal.

2.3.2 Different Photothermal Techniques

The orientation of the probe beam with regards to the sample cell leads to different methods. When the experimental set-up consists of a beam parallel to the pump (excitation) beam it is called time-resolved thermal lensing (TRTL). This detection results in a defocused probe beam that is monitored in the form of a blooming effect. Photothermal beam deflection (PDB) is also a coaxial arrangement, but the refractive index is measured by the amount the probe beam horizontally displaces. Only a fraction of the beam in monitored due to a slit placed between the sample holder and the detector. When the probe beam is placed perpendicular to the pump beam, the method is referred to as photothermal deflection (PTD).[13] The current set-up at the University of Ottawa is the TRTL method where the probe beam is a continuous wave from a helium-neon laser emitting at 632.8 nm. The general set-up is shown in Figure 2-4.

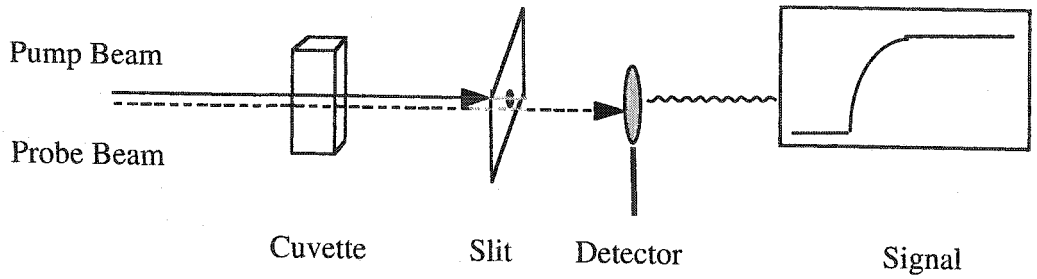

Figure 2-4. Schematic representation of TRTL method at the University of Ottawa.

2.3.3 General Experimental Set-up

This set-up requires perfect parallel alignment of the pump and probes beams through the sample. Also, the two beams must be relatively close to ensure the probe beam monitors the heat deposited within the irradiated area. It is important that the probe beam not be absorbed by any of the species present, including the ground state and metastable species. Because this method is extremely sensitive to beam position and shape, only the wavelengths emitted from the solid state lasers can be used as their shape and power are relatively homogenous compared to those of the excimer lasers available in our laboratory.[13,14]

2.3.4 Merits and Faults

There are many benefits to the photothermal techniques. The principal benefit is it is a self-calibrating technique and therefore does not require any references. This makes for easier studies since only one measurement is required with this technique. Since no reference is required, absolute values can be measured that normally require relative actinometry. This allows for the measurements of new fluorescence standards and dyes with high accuracy for subsequent relative actinometry work.

The major difficulty with the method in general is concerning the alignment of the system. The probe and pump beam must be aligned in parallel for greater sensitivity and accuracy. Any divergence from the parallel arrangement leads to local hot spots or the wrong area being probed.

2.4 Photoacoustic Calorimetry

2.4.1 General Description

Photoacoustic calorimetry (PAC) and laser induced optoacoustic calorimetry (LIOAC) are interchangeable terms used to describe the method that measures reaction energies by monitoring acoustic waves. This method is similar to the photothermal method as it detects the heat released following absorption of radiation. The heat deposited into the medium causes a local disturbance, as with PTM, but is in the form of an acoustic wave that propagates through the solution. The pressure wave is subsequently recorded when it contacts the cuvette walls by means of a high frequency piezoelectric detector. The amplitude of the recorded signal (S) is proportional to the amount of heat (H) deposited into the system by the reaction studied, the amount of energy absorbed (A) at the irradiation wavelength (E_{hv}), and a system specific parameter (k) as expressed in Equation 2-5. This is in agreement with Bell's original findings in 1881, including an additional component, α/C_p. The α parameter is related to the solvent's thermoelastic properties, which is its capacity to undergo compression and expansion. The C_p term is the solvent's heat capacity at constant pressure. These terms will be discussed in a following section and explain Bell's difficulty in detecting signals in liquid and solid media.

$$S = k\left(\frac{\alpha \cdot MW}{C_p}\right) \cdot H \cdot E_{hv}\left(1 - 10^{-A}\right)$$

Equation 2-5. PAC signal parameters.

Unlike the photothermal method, PAC is not a self-calibrated technique and therefore requires the use of a reference compound. This isolates the parameter k and correlates the signal amplitude with the amount of heat deposited into the medium. Typical choice references deposit all the excitation energy into the medium as heat within the response time of the detector, such as *o*-hydroxy benzophenone (OHBP). The ratio of the studied sample (S_{sample}) and reference ($S_{reference}$) signals is proportional to the observed reaction enthalpy (ΔH_{obs}) and the quantum yield for the reaction (Φ) as expressed in Equation 2-6. This requires measuring the reference and sample compounds under identical conditions including matched absorbances at the excitation wavelength.

$$\frac{S_{sample}}{S_{reference}} = 1 - \frac{\Phi \Delta H_{obs}}{E_{h\upsilon}}$$

Equation 2-6. Standard enthalpic PAC equation.

Normally the ratio required for Equation 2-6 is determined by measuring the two signal amplitudes as a function of laser power. This approach is graphically represented in Figure 2-5 where the ratio of the two slopes is the desired variable for Equation 2-6. Not only does this approach inherently reduce the error associated with the final calculated energy, but it also verifies whether the observed reaction is monophotonic. Monophotonic behavior is crucial for correct signal deconvolution and is assumed by a linear trend over the laser dose range. Many acoustic waves are acquired at each laser power and averaged to reduce the error since the final enthalpy calculated is extremely sensitive to all the variables including quantum yield, excitation wavelength, in addition to the PAC signals. For example, a 2 % error in the slope for a given system with an overall quantum yield of 0.7, excited with 248 nm leads to a 15 % variance in the final enthalpy calculated. Small quantum yields and large ratios tend to give larger errors, therefore all experimental errors must be minimized through repeated measurements.

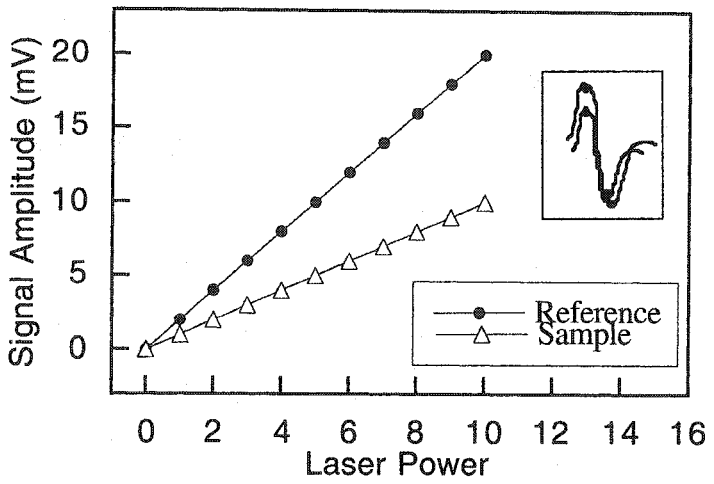

Figure 2-5. Typical plot for ratio determination for Equation 2-6. Inset: PAC signal of reference (•) and sample (Δ).

2.4.2 Molecular Volume Effects

In order for the acoustic wave to propagate through the medium and eventually be detected, a reorganization must occur.[15] In the absence of media no wave can be supported, which is the case in the vacuum of space. The reorganization leads to a volume change (ΔV_{th}) in the medium expressed by Equation 2-7. The volume change is proportional to the heat change per volume ($\Delta T(V)$), the molecular weight of the medium (MW), and its thermal compressive parameter (α). The developed right hand term accounts for the heat capacity of the medium at fixed pressure (C_p) and its density (ρ). These terms describe the medium's capability to absorb the heat deposited by an induced reaction, subsequently influencing the amplitude of the acoustic wave. Hence, the size of the observed optoacoustic signal is dependent on the solvent selected. For example, the observed signal will be larger with hexane than with acetonitrile (see Table 2-1).

$$\Delta V_{th} = \alpha \cdot MW \cdot \Delta T(V) = \frac{\alpha \cdot MW \cdot E_{h\upsilon}}{C_p \cdot \rho}$$

Equation 2-7. Solvent volume change for photoacoustic studies.

The thermoelastic parameters required for Equation 2-7 are readily found in literature such as Riddick et al.[16] Values are known for most typically used organic solvents where a few representative thermoelastic and solvent dependent values are found in Table 2-1. There are only slight differences between the organic solvent's physical properties, but these are generally smaller than those for gases by one or two orders of magnitude accounting for the larger signals observed with gases.

Table 2-1. Physical properties of some typical organic solvents at room temperature.[16,17]

Solvent	MW (g mol^{-1})	α (x 10^{3} K^{-1})	C_p (Cal mol^{-1} K^{-1})	ρ (g cm^{-3})	X_s (ml Kcal^{-1})
Hexane	87.18	1.391	46.72	0.655	3.912
Benzene	78.11	1.10	32.45	0.877	3.019
Acetonitrile	41.05	1.368	21.86	0.786	3.310
Dichloromethane	125.0	1.13	24.11	1.327	4.415
Methanol	32.04	1.09	19.47	0.791	2.268

For some solvents, the thermoelastic parameter (α) has not been measured, but can easily be calculated from Equation 1-8. It is proportional to the solvent's density (d) measured at two different temperatures (ΔT).

$$\alpha = \frac{\left(d_1 / d_2\right) - 1}{\Delta T}$$

Equation 2-8. Thermoelastic parameter determination required for PAC.

The volume change recorded in the acoustic signal in not entirely related to the solvent's dampening effect. It is also related to the volume change (ΔV_{rx}) associated with the chemical reaction studied.[18] Therefore, the volume change from reactant to product can be measured by the amount of heat deposited into the medium. The observed signal can now be represented as a linear combination of the two volume changes expressed in Equation 2-9.

$$S_{sample} = k'\left(\Delta V_{th} + \Delta V_{rx}\right)$$

Equation 2-9. PAC signal as a function of volume effects.

Substituting Equation 2-7 into 2-9 leads to the expanded form of Equation 2-10. Without the use of a reference it is nearly impossible to isolate the two volume

contributions from the calorimetric portion of the signal and in turn gives incorrect enthalpy calculations. Assuming the reaction volume change for the reference is negligible, the reference signal measured is proportional only to the volume change induced by the solvent. Taking the ratio of the sample and reference signals, similarly to Equation 2-6, leads to the new PAC Equation 2-11, which includes volume effects.

$$S_{sample} = k'\left(\frac{\alpha \cdot E_a \cdot MW}{C_p \cdot \rho} + \Delta V_r\right)$$

Equation 2-10. Expanded form of sample signal.

Equation 2-11 shows the ratio of the two signals is a linear combination of the enthalpic term (Θ) and the volume contributions. Through isolation of the volume contributions, the enthalpic portion of the observed reaction can be obtained. This is done by varying the solvent's contribution through the use of different solvents, in the case for organic solvents (*vide infra*), and also yields the reaction volume change as additional information. Some earlier PAC work neglected these volume contributions, and subsequently led to slightly lower enthalpy values than expected.[19,20]

$$\frac{S_{sample}}{S_{reference}} = \Theta + \left(\frac{\Delta V_{rx}}{E_a^{sample}}\right) \cdot \frac{C_p \cdot \rho}{\alpha \cdot MW}$$

Equation 2-11. Ratio of PAC signals used for isolating ΔV_{rx}.

Equation 2-12 is typically used in the literature to represent the thermoelastic properties of the solvent's volumes contribution. This in turn simplifies the standard PAC equations.

$$X_s = \frac{\alpha \cdot MW}{C_p \cdot \rho}$$

Equation 2-12. Simplified equation for thermoelastic properties required for volume effect determination in PAC measurements.

Substituting Equation 2-11 into the Equation 2-6 and using the identity from Equation 2-12 leads to the standard and most widely used PAC equation

represented below. The experimentally observed calorimetric value is linearly proportional to the true reaction enthalpy (ΔH_{rx}) and the reaction volume change (ΔV_{rx}). Through the use of a homologous solvent series, the influence of the solvent on the signal can be isolated. The thermal volume parameter can be isolated by varying the X_s parameter by repeating the PAC measurements in different organic solvents of the same family (i.e., linear alkanes). Monitoring the influence of the acoustic signal in different solvents leads to easy graphic extrapolation of the desired values according to Equation 2-13 and shown in Figure 2-6. The slope gives rise to the reaction volume change while the intercept gives the true reaction enthalpy. A positive slope denotes an overall expansion upon going from reagent to product. Conversely, a negative slope indicates the reaction has undergone a net contraction.

$$\Phi\Delta H_{obs} = \Phi\Delta H_{rx} + \frac{\Delta V_{rx}}{X_s}$$

Equation 2-13. Typical reduced PAC equation.

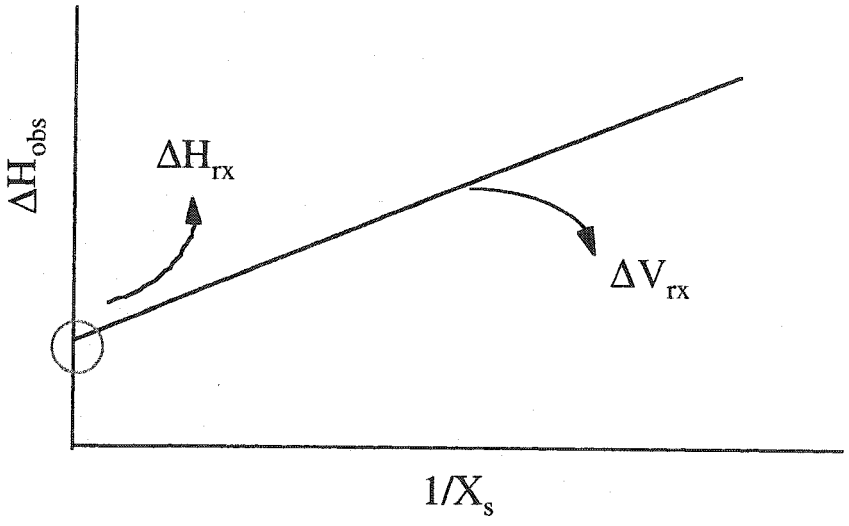

Figure 2-6. Graphical approach used for extrapolating ΔH_{rx} and ΔV_{rx}. The slope shown denotes a volume expansion.

The graphical approach shown in Figure 2-6 leads to ΔV_{rx} with relatively small uncertainties. However, ΔH_{rx} is associated with an extremely large error, as high as 100%, simply from extrapolating over a large range of $1/X_s$ values. Typical $1/X_s$ for homologous linear alkane series range from 0.25-0.7 kcal/ml with no

values in the range of 0-0.24 kcal/mol. Therefore an intercept leading to ΔH_{rx} must be extrapolated over a large range leading to an increased uncertainty. This shortcoming can mathematically be remedied by applying the approach introduced by Grabowski et al.[21] Equation 2-14 shows the new interpretation leading to ΔV_{rx} as the intercept at ΔH_{rx} as the slope. This method gives an increased linear correlation because the X_s parameter is multiplied on the left hand term. Regardless, the ΔH_{rx} is interpolated more accurately as it is derived from the slope and not the intercept.

$$X_s \cdot \Phi\Delta H_{obs} = X_s \cdot \Phi\Delta H_{rx} + \Delta V_{rx}$$

Equation 2-14. Grabowski approach to interpolating ΔH_{rx} for PAC studies.

Typically, a series of linear alkane solvents are used for extrapolating the volume effects as they provide a large range of X_s values. Pentane is normally the first point when using Equation 2-13 and increasing the chain size increases $1/X_s$. Therefore, the use of long *n*-alkanes is desirable in order to increase the $1/X_s$ range used for extrapolation the values used for Equations 2-13 and 2-14. However, there are a few problems that arise when using extremely long *n*-alkanes, specifically, increased viscosity and reduced reagent solubility. Recently, cyclic alkanes have also been examined as a potential new homologous series for PAC measurements.[22,23] Good signals and linear correlation with X_s were obtained, however the range is limited as shown in Table 2-2. The use of aromatic solvents as a new homologous series was also investigated and was found to give the anticipated values for the standard diphenylcyclopropenone system.[24] However, the limitation of these solvents is their small X_s range seen in Table 2-2.

Table 2-2. X_s values of cyclic alkanes and aromatic solvents.[16,17]

Solvent	α ($\times 10^3$ K^{-1})	ρ (kg m^{-3})	C_p (Cal g^{-1} K^{-1})	X_s (ml $Kcal^{-1}$)
c-Pentane				4.089
c-Hexane	1.220	0.774	37.29	3.499
cis-Decalin[25]	0.867	0.893	55.45	2.421
trans-Decalin[25]	0.865	0.866	54.61	2.529
Benzene	1.213	0.879	32.45	3.343
Toluene	1.067	0.862	37.59	3.033
o-Xylene	0.952	0.876	44.95	2.567
m-Xylene	0.981	0.860	43.84	2.762
p-Xylene	0.956	0.857	43.42	2.729

Unlike organic solvents, isolating volume contributions cannot be easily done through the use of a homologous series for aqueous studies. Goodman et al. originally took the approach of varying the X_s parameter through the use different solvent mixtures of acetonitrile/water.[26] His studies were done on the photodecomposition of diphenylcyclopropenone that has recently become the standard for PAC calibration and method validation. The results obtained from this approach led to a linear correlation, however the values extrapolated were different from those done in an organic homologous series.[21,27] PAC aqueous studies have subsequently been successfully refined by the research group at the Max-Planck-Institut für Strahlenchemie in Germany by taking advantage of water's temperature dependent properties. As seen in Table 2-3, the properties that lead to X_s show an immense dependence on temperature. Therefore, doing PAC measurements at various temperatures leads to the same effect as changing the solvent as with an organic homologous series. This in turn allows for relatively easy extrapolation of the desired enthalpic and volume terms.

However, the major assumption made for the aqueous approach is the reaction under study must be temperature independent.

Table 2-3. Thermoelastic properties of water at various temperatures.[16,17]

Temperature (°C)	α ($\times 10^3$ K^{-1})	ρ (kg m^{-3})	C_p (Cal g^{-1} K^{-1})	$1/X_s$ (Kcal ml^{-1})
0	-0.681	999.84	1.00738	-14.801
2	-0.327	999.94	1.00571	-30.726
4	0.000	999.98	1.0043	3719.5
6	0.031	999.94	1.00313	32.109
8	0.060	999.85	1.00213	16.586
10	0.088	999.70	1.00129	11.379
12	0.114	999.50	1.0006	8.7667
14	0.139	999.25	1.0002	7.1941
16	0.162	998.95	0.99955	6.1427
18	0.195	998.59	0.99914	5.1127
20	0.207	998.21	0.99883	4.8217
25	0.257	997.05	0.99828	3.8697

The advantage of PAC in aqueous media is the number of measurements required to extrapolate the desired information is significantly reduced. At 3.9 °C, the α value of water is zero and the observed acoustic signal is exclusive from ΔV_{rx}. Figure 2-7 shows the PAC signal for the reference and the signal from ΔV_{rx} for the sample recorded at 3.9 °C.

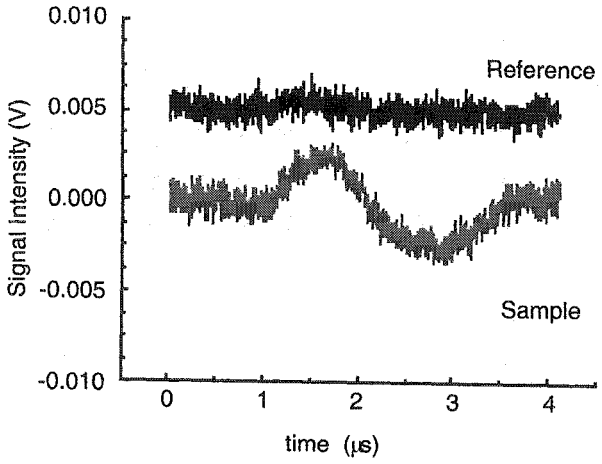

Figure 2-7. PAC signal from reference and sample in water at 3.9 °C.

Equation 2-11 must be modified when using the α=0 method to reflect the lack of signal arising from the solvent volume effect. Equation 2-15 incorporates this phenomenon and the fraction of heat deposited into the system (Θ) can be obtained by measuring the sample at two temperatures (3.9 °C and another) relative to that of the reference at one temperature.

$$\Theta = \frac{S_{sample}^{\alpha \neq 0} - S_{sample}^{\alpha = 0}}{S_{reference}^{\alpha \neq 0}}$$

Equation 2-15. Two temperature equation for aqueous PAC studies.

The reaction volume change can also be easily determined by the two temperature method according to Equation 2-16. This approach has been successfully applied for determining the enthalpic and volume changes for aqueous studied reactions.[22,28-31] However, in addition to assuming the studied reactions are temperature independent, the compressibility of the solvent at both temperatures is assumed to be identical.

$$\Delta V_{rx} = \left(\frac{S_{sample}^{\alpha = 0}}{S_{reference}^{\alpha \neq 0}} \right) \cdot \left(\frac{\beta}{C_p \rho} \right)_{\alpha \neq 0} \cdot \left(\frac{E_{h\upsilon}}{\Phi} \right)$$

Equation 2-16. Reaction volume change from the two temperature method in aqueous media.

Many of the processes leading to volume effects in PAC studies may also undergo a thermally reversible reaction. This provides a means of verifying the PAC data, as a wealth of data for thermal volume changes are available.[32]

2.4.3 Additional Volume Contributions

The ΔV_{rx} term previously discussed refers to all the volume changes occurring within the reaction. It can be further subdivided into the individual volume contributions arising from van der Waals effects (ΔV_{vdw}), electrostriction (ΔV_{el}), or solvent-solute interaction(ΔV_{ss}). The choice of solvent for PAC measurements can influence these volume contributions and measurements in several solvents can lead to the isolation of the individual volume contributions.[28,33]

$$\Delta V_{rx} = \Delta V_{vdw} + \Delta V_{el} + \Delta V_{ss}$$

Equation 2-17. Breakdown of contributions arising from reaction volumes in PAC.

2.4.4 Detectors

There are two general types of detectors used for PAC studies. They are a piezoelectric detector and a thin film detector. The most widely used piezoelectric detector is a lead-zirconate-titanate (PZT) because it is inexpensive with fast rise times and typically resonate with low frequency rates. It works much on the same principle as the needle used in traditional LP turn tables. It senses the pressure wave from the studied reaction and immediately translates this into a voltage that can be subsequently amplified and recorded. The response of these detectors is normally linear across the working window. This is a versatile detector that is readily used for calorimetric work, but cannot be used for time resolution. The detector begins to ring once activated by the primary wave. The trailing pressure waves required for time deconvolution cannot be resolved because they are masked by the dominant ringing from the primary wave.

Contrary to the piezoelectric PZT design, the thin film detectors can allow for mathematical deconvolution of the PAC signal to obtain kinetic in addition to calorimetric information. A dielectric polymeric disk, such as Teflon or β-polyvinylidene difluoride (PVF_2), 1 cm in diameter is used. It consists of

aluminum coating on both sides and is placed between the cuvette and detector. The two sides of the polymer act as charged poles and react differently when triggered by an acoustic wave. In short, the response is different than the PZT transducer. In essence, the film renders the detector nonringing and the pressure waves following the primary wave can be measured.[34] This additional information is crucial for kinetic deconvolution.

The advantage of the PVF_2 detector is the accessibility of deconvolution of kinetic information, but its sensitivity is considerably less than the PZT transducer.[35,36] Its sensitivity is 2-50 fold less than the PZT depending on the PVF_2 film selected.[24] Typically thinner films give the highest sensitivity. A choice must therefore be made whether kinetic information or sensitivity is required in order to select the best detector.

Currently there are two PZT based detectors available for acoustic studies in our laboratory being 1" in diameter from Panametrics. They have similar rise times,[37] but vary in resonant frequency between 0.5 MHz and 1 MHz.

2.4.5 Reference Compounds

The choice of a reference compound is important because the enthalpic and volume contributions of the reactions studied are dependent on it. Good references are compounds that strongly absorb at the irradiation wavelength and do not fluoresce. If they do, their yield of fluorescence must be known. They also must deliver all the absorbed heat back into the medium as prompt heat within the detector's time resolution, normally faster than the heat integration time of the reaction studied. The use of an external reference is standard, but internal references can also be used. However, their use complicates the data treatment and their specific interaction with the reagents must be exactly known.

For studies in organic media, the choice reference compound is *o*-hydroxy benzophenone (OHBP) as it absorbs readily at all the excitation wavelengths available in laser laboratories (248-370 nm). Upon excitation, its excited state is rapidly deactivated by intramolecular excited state proton transfer. Other acceptable references are laser dyes as they have high extinction coefficients. Ferrocene is yet another highly used standard for the 300-350 nm wavelength range. For studies at longer wavelengths, carotenes are regularly employed in the wavelength range of 400-800 nm.

PAC studies in aqueous medium are more problematic as good references must be pH and temperature independent. Some of the more popular laser dyes used as organic standards have limited solubility in water and tend to form undesired aggregates. However, because of their high absorbances, very little of the dye is required and they can be filtered to prevent aggregate formation. A few dyes currently used as reference compounds for aqueous studies are: bromocresol purple, bromocresol green, Evan's blue, and Evan's green.

2.4.6 Time Resolution

Valuable time dependent information leading to transient lifetimes and kinetics can be extrapolated from the PAC signal. The time dependent PAC signal (S(t)) can be expressed as a linear combination of the lifetimes (τ) and fractional heat deposited (ϕ) by the species produced as shown in Equation 2-18. The signal is then deconvoluted by mathematical treatment to resolve for the four unknowns; two fractional heat terms and two lifetimes for a two transient system. The sample equation shown refers to a two component system.

$$S(t) = \phi_1 \exp\left(-\frac{1}{\tau_1}\right) + \phi_2 \exp\left(-\frac{1}{\tau_2}\right)$$

Equation 2-18. Time resolution of PAC signal.

Melton and Caldwell have carried out substantial work concerning optimal cell design and mathematical treatment to extract the lifetimes and fractional heat components for reactions producing many transients.[33,38-41] Currently, a commercial software package has been released by Sound Analysis that deconvolutes the signal by a *quadratic-fit-convolution* to solve for a three or more component system.[42,43] The general equation to be solved for multi-component systems is merely a linear combination of the number of components and is an expansion of that represented by Equation 2-18. All these methods compare the reference and sample signals and then solve for a series of exponential decays. This gives a new simulated signal, which is then compared to the reference signal and the residuals analyzed. The number of components expected and the number of variables to fit can be selected to derive the correct answer. The accuracy of the simulated fit depends on the number of data points selected. For this reason, the PVF_2 detector is the choice detector for time-resolved PAC studies as the entire signal over the response frequency of the

detector can be monitored. PZT detectors are not suitable for kinetic studies because they begin to ring with the first wave and the secondary and trailing waves required for the fitting programs are lost. A typical wave form with reference, sample, and simulated signals is shown in Figure 2-8.

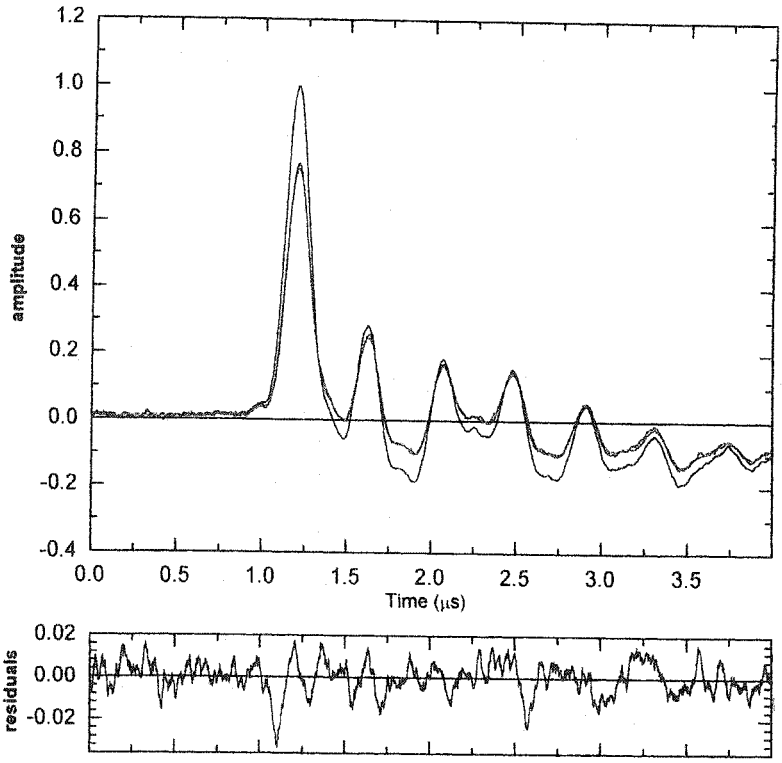

Figure 2-8. Typical PAC deconvolution signal fitted with the Sound Analysis program.[42] Top figure shows the reference signal (large), the sample signal (small), and the mathematically fitted signal. Lower figure shows the residual data between the calculated and experimental data.

2.4.7 General Experimental Set-up

Standard PAC experimental set-up consists of a sample holder (cuvette), transducer for signal detection, signal recorder, and a power meter. The set-up at the University of Ottawa has a traditional set-up with the incoming laser beam being split with a quartz plate. Part of the beam is measured using a diode detector, capable of monitoring all the laser wavelengths available in the laboratory. The output of the power meter is connected to Channel B of a Tectronix 2440 scope and the power measured is recorded once the system has

been triggered by the laser hitting a fiber optic cable. The remaining laser light is passed through a 1 mm pinhole prior to the sample holder in order to reduce the amount of light hitting the sample. Only a small amount of light is required to induce a detectable pressure wave without swamping the detector.[12] A standard quartz 10 x 10 mm fluorescence cell is used as the reaction vessel, which is placed on top of the transducer with a layer of silicon grease assuring good acoustic transference. A brass plate is mounted on top of the cell and tightened with four brass screws to secure the cell to the transducer and to heighten acoustic transference. The transducer is connected to a home-built amplifier for signal enhancement and then connected to Channel A of the scope without further filtering. The PAC set-up at the University of Ottawa is shown in Figure 2-9 and there experimental set-up is shown at the conclusion of this chapter.

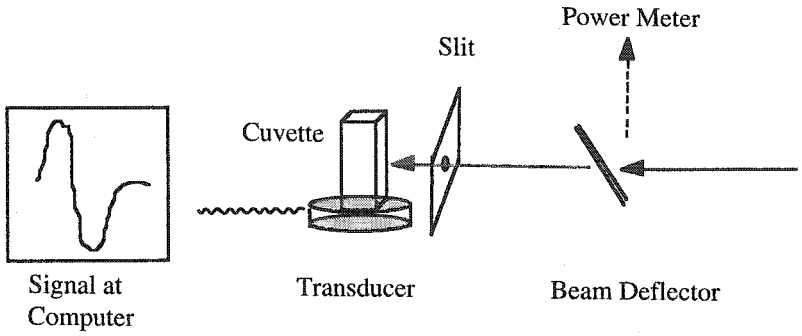

Figure 2-9. Schematic representation of PAC set-up at the University of Ottawa.

The signal acquired from both channels is digitized and the first 1024 data points are sent to a Mac computer after each laser pulse. At each laser power, the data are averaged and after complete acquisition, they are analyzed with an in-house program written in the LabVIEW environment. The program automatically searches for the maximum and minimum amplitude of the PAC signal from the transducer on Channel A and calculates the difference. The software then averages the 50 data points of the laser power on Channel B at the maximum found for Channel A. Both data sets (amplitude difference and average laser power) are automatically stored in a text file after each analysis for easy generation of power dependence plots of the type shown in Figure 2-5. A typical screen found in the LabVIEW environment for PAC analysis is represented in Figure 2-10 for *o*-hydroxybenzophenone in acetonitrile with the number of points on the axis and transducer response in millivolts on the abscise.

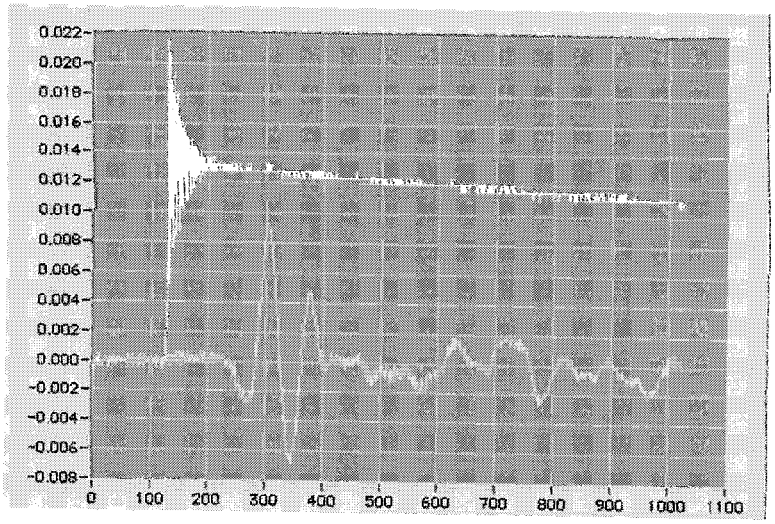

Figure 2-10. Window from LabVIEW environment showing laser power (top) and PAC wave signal (bottom).

This set-up is conducive to studying all organic reactions, but studies in aqueous medium cannot be done due to the lack of thermocontrol (*vide supra*). The major drawback to this cell-transducer arrangement is the laser beam must be aligned close to the bottom of the cell for a maximum signal to be produced. This results in the PAC signal overlapping with the laser trigger noise and leads to erroneous results. There is also potential for the laser beam reflecting off the cuvette bottom causing multiple waves that are difficult to deconvolute and also cause multiple heating. Moving the beam vertically (away from the cuvette bottom) reduces the signal intensity and eventually moves the signal outside the resolution window of the detector. Moving the laser beam horizontal also decreases the signal amplitude and causes a decrease in favorable wave symmetry. Placing the transducer in the same plane as the incident beam eliminates most of these problems and allows for the placement of a temperature controller for aqueous based studies. This is the design used in many laboratories that do PAC studies on a regular basis including the Max-Planck-Institut für Strahlenchemie. The schematic of this design is shown in Figure 2-11.

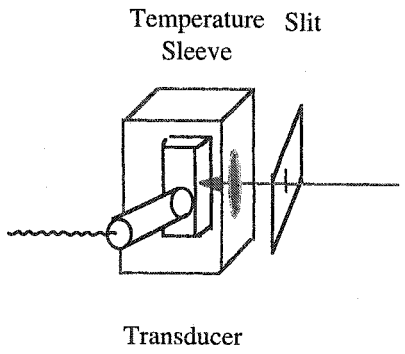

Figure 2-11. Coaxial detector set-up with temperature sleeve.

The coaxial detector approach is not without its disadvantages. However, the disadvantages are trivial compared to the perpendicular approach in Figure 2-9. In the coaxial arrangement, the detector must be securely supported at the free end to provide constant pressure between the detector and the cuvette. However, the cuvette is firmly anchored within the temperature sleeve and is more tolerable to disturbances, hence less effect on the parameter k (Equation 2-5) than with the perpendicular design. The cuvette can also be easily cleaned without risk of disturbing the system. A magnetic stirrer can also be placed under the cuvette for sample stirring between shots to ensure complete solution homogeneity and avoid product build-up.

Some experimental conditions that must be met to give reproducible and accurate results are summarized here. The sample must be thoroughly de-oxygenated as any residual oxygen can lead to erroneous charge-transfer effects being measured.[44] The absorbances of the reference and sample must be as closely matched as possible at the excitation wavelength. Normally they are matched within 2%. The exact same experimental conditions must be used when measuring the reference and sample, so extreme care must be used when exchanging samples and cleaning the cuvette.

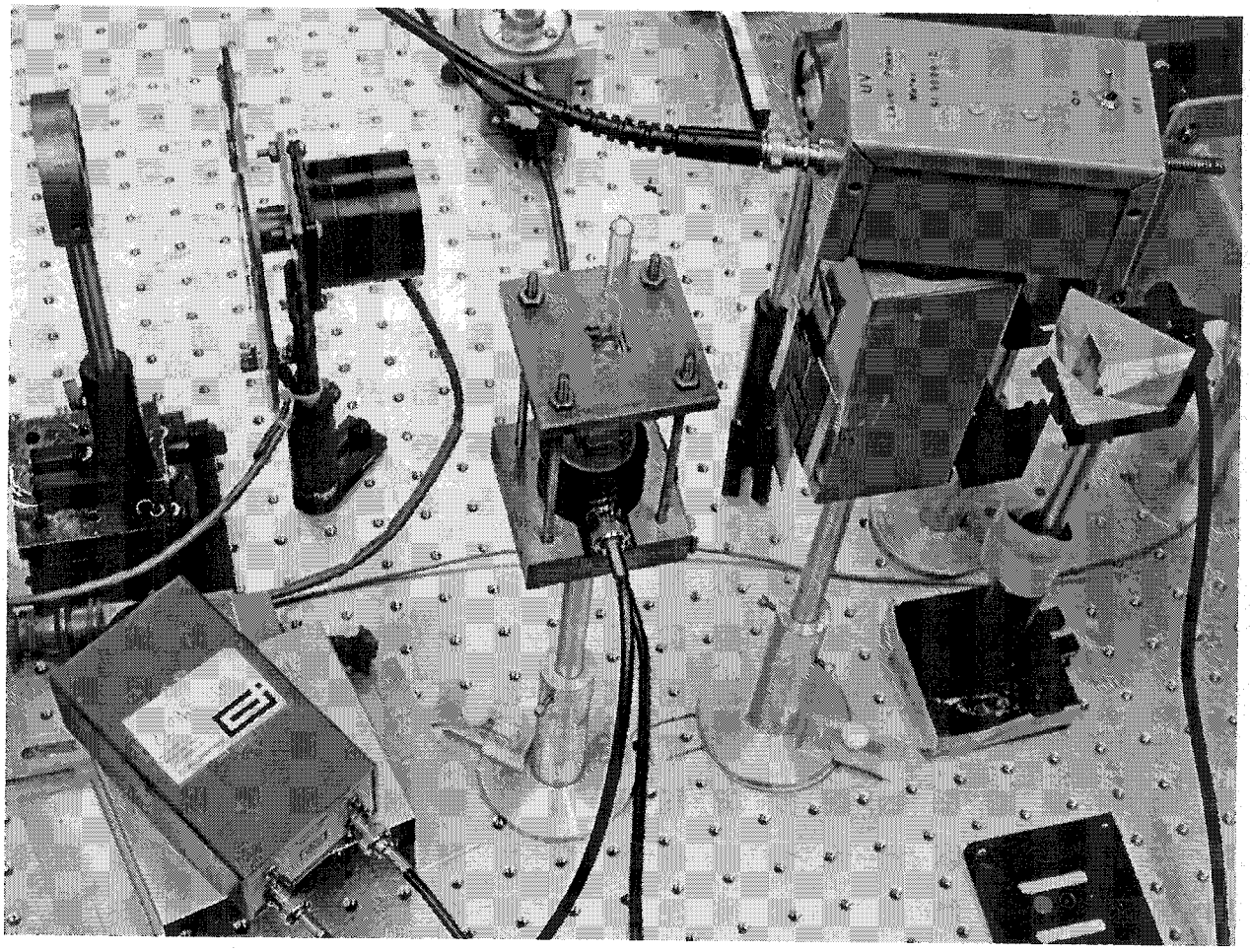

Figure 2-12. General experimental set-up for PAC studies at the University of Ottawa.

2.5 Chapter References

1. Berinstain, A. Development of Laser Techniques for Applications in Biomolecules and Cellular Systems, University of Ottawa, 1997.
2. Weldon, D. The Detection and Fate of Bromine Atoms and β-Bromo Radicals Generated Via the Photochemical Debromination of *Vicinal* Dibromides in Acetonitrile, University of Ottawa, 1998.
3. Porter, G.; Topp, M. R. *Proc. Roy. Soc., Ser. A* **1970**, *315*, 163-184.
4. Porter, G.; Tchir, M. F. *J. Chem. Soc., Chem. Comm.* **1970**, 1372-1373.
5. Lindqvist, L. *Hebd. Séances Acad. Sci., Ser. C* **1966**, *263*, 852-854.
6. Kosonocky, W. F.; Harrison, S. E.; Stander, R. *J. Chem. Phys.* **1965**, *43*, 831-833.
7. PAC can only resolve kinetics through complicated data deconvolution with a PVF_2 detector.
8. Bell, A. G. *Am. J. Sci.* **1880**, *20*, 305.
9. Bell, A. G. *Philos. Mag.* **1881**, *11*, 510.
10. Atkins, P. W. *Physical Chemistry*, 5th ed.; W.H. Freeman and Company: New York, 1994, pp 1031.
11. Braslavsky, S. E.; Heihoff, K. Photothermal methods. In *Handbook of Photochemistry*; Scaiano, J. C., Ed.; CRC Press, Inc.: Boca Raton, 1989; Vol. 1; 327-355.
12. Braslavsky, S. E.; Heibel, G. E. *Chem. Rev.* **1992**, *92*, 1381-1410.
13. Bailey, R. T.; Cruickshank, F. R. Thermal Lensing. In *Photoacoustic, Photothermal and Photochemical Processes in Gases*; Hess, P., Ed.; Springer-Verlag: New York, 1989; Vol. 46; 252.
14. The beam homogeneity is discussed in the following chapter.
15. Holbrow, C. H.; Lloyd, J. N.; Amato, J. C. *Modern Introductory Physics*; Springer: New York, 1999, pp 519.

16. Riddick, J. A.; Bunger, W. A.; Sakano, T. K. *Organic Solvents: Physical Properties and Methods of Purification*, 4th ed.; John Willey and Sons: New York, 1986; Vol. II, pp 1325.
17. Reichardt, C. *Chem. Rev.* **1994**, *94*, 2319-2358.
18. Callis, J. B.; Parson, W. W. *Biochim. Biophys. Acta* **1972**, *267*, 348.
19. Burkey, T. J.; Makewski, M.; Griller, D. *J. Am. Chem. Soc.* **1986**, *108*, 2218-2221.
20. Clark, K. B.; Griller, D. *Organometallics* **1991**, *10*, 746-750.
21. Hung, R. R.; Grabowski, J. J. *J. Am. Chem. Soc.* **1992**, *114*, 351-353.
22. Williams, R.; McDonagh, A. F.; Braslavsky, S. E. *Photochem. Photobiol.* **1998**, *68*, 433-437.
23. PAC measurements in different homologous series is also discussed in a following chapter.
24. Skene, W. G., Final report for PAC studies done at the Max-Planck-Institut für Strahlenchemie, Germany under the auspices of a DAAD scholarship.
25. Also known as decahydronaphthalene.
26. Herman, M. S.; Goodman, J. L. *J. Am. Chem. Soc.* **1989**, *111*, 1849-1854.
27. Schmidt, R.; Schütz, M. *Chem. Phys. Lett.* **1996**, *263*, 795-802.
28. Jiwan, J.-L. H.; Wegewijs, B.; Indelli, M. T.; Scandola, F.; Braslavsky, S. E. *Recl. Trav. Chim. Pays-Bas* **1995**, *114*, 542-548.
29. Malkin, S.; Churio, M. S.; Shochat, S.; Braslavsky, S. E. *J. Photochem. Photobiol. B.* **1994**, *23*, 79.
30. Yruela, I.; Churio, M. S.; Gensch, T.; Braslavsky, S. E. *J. Phys. Chem.* **1994**, *98*, 12789.
31. van Brederode, M. E.; Gensch, T.; Hoff, W. D.; Hellingwerf, K. J.; Braslavsky, S. E. *Biophys. J.* **1995**, *68*, 1101.
32. Asano, T.; Le Noble, W. J. *Chem. Rev.* **1978**, *78*, 407-489.

33. Schmidt, R.; Schütz, M. *J. Photochem. Photobiol. A: Chem.* **1997**, *103*, 39-44.

34. Kuo, C. Y.; Vieira, M. M. F.; Patel, C. K. N. *J. Appl. Phys.* **1984**, *55*, 3333-3336.

35. Berlincourt, D. A.; Curran, D. R.; Jaffe, H. Piezoelectric and Piezomagnetic Materials and Their Function in Transducers. In *Physical Acoustics, Principles and Methods*; Mason, W. P., Ed.; Academic Press: New York, 1964; Vol. 1A; 515.

36. Krautkrämer, J.; Krautkrämer, H. *Ultrasonic Testing of Materials*; Springer-Verlag: Berlin, 1983, .

37. Panametrics Inc. http://www.panametrics.com/ (10 November 1999).

38. Strickland, A. D.; Caldwell, R. A. *J. Phys. Chem.* **1993**, *97*, 13394-13402.

39. Arnaut, L. G.; Caldwell, R. A.; Elbert, J. E.; Melton, L. A. *Rev. Sci. Instrum.* **1992**, *63*, 5381-5389.

40. Peters, K. S.; Snyder, G. J. *Science* **1988**, *241*, 1053-1057.

41. Melton, L. A.; Ni, T.; Lu, Q. *Rev. Sci. Instrum.* **1989**, *60*, 3217-3223.

42. Quantum Northwest Inc. http://www.qnw.com/ (7 March 2000).

43. Small, J. R.; Libertini, L. J.; Small, E. W. *Biophys. Chem.* **1992**, *42*, 29-48.

44. Scaiano, J. C.; Martin, A. J.; Yap, G. P. A.; Ingold, K. U. *Org. Lett.* **2000**, *2*, 899-901.

3. Initiator Decomposition

3.1 Introduction

The introductory chapter has dealt with the different ways of obtaining living polymers by the so called living free radical polymerization (LFRP) process. This included the nitroxide mediated LFRP which is of great interest commercially since it is a viable method of achieving living polymers without the contamination of metals. Work in this field was originally spawned by the seminal findings of the Xerox group that successfully achieved narrow polydispersity and high molecular weights polymers from styrene in the presence of nitroxides.[1] Nitroxide mediated polymerization was originally conceived by the CSIRO group in Australia who patented the general concept in the early '80s.[2] Since these two original reports, there has been exhaustive research concerned with applied polymerization mediated by nitroxides.[3-10] Most of the published material deals primarily with commercialization of the process attempting to make it a more viable means of achieving living polymers relative to ionic methods. As a result, the amount of applied research has superseded that of fundamental study dealing with the mechanistic aspects of this process. The focus of this research originally dealt with examining the fundamental sequences involved in the LFRP process responsible for living polymers since little work was concerned with this area prior to the beginning of this project.[2-6,11,12]

The general scheme for the LFRP is represented in Scheme 3-1. The primary LFRP steps are similar to conventional free radical polymerization involving the initiation and propagation steps represented by Equations 1, 2, and 4 in the scheme. The major difference is the presence of free nitroxides during the polymerization which trap the propagating radicals. This in effect gives a dormant polymer, which at the polymerization temperatures, undergoes cleavage of the C-O bond to regenerate the propagating carbon centered radical. These reversible processes, shown in Equations 3 and 5, are responsible for controlling the polymerization and ultimately leading to narrow molecular weight distributions and high molecular weights when applied to styrene.[7,13-26] The success achieved with nitroxide mediated LFRP is principally attributed to the labile C-O bond. Prior to the work presented here, little experimental and conclusive research had examined the strength of the labile C-O bond.[27-31] Semi-empirical studies had only been performed as approximations for the bond dissociation energy (BDE) of this C-O bond crucial for the LFRP process.[32-34] The focus of this chapter examines the BDE of the important C-O bond through

thermal decomposition kinetics of a series of alkoxyamine initiators typically used for promoting the LFRP process (*vide infra*). In addition to the desired BDE value, the bond dissociation energies arising from N-O homolysis reactions and the energetics of disproportionation product formation have also been examined.

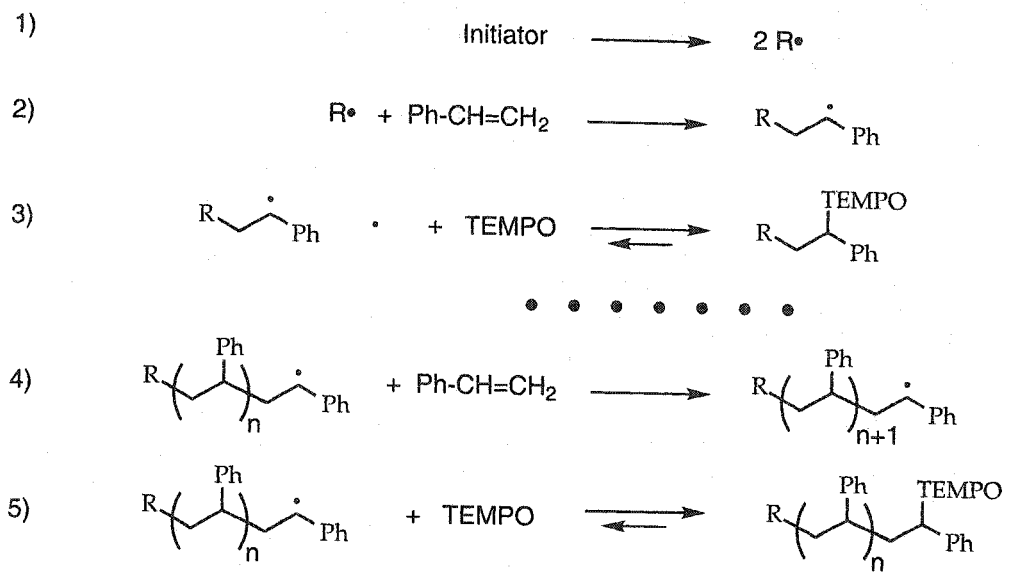

Scheme 3-1. General LFRP scheme as applied to styrene monomer.

3.2 Results and Discussion

Two general experimental methods have been used to obtain the desired energetic values. Each method is treated separately in its appropriate section since they are specific to the decomposition energy. The first method deals with the thermal decomposition of alkoxyamine initiators to determine the C-O BDE relevant to the LFRP. The other method is photoacoustic calorimetry (PAC) which calls upon the measured C-O BDE values to calculate the bond strength of the N-O homolysis reaction in addition to the energies leading to the formation of disproportionation products.

3.2.1 Thermal Studies

A limited number of reports have dealt with measuring the labile C-O bond energies important in the LFRP process where it undergoes reversible cleavage at the polymerization temperature. The reported decomposition values have primarily been measured using the techniques of ESR,[35-37] NMR,[38-41] HPLC,[28-31,42,43] and semi-empirical[32-34,44-47] calculations with values ranging from 19 to 42 kcal/mol. The large range of 13 kcal/mol for the reported values is not exact and a representative value for the labile C-O bond is of importance for understanding the LFRP process and for the design of better initiators.

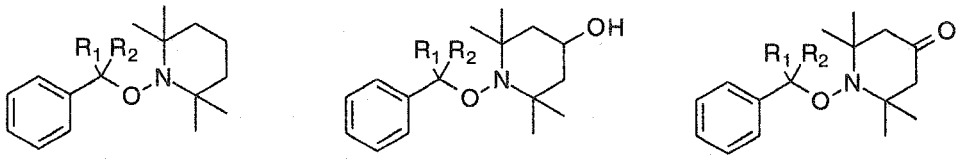

1a $R_1=R_2=H$
1b $R_1=H; R_2=CH_3$
1c $R_1=R_2=CH_3$

2a $R_1=R_2=H$
2b $R_1=H; R_2=CH_3$
2c $R_1=R_2=CH_3$

3a $R_1=R_2=H$
3b $R_1=H; R_2=CH_3$
3c $R_1=R_2=CH_3$

Figure 3-1. Specific types of LFRP alkoxyamine initiators investigated.

The method used for the current research was based on product analysis by HPLC arising from the thermal decomposition of various alkoxyamines. In general, this method is not dissimilar to the previously reported methods, but an external trap was used to prevent the back reaction from occurring (*vide infra*) validating the results presented here. These alkoxyamine initiators were used as they are good mimetics for the reaction occurring in the LFRP process. They

have successfully been used by this research group[48-51] and others[7,35,52,53] as probes for measuring the reaction kinetics and thermodynamics for the LFRP process. They are also commercially used for LFRP initiation because they are shelf-stable and easily synthesized. More importantly upon thermal decomposition, they afford stoichiometric amounts of nitroxide relative to the propagating radical crucial for the synthesis of polymers with living properties. The advantage of these unimolecular initiators for fundamental work is practical in nature. They are readily soluble in any solvent, are monodisperse, and are easily characterized by standard analytical techniques, unlike polymers, oligomers, or other analogues. The series of unimolecular initiators examined herein is represented in Figure 3-1. The initiators **1-3b** are the most relevant to the LFRP of styrene as they produce the identical propagating radical upon thermal decomposition as that for the polymerization of styrene.

The decomposition method selected for determining the BDE of the labile C-O bond was based on thermal decomposition of the alkoxyamines seen in Figure 3-1. In the absence of radical scavengers, the main pathway for the decomposition of these initiators is through the formation of disproportionation products shown in Scheme 3-2. Initiators **1-3c** cannot undergo this reaction because they do not posses the necessary α-hydrogens. In the presence of radical scavengers, such as monomers,[16] oxygen,[54] or other nitroxides,[49] decomposition of the alkoxyamines occurs with faster apparent rates, and gives other products, indicative of scavenging of carbon centered radicals, along with small amounts of disproportionation products.[38,49,54] The difference in behavior, particularly the relative thermal stability of alkoxyamines in the absence of scavengers, can be readily explained with the Fischer-Ingold persistent free radical effect which in this case favors cross combination of the radicals to regenerate the starting material.[35,55,56] Many of the previous decomposition studies have been done under reversible conditions where the radicals produced are not scavenged and subsequently undergo the reaction shown in Scheme 3-2. Under these conditions, the two radicals formed can also undergo the radical recombination or back reaction represented in Equation 6 of Scheme 3-3. This has the result of leading to erroneous results because both processes are known not to be iso-energetic (*vide infra*).[53,54,57,58] A prime example of erroneous values measured under reversible conditions is the work of Engel et al.[37] The BDE measured for the di-*tert*-butyl alkoxyamine (see structure in entry 1 of Table 3-2) was 34.3 kcal/mol which is too high since this initiator decomposes at room temperature. The BDE is anticipated to be less than **1c** as this initiator also decomposes at room

temperature, but at a slower rate. This is based upon qualitative observation by the amount of orange color produced from the free nitroxide formed on decomposition. The lower BDE value is also supported by the calculated value by the density function theory method (*vide infra*).

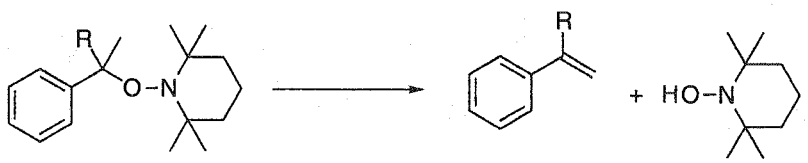

Scheme 3-2. General reaction leading to decomposition products.

The addition of scavengers prevents the back reaction from occurring and ultimately leads to accurate decomposition energies. This was the strategy adopted for a study of alkoxyamines. The addition of a nitroxide different from that produced upon thermal decomposition of the initiator was chosen. This has a two fold effect: suppression of the back reaction (Equation 6), and easy analytical quantification of the trapped product (Equation 7). Under irreversible conditions, analysis of the trapped product represents the decomposition kinetics of the alkoxyamine. The nitroxide experiment was run under conditions such that the concentration of the added nitroxide guarantees that ≥ 95 % of the carbon centered radicals produced were trapped exclusively via reaction 7. This was achieved by selecting the nitroxide concentration to be ≥ 20 times the rate constant of radical trapping between the carbon centered radical and the nitroxide measured in the following chapter, assuming the radical concentration upon thermal decomposition to be in the μM range.[53,57,59]

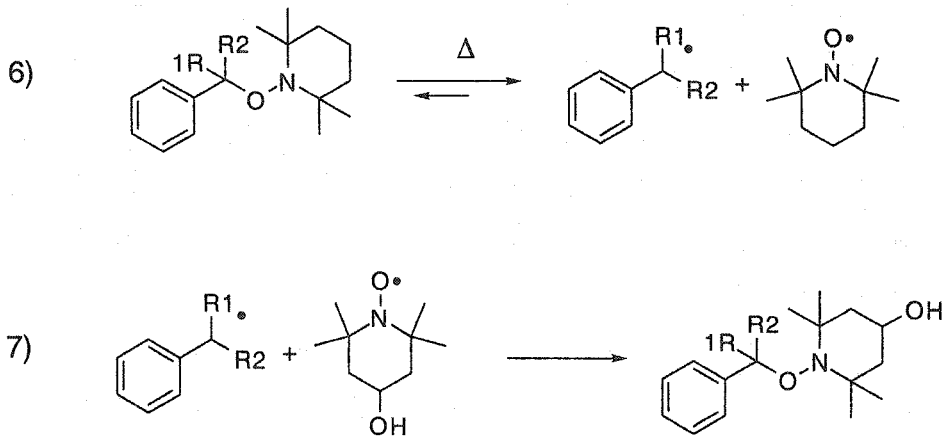

Scheme 3-3. Nitroxide exchange experiment preventing the back reaction upon thermal decomposition leading to N-O BDEs.

Monitoring the growth of the trapped product can easily be done through HPLC analysis. At relatively low conversions, this leads to the typical plot of the type shown in Figure 3-2 where the slope represents the rate constant at the given temperature. Measuring the decomposition kinetics over a series of temperatures leads in part to the desired C-O energetics. This is done through the Arrhenius equation represented by Equation 3-1. The parameter k in this equation represents the rate constant for a given temperature derived from the slopes of plots typical to those shown in Figure 3-2. The other parameters in this equation are the pre-exponential factor (log A) related to the structure of the transition state,[60,61] E_a is the activation energy required for C-O bond homolysis, R is the universal gas constant and T is the temperature. The two parameters (log A and E_a) are found by decomposition experiments at different temperatures. Measuring the rate constants over a series of temperatures leads to the desired value according to Equation 3-1.

$$\log k = \log A - 2.303 \cdot \frac{E_a}{RT}$$

Equation 3-1. Arrhenius equation used for obtaining thermodynamic information from kinetic measurements.

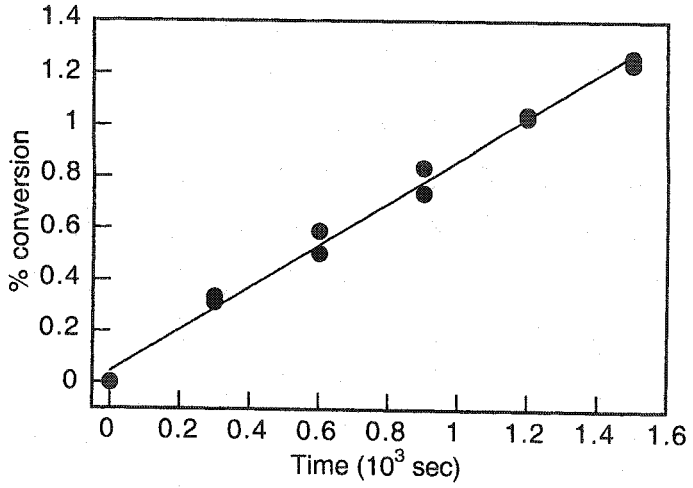

Figure 3-2. Product formation upon the thermal decomposition of 2a by the nitroxide exchange experiment at 155 °C.

Measuring the decomposition kinetics of the alkoxyamine initiators by monitoring the amount of trapped product gives the rate constant necessary for Equation 3-1. The trapped products in the case of initiators **1a** and **2a** are easily represented by Equation 7 (Scheme 3-3) and the rate constant can effortlessly be derived from the slope of plots similar to Figure 3-2. However, the initiators **1b-c** and **2b-c** give more than one product upon thermal decomposition. Preliminary results concerning this thermal decomposition were originally obtained by Peter Hahn, a fourth year honours student under the supervision of the author of this thesis. This preliminary work found that disproportionation products for the initiators **1b** and **1c** were formed during their thermal decomposition under the nitroxide exchange experiment. At the polymerization temperature, the amount of styrene and α-methyl styrene corresponding to the disproportionation products for **1b** and **1c** were found to be 2.8 % and 5 %, respectively. The formation of these disproportionation products must be accounted for and complicates determination of the rate constant. The total amount of the products formed from nitroxide exchange and disproportionation are taken to be equal to the total amount of initial alkoxyamine decomposition allowing for easy determination of the desired rate constant similar to **1b** and **1c**. The extinction coefficients of the trapped and disproportionation products are considerably different thereby requiring re-calibration for these differences in order to derive the correct rate constant.

The formation of disproportionation products implies a lack of controlled polymerization because the products formed are hydroxylamine and a vinyl terminated polymer or oligomer. This is of importance because the vinyl group formed can undergo polymerization in an uncontrolled fashion leading to polymers with broad molecular weight distributions. The amount of disproportionation products formed for **1b** suggest 1 in approximately 30 polymer chains undergoes the reaction leading to disproportionation products. If this was a dominant process during the LFRP process, polymers with high polydispersities should be observed. Also, the polymer terminus should be free of any nitroxide cap due to chain transfer. However from the number of successful LFRP polymerization reports for styrene, the formation of disproportion products must not be present during the polymerization reaction.[14,16,21,28-31,41,57,62-78] The origins of these disproportionation products are fully investigated and discussed in a following chapter and a new initiator is proposed.

The desired activation energy required for homolytic cleavage of the labile C-O bond can be determined by measuring the decomposition kinetics over a series of temperatures. The plots shown in Figure 3-3 represent such a study for the alkoxyamines from Figure 3-1 as derived from Equation 3-1. The slope obtained from these plots leads to the activation energies (E_a) required for the homolytic C-O bond cleavage, while the intercepts lead to the pre-exponential factors (log A). The values derived from the plots shown in Figure 3-3 for the four alkoxyamine initiators studied are summarized in Table 3-1.

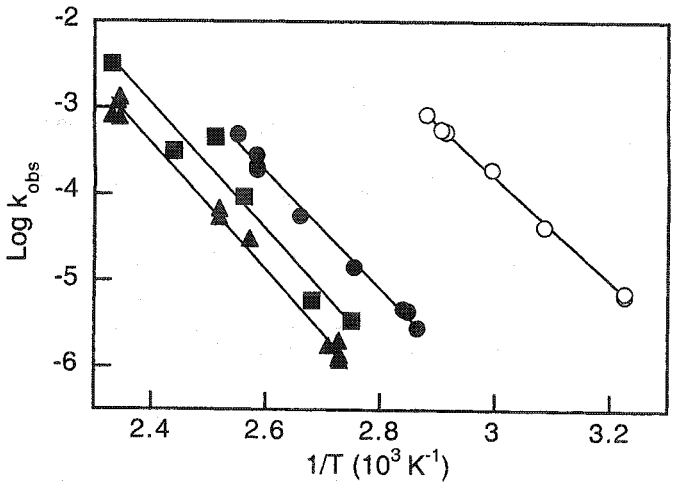

Figure 3-3. Arrhenius plots from the thermal decomposition of LFRP initiators 1a (▲), 1b (●), 1c (○), and 2a (■). Each point in the plot is based upon at least 2 averages of the corresponding data shown in Figure 3-2.

The values of the pre-exponential factors measured are of the same order of magnitude and are consistent with homolytic bond cleavage processes for similar reactions.[61] The transition states for the thermal decomposition of these initiators lies close to the products as implied by the high frequency factor. Also, a transition state with many degrees of freedom and a high entropy gain is implied by the large pre-exponential value. The other parameter derived from Figure 3-3 and Equation 3-1 is the activation energy. These measured values are indicative of the strength of the C-O bond, but are not the desired BDE values. This is because the activation energy for the back reaction of Equation 6 (Scheme 3-3) is not zero and must be known to calculate the BDE.[52,53,57] The desired BDE values are the difference between the activation energies for the forward (decomposition) and the back reaction (recombination) of Equation 6. The recombination of the nitroxide and the carbon centered radicals must also overcome an energy barrier as illustrated in Figure 3-4. The activation energy for this reaction is not included in the thermolysis measurements, but can be calculated. The value is easily calculated for similar reactions of similar structures and falls in the area of 2 kcal/mol.[52,53,57] The desired BDEs calculated including the activation energies for the recombination reaction are reported in Table 3-1.

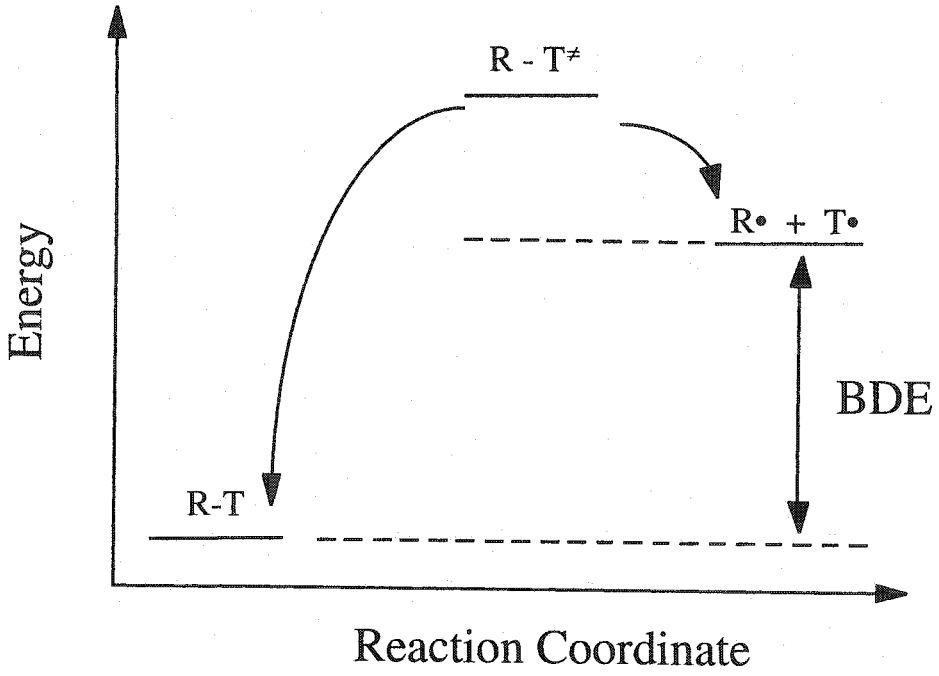

Figure 3-4. Schematic representation for bond dissociation energy (BDE) calculation.

Table 3-1. Values derived from the thermolysis reaction involving the nitroxide exchange experiment according to the Arrhenius equation.

Initiator	E_a (kcal mol^{-1})	log A (s^{-1})	E_a (reverse) (kcal mol^{-1})	BDE[a] (kcal mol^{-1})	τ[b] (s) at 398 K	T range (K)
1a	32.6[c]	13.6[d]	1.8[e]	30.8	16 100	366-427
1b	30.7[f]	13.7[g]	2.3[h]	28.4	1500	348-393
1c	27.2[i]	14.0	2.6[h]	24.6	7	308-348
2a	33.2	13.6	1.8[e]	31.4	34 500	363-428

a) BDE refers to bond dissociation energy.
b) Lifetime in seconds calculated as 1/k where k denotes the rate constant obtained from the plots similar to those of Figure 3-2.
c) A value of 23.4 kcal/mol has been reported.[47]
d) A value of 11.9 has been reported.[47]
e) Value derived from literature.[52,57]
f) Values of 24.2,[38] 28.4,[38] 29.7,[31] 31.1,[36,65,79] 29.7,[28,30] 36.7,[28,30] 19.0,[69] 27.0[69] kcal/mol have also been reported.
g) Other reported values are 13.5,[31] 13.3,[28,30] and 14.8.[28,30]
h) Value derived from literature.[53]
i) A value of ~ 25 kcal/mol has also been determined.[35]

The BDE values shown in this table illustrate the influence of radical structures upon the C-O bond stability and are consistent with benzylic radicals. The previously reported BDEs for similar compounds are also given in this table for comparison. Increasing substitution at the benzylic center with methyl groups decreases the bond strength as the radical center generated is stabilized.[52,53,57] The influence of the radical structure is also confirmed by the calculated BDEs reported in Table 3-2. Even though semi-empirical methods are not parameterized for nitroxides or open shelled species, their errors are systematic and relative trends can be accurately predicted.[33,80-90] The theoretical density function theory method (DFT) yields relatively accurate heats of formation and

the reported values and trends are consistent with the semi-empirical calculated values.[91-93] Conversely to the carbon centered radical structure, the nitroxide structure has no influence on the decomposition kinetics as the value for **1a** and **2a** are essentially identical. The lack of influence of the nitroxide structure upon the C-O bond strength is also supported by the calculations presented in this table. Recently, it was shown that electronic effects from substitution only in the 2 and 6 positions of the nitroxide are able to influence the C-O bond strength.[35,45,70,94-99] Electron withdrawing groups stabilize the bond while electron donating groups destabilize it ultimately decreasing the BDE of the C-O bond.[34]

Even though the reported BDEs in Table 3-1 suggest **1c** would be a better initiator because of its weak C-O bond, its lifetime is too short for the polymerization of styrene. It would rapidly decompose leading to fast polymer initiation without much nitroxide control. The initiators **1a** and **2a** have high BDEs leading to their slow decomposition at the polymerization temperature where the polymer chains would be initiated at different times. Their lifetimes are also too long to be useful for the initiation of styrene and would lead to polymers without any living properties. Alkoxyamine **1c** would be a more useful initiator for monomers whose polymerization can be carried out at lower temperatures. At lower temperatures, the C-O bond could still be cleaved and its lifetime may be suitable for the living polymerization of acrylates.

The BDE values measured represent the first study concerned with the irreversible decomposition of alkoxyamines. All other reports were done under reversible conditions and neglected the energetics association with the build-up of nitroxides under these conditions (*vide supra*). Fischer et al. kinetically took this build-up into account through the use of complicated mathematics involving a $t^{1/3}$ rate law. Their measured BDE value of 27 kcal/mol for **1c** does not account for the back reaction and as a result is consistent with the E_a measured here.[35] The HPLC method presented here is an attractive choice because it is relatively simple and does not require complicated kinetic studies to arrive at the correct answer, which others have not successfully done. The value measured in this study under irreversible conditions is also identical to Fukuda et al. who determined their value using nitroxide capped polymers with M_w=1700 and PD=1.2.[30,31] Their study was done under typical LFRP conditions and the similarity of the results validates our method for measuring the BDE using unimolecular initiators as probes for the LFRP process. Therefore, the

thermal decomposition of alkoxyamine probes under nitroxide exchange conditions is representative of the kinetics and thermodynamics occurring during the LFRP process. This is further supported by the calculated values in Table 3-2 which are similar in value and represent the same trend for the experimentally measured BDEs. More recently, reports have appeared in the literature confirming the thermolysis results presented here.[42,43,100,101]

From the measured BDE of **1b** and the rate constant measured in the following chapter, the equilibrium constant for Equation 6 (Scheme 3-3) is calculated to be 1.4×10^{-11} M^{-1} at 125 °C. This value is similar to that found by Fukuda et al. for their study involving nitroxide capped polymers. The small value indicates the equilibrium is shifted to the side of nitroxide capped polymers where very few propagating radicals are produced. Most of the polymer chains are dormant at the polymerization temperature where any uncapped chains add to the monomer and are rapidly capped by nitroxide leading to controlled polymer growth.

Table 3-2. Reported calculated BDE[a] of benzylic-based alkoxyamines containing various nitroxide structures.

Alkoxyamine	ΔH_{rx} (kcal mol^{-1}) AM1[b]	ΔH_{rx} (kcal mol^{-1}) PM3[b]	ΔH_{rx} (kcal mol^{-1}) DFT[c]
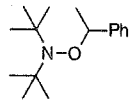	-	-	22.2
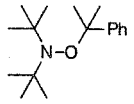	-	-	18.8
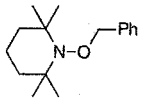	-	-	29.0
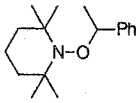	22.0 (23.2[c])	26.0	26.3
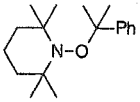	-	-	21.3
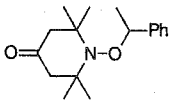	19.0	24.0	-
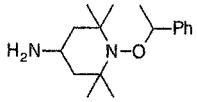	22.0	26.0	-
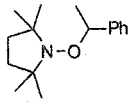	23.2[c]	-	
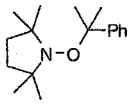	14.5[c]	-	-
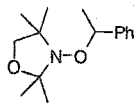	17.0	19.0	-

a) Refers to the bond dissociation energy calculated from the reaction enthalpy (ΔH_{rx}) derived from the individual heats of formations (ΔH_f) for the reagents and products.
b) Values taken from literature.[32]
c) Values taken from literature.[34]
d) Refers to Density Function Theory[91,92] where values were taken from literature.[45]

3.2.1.1 Thermal Study Conclusion

The decomposition energy study is relevant to the LFRP process as it provides exact BDE values for the labile C-O bond previously measured under reversible conditions. The value is relatively weak compared to a normal C-C bond and confirms the measured bond cleavage at the polymerization temperatures. The results obtained show that the BDE is influenced by the stability of the carbon centered radical produced upon thermal decomposition and is lower when a more stable carbon centered radical is produced. Furthermore, the C-O BDE can be tuned to a specific value by careful selection of the appropriate carbon centered radical produced upon thermal decomposition. The C-O BDE for acrylate systems is expected to be higher than for styrene systems as the radical generated is less stable than its styrene analogue.

3.2.2 Photoacoustic Calorimetry Studies

Photoacoustic calorimetry (PAC) measurements were done with the unimolecular initiators to determine the reaction enthalpies of photodecomposition. This method of analysis is extremely sensitive to all reaction processes, providing they occur within the time response of the transducer. This sensitive technique cannot selectively isolate the individual contributions for each process from the overall acoustic signal. As a result, the exact nature and pathways of the photochemical processes encountered after excitation must be known. This was the problem with the original studies concerning these initiators, because the C-O cleavage was believed to be the sole decomposition pathway. In fact, the apparent C-O BDE measured for these unimolecular initiators in this preliminary PAC study were greater than those found in Table 3-1 because the photodecomposition pathway is more complicated than simple C-O bond fragmentation (*vide infra*).

The general equation used for PAC data analysis is found in Equation 3-2 and relates the observed PAC signal ratio (α) of the sample and reference to the excitation wavelength ($E_{h\nu}$), the enthalpy of the overall reaction studied (ΔH_{obs}), and its photochemical efficiency (Φ). The origins of the necessary equations and full description of the PAC theory is covered in the experimental section in a preceding chapter. Only the value of α is derived from the PAC measurements and either the quantum yield or the enthalpy of the studied reaction must be

known in order to solve this equation. Since the initiator decomposition energetics are the desired values, the quantum yields for this reaction must be independently known. However, these values had not been previously measured and therefore had to be established before any thermodynamic information could be extrapolated from the PAC data.

$$\frac{\Phi \Delta H_{obs}}{E_{h\nu}} = (1 - \alpha_{obs})$$

Equation 3-2. General PAC equation for determining the enthalpy of the desired reaction.

3.2.2.1 Quantum Yield Determination

Studies involving the quantum yields of photodecomposition are required since these values are unknown. This can be obtained by relative actinometry which compares the product concentration formed upon decomposition of the desired compound relative to a material that undergoes a known yield of decomposition for a given light intensity. The reference compound is referred to as an actinometer. Steady state irradiations involving actinometers are quite common, but involve analytical methods requiring concentrations to be known and are typically more laborious than other methods.[102] This approach also leads to errors in the quantum yield arising from analysis and compounds the error already associated with the actinometers.[103] The method of choice selected for the quantum yield determination was transient actinometry. This method involves comparing the maximum transient absorbance of the transient under study relative to the actinometer over a range of laser dosages. Dibenzyl type ketones such as those shown in Figure 3-5 were used as actinometers because their photodecomposition leads to transients visible by the LFP instrument identical to those produced upon decomposition of the LFRP initiators. This eliminates the need to know the transient's extinction coefficients, thereby reducing the uncertainties of the measured values (*vide infra*).

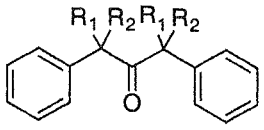

4a $R_1=R_2=H$
4b $R_1=CH_3$; $R_2=H$
4c $R_1=R_2=CH_3$

Figure 3-5. Structures of substituted dibenzyl ketones used as actinometers for carbon centered radicals by LFP.

Upon irradiation, dibenzyl ketone (**4a**) and its substituted analogues (**4b-c**) are known to undergo homolytic α-cleavage (Norrish type I) with relatively high efficiencies followed by an equally efficient release of carbon monoxide.[104,105] The first step occurs almost instantaneously after n,π* excitation and the subsequent loss of CO occurs quite fast (< 10 ns) for **4b-c**, but is slower for **4a**.[105] The general scheme as applied to **4b** is represented by Equation 8 in Scheme 3-4 where the generated carbon centered radical is detectable at ca. 318 nm on the LFP system.

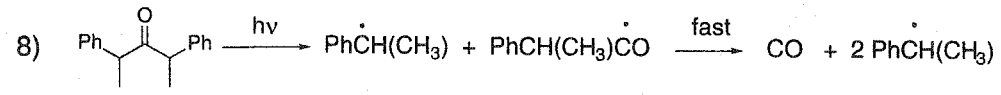

4b

Scheme 3-4. Photodecomposition of actinometer 4b to give 2 1-phenylethyl radicals and carbon monoxide as products.

The quantum yields of **4a** and **4b** are known at excitation wavelengths and solvents different from those used for the PAC studies. Since some photochemical processes are known to be wavelength[102,106] and solvent[107] dependent, the quantum yields of these actinometers were examined at 254 nm in cyclohexane. This was done to match the experimental conditions used in the PAC measurements (*vide infra*) since this method is known to be extremely sensitive and dependent on the solvent as well as the data subsequently used to deconvolute the PAC measurements.[108,109] Therefore, every precaution was taken to ensure identical experimental conditions including the actinometer quantum yield measurements in cyclohexane used for the PAC studies. This was done by comparing the appearance of bibenzyl by GC and NMR after the irradiation of **4a** at 300 nm in cyclohexane to that in benzene. The quantum

yield in the two solvents were slightly different to the previously reported values.[110,111] The measurements were done in cyclohexane to ensure an accurate value was found for subsequent transient absorption actinometry.

The actinometer of choice for steady state irradiation was valerophenone (**5**). Upon irradiation, the ketone is excited to its singlet state and intersystem crosses to the triplet state. From its n,π* triplet state, valerophenone undergoes the Norrish type II process.[112,113] This involves hydrogen abstraction by the excited ketone at the γ-position leading to a 1,4-biradical. This intermediate subsequently either undergoes cyclization affording the cyclobutane **6a** or decomposes leading to vinyl products. The 1,2-allylic alcohol formed further rearranges to give acetophenone (**6b**) as the predominant product, which can easily be identified and quantified by HPLC analytical methods because it is less volatile. The quantum yield of **6b** produced upon photodecomposition of valerophenone at 313 nm has been measured to be 0.4 and is sensitive to solvent polarity.[107,112] It is assumed that the measured value does not vary with irradiation wavelength allowing for its use as a steady state actinometer for the studies discussed here.

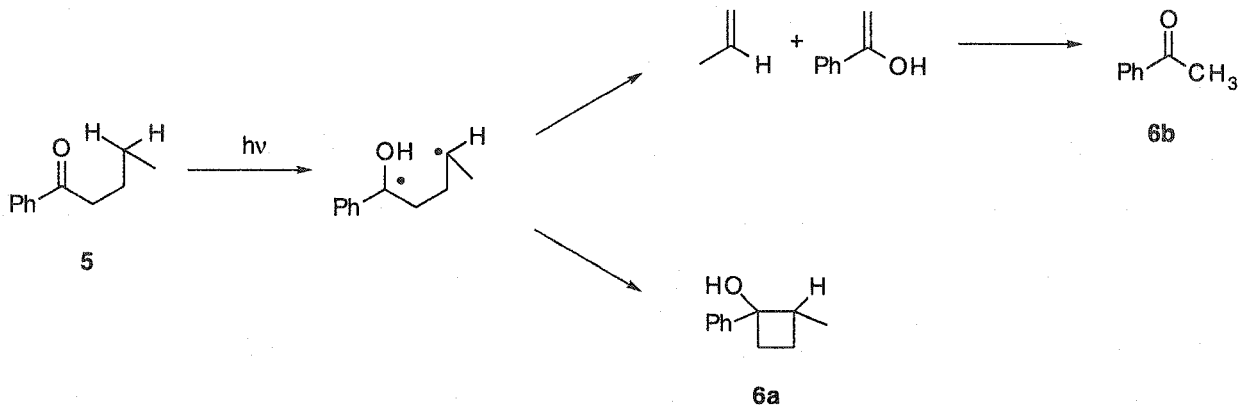

Scheme 3-5. Photodecomposition of valerophenone (5) to acetophenone (6b).

The quantum yield for **4c** is unknown and was consequently measured by steady state irradiation at 254 nm in cyclohexane to match the experimental PAC conditions. This value was determined by product formation upon photodecomposition according to Equation 9 represented in Scheme 3-6. The concentrations were subsequently compared to the amount of type II cleavage from the actinometer, valerophenone, at identical irradiation wavelengths. HPLC and NMR analytic methods were used to measure the products arising

from carbon centered radical recombination (~ 90 %) and disproportionation. Only minor disproportionation products were observed and the analytical techniques used did not detect any aldehyde product, which was previously reported in small amounts.[114] The quantum yields of the other ketones, summarized in Table 3-3, were also measured under identical conditions at low conversions and compared to **4c**. These values have not previously been reported for irradiation at 254 nm or in cyclohexane. The previously unmeasured values at 254 nm in cyclohexane are similar to those previously measured being relatively close to unity, but consistently lower for **4b** as found in Table 3-3. Reasons for change in any of the excited states leading to the observed lower quantum yield for this compound is still elusive.[104,105,111,115-118]

9) 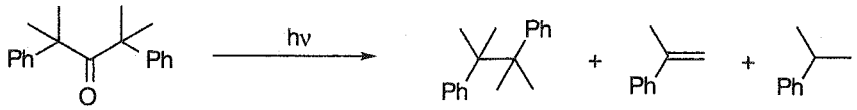

4c **5c**

Scheme 3-6. Photodecomposition products of substituted dibenzylketone actinometer 4c.

Table 3-3. Quantum yields of product formation for substituted dibenzyl ketones determined by GC.

Ketone	Φ^a	Φ^b
4a	0.93[c]	0.87[d]
4b	0.56[c]	0.62[e]
4c	0.70[f]	-

a) Irradiated at 254 nm in cyclohexane.
b) Values taken from literature irradiated at 313 nm.
c) Value determined relative to **4c**.
d) Literature value in benzene.[104,111]
e) Literature value in pentane.[114]
f) Value determined relative to valerophenone actinometer in cyclohexane, Φ=0.4.[107,119,120]

The quantum yield measured for the ketone actinometers were subsequently used to determine the quantum yield of formation of the carbon centered radicals arising from photodecomposition of the LFRP initiators (**4a-b** and **2a-c**) by relative transient actinometry. In brief, this method involves comparing the top absorbance of the generated carbon centered radicals from the sample relative to the reference as a function of laser power. A typical plot generated from this type of study is shown in Figure 3-6 where the linear trend indicates simple monophotonic chemistry. An upward curvature denotes multiphotonic processes while a quadratic function implies a saturation effect. Since the transient observed for the actinometer and initiator are identical, there is no need for their extinction coefficients (ε) to be known. This has the added advantage of giving calculated yields with higher certainty since ε values typically change with solvent and reported literature values vary extensively for the same transients.[121,122] The quantum yield can then be easily calculated according to Equation 3-3 inherently giving more accurate results as it does not rely on knowing the value of ε. The factor of two in this equation accounts for the production of two benzylic type radicals upon decomposition of the

actinometer, $\Phi_{actinometer}$ represents the quantum yield of the actinometer, and $Slope_x$ represents the slope derived from Figure 3-6.

The initiator quantum yields calculated according to Equation 3-3 for the generation of carbon centered radicals are found in Table 3-7. The quantum yield values appear to be consistently lower for the 4-hydroxy-TEMPO based initiators regardless of the nature of the carbon radical generated. Any trend implied by the measured values is most likely due to coincidence and experimental error and not due to difference in the polarity of the generated nitroxide, even though these radical trapping reactions with nitroxides are known to be slower in polar solvents.[57] There is a large uncertainty associated with the measured quantum yields for **1c** and **2c** as the power dependence plots showed a quadratic trend over the laser powers measured and are inconsistent with the values measured by steady state irradiation. Also, only a small region of linearity was observed leading to the improbable value of $\Phi > 1$. These skewed values are also probably from the formation of a high fraction of disproportionation products (*vide infra*). For this reason, the quantum yields measured by steady state irradiation for this initiator were exclusively chosen for the calculations involving the PAC data.

$$\Phi_{initiator} = 2 \cdot \frac{Slope_{initiator} \cdot \Phi_{actinometer}}{Slope_{actinometer}}$$

Equation 3-3. Quantum yield determination of LFRP initiators using ketones 4a-c.

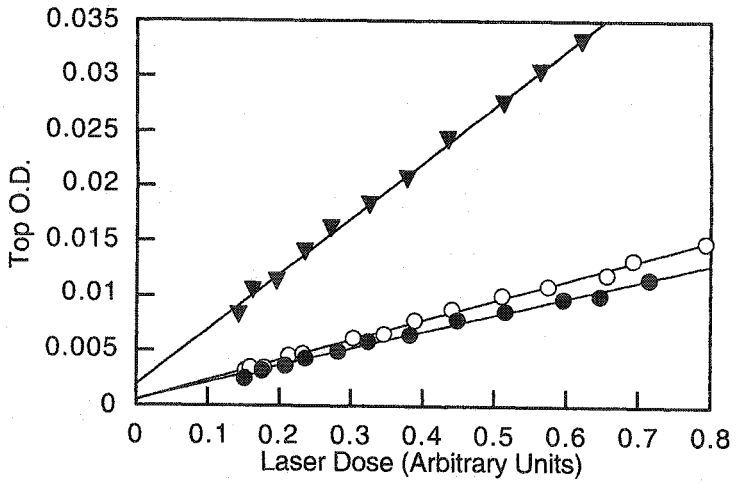

Figure 3-6. Relative transient actinometry for benzylic radical generation for 1a (▼), 2a (○), and 4a(●) monitored at 319 nm after 266 nm excitation in cyclohexane

Transient actinometry gives the quantum yield of generation only for the carbon centered radicals since all other transients produced are invisible to the laser system. Therefore, steady state irradiation was used to detect and isolate other photoproducts. In addition to the expected C-O bond cleavage, a considerable amount of N-O cleavage and disproportionation products were observed with this technique. An additional radical trap (4-hydroxy-TEMPO) was added to the samples, similar to the work discussed above,[49] to prevent the back reaction between carbon radicals with TEMPO represented in Equation 6 of Scheme 3-3. The observed quantum yields would be lower if this reaction was allowed to proceed. Lower concentrations of the trap were required, relative to the thermal studies, to avoid direct excitation of the nitroxide, as it absorbs at the irradiation wavelength. Typical trap absorbances at the irradiations wavelength were < 0.08. Subsequently, the conversions used for the steady state irradiation were also low (< 5 %) to prevent trap depletion and excitation of the photoproducts. The quantum yield of initiator photodecomposition ($\Phi_{initiator}$) can be calculated through Equation 3-4 by determining the concentration of all the products formed. The concentration of acetophenone produced upon photodecomposition of valerophenone at 254 nm must be calculated. The parameter χ is a correction factor accounting for different irradiation times between the initiator and actinometer.

$$\Phi_{initiator} = \chi \cdot \frac{[Products_{initiator}]}{[Acetophenone]} \cdot \Phi_{Valerophenone}$$

Equation 3-4. Quantum yield calculation from steady state irradiation.

The LFRP initiators (**1b-c** and **2b-c**) examined were shown to give disproportionation products in low yields under the thermal conditions as discussed above. The mechanism by which these products are formed is a concerted process[38,49] upon thermal decomposition and may change under photochemical conditions.[37,123-130] The proof for this specific concerted mechanism is the focus of a subsequent chapter. Hydroxylamine derived from the external trap, in addition to ethylbenzene and cumene, were not observed during the photochemical studies. This does not infer an identical concerted mechanism for the photochemical process as its thermal analogue. However, recent reports confirm the disproportionation process pathway for thermal decomposition.[49,73,131,132]

The general mechanism for the photodecomposition of LFRP was found to proceed by two competitive homolytic pathways arising from N-O and C-O bond cleavage. This N-O photoinduced decomposition was also observed previously by an independent study.[35] The subsequently generated radicals from N-O fragmentation can decay by hydrogen abstraction from the solvent (pathway d in Scheme 3-7) when cyclohexane is used as the solvent. The fate of the radicals from C-O bond cleavage conversely undergo trapping by the excess nitroxide added (pathway b). There also exists a third decomposition pathway being the concerted disproportionation reaction (pathway c).[59] The amount of trapped-to-disproportionation products observed is dependent on the carbon centered radical generated; **1c** has a greater number of β-hydrogens than **1b** and gives more disproportionation products. The photodecomposition of the LFRP initiators and the subsequent product formation determined by steady state irradiation are found in Scheme 3-7. The quantitative product distribution including the quantum yields of decomposition are also shown in Table 3-4.

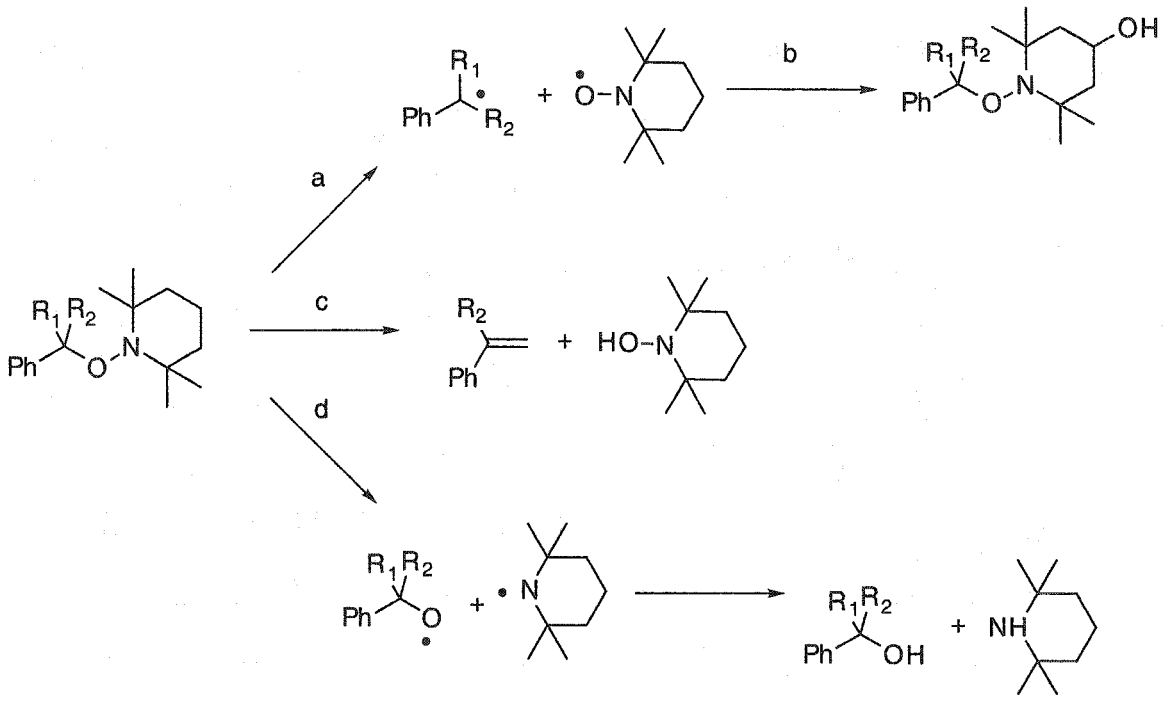

Scheme 3-7. Photodecomposition pathways for LFRP initiators determined through product analysis after steady state irradiation.

The quantum yield and product distribution for **1a** and **2a** are essentially identical implying there is no significant influence from the substitution in the 4 position. Kinetic work presented in a following chapter also supports this conclusion.[59] However, we observed inconsistent results when the nitroxide moiety in the initiator was substituted with 3-oxo-TEMPO. At the irradiation wavelength used for this study, some of the energy is localized in the ketone moiety of this nitroxide causing inconsistent PAC results possibly arising from triplet formation and energy transfer. Therefore, studies involving the oxo based nitroxides were not pursued after discouraging preliminary studies.

Table 3-4. Product photodecomposition percentage and quantum yields in cyclohexane.

Initiator	C-O	N-O	Disproportionation	Total
1a (%)	70.5	29.9	-	100
Φ^a	0.63	0.27	-	0.90[b]
1b (%)	53	17	30	100
Φ^a	0.48	0.15	0.24	0.90[b]
2b (%)	62	15	22	100
Φ^a	0.53	0.13	0.19	0.85[b]
1c (%)	20	24	56	100
Φ^a	0.19	0.23	0.53	0.95[b]

a) Quantum yields determined by steady state actinometry versus valerophenone.
b) Total quantum yield based on all products formed from steady state irradiation at 254 nm.

For the different initiators examined, the major decomposition pathway is from C-O bond cleavage (pathway a, Scheme 3-7). This is not surprising since the C-O bond is known to be relatively weak, measured in the previous section.[49,101] The N-O bond must be stronger as only smaller amounts of products from this cleavage are observed. The excitation energy used for these experiments is quite high, ca. 115 kcal/mol, and is obviously sufficient to excite the initiators directly to a dissociative state leading to N-O bond cleavage in addition to the expected C-O cleavage. However, in some systems this bond must not be significantly stronger than the C-O bond since products from N-O homolytic fragmentation have also been observed under thermal conditions.[73] The amounts produced

upon thermolysis are less than those generated from photochemical means implying the reaction barrier is more easily overcome photochemically.

An interesting observation lies with the amount of cross-trapped products versus disproportionation (pathways b and c) for **1b** and **1c**. The amount of photoproducts for these two initiators is reversed with respect to one another. The previous thermolysis investigation (*vide supra*) of these initiators showed a marginal increase in the amount of disproportionation products for **1c** relative to **1b** for this concerted process.[49] More recently, we have found that a combination of steric and kinetic factors are responsible for a change in disproportionation products and are discussed in a following chapter.[132] The significant amount of disproportionation products observed for **1c** is possibly a result of the greater number of abstractable hydrogens available. This is likely compounded with a lower rotational barrier leading to the correct four centered eliminating configuration required for disproportionation product formation (see Formation of Disproportionation Products chapter).

3.2.2.2 Disproportionation Energies

The energetics for reactions leading to disproportionation products are known to be significant.[37,125-130,133] Since these values are not negligible and the PAC measurements record the energetics of all the processes occurring within the time scale of the transducer, the thermodynamics of the reaction leading to disproportionation products must be considered when solving the PAC data. The values for the reaction specific to these initiators have not been previously examined, but can easily be calculated from literature values. The thermodynamic cycle used to calculate the desired disproportionation reaction enthalpy is represented in Scheme 3-8 involving the known C-O bond homolysis. More specifically, the formation of disproportionation products can be accounted for by Equations 10 and 11 shown in Scheme 3-9 involving the exchange of a hydrogen.

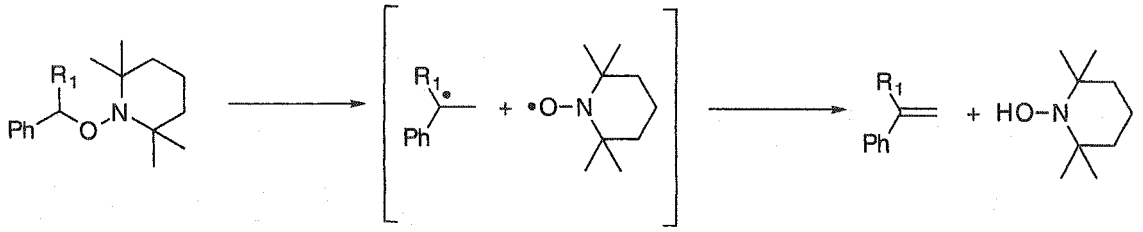

Scheme 3-8. Schematic representation of the equation used to determine the disproportionation reaction enthalpy (ΔH_{rx}).

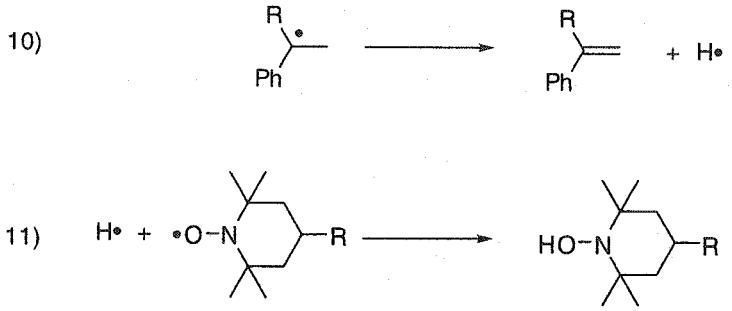

Scheme 3-9. Breakdown of reactions used to calculate the disproportionation reaction enthalpy.

The individual enthalpies of formation (ΔH_f) for the species shown in Scheme 3-9 can be used to calculate the overall reaction enthalpy of the reaction leading to disproportionation products. The values used for this calculation are summarized in Table 3-5, and when used with the reported values in Equation 3-4, easily lead to the desired disproportionation reaction enthalpy for the initiators studied. The ΔH_f values required for TEMPO and its hydroxylamine analogue have not been reported, but the BDE for the reaction expressed in Equation 11 of Scheme 3-9 was previously found to be 69.6 kcal/mol.[134] The reported BDE involving 4-oxo-TEMPO was 71.8 kcal/mol, which is consistent with the calculated value using the individual numbers from Table 3-5.

$$\Delta H_{disproportionation} = \Delta H_{C-O} + \Delta H_{Equation\ 10} + \Delta H_{Equation\ 11}$$

Equation 3-5. Calculation of disproportionation reaction enthalpy.

Table 3-5. Thermodynamic values for compounds leading to disproportionation products.

Structure	ΔH_f (kcal mol^{-1})[135]	Structure	ΔH_f (kcal mol^{-1})[135]
	49.0[45,136,137]	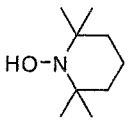	-
	39.6[45,137,138]	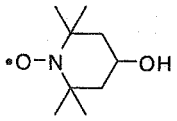	-69.6[139]
	35.1[140,141]	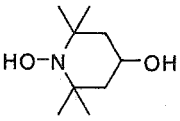	-85.5[139]
	32.4[45,137,138]	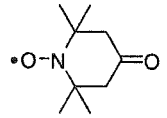	-51.5[139]
	27.0[140,142]	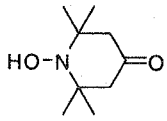	-71.2[139]
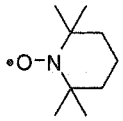	26.0[143,144]	H•	52.1[145]

The calculated disproportionation reaction enthalpies for the studied initiators using Equation 3-5 and the individual values from Table 3-5 are represented in Table 3-6. The calculated values are all endothermic and are relatively small compared to the thermally measured BDEs for these initiators, but are consistent with similar reactions.[133] When these values are taken together with their respective quantum yields from Table 3-4, their contributions to the PAC measurements are consistently small relative to the energetically dominant N-O and C-O homolysis reactions. Nonetheless, these values are important for deconvoluting the PAC data and for accurately determining the N-O BDEs for the LFRP initiators.

Table 3-6. Disproportionation reaction enthalpies involving different nitroxides and benzylic type centers and their subsequent contributions to the PAC calculations.

Products	$\Delta H_{disproportionation}$ (kcal mol^{-1})		$\Phi \cdot \Delta H_{disproportionation}$ (kcal mol^{-1})[a]	
			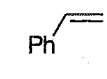	
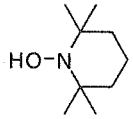	6.4	3.3	1.5	1.8
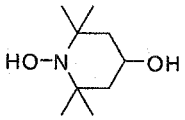	8.0	4.6	1.5	-
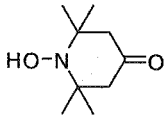	4.2	0.8	-	-

a) Quantum yield value taken from Table 3-4.

3.2.2.3 N-O Bond Energies

The bond dissociation enthalpy of the N-O bond for the initiators found in Figure 3-1 can be determined through deconvolution of the PAC data. The PAC measurements done in cyclohexane with initiators **1a-c** and **2a-c** with excitation at 254 nm lead to the data represented in the second column of Table 3-7. These values are derived from the PAC measurements and are extrapolated through the use of Equation 3-2. The parameter α in this equation refers to the ratio of the two slopes derived from plots similar to that represented in Figure 3-7. The reaction enthalpies are linearly related to α, being the ratio of the resulting pressure wave amplitudes for the reference (*o*-hydroxybenzophenone) and the compound studied. Figure 3-7 shows the change in the measured pressure wave amplitude as a function of laser dose for the reference compound and **1a** and the ratio of the two slopes leads to α. The linear trend implies the photodecomposition process for the initiators is monophotonic over the entire laser dose range, and is important for deconvoluting the data.

Table 3-7. Quantum yield of carbon centered radical generation determined by relative transient actinometry and PAC enthalpy values for homolytic bond scission.

Initiator	$\Phi\Delta H_{obs}$ (kcal/mol)	Φ^a (C-O) (± 4%)	$\Delta H_{thermal}$ (C-O) (kcal/mol)	ΔH^c (N-O) (kcal/mol)
1a	34 ± 2	0.66	30.8[b]	42 ± 4
1b	25 ± 2	0.52	28.4[b]	44 ± 4
1c	19 ± 1	(0.19)	24.6[b]	40[e] ± 4 (46)[f]
2a	33 ± 2	0.58	31[b]	40 ± 4
2b	24 ± 2	0.51	27 ± 3[d]	-
2c	20 ± 1	(0.16)	23 ± 3[d]	-

a) Values based on transient LFP actinometry measured in cyclohexane against their respective ketone actinometers in Figure 3-6.
b) Values for C-O bond cleavage taken from thermolysis studies presented above.[49]
c) N-O bond dissociation energy determined by PAC measurements according to Equation 3-7.
d) Value calculated from Equation 3-6 assuming the same N-O bond energies from **1b** and **1c** analogues are approximately the same. The values in parentheses are uncertain because of a quadratic power dependence relationship.
e) Calculated based upon value derived from PAC measurements.
f) Calculated from value free of volume effects from Figure 3-8.

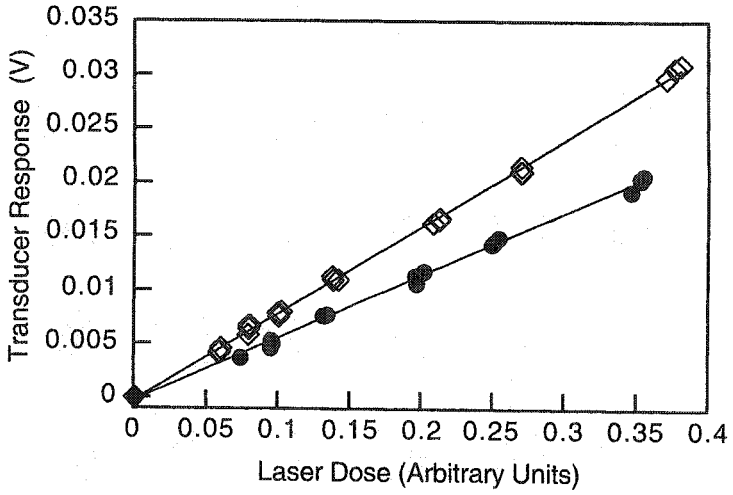

Figure 3-7. Photoacoustic calorimetry response of 1a (●) versus the reference (✧), *o*-hydroxybenzophenone, as a function of laser power measured in cyclohexane.

The data obtained from the PAC measurements (ΦΔH) contains the quantum yield for the observed process and is also dependent on the solvent (*vide infra*). Therefore, the exact photodecomposition pathway and its respective amount must be known. The data summarized in Tables 3-5 and 3-7 are crucial for deconvoluting the PAC data into energetics of the different decomposition pathways. The deconvolution can easily be done according to Equation 3-6 since the total observed PAC signal is a linear combination of all the individual processes occurring within the time resolution of the transducer. The processes detected by the transducer are N-O and C-O bond homolysis in addition to the reaction leading to disproportionation products exclusively (*vide infra*).

$$\Phi\Delta H_{true} = \Phi_{N-O}\Delta H_{N-O} + \Phi_{C-O}\Delta H_{C-O} + \Phi_{Disprop.}\Delta H_{Disprop.}$$

Equation 3-6. Deconvolution of the PAC data into discrete thermodynamic processes occurring photochemically.

The parameter $\Phi\Delta H_{true}$ is the enthalpic term devoid of any volume effects. It is related to the observed enthalpy ($\Phi\Delta H_{obs}$) according to Equation 3-7.

$$\Phi\Delta H_{obs} = \Phi\Delta H_{true} + \frac{\Delta V}{X_s}$$

Equation 3-7. General PAC equation leading to reaction enthalpies as a function of the solvent properties.

The $\Phi\ \Delta H_{obs}$ values for all three types of initiators (**Xa-c**) observed are relatively similar, suggesting the time response window of the transducer is capable of recording only the primary processes. The disproportionation process is known not to be iso-energetic[127,130,133,146] and would lead to significantly different values for **1b-c** and **2b-c** since these give substantial amounts of disproportionation products. Since the values or these initiators are relatively close to **1a**, which cannot undergo any disproportionation, the processes recorded by the transducer are uniquely from N-O and C-O bond fragmentations. The rate constant for hydrogen abstraction by cumyl alkoxyl from cyclohexane was measured and found to be $9.7 \times 10^5\ M^{-1}\ s^{-1}$. Under these experimental conditions, this leads to an observed lifetime of 1.3 μs for the alkoxyl radical, which is outside the response time of the transducer. Therefore, the hydrogen abstraction thermodynamics are excluded from the calculations as they are not recorded by the transducer and subsequently simplify the data treatment to that represented by Equation 3-6. Only the reactions of N-O and C-O homolytic bond cleavage, in addition to the reaction leading disproportionation products, are accounted for in the PAC calculations because they occur instantaneously, hence within the laser pulse.

The observed enthalpy (ΔH_{obs}) of the measured reactions is a function of the volume contributions (right hand term in Equation 3-7) and the true reaction enthalpy (ΔH_{true}). The former term accounts for the reaction volume change arising from bond cleavage during the course of the fragmentation reaction. It also considers the chemical volume change of the solvent related to its thermoelastic properties (X_s). The latter term can be ignored for isothermal studies since its contributions at room temperature is small.[109] However, the amplitude of the observed PAC signal is solvent dependent and can be isolated through the study of PAC measurements in a series of homologous solvents.

Isolating the volume contributions in order to determine true enthalpy values for the reaction studied (ΔH_{true}) is typically done through the use of a homologous series of solvents. This has the effect of varying X_s without influencing the detectable energetics of the reaction studied. This value is

specific to each solvent and is a function of the solvent's molecular weight (MW), heat capacity (C_p), density (ρ), and thermal compressive parameter (α) as expressed in Equation 3-8. The derivation of this equation and its chemical significance is thoroughly explored in the chapter dealing with photothermal and photoacoustic methods.

$$X_s = \frac{\alpha \cdot MW}{C_p \cdot \rho}$$

Equation 3-8. Method for calculating the solvent specific parameter X_s.

The values of ΔH_{obs} are measured in a series of homologous solvents, typically linear alkanes, and the desired true enthalpy values are extrapolated according to Equation 3-7. This approach yields ΔV as the slope and ΔH_{true} as the intercept.[108,147] Since the extrapolation is done over a long range, there is a significant error associated with the intercept, providing only a rough estimate for the value of ΔH_{true}. Treating the PAC data according to Equation 3-7 leads to a typical plot shown in Figure 3-8 where the slope yields relatively accurate information compared to the intercept. The approach gives the volume contribution being $\Delta V = 11.8 \pm 5$ ml/mol for the decomposition of **1c**. Since, all the PAC measurements for the remaining initiators were done in cyclohexane ($X_s = 3.557$ ml/kcal), the volume correction factor for Equation 3-7 in this solvent is 3.3 kcal/mol.

The extrapolated volume factor of 11.8 ± 5 ml/mol lies in the specific range of ~10 ml/mol[148-150] expected for typical homolytic C-C bond cleavage measured by pressure methods. These studies are normally good sources for verifying the PAC measurements as many of the reverse reactions have been studied.[151] A volume factor similar to literature values is expected since the process measured in the PAC studies involves a bond homolysis being; C-O and N-O bond cleavages. Regardless, the observed volume contribution is consistent with previously measured homolytic bond cleavages by pressure methods.[151] As a result of the simultaneous bond cleavages, the ΔH_{true} value reflects the sum of the two processes and their respective quantum yields in addition to the reaction leading to disproportionation products.

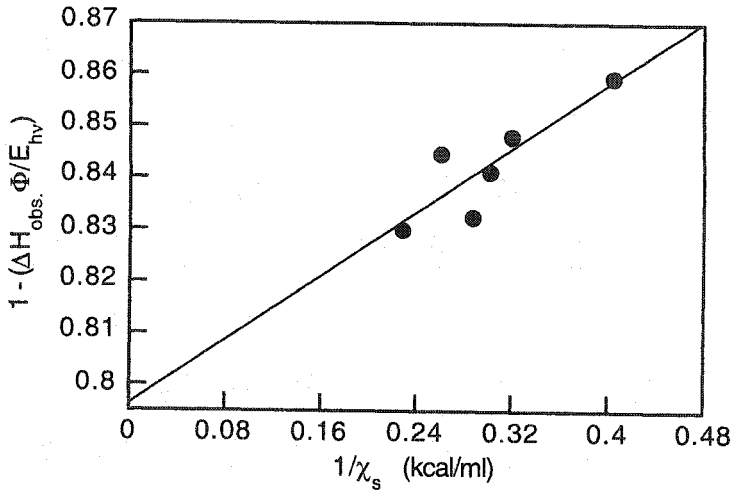

Figure 3-8. Graphical approach used for determining the volume contributions derived from the slope in a series of cyclic alkane solvents.

The shortcomings for determining ΔH_{true} from Equation 3-7 can be circumvented by treating the data by the method of Grabowski et al.[150] This approach involves rearranging the equation to give ΔV as the intercept, and more accurate values of ΔH_{true} from the slope. Equation 3-9 represents Grabowski's approach in which the solvent parameter is multiplied throughout. This becomes a weighting factor and increases the linearity of the plots derived from this equation. The value extrapolated from the slope of Figure 3-9 using Equation 3-9 is ΔH_{true} = 17.9 ± 2 kcal/mol. This value represents the sum of all the processes accounted for in Equation 3-6 and is void of any volume contribution or PAC solvent effect. The volume contribution (ΔV) **cannot** be accurately calculated from this equation because the intercept contains a large error. Only the enthalpy of the reaction can be accurately determined from this approach, unlike Equation 3-7.

$$\Phi\Delta H_{obs} \cdot X_s = \Delta V + \Phi\Delta H_{true} \cdot X_s$$

Equation 3-9. Grabowski's approach for determining the true reaction enthalpy (ΔH_{true}) as the slope.

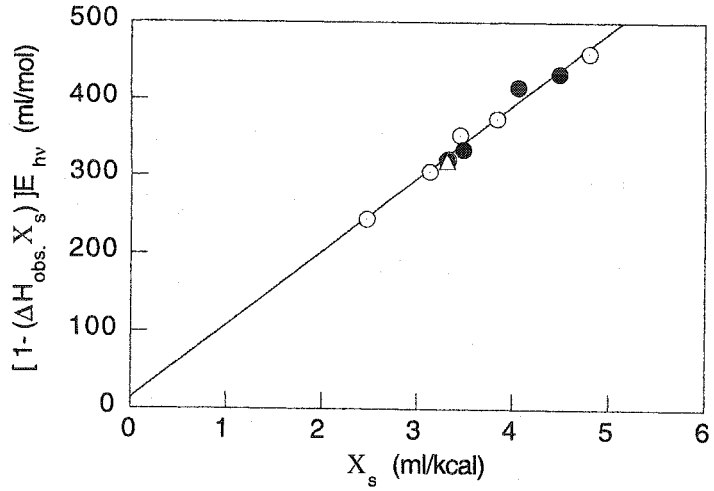

Figure 3-9. ΔH_{true} determination for initiator 1c derived from the slope. PAC response in various linear (○), cyclic (●) alkane solvents, and acetonitrile (Δ).

From the previously known C-O bond dissociation enthalpies[49] of the initiators in conjunction with the measured quantum yields and product distributions from this study, the N-O bond dissociation enthalpies for these initiators can finally be calculated. The calculated values found in Table 3-7 are in the range of 40 kcal/mol and are slightly lower than expected for N-O cleavage.[152,153] This is expected since the nitrogen radical generated is stabilized more than a simple substituted amine. It also shares the similar steric structure to TEMPO, thus some comparable persistent behavior similar to its parent nitroxide from the tetra-substitution in the 2 and 6 positions is expected.

Semi-empirical calculations have previously been done concerning the desired N-O bond cleavage, however the values calculated are 5-10 kcal/mol smaller than the experimentally measured ones.[33] Also, the system analyzed in the literature gives an aliphatic alkoxyl radical which is by far less stable than the ones derived in this study, and would therefore be expected to be higher. This study shows the shortcomings of the semi-empirical method to accurately handle open shell systems as they are not parameterized for such N-O nitroxide studies.[80,81,85,90] However, absolute values from these types of calculations can be used to accurately predict trends because the errors associated with the calculations are systematic.[81-83,85,89] The N-O bond dissociation enthalpy calculated semi-empirically is consistent with the experimental data and predicts a 15 kcal/mol stronger bond for N-O homolytic cleavage relative to C-O cleavage.

The calculated N-O BDEs are consistent regardless of the initiator examined. There should be little difference between these values as the radicals generated upon cleavage are structurally similar, being the alkoxyl and hindered amino radicals. The only difference between the species generated is the methyl substitution α to the oxygen radical center. There should be little stability influence from this substitution compared to benzylic centers because the radical center is located on the oxygen and cannot be stabilized through resonance effects. Therefore, the difference in the calculated N-O BDEs reflects the uncertainties arising from experimental errors in many forms, i.e., the PAC data, quantum yield measurements, volume calculations, and C-O BDEs.

The N-O BDEs reported in Table 3-7 are consistent within experimental error for the three different initiators examined. The BDEs values obtained were calculated by different methods for each of the initiators and their self-consistency suggests the values calculated are correct. The benzylic initiators (**1a** and **2a**) cannot form disproportionation products and subsequently contain only the N-O BDE as the only unknown in the PAC data. The calculated value for this initiator in known with higher certainty as it does not rely on data from disproportionation products. The $\Phi\Delta H_{true}$ value for initiator **3a** can be graphically derived without the volume effect and is therefore also known with greater certainty. The self-consistency between this value and that calculated in the same fashion as **1-3b** confirms the correct N-O BDE value is derived.

The bond enthalpies for the TEMPO and 4-hydroxy-TEMPO initiators are assumed to be identical since the radicals formed upon decomposition are similar in structure and the 3-position substitution has little effect (*vide supra*). These values in turn were used to calculate the unknown C-O enthalpies for the two initiators, **2b-c**. They are identical within experimental error to the corresponding TEMPO initiators validating the PAC measurements previously measured. This is understandable since the substitution at the 3-position should not influence the bond energies. The self-consistent correlation between these values for the two sets of initiators implies the volume contribution for all three types of initiators is identical and further confirms the response time of the transducer is too short to resolve the processes after initial bond fragmentation.

3.2.2.4 Volume Contributions

The volume contribution (ΔV) is incorporated into the PAC data collected and must be known in order to accurately determine the value of ΔH_{true}. In certain reported cases these contributions have inadvertently been neglected and only by chance have the correct enthalpic values been obtained.[154-156] To recapitulate, the standard method for isolating the volume contribution from the true reaction enthalpy (ΔH_{true}) is normally done graphically by extrapolation involving PAC studies in a series of homologous solvents, typically linear alkanes. This method is reserved for reactions that can be exclusively studied in organic solvents. The same effect of varying X_s can be achieved for aqueous studies through a change in temperature or by a two point method.[157] This involves measuring the enthalpic contribution at a given temperature and at 3.8 °C at which temperature the volume effect from the aqueous solvent is nonexistent. The observed signal at this temperature exclusively comes from the observed reaction devoid of any volume effects. The advantage of this approach, called the β=0 method, is that only two accurate measurements are required, thereby simplifying the technique. A more laborious and time consuming effort is required for analysis for reactions done in organic solvents. Normally the desired PAC studies must be repeated in 5-6 linear alkane solvents in order to isolate the volume contributions.

The solvents of choice for isolating the volume effects have a large range of X_s values in order to introduce a small uncertainty when extrapolating the desired values from the graphical approach similar to that shown in Figures 3-8 and 3-9. Mathematically the graphical approach is feasible for isolating the desired values, however practically many problems arise. Exact measurements under identical conditions must be repeated in the different solvents which becomes laborious and time consuming. The longer alkane solvents required to obtain a large difference between the X_s values are relatively viscous and difficult to work with compared to shorter alkane solvents. This affects some reactions studied, but most importantly, the solubility of polar reagents and products is affected. This in turn limits the excitation wavelength used and the reagent concentration used for the PAC studies. The use of solvents other than a conventional linear alkane homologous series for isolating the volume contributions will be presented.

The linear alkane studies have recently been expanded to include some work with cyclic alkanes including *cis* and *trans* decalin as a new means to extrapolate

the volume contributions.[158] The difficulty with working with cyclic alkanes is their availability in large quantities and in high purity. The decalin solvents require exhaustive purification to remove aromatic contaminants. Success has also recently been met with aromatic solvents such as benzene and its methylated analogues as a homologous series.[131] However, the use of these solvents as a homologues series must be employed in conjunction with other homologous series in order to obtain accurate volume contribution because their total X_s range is relatively small compared to the range available for linear alkane solvents.

The work explored here combines cyclic and acyclic alkane solvents to show the volume contributions arising from homolytic cleavage processes can be extrapolated without the use of a *true* homologous series. The important solvent parameters, including X_s, required for isolating the volume contributions are reported in Table 3-8. The linear trend represented in Figures 3-8 and 3-9 supports the fact that the volume contribution is consistent regardless of the homologous series chosen. Also included in these measurements is acetonitrile to prove PAC studies of homolytic bond cleavage are insensitive to the solvent chosen for examining radical reactions. Preliminary studies have shown that the reaction of study is insensitive to the choice of solvent. The benefit to this approach is different solvents can be used to give a larger range of X_s without being confined to a homologous series of solvents such as linear or cyclic alkanes. This assumes the quantum yields for the reactions in different solvents are known. A further advantage to this approach is reactant solubility problems encountered with apolar solvents can be avoided by using a series of polar and smaller apolar non-homologous solvents series to determine reaction enthalpies for radical reactions. The linear trend shown in Figure 3-9 for the various solvents supports the claim that a strict homologous series is not required for PAC studies involving radical reactions.

Table 3-8. Solvent thermoelastic properties used for PAC volume contributions determination.

	Solvent	α^a ($\times 10^3 K^{-1}$)	X_s^b (ml $kcal^{-1}$)
Cyclic	Cyclopentane	1.347	4.089
	Cyclohexane	1.220	3.558
	Methyl-cyclohexane	1.132[c]	4.49
Linear	Pentane	1.610	4.678
	Hexane	1.391	3.918
	Heptane	1.263[c]	3.467
	Octane	1.164	3.133
	Iso-Octane	1.198[c]	3.450
	Undecane	0.974	3.331
	Acetonitrile	1.368	3.310

a) From literature.[159]
b) Value calculated from Equation 3-10.
c) Calculated from Equation 3-8.

Only limited values of the thermal compressive parameter (α) have been experimentally measured.[159] However, the desired values can be calculated from other parameters according to Equation 3-10. The desired α value is

proportional to the ratio of the solvent's density (d_1 and d_2) at two given temperatures over the difference between these two temperatures.

$$\alpha = \frac{(d_1 / d_2) - 1}{\Delta T}$$

Equation 3-10. Method for calculating the thermal compressive parameter.

The disadvantage of using a mixed solvent series for PAC studies is that investigations are limited to homolytic bond scission or isomerization reactions. For other reactions, such as electron transfer or heterolytic processes, the choice of solvent influences the efficiency and rate of these reactions, hence precludes the use of a mixed solvent series. Different homologous solvent series used for studying these types of reactions leads to the isolation of the individual volume contributions arising from Van der Waals effects, electrostriction, and solvent-solute interactions. However for radical and isomerization reactions, the predominant volume contribution arises from solvent reorganization from reagent to product and a mixed series of solvents can be used for isolation of the parameter ultimately leading to ΔH_{true}.[58,150,151,158,160-168]

3.3 Conclusion

The BDEs of several alkoxyamines used as initiators for LFRP were examined through their decomposition at various temperatures. The C-O bond strength calculated from these measurements was found to be a function of the carbon centered radical produced upon thermal bond cleavage. Weaker bonds were observed for relatively stable radicals, while the nitroxide structure did not appear to influence the bond strength. A minor side reaction leading to disproportionation products was observed at typical styrene polymerization temperatures. The significance of this side reaction is important because it implies a substantial amount of chain termination would occur during the polymerization process leading to poor living polymer like properties.

The quantum yield of photodecomposition of the alkoxyamine initiators were measured by steady state and relative transient actinometry and found to be close to unity. However, the ratio of the isolated decomposition products vary as a function of the initiator structure. The major pathway for decomposition for **1-2a** occurs by C-O homolytic cleavage and the remainder arises from N-O homolytic cleavage. Homolytic C-O was found to also be the predominant decomposition pathway for **1-2b**, followed by the formation of disproportionation products and minor N-O homolytic bond fragmentations. Disproportionation products are the major decomposition products for **1c** possibly due to the increased number of abstractable β-hydrogens and low rotational barrier.

The photodecomposition quantum yield of the ketones used as actinometers were measured in experimental conditions comparable to the PAC studies and were found to be similar to reported values. The values were subsequently used in conjunction with the photodecomposition quantum yields of the LFRP initiators to determine the energetics involved for homolytic N-O bond cleavage and the formation of disproportionation products. The BDE for the previously unreported N-O bond was found to be higher than for the C-O bond, yet smaller than similar bonds yielding less stable products.

The volume contributions and true enthalpic values for PAC studies involving the production of radicals from homolytic bond cleavage can be done without the use of a homologous solvent series. The desired values can be obtained

through the use of different solvents including linear and cyclic hydrocarbons and acetonitrile.

3.4 Experimental

All chemicals were used as received from Aldrich unless otherwise stated. Hexanes used for chromatographic purposes was washed and distilled over calcium chloride prior to use. OmnioSolv grade solvents for laser work and HPLC grade solvents for analytic work were used as received from VWR.

3.4.1 Thermolysis Studies

The stock solution for thermolysis studies of **1a** was prepared in the following fashion. The compound **1a** (179 mg, 0.72 mmol) was dissolved along with 4-hydroxy-TEMPO (233 mg, 1.36 mmol) and 1,1′ binaphthalene (13 mg, 0.05 mmol) in 25 mL cyclohexanol. The orange colored solution was sonicated for 25 minutes to ensure complete dissolution of all the reagents and then refrigerated for future use. Stock solution of **2a** was prepared by dissolving it (126 mg, 0.48 mmol) along with TEMPO (201 mg, 1.29 mmol) and 1,1′ binaphthalene (10 mg, 0.04 mmol) in 25 mL cyclohexanol and sonicating it till thoroughly dissolved. The stock solution for **1a** was done by mixing **1a** (175 mg, 0.67 mmol), 4-hydroxy-TEMPO (240 mg, 1.39 mmol), and 4-di-*tert*-butylbenzene (7.7 mg, 0.04 mmol) as an internal reference in 25 mL cyclohexanol. The solution was sonicated for 20 minutes to ensure complete dissolution. The solution for **1b** was prepared in a similar manner where **1b** (192 mg, 0.69 mmol), 4-hydroxy-TEMPO (254 mg, 1.47 mmol), and 4-di-*tert*-butylbenzene (9.1 mg, 0.05 mmol) were dissolved in 25 mL cyclohexanol and sonicated.

Approximately 1 mL of the stock solution was placed in a 7 cm x 7 mm glass tube and subjected to three cycles of freeze-pump-thaw. The samples were then flame sealed under vacuum and placed in a thermostated aluminum block equipped with a thermocouple and voltage meter for temperature measurements. The samples were heated at the desired temperature and removed at given intervals and immediately cooled in ice water. A minimum of five samples were heated per temperature. They were subsequently cracked open and the ratio of trapped product to internal standard were measured by HPLC analysis. The products were detected at 220 and 254 nm with a diode array detector and separated on a Zorbax® C-18 reverse phase column with a flow rate of 0.5 mL / min and 85% methanol / 15% water as eluent.

Known amounts of the trapped products, styrene, α-methylstyrene, and internal standards were made up in methanol and subsequently injected for HPLC analysis. These led to the generation of calibration curves for determining the product concentrations based upon the trapped product to internal standard ratios.

3.4.2 Quantum Yield Determination

Dibenzyl ketone actinometry: i) Samples of recrystallized and sublimed dibenzyl ketone (**4a**) were prepared in OmniSolv cyclohexane or benzene (12 mM) with (absorbances > 2 at 300 nm) and 1,4-di-*tert*-butylbenzene (7 mM) as internal reference. The samples were dearated with oxygen-free nitrogen, sealed in 7 m m quartz test tubes and irradiated at 300 nm with 2 lamps from 2.5 to 12 minutes. The ratio of starting material to internal reference for the two irradiated samples was determined by GC equipped with a FID detector. ii) Two sets of dibenzyl ketone (35 mM) solutions were made in C_6D_6 and C_6D_{12} in 5 mm quartz NMR tubes and dearated with nitrogen. The samples were irradiated at 300 nm with 2 lamps for a total period of 12 minutes. The amount of bibenzyl produced as a function of time was monitored on a Brüker 500 MHz NMR spectrometer by analyzing the growth of the product protons.

Steady state actinometry: All samples were dissolved in OmniSolv grade cyclohexane in 7 mm quartz test tubes and their concentrations adjusted to give absorbances of 2 at the irradiation wavelength. Typical concentrations for samples **1a-c** were approximately 15 mM with the addition of 0.2 mM of 4-hydroxy-TEMPO as a radical trap. For **2a-c**, the sample concentrations were about 10 mM. All samples were dearated with nitrogen for 20 minutes and irradiated in a merry-go-round photoreactor with 2 lamps at 254 nm. The series were irradiated simultaneously side-by-side with the actinometer, valerophenone (51 mM), for 2 minutes and the product concentrations determined by HPLC. The products were detected at 220 and 254 nm with a diode array detector and separated on a Zorbax® C-18 reverse phase column with a flow rate of 0.5 ml / min and 85% methanol / 15% water as eluent. The retention times and concentrations were calibrated against authentic samples.

Transient Actinometry: About 60 ml of the initiator solution was prepared in OmniSolv grade cyclohexane in a Suprasil 7 x 7 mm^2 quartz cells and their absorbances matched to within 2% at 266 nm against their respective

actinometers and dearated for 20 minutes with nitrogen. The samples were excited from the fourth harmonic of a Nd-YAG Surelite laser from Continuum with 15 mJ of 266 nm irradiation in 6 ns pulses. Other details for the laser setup can be found elsewhere and presented in the experimental LFP chapter.[169,170] The samples were irradiated under flow conditions and approximately 30 to 40 shots collected till a constant signal was observed. The radicals generated upon photolysis were monitored at 317 nm for **1-2a** and **4a**, 319 nm for **1-2b** and **4b**, and 321 nm for **1-2c** and **4c** and their top O.D. monitored as a function of laser power.

3.4.3 Photoacoustic Calorimetry Studies

The measurements were done with a home-built apparatus consisting of a 10 x 10 mm^2 quartz Suprasil cuvette placed on top of a 0.5 MHz 1″ Videoscan transducer from Panametrics and the signal digitized with a Tektronix 2440 scope. A layer of silicon grease between the cuvette and transducer was used to ensure good acoustic transference. Samples were thoroughly degassed with nitrogen and their absorbances verified before and after the measurements to ensure they matched within 2 % the reference compound (*o*-hydroxybenzophenone) at the excitation wavelength. Excitation pulses (248 nm) from an excimer Lumonics E4-500 laser were used to excite the sample with pulse durations < 10 ns and typical energies of 70-90 mJ. The laser beam was focused behind the cuvette after passing through a 1 mm pinhole slit and its power measured by sampling a fraction of the beam. The data were digitized and sent to a computer and subsequently analyzed using an in-house data program written in the LabVIEW environment. The acoustic wave amplitude was monitored as a function of laser power and the heat of reaction was determined similarly to other methods.[171,172]

3.4.4 Synthesis

The coupled photoproducts from **4b** and **4c** (2,3-diphenylbutane (**5b**) and 2,3-dimethyl 2,3-diphenylbutane (**5c**) were photochemically synthesized. In a 15 cm Pyrex test tube was added 500 mg (3.4 mmol) of purified di-*tert*-butylperoxide and either 50 mL of ethylbenzene (408 mmol) for **5b** or cumene (359 mmol) for 5c. The solution was degassed followed by irradiation at 300 nm for a period of 2 days. The unreacted solvent was removed under vacuum and the white solid

purified by flash column chromatography with 100 % hexanes. The other photoproducts[104,105] were commercially available from Aldrich.

2,3-diphenylbutane (5b): Isolated as a white solid. M.p. 110-114 °C. ^{1}H NMR (200 MHz, $CDCl_3$ TMS) δ 7.34-7.15 (m, 10H), 2.79-2.76 (m, 2H), 1.05-0.98 (d, 6H). ^{13}C NMR (300 MHz, $CDCl_3$) δ 128.3, 127.6, 126.0, 99.4, 47.3, 20.9. MS (EI) m/z (%) 210 (19), 178 (27), 152 (5), 129 (22), 115 (8), 105 (100), 91 (23), 77 (49), 65 (7), 51 (20).

2,3-dimethyl 2,3-diphenylbutane (5c): Isolated as a white solid. M.p. 88-96 °C. ^{1}H NMR (200 MHz, $CDCl_3$ TMS) δ 7.24-7.03 (m, 10H), 1.29 (s, 12H). ^{13}C NMR (300 MHz, $CDCl_3$) δ 128.6, 128.6, 127.5, 126.6, 126.6, 125.5, 99.4, 43.6, 25.2. MS (EI) m/z (%) 238 (6), 206 (13), 178(20), 152 (3), 129 (18), 119 (100), 103 (36), 91 (92), 77 (37), 65 (12), 51 (17), 41 (53).

The syntheses of compounds **1a-c**, **2a-c**, and **3a-c** were done according to the literature procedure of Connolly.[48] In general, the method consisted of 1 equivalent nitroxide dissolved in 5 mass equivalents of di-*tert*-butylperoxide previously purified by passing it through a plug of neutral aluminum oxide. The orange colored solution was further diluted with 30 - 40 mL of the appropriate hydrocarbon solvent, charged into a Pyrex test tube, and purged with nitrogen for a minimum of 25 minutes. The solution was then irradiated at 300 nm till the color bleached, then the residual solvent removed by a stream of nitrogen, and subjected to further purification by flash chromatography and crystallization. Products **1a-c** and **3a-c** were isolated in greater than 90 % yield. **2a-c** could only be isolated in moderate to good yields because the photo-oxidation of the alcohol functionality to the ketone could not be controlled.

1-Benzyloxy-2,2,6,6-tetramethyl-piperidine (1a): ^{1}H (200 MHz, $CDCl_3$, TMS) δ 7.20-7.31 (m, 5H), 4.76 (q, 1H), 1.45 (d, 3H), 1.33 (m, 5H), 1.26 (s, 3H), 1.14 (s, 3H), 1.01 (s, 3H), 0.67 (s, H). ^{13}C (300 MHz, $CDCl_3$) δ 149.8, 127.8, 126.2, 125.3, 59.4, 40.8, 33.9, 20.6, 17.1. MS (EI) m/z (%) 157 (40), 156 (37), 143 (12), 142 (100), 123 (21), 115 (7), 105 (77), 104 (23), 103 (13), 77 (13), 74 (20), 69 (40), 56 (14), 55 (20), 41 (21). MS (FAB) m/z (%) 262 (5, M+1), 158 (11), 156 (95), 126 (100), 121 (30), 105 (14), 91 (8), 82 (16), 77 (2), 69 (85), 56 (10), 42 (13).

2,2,6,6-Tetramethyl-1-(1-phenyl-ethyoxy)-piperidine (1b): M.p. 42 °C. ^{1}H (200 MHz, $CDCl_3$, TMS) δ 7.25-7.45 (m, 5H), 4.76 (q, 1H),1.45 (d, 3H), 1.35 (m, 6H), 1.26 (s, 3H), 1.14 (s, 3H), 1.01 (s, 3H), 0.67 (s,3H). ^{13}C (300 MHz, $CDCl_3$) δ 145.8, 127.9, 126.7, 126.6, 83.1, 59.7, 40.4, 34.5, 34.1, 23.5, 20.3, 17.2. MS (EI) m/z (%) 156 (37), 142

(100), 123 (21), 105 (77), 104 (23), 91 (2), 77 (13), 69 (40), 56, (19), 41 (17). MS (FAB) m/z (%) 262 (5, M+1), 156 (95), 126 (100), 121 (30), 105 (14), 91 (7), 69 (85), 56 (10), 42 (12).

2,2,6,6-Tetramethyl-1-(1-methyl-1-phenyl-ethyoxy)-piperidine (1c): M.p. 50 °C. ^{1}H (200 MHz, $CDCl_3$, TMS) δ 7.47 (m, 2H), 7.28 (m, 2H), 7.17 (m, 1H), 1.59 (s, 6H), 1.51 (m, 4), 1.39 (q, 2H), 1.08 (s, 6H), 0.82 (s, 6H). ^{13}C (300 MHz, $CDCl_3$) δ 150.8, 127.6, 126.0, 125.3, 59.4, 40.8, 33.9, 28.2, 20.6, 17.1. MS (EI) m/z (%) 156 (24), 142 (45), 141 (20), 126 (54), 125 (11), 119 (41), 118 (100), 117 (97), 115 (47), 105 (17), 103 (86), 97 (22), 91 (45), 82 (29), 77 (59), 69 (90), 55, (61), 41 (81). MS (FAB) m/z (%) 276 (8, M+1), 156 (65), 142 (77), 140 (41), 119 (100), 91 (46), 83 (25), 69 (51), 58 (28).

1-Benzyloxy-2,2,6,6-tetramethyl-piperidin-4-ol (2a): M.p. 82 °C. ^{1}H (200 MHz, $CDCl_3$, TMS) δ 7.40 (m, 2H), 7.22 (m, 2H), 7.18 (m, 1H), 4.86 (s, 2H), 3.76 (q, 1H), 1.65-1.80 (m, 4H), 1.28 (s, 6H), 1.15 (s, 6H). ^{13}C (300 MHz, $CDCl_3$) δ 143.2, 127.8, 126.9, 125.8, 77.4, 63.4, 59.9, 48.9, 34.0, 28.6. MS (EI) m/z (%) 172 (58), 142 (50), 140 (20), 124 (39), 116 (32), 108 (64), 105 (66), 98 (70), 91 (72), 77 (84), 67 (47), 58 (86), 42 (100), 40 (87). MS (FAB) m/z (%) 264 (46, M+1), 172 (100), 156 (25), 142 (22), 119 (20), 16 (10), 91 (52), 77 (5), 69 (6), 57 (10).

2,2,6,6-Tetramethyl-1-(1-phenyl-ethyoxy)-piperidin-4-ol (2b): M.p. 92 °C. ^{1}H (200 MHz, $CDCl_3$, TMS) δ 7.22-7.30 (m, 5H), 4.73 (q, 1H), 3.94 (q, 1H), 1.65-1.79 (m, 4H), 1.48 (d, 3H), 1.31 (s, 3H), 1.19 (s, 3H), 1.06 (s, 3H), 0.65 (s, 3H). ^{13}C (300 MHz, $CDCl_3$) δ 145.4, 128.0, 126.9, 126.6, 83.3, 63.3, 30.2, 59.9, 48.9, 34.2, 23.4,m 21.3. MS (FAB) m/z (%) 278 (14, M+1), 209 (22), 186 (14), 172 (8), 105 (100), 91 (25), 77 (13), 65 (5).

2,2,6,6-Tetramethyl-1-(1-methyl-1-phenyl-ethyoxy)-piperidin-4-ol (2c): M.p. 106 °C. ^{1}H (200 MHz, $CDCl_3$, TMS) δ 7.45 (m, 2H), 7.25 (m, 2H), 7.18 (m, 1H), 3.32 (q, 1H), 3.73 (m, 1H), 1.84 (3, 4H), 1.59 (s, 6H), 1.13 (s, 6H), 0.86 (s, 6H). ^{13}C (300 MHz, $CDCl_3$) δ 150.5, 127.7, 126.2, 125.3, 79.9, 63.2, 59.9, 49.3, 33.8, 28.2, 21.5. MS (EI) m/z (%) 173 (7), 172 (5), 158 (16), 142 (21), 140 (13), 123 (13), 118 (100), 117 (87), 115 (40), 108 (15), 105 (15), 103 (66), 98 (31), 91 (38), 83 (16), 77 (46), 58 (51), 55 (31), 44 (21), 41 (52). MS (FAB) m/z (%) 292 (32, M+1), 174 (44), 173 (11), 172 (11), 158 (27), 156 (12), 119 (100), 91 (19), 74 (15).

1-Benzyloxy-2,2,6,6-tetramethyl-piperidin-4-one (3a): M.p. 76 °C. ^{1}H (200 MHz, $CDCl_3$, TMS) δ 7.30-7.35 (m, 5H), 4.89 (s, 2H), 2.19-2.63 (dd, 4H), 1.38 (s, 6H), 1.19 (s, 6H). ^{13}C (300 MHz, $CDCl_3$) δ 208.1, 137.3, 128.3, 127.7, 127.6, 78.9, 63.2, 53.3, 32.5,

22.6. MS (FAB) m/z (%) 262 (73, M+1), 246 (15), 170 (75), 164 (76), 153 (20), 114 (26), 91 (100), 83 (14), 77 (5), 70 (6), 59 (10).

2,2,6,6-Tetramethyl-1-(1-phenyl-ethyoxy)-piperidin-4-one (3b): M.p. 74 °C. ^{1}H (200 MHz, $CDCl_3$, TMS) δ 7.23-7.37 (m, 5H), 4.84 (q, 1H), 2.19-2.63 (dd, 4H), 1.58 (d, 3H), 1.38 (s, 6H), 1.19 (s, 6H). ^{13}C (300 MHz, $CDCl_3$) δ 208.4, 144.6, 128.1, 127.2, 126.8, 83.4, 62.9, 62.7, 5.6, 33.9, 33.6, 22.9, 22.7, 22.6. MS (EI) m/z (%) 171 (22), 156 (23), 123 (12), 114 (24), 105 (100), 104 (90), 103 (61), 98 (12), 91 (10), 83 (65), 77 (50), 69 (14), 56 (91), 51 (43), 41 (48), 39 (45). MS (FAB) m/z (%) 276 (22, M+1), 220 (10), 206 (18), 185 (67), 177 (20), 156 (21), 132 (56), 120 (11), 105 (100), 91 (20), 77 (32), 57 (20).

2,2,6,6-Tetramethyl-1-(1-methyl-1-phenyl-ethyoxy)-piperidin-4-one (3c): M.p. 89 °C. ^{1}H (200 MHz, $CDCl_3$, TMS) δ 7.48 (d, 2H), 7.18-7.32 (m, 3H), 2.10-2.59 (dd, 4H), 1.65 (s, 6H), 1.12 (s, 6H), 0.97 (s, 6H). ^{13}C (300 MHz, $CDCl_3$) δ 210.2, 157.2, 127.8, 126.5, 125.3, 125.2, 118.8, 83.6, 62.7, 60.1, 54.1, 33.5, 30.6, 28.2, 22.5. MS (FAB) m/z (%) 290 (11, M+1), 185 (16), 172 (27), 119 (100), 91 (33), 77 (4), 75 (13), 56 (4).

2,4-Diphenyl-pentane-3-one (4b): A modified synthesis based upon the literature procedure was used.[114] A solution of 35 % weight (1.73 M) of potassium hydride (1.53 g, 13.4 mmol) was dissolved in dry THF along with 1.73 M *n*-butyllithium (7 mL, 12.1 mmol) and cooled to 0 °C. Dibenzyl ketone (2.1 g, 9.98 mmol) was dissolved in 40 mL dry THF and added drop-wise to the cooled solution. After complete addition, the solution was warmed to room temperature and stirred for an additional 30 minutes. The solution was cooled down to 0 °C and methyl iodide (1.4 mL, 22.4 mmol) dissolved in 10 mL dry THF was added drop-wise to the ketone solution. The solution was stirred overnight at room temperature and then quenched with the addition of a saturated brine solution. The organic layer was extracted three times with dichloromethane. The organic layer was dried over anhydrous magnesium sulfate, filtered and purified by flash column chromatography with 20 % ethylacetate/hexanes to afford the product as an oil in 17 % yield. ^{1}H (200 MHz, $CDCl_3$, TMS) δ 7.21-7.38 (m, 10H), 3.81 (t, 4H), 1.29 (d, 6H). ^{13}C (300 MHz, $CDCl_3$) δ 210.1, 140.8, 129.4, 128.9, 128.5, 128.3, 128.2, 127.9, 127.4, 127.0, 126.7, 51.4, 408, 10.3, 10.0. MS (EI) m/z (%) 238 (11), 232 (9), 203 (3), 133 (45), 132 (16), 106 (38), 105 (100), 104 (43), 79 (41), 78 (19), 77 (50), 51 (21), 44 (21), 40 (35).

2,4-Dimethyl-2,4-diphenyl-pentane-3-one (4c): A modified synthesis based upon the literature procedure was used.[118] Dibenzyl ketone (1.99 g, 9.46 mmol) was dissolved in 100 mL dry THF and cooled to 0 °C followed by the addition of

sodium hydride (1.24 g, 51.7 mmol). Once the orange solution had turned milky white in color, methyl iodide (5 mL, 80.3 mmol) was added drop-wise to the solution at room temperature followed by refluxing overnight. The reaction was quenched with a saturated brine solution and the organic layer separated with dichloromethane. The organic layer was dried over anhydrous magnesium sulfate followed by purification by flash chromatography with 15 % ethylacetate/hexanes. The product was isolated as white needles in 10 % yield. M.p. 112 °C. ^{1}H (200 MHz, $CDCl_3$, TMS) δ 7.11-7.22 (m, 10H), 1.2 (s, 12H). ^{13}C (300 MHz, $CDCl_3$) δ 213.2, 144.3, 128.6, 128.4, 128.3, 125.8, 52.9, 27.8. MS (EI) m/z (%) 266 (5), 238 (8), 219 (3), 181 (6), 118 (42), 131 (4), 121 (80), 119 (100), 118 (48), 117 (30), 115 (20), 105 (38), 104 (20), 103 (46), 92 (33), 90 (91), 79 (57), 78 (37), 77 (63), 65 (23), 63 (12), 52 (11), 51 (35), 50 (35), 41 (82), 40 (24), 39 (42).

3.5 Chapter References

1. Georges, M. K.; Veregin, R. P. N.; Kazmaier, P. M.; Hamer, G. K. *Macromolecules* **1993**, *26*, 2987-2988.
2. Solomon, D. H.; Rizzardo, E.; Cacioli, P. U.S. Patent 4,581,429, **1986**.
3. Davis, T. P.; Haddleton, D. M.; Richards, S. N. *J. Macromol. Sci. Rev. Macromol. Chem. Phys.* **1994**, *C34*, 243-324.
4. Matyjaszewski, K.; Pugh, C. *Makromol. Chem., Macromol. Symp.* **1993**, *67*, 67-82.
5. Matyjaszewski, K. *New Polym. Mater.* **1990**, *2*, 115-123.
6. Penczek, S.; Szymanski, R.; Duda, A. *Macromol. Symp.* **1995**, *98*, 193-216.
7. Malmström, E. E.; Hawker, C. J. *Macromol. Chem. Phys.* **1998**, *6*, 923-935.
8. Szwarc, M. *Contemp. Top. Polym. Sci.* **1978**, *1*, 265-281.
9. Szwarc, M. *Science* **1970**, *170*, 23-31.
10. Szwarc, M. *Carbanions, Living Polymers, and Electron Transfer Processes*; Interscience: New York, 1968, pp 685.
11. Harwood, H. J. Living Polymerization Systems. In *Encyclopedia of Polymer Science and Engineering*; 2nd ed.; Kroschwitz, J. I., Ed.; John Wiley and Son: New York, 1990; Vol. Supplement; 380-469.
12. Moffat, K. A.; Saban, M. D.; Veregin, R. P. N.; Georges, M. K.; Hamer, G. K.; Kazmaier, P. M. U.S. Patent 5,449,724, **1995**.
13. Hawker, C. J.; Hedrick, J. L. *Macromolecules* **1995**, *28*, 2993-2995.
14. Hawker, C. J.; Barclay, G. G.; Dao, J. *J. Am. Chem. Soc.* **1996**, *118*, 11467-11471.
15. Hawker, C. J. *J. Am. Chem. Soc.* **1994**, *116*, 11185-11186.
16. Hawker, C. J.; Barclay, G. G.; Orellano, A.; Dao, J.; Devonport, W. *Macromolecules* **1996**, *29*, 5245-5254.

17. Barclay, G. G.; Hawker, C. J.; Ito, H.; Orellana, A.; Malenfant, P. R. L.; Sinta, R. F. *Macromolecules* **1998**, *31*, 1024-1031.
18. Devonport, W.; Michalak, L.; Malmstrom, E.; Mate, M.; Kurdi, B.; Hawker, C. J. *Macromolecules* **1997**, *30*, 1929-1934.
19. Hawker, C. J.; Fréchet, J. M. J. *J. Am. Chem. Soc.* **1990**, *112*, 7638-7647.
20. Doa, J.; Benoit, D.; Hawker, C. J. *J. Polym. Sci. A. Polym. Chem.* **1998**, *36*, 2161-2167.
21. Marestin, C.; Noel, C.; Guyot, A.; Claverie, J. *Macromolecules* **1998**, *31*, 4041-4044.
22. Hawker, C.; Benoit, D.; Rivera, F., Jr.; Piotti, M.; Rees, I.; Hedrick, J. L.; Zech, C.; Maier, G.; Voit, B.; Braslau, R.; Fréchet, J. M. J. *Polym. Prepr.* **1999**, *40*, 315-316.
23. Benoit, D.; Chaplinski, V.; Braslau, R.; Hawker, C. J. *J. Am. Chem. Soc.* **1999**, *121*, 3904-3920.
24. Hawker, C. J. *Acc. Chem. Res.* **1997**, *30*, 373-382.
25. Lokaj, J.; Vlcek, P.; Kriz, J. *Macromolecules* **1997**, *30*, 7644-7646.
26. Harth, E.; Benoit, D.; Helms, B.; Hawker, C. J. *Polym. Prepr.* **2000**, *41*, 42-43.
27. Fukuda, T.; Goto, A.; Ohno, K.; Tsujii, Y. "Mechanism and Kinetics of Nitroxide-Controlled Free-Radical Polymerization"; Controlled Radical Polymerization, 1998, San Francisco, CA.
28. Fukuda, T.; Tsujii, Y.; Miyamoto, T. *Polym. Prepr.* **1997**, *38*, 723-724.
29. Fukuda, T.; Terauchi, T.; Goto, A.; Ohno, K.; Tsujii, Y.; Miyamoto, T. *Macromolecules* **1996**, *29*, 6393-6398.
30. Fukuda, T.; Goto, A. *Macromol. Rapid Commun.* **1997**, *18*, 683-688.
31. Goto, A.; Rerauchi, T.; Fukuda, T.; Miyamoto, T. *Macromol. Rapid Commun.* **1997**, *18*, 373-381.
32. Kazmaier, P. M.; Moffat, K. M.; Georges, M. K.; Veregin, R. P. N.; Hamer, G. K. *Macromolecules* **1995**, *28*, 1841-1846.

33. Cogen, J. M. *Polymer Degrad. Stab.* **1994**, *44*, 49-53.
34. Moad, G.; Rizzardo, E. *Macromolecules* **1995**, *28*, 8722-8728.
35. Kothe, T.; Marque, S.; Martschke, R.; Popov, M.; Fischer, H. *J. Chem. Soc., Perkin Trans. 2* **1998**, *7*, 1553-1559.
36. Veregin, R. P. N.; Georges, M. K.; Hamer, G. K.; Kazmaier, P. M. *Macromolecules* **1995**, *28*, 4391-4398.
37. Engel, P. S.; Duan, S.; Arhancet, G. G. *J. Org. Chem.* **1997**, *62*, 3537-3541.
38. Li, I.; Howell, L.; Matyjaszewski, K.; Shigemoto, T.; Smith, P. B.; Priddy, D. B. *Macromolecules* **1995**, *28*, 6692-6693.
39. Howell, B. A.; Priddy, D. B.; Li, I. Q.; Smith, P. B.; Kastl, P. E. *Polym. Bull.* **1996**, *37*, 451-456.
40. Odell, P. G.; Veregin, R. P. N.; Michalak, L. M.; Brousmiche, D.; Georges, M. K. *Macromolecules* **1995**, *28*, 8453-8455.
41. Puts, R. D.; Sogah, D. Y. *Macromolecules* **1996**, *29*, 3323-3325.
42. Fukuda, T.; Atsushi, G. *Polym. Prepr.* **1999**, *40*, 311-312.
43. Goto, A.; Fukuda, T. *Macromolecules* **1999**, *32*, 618-623.
44. Rychnovsky, S. D.; Vaidyanathan, R.; Beauchamp, T.; Lin, R.; Farmer, P. J. *J. Org. Chem.* **1999**, *64*, 6745-6749.
45. Marsal, P.; Roche, M.; Tordo, P.; de Sainte Claire, P. *J. Phys. Chem. A* **1999**, *103*, 2899-2905.
46. Kysel, O.; Mach, P.; Micov, M. *Polymer Degrad. Stab.* **1993**, *40*, 31-35.
47. Stipa, P.; Greci, L.; Carloni, P.; Damiani, E. *Polymer Degrad. Stab.* **1997**, *55*, 323-327.
48. Connolly, T. J.; Baldovi, M. V.; Mohtat, N.; Scaiano, J. C. *Tetrahedron Lett.* **1996**, *37*, 4919-4922.
49. Skene, W. G.; Belt, S. T.; Connolly, T. J.; Hahn, P.; Scaiano, J. C. *Macromolecules* **1998**, *31*, 9103-9105.

50. Baldovi, M. V.; Cozens, F. L.; Fornes, V.; Garcia, H.; Scaiano, J. C. *Chem. Mater.* **1996**, *8*, 152-160.
51. Korolenko, E. C.; Cozens, F. L.; Scaiano, J. C. *J. Phys. Chem.* **1995**, *99*, 14123-14128.
52. Chateauneuf, J.; Lusztyk, J.; Ingold, K. U. *J. Org. Chem.* **1988**, *53*, 1629-1632.
53. Bowry, V. W.; Ingold, K. U. *J. Am. Chem. Soc.* **1992**, *114*, 4992-4996.
54. Howard, J. A.; Tait, J. C. *J. Am. Chem. Soc.* **1978**, *43*, 4279-4283.
55. Fischer, H. *J. Am. Chem. Soc.* **1986**, *108*, 3925-3927.
56. Fischer, H. *J. Polym. Sci., Part A: Polym. Chem.* **1999**, *37*, 1885-1901.
57. Beckwith, A. J.; Bowry, V. W.; Ingold, K. U. *J. Am. Chem. Soc.* **1992**, *114*, 4983-4992.
58. Skene, W. G.; Scaiano, J. C. **2000**, Manuscript in preparation.
59. Skene, W. G.; Scaiano, J. C.; Listigovers, N. A.; Kazmaier, P. E.; Georges, M. K. *Macromolecules* **2000**, *33*, 5065-5072.
60. Atkins, P. W. *Physical Chemistry*, 5th ed.; W.H. Freeman and Company: New York, 1994, pp 1031.
61. Laidler, K. J.; Meiser, J. H. *Physical Chemistry*; The Benjamin/Cummings Publishing Company, Inc.: Menlo Park, 1982, pp 919.
62. Georges, M. K.; Kee, R. A.; Veregin, R. P. N.; Hamer, G. K.; Kazmaier, P. M. *J. Phys. Org. Chem.* **1995**, *8*, 301-305.
63. Saban, M. D.; Georges, M. K.; Veregin, R. P. N.; Hamer, G. K.; Kazmaier, P. M. *Macromolecules* **1995**, *28*, 7032-7034.
64. Georges, M. K.; Veregin, R. P. N.; Kazmaier, P. M.; Hamer, G. K. *Polym. Prepr.* **1994**, *38*, 870-871.
65. Veregin, R. P. N.; Odell, P. G.; Michalak, L. M.; Georges, M. K. *Macromolecules* **1996**, *29*, 2746-2754.
66. Veregin, R. P. N.; Odell, P. G.; Michalak, L. M.; Georges, M. K. *Macromolecules* **1996**, *29*, 3346-3352.

67. Hammouch, S. O.; Catala, J.-M. *Macromol. Rapid. Commun.* **1996**, *17*, 683-691.

68. Georges, M. K.; Listigovers, N. A.; Odell, P. G.; Hamer, G. K.; Quilan, M. H.; Veregin, R. P. N. *Polym. Prepr.* **1997**, *38*, 454-455.

69. Veregin, R. P. N.; Kazmaier, P. M.; Odell, P. G.; Georges, M. K. *Chem. Lett.* **1997**, *5*, 467-468.

70. Grimaldi, S.; Finet, J.-P.; Zeghdaoui, A.; Tordo, P.; Benoit, D.; Gnanou, Y.; Fountanille, M.; Nicol, P.; Pierson, J.-F. *Polym. Prepr.* **1997**, *38*, 651-653.

71. Georges, M. K.; Veregin, R. P. N.; Kazmaier, P. M.; Hamer, G. K. *Trends Polym. Sci.* **1994**, *2*, 66-72.

72. Kobatake, S.; Harwood, H. J.; Quirk, R. P.; Priddy, D. B. *J. Polym. Sci. A. Polym. Chem.* **1998**, *36*, 2555-2561.

73. Moffat, K. A.; Hamer, G. K.; Georges, M. K. *Macromolecules* **1999**, *32*, 1004-1012.

74. Yoshida, E.; Nakamura, M. *Polym. J.* **1998**, *30*, 915-920.

75. Yoshida, E.; Sugita, A. *J. Polym. Sci. A. Polym. Chem.* **1998**, *36*, 2059-2068.

76. Georges, M. K.; Odell, P. G.; Veregin, R. P. N.; Keoshkerian, B. *Polym. Prepr.* **1997**, *38*, 721-722.

77. Platkowski, K.; Reichert, K.-H. *Chem. Ing. Techn.* **1999**, *71*, 493-496.

78. Bon, S. A. F.; Chambard, G.; German, A. L. *Macromolecules* **1999**, *32*, 8269-8276.

79. Veregin, R. P. N.; Odell, P. G.; Michalak, L. M.; Georges, M. K. *Macromolecules* **1996**, *29*, 4161-4163.

80. Dewar, M. J. S.; Zoebisch, E. G.; Healy, E., F.; Stewart, J. J. P. *J. Am. Chem. Soc.* **1985**, *107*, 3902-3909.

81. Stewart, J. J. P. *J. Comput. Chem.* **1989**, *10*, 209-220.

82. Zerner, M. C. Semiempirical Molecular Orbital Methods. In *Reviews in Computational Chemistry II*; Lipkowitz, K. B., Boyd, D. B., Eds.; VCH:, 1991; 313-359.

83. Stewart, J. J. P. Semiempirical Molecular Orbital Methods. In *Reviews in Computational Chemistry I*; Lipkowitz, K. B., Boyd, D. B., Eds.; VCH:, 1990; 45-81.

84. Fabian, W. M. F. *J. Comput. Chem.* **1988**, *9*, 369-677.

85. Stewart, J. J. P. *J. Comput. Chem.* **1989**, *10*, 221-264.

86. Feigel, M.; Strassner, T. *Theochem.* **1993**, *283*, 33-48.

87. Coussens, B.; Pierloot, K.; Meier, R. J. *Theochem.* **1992**, *259*, 331-344.

88. Burke, L. A.; Krishnan, P. N.; Morris, R. E.; Famini, G. R. *J. Org. Chem.* **1992**, *5*, 614-616.

89. Dos Santos, H. F.; De Almeida, W. B. *Theochem.* **1995**, *335*, 129-139.

90. Karelson, M.; Katritzky, A. R.; Zerner, M. C. *J. Org. Chem.* **1991**, *56*, 134-137.

91. Hohenberg, P.; Kohn, W. *Phys. Rev. B.* **1964**, *136*, 864.

92. Kohn, W.; Sham, L. J. *Phys. Rev. A* **1965**, *140*, 1133.

93. Olah, G. A.; Rasul, G.; Heiliger, L.; Prakash, G. K. S. *J. Am. Chem. Soc.* **1996**, *118*, 3850-3583.

94. Chachaty, C.; Mathieu, C.; Mercier, A.; Tordo, P. *Mag. Res. Chem.* **1998**, *36*, 46-54.

95. Le Mercier, C.; A., G.; Siri, D.; Tordo, P.; Marque, S.; Martschke, R.; Fischer, H. *Polym. Prepr.* **1999**, *40*, 313-314.

96. Le Mercier, C.; Bernard-Henriet, C.; de Sainte-Claire, V.; Le Moigne, F.; Tordo, P. *Polym. Prepr.* **1999**, *40*, 403-404.

97. Le Moigne, F.; Mercier, A.; Tordo, P. *Tetrahedron Lett.* **1991**, *32*, 3841-3844.

98. Mathieu, C.; Tuccio, B.; Lauricella, R.; Mercier, A.; Tordo, P. *J. Chem. Soc., Perkin Trans. 2* **1997**, *12*, 2501-2505.

99. Stipa, P.; Finet, J.-P.; Le Moigne, F.; Tordo, P. *J. Org. Chem.* **1993**, *58*, 4465-4468.

100. Fukuda, T.; Goto, A.; Ohno, K. *Macromol. Rapid Commun.* **2000**, *21*, 151-165.

101. Ciriano, M. V.; Korth, H.-G.; van Scheppingen, W. B.; Mulder, P. *J. Am. Chem. Soc.* **1999**, *121*, 6375-6381.

102. Turro, N. J. *Modern Molecular Photochemistry*; University Science Books: Sausalito, 1991, pp 628.

103. Wintgens, V.; Johnston, L. J.; Scaiano, J. C. *J. Am. Chem. Soc.* **1988**, *110*, 511-517.

104. Turro, N. J.; Anderson, D. R.; Chow, M.-F.; Chung, C.-J.; Kraeutler, B. *J. Am. Chem. Soc.* **1981**, *103*, 3892-3896.

105. Gould, I. R.; Baretz, B. H.; Turro, N. J. *J. Phys. Chem.* **1987**, *91*, 925-929.

106. Baumann, N. *Helv. Chim. Acta* **1972**, *55*, 2716-2723.

107. Wagner, P. J. *Tetrahedron Lett.* **1967**, *1*, 1753-1756.

108. Braslavsky, S. E.; Heihoff, K. Photothermal Methods. In *Handbook of Photochemistry*; Scaiano, J. C., Ed.; CRC Press, Inc.: Boca Raton, 1989; Vol. 1; 327-355.

109. Braslavsky, S. E.; Heibel, G. E. *Chem. Rev.* **1992**, *92*, 1381-1410.

110. Robbins, W. K.; Eastman, R. H. *J. Am. Chem. Soc.* **1970**, *92*, 6076-6077.

111. Turro, N. J.; Kraeutler, B.; Anderson, D. R. *J. Am. Chem. Soc.* **1979**, *101*, 7435-7437.

112. Barltrop, J. A.; Coyle, J. D. *J. Am. Chem. Soc.* **1968**, *90*, 6584-6588.

113. Baum, E. J.; Wan, J. K. S.; Pitts, J. N. J. *J. Am. Chem. Soc.* **1966**, *88*, 2652-2659.

114. Baretz, B. H.; Turro, N. J. *J. Am. Chem. Soc.* **1983**, *105*, 1309-1316.

115. Turro, N. J.; Gould, I. R.; Baretz, B. H. *J. Phys. Chem.* **1983**, *87*, 531-532.

116. Step, E. N.; Buchachenko, A. L.; Turro, N. J. *J. Am. Chem. Soc.* **1994**, *116*, 5462-5466.

117. Step, E. N.; Tarasov, V. F.; Buchachenko, A. L.; Turro, N. J. *J. Phys. Chem.* **1993**, *97*, 363-373.

118. Gould, I. R.; Zimmt, M. B.; Turro, N. J.; Baretz, B. H.; Lehr, G. F. *J. Am. Chem. Soc.* **1985**, *107*, 4607-4612.

119. Wagner, P. J.; Kelso, P. A.; Kemppainen, A. E.; McGrath, J. M.; Schott, H. N.; Zepp, R. G. *J. Am. Chem. Soc.* **1972**, *94*, 7506-7512.

120. Wagner, P. J.; Kelso, P. A.; Zepp, R. G. *J. Am. Chem. Soc.* **1972**, *94*, 7480-7488.

121. Carmichael, I.; Hug, G. L. *J. Phys. Chem. Ref. Data* **1986**, *15*, 1-250.

122. Carmichael, I.; Helman, W. P.; Hug, G. L. *J. Phys. Chem. Ref. Data* **1987**, *16*, 239-260.

123. Weiner, S. A.; Hammond, G. S. *J. Am. Chem. Soc.* **1969**, *91*, 986-991.

124. Tanner, D. D.; Rahimi, P. M. *J. Am. Chem. Soc.* **1982**, *104*, 225-229.

125. Benson, S. W. *J. Phys. Chem.* **1985**, *89*, 4366-4369.

126. Bradley, J. N.; Rabinovitch, B. S. *J. Chem. Phys.* **1962**, *361*, 3498-3499.

127. Gibian, M. J.; Corley, R. C. *J. Am. Chem. Soc.* **1972**, *94*, 4178-4183.

128. Gleixner, G.; Olaj, O. F.; Breitenbach, J. W. *Angew. Makromol. Chem.* **1979**, *180*, 2581-2590.

129. Koroli, L. L.; Kuzmin, V. A.; Khudyakov, I. V. *Int. J. Chem. Kin.* **1984**, *16*, 379-396.

130. Roginskii, V. A. *Zh. Org. Khim.* **1989**, *25*, 449-461.

131. Skene, W. G. "Final report for PAC studies done at the Max-Planck-Institut für Strahlenchemie, Germany under the auspices of a DAAD scholarship.," Max-Planck-Institut für Stralhenchemie, 1998.

132. Skene, W. G.; Scaiano, J. C.; Yap, G. P. A. *Macromolecules* **2000**, *33*, 3536-3542.

133. Gratton, D. W.; Carlsson, D. J.; Howard, J. A.; Wiles, D. M. *Can. J. Chem.* **1979**, *57*, 2834-2842.

134. Mahoney, L. R.; Mendenhall, G. D.; Ingold, K. U. *J. Am. Chem. Soc.* **1973**, *95*, 8610-8614.

135. National Institute of Standards and Technoloy Chemistry Web Book. http://webbook.nist.gov/chemistry/ (21 March 2000).

136. Tsang, W. *Shock Tubes in Chemistry*; M. Dekker: New York, 1981, .

137. Wayner, D. D. M.; Parker, V. D. *Acc. Chem. Res.* **1993**, *26*, 287-229.

138. Robaugh, D. A.; Stein, S. E. *Int. J. Chem. Kin.* **1981**, *13*, 445-462.

139. Lebedev, Y. A.; Rozantzev, E. G.; Kalashnikova, L. A.; Lebedev, V. P.; Neiman, M. B.; Apin, A. Y. *Dokl. Phys. Chem.* **1966**, *168*, 460-462.

140. Yaws, C. L.; Chiang, P.-Y. *Chem. Eng.* **1988**, 81-87.

141. Prosen, E. J.; Rossini, F. D. *J. Res. N.B.S.* **1945**, *34*, 59-63.

142. Guthrie, J. P. *Can. J. Chem.* **1978**, *56*, 962-973.

143. Lias, S. G.; Bartmess, J. E.; Liebman, J. F.; Holmes, J. L.; Levin, R. D.; Mallard, W. G. *J. Phys. Chem. Ref. Data* **1988**, *17*, 1-188.

144. Morishima, I.; Yoshikawa, K.; Yonezawa, T.; Matsumoto, H. *Chem. Phys. Lett.* **1972**, *16*, 336-340.

145. Chase, M. W.; Davies, C. A.; Downey, J. R.; Frurip, D. J.; McDonald, R. A.; Syverud, A. N. *J. Phys. Chem. Ref. Data* **1985**, *14*, 1-1856.

146. Noelke, M.; Verevkin, S. P.; Beckhaus, H.-D.; Ruchardt, C. *Liebigs. Ann.* **1995**, *1*, 41-51.

147. Laarhoven, L. J. J.; Mulder, P.; Wayner, D. D. M. *Acc. Chem. Res.* **1999**, *32*, 342-349.

148. Benson, S. W. *Thermochemical Kinetics*, 2nd ed.; John Wiley & Sons: New York, 1976, pp 320.

149. le Noble, W. J.; Kelm, H. *Ang. Chem. Int. Eng. Ed.* **1980**, *19*, 841-946.

150. Hung, R. R.; Grabowski, J. J. *J. Am. Chem. Soc.* **1992**, *114*, 351-353.

151. Asano, T.; Le Noble, W. J. *Chem. Rev.* **1978**, *78*, 407-489.

152. Roberts, J. D.; Caserio, M. C. *Basic Principles of Organic Chemistry*, 2nd ed.; W.A. Benjamin, Inc.: Menlo Park, 1977, pp 1596.

153. Tamagaki, S.; Ogino, K.; Kozuka, S.; Oae, S. *Tetrahedron* **1970**, *26*, 4675-4689.

154. Burkey, T. J.; Makewski, M.; Griller, D. *J. Am. Chem. Soc.* **1986**, *108*, 2218-2221.

155. Griller, D.; Simoes, J. A. M.; Mulder, P.; Sim, B. A.; Wayner, D. D. M. *J. Am. Chem. Soc.* **1989**, *111*, 7872-7876.

156. Clark, K. B.; Griller, D. *Organometallics* **1991**, *10*, 746-750.

157. Gensch, T.; Churio, M. S.; Braslavsky, S. E.; Schaffner, K. *Photochem. Photobiol.* **1996**, *63*, 719-725.

158. Williams, R.; McDonagh, A. F.; Braslavsky, S. E. *Photochem. Photobiol.* **1998**, *68*, 433-437.

159. Riddick, J. A.; Bunger, W. A.; Sakano, T. K. *Organic Solvents: Physical Properties and Methods of Purification*, 4th ed.; John Willey and Sons: New York, 1986; Vol. II, pp 1325.

160. Schmidt, R. *J. Phys. Chem.* **1998**, *102*, 9082-9086.

161. Itoh, Y.; Gouki, M.; Goshima, T.; Hachimori, A.; Kojima, M.; Karatsu, T. *J. Photochem. Photobiol. A.* **1998**, *117*, 91-98.

162. Churio, M. S.; Angermund, K. P.; Braslavsky, S. E. *J. Phys. Chem.* **1994**, *98*, 1776-1782.

163. Gensch, T.; Braslavsky, S. E. *J. Phys. Chem. B* **1997**, *101*, 101-108.

164. Strassburger, J., M.; Gärtner, W.; Braslavsky, S. E. *Biophys. J.* **1997**, *72*, 2294-2303.

165. Schulenberg, P. J.; Gärtner, W.; Braslavsky, S. E. *J. Phys. Chem.* **1995**, *99*, 9617-9624.

166. Schmidt, R.; Schütz, M. *Chem. Phys. Lett.* **1996**, *263*, 795-802.

167. Clark, K. B.; Wayner, D. D. M.; Demirdji, S. H.; Koch, T. H. *J. Am. Chem. Soc.* **1993**, *115*, 2447-2453.

168. Wayne, G. S.; Synder, G. J. *J. Am. Chem. Soc.* **1993**, *115*, 9860-9861.

169. Scaiano, J. C. *J. Am. Chem. Soc.* **1980**, *102*, 7747-7753.

170. Scaiano, J. C.; Tanner, M.; Weir, D. *J. Am. Chem. Soc.* **1985**, *107*, 4396-4403.

171. Belt, S.; Scaiano, J. C.; Whittlesey, M. K. *J. Am. Chem. Soc.* **1993**, *115*, 1921-1925.

172. Peters, K. S.; Snyder, G. J. *Science* **1988**, *241*, 1053-1057.

4. LFRP Initiator Kinetics

4.1 Introduction

The living properties of polymers derived from nitroxide mediated polymerization were shown to be a result of the labile C-O bond that undergoes reversible capping at the polymerization temperatures. This was discussed in depth in the two preceding chapters. The importance of this labile bond and the measurement of the bond dissociation energies (BDE), represented by k_1 in Scheme 4-1, were the focus of the preceding chapter. The complementary reaction to this bond breaking reaction is the carbon center radical trapping by nitroxides. The rate constant for this reaction is represented by k_{-1} in Scheme 4-1. These two reactions occur during the LFRP reaction and an equilibrium is established being in favor of the trapped or dormant species. Like the C-O cleavage measurements, investigation of the rate constants for nitroxide trapping of the carbon centered radical gives valuable information pertaining to the LFRP process. Different trapping rate constants for this back reaction shift the equilibrium of Scheme 4-1 and ultimately affect the amount of propagating radicals produced. The change in equilibrium and radical concentration influences the controlling nature of the polymerization and subsequently modifies the living properties of the polymers obtained. Laser flash photolysis studies were used to examine the influence of nitroxide and carbon centered radical structures upon the bi-molecular rate constant represented by k_{-1}.

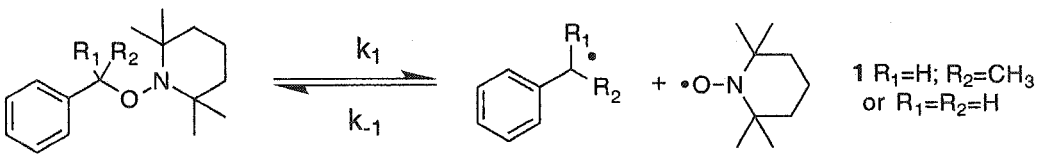

Scheme 4-1. Reversible trapping of the 1-phenylethyl radical or benzylic radicals by nitroxide characteristic of the LFRP process.

The focus of the first section is the investigation of trapping rate constants for a series of unimolecular LFRP initiators that generate different carbon centered radicals and nitroxides upon decomposition. The original investigation was a collaboration between the research groups at the University of Ottawa and the Xerox Research Centre. The following section also examines the nitroxide trapping rate constants for a series of group IV organometallic radicals. The second section equally uses laser flash photolysis to measure the bi-molecular rate constants for a class of organometallic radicals as a tool for the

characterization of a new series of unimolecular LFRP initiators. Common to both of these is the method of laser flash photolysis used to photochemically generate the radicals and ultimately determine the desired rate constants. This technique is primarily used because the rate constants for the coupling reactions are known to be fast yet below the diffusion controlled limit.[1-3]

4.2 Results and Discussion

The usefulness of macromolecular initiators as mimics for the kinetics in the LFRP process were established in the previous chapter. These alkoxyamines were found to be good mimetics for the LFRP reactions and the trapping reaction examined here is also expected to be representative of the LFRP kinetics. The series of unimolecular initiators studied are represented in Figure 4-1. The candidates found in this figure were selected because of the specific radicals they produce upon decomposition. In general, two major classes of carbon centered radicals are produced upon photolysis of these initiators. The first type of carbon centered radical is the 1-phenylethyl radical, which has identical substitution as the propagating radical in the polymerization of styrene. The other radical produced is derived from structure **2** and mimics the propagating propionate radical in the polymerization of acrylates.

4.2.1 Alkoxyamine Initiators

Alkoxyamines initiators, such as those in Figure 4-1, among many others, produce carbon centered radicals and nitroxides in stoichiometric ratios, usually 1:1, either by thermal[4] or photolytic decomposition.[4-13] It is further assumed that the back reaction involving combination of TEMPO or a nitroxide analogue with the carbon centered radical provides a reasonable model for the re-capping reaction involved in the reversible termination of nitroxide-regulated free radical polymerizations. In this sense, the back reaction of the radicals derived from **1-6** can be expected to provide some insight into the dynamics of LFRP. The series of unimolecular initiators were examined to determine the influence of nitroxide and carbon centered radical structure on the back reaction. This provides information pertaining to their capabilities as suitable candidates for LFRP.

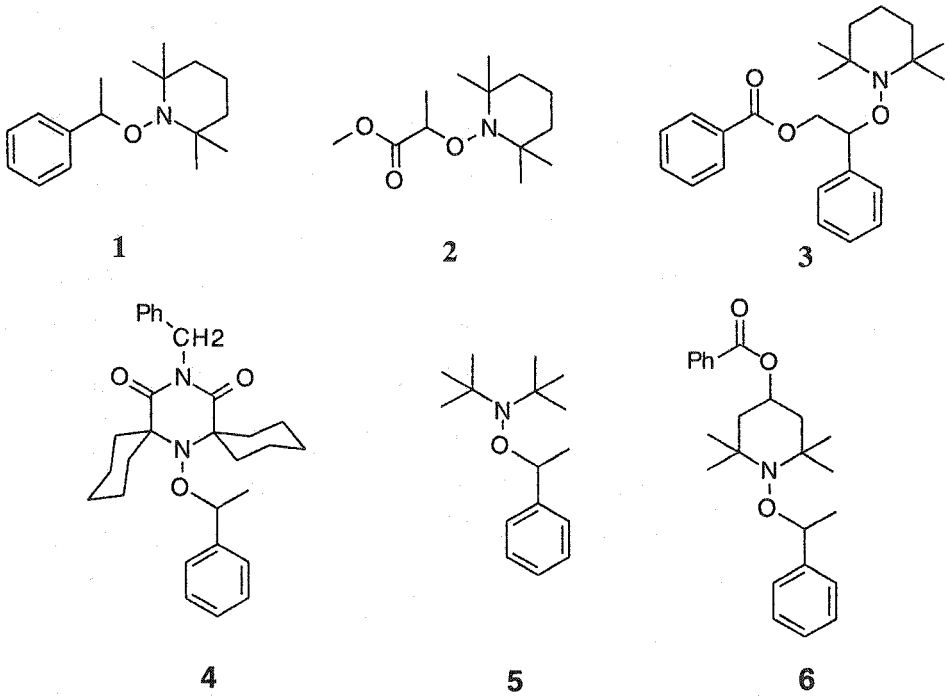

Figure 4-1. Different alkoxyamines initiators for LFRP studied. Compounds 2, 4, and 6 were studied as part of a collaboration with the Xerox Research Centre.

The reactions of carbon centered radicals (R•) with nitroxides have been examined in considerable detail by Ingold et al.[1-3] In general, these reactions are quite fast, but below the diffusion controlled limit (~ 10^{10} M^{-1} s^{-1} for acetonitrile), and show a dependence on the polarity of the solvent, being slower in polar solvents. A few representative rate constants for TEMPO at room temperature are given in Table 4-1; they show that the rate constant for trapping is greater for aliphatic radicals. This is due primarily to the difference in thermodynamic stability of the radical in addition to steric effects.[1-3]

Table 4-1. Rate constants for the reactions of carbon-centered radicals with TEMPO.[2,3,14]

Radical	Solvent	k (10^{-7} $M^{-1}s^{-1}$)
n-Nonyl	Acetonitrile	15
$C_6H_5CH_2\bullet$	Acetonitrile	9.5
n-Nonyl	Cyclohexane	85
$C_6H_5CH_2\bullet$	Cyclohexane	41
n-Nonyl	Isooctane	123
$(CH_3)_3CCH_2\bullet$	Isooctane	96
$C_6H_5CH_2\bullet$	Isooctane	48
$C_6H_5CH\bullet(CH_3)$	Isooctane	16
$C_6H_5C\bullet(CH_3)_2$	Isooctane	12

In the simplest of cases, such as **1**, the decay of the radicals can be monitored under two distinct set of conditions with reference to the relative concentrations of the two radicals. The first case concerns two radicals that are produced in *identical* concentrations, as in reaction 1; then, their back reaction should follow second-order kinetics. In general, k_2 (Equation 2) is faster than k_3 (Equation 3) shown in Scheme 4-2. Thus, self reaction (e.g. benzyl radicals) tends to dominate when both radicals are present in equal concentrations. The example given in Scheme 4-2 illustrates the reaction with TEMPO, but the same ideas apply to other nitroxides.

In the second case, when the persistent radical (nitroxide) is present in higher concentration, or if it accumulates during the experiment, reaction 3 dominates and the process follows pseudo-first-order kinetics.[15,16] This is a characteristic example of the Fischer-Ingold persistent free radical effect.[17,18] The experiments were carried out under these conditions (either by accumulation or addition of TEMPO) since they are more relevant to LFRP. The simplest way to achieve this is by direct photolysis of the initiators in the presence of various concentrations of added nitroxides in order to determine the pseudo-first order rate constant for

radical decay. However, some of the initiators in the series were not easily analyzed by this method and other methods were required (*vide infra*). The rate constants measured in this study refer exclusively to the coupling reaction of the carbon centered radical by the nitroxide shown in Equation 3.

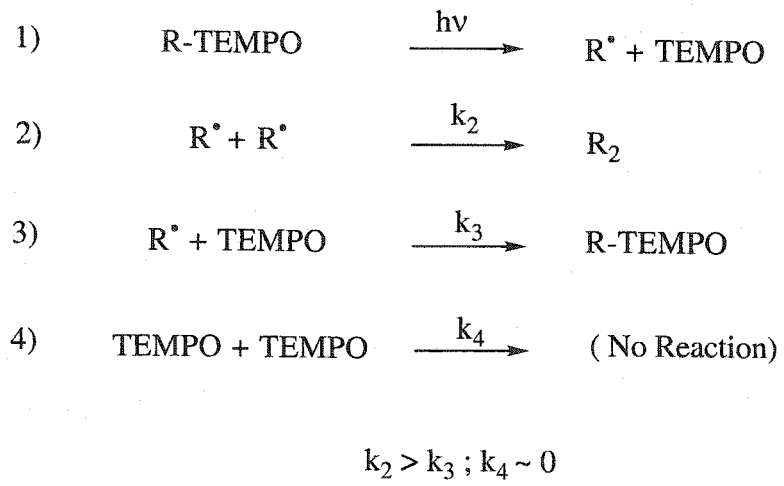

Scheme 4-2. Reaction scheme for LFRP process of alkoxyamines.

Initiators **1** and **3** have also been extensively studied[1-3,14,19-26] as model compounds to probe the properties of LFRP. The initiator **1** is a relatively simple system that has previously been studied by this research group both in terms of thermodynamics[4,5] and kinetics.[27,28] Therefore, the rate constants derived from this initiator should shed some insight into the kinetics of the polymerization of styrene systems. Upon laser excitation at 266 nm, **1** undergoes the C-O bond fragmentation within the laser pulse (~ 10 ns) and subsequently gives rise to the characteristic signal due to 1-phenylethyl radical with λ_{max} 319 nm (compare with benzyl radicals, λ_{max} 317 nm).[29] An expanded section of the relevant part of the transient spectrum is shown in Figure 4-2.

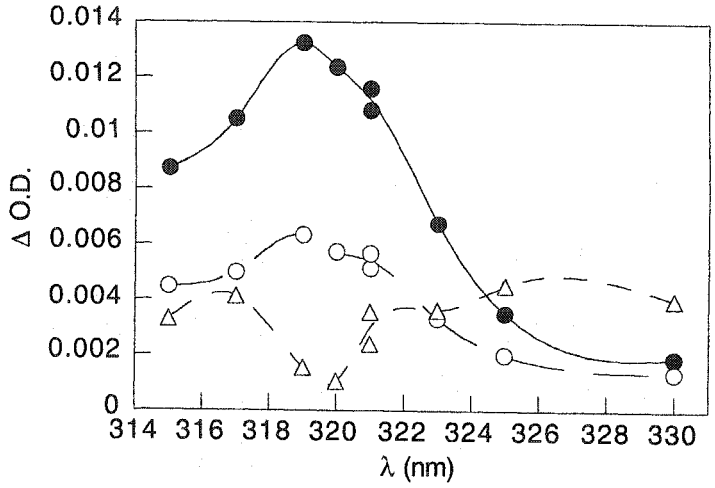

Figure 4-2. 1-Phenylethyl radical recorded in acetonitrile, recorded at 2.32 (●), 8.88 (○), and 11.9 (Δ) μs after laser pulse derived from direct photolysis of 1 with 266 nm excitation.

Carbon centered radicals are rapidly scavenged by free nitroxides and any residual nitroxide may influence the radical lifetimes. In order to avoid erroneous results arising from this possibility, the nitroxide concentration was carefully determined by two methods. The two slightly different approaches were used in the determination of the rate constants. In one method (referred to as the 'multiple cell' method), a series of samples were prepared containing equal concentrations of 1 and variable concentrations of added nitroxide. The lifetimes of the 1-phenylethyl radical were determined for each sample (a representative trace is shown in the inset of Figure 4-3) and the TEMPO concentration quenching plot obtained by this method as seen in Figure 4-3, where k_{obs} is the reciprocal of the radical lifetime. Note that the values of k_{obs} correspond to k_3[TEMPO] under strictly pseudo-first order conditions. The desired k_3 value (Equation 3) is obtained from the slope of various nitroxide concentrations as a function of k_{obs}, as shown in Figure 4-3.

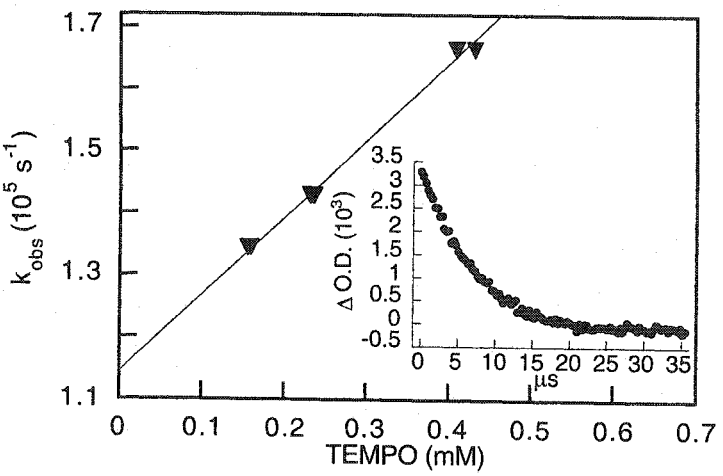

Figure 4-3. Quenching plot of 1-phenylethyl radical as a function of TEMPO concentration monitored at 319 nm in acetonitrile using the multiple cell method. Inset: Decay of 1-phenylethyl radical also in acetonitrile also monitored at 319 nm.

In the second method (referred to as the 'single cell' method), portions of a TEMPO stock solution were added to a single cell and the radical lifetime determined after each addition. At the end of the experiment the nitroxide concentration was determined based on HPLC analysis. In the example of Figure 4-4, the nitroxide was found to be 0.287 mM compared with 0.259 mM based on the sum of injected amounts. The difference is consistent with some accumulation of TEMPO due to photolysis of 1 combined with minor HPLC calibration errors. The difference is relatively small and influences the rate constant only marginally. All measurements were performed under conditions where the radical decay followed first-order kinetics.

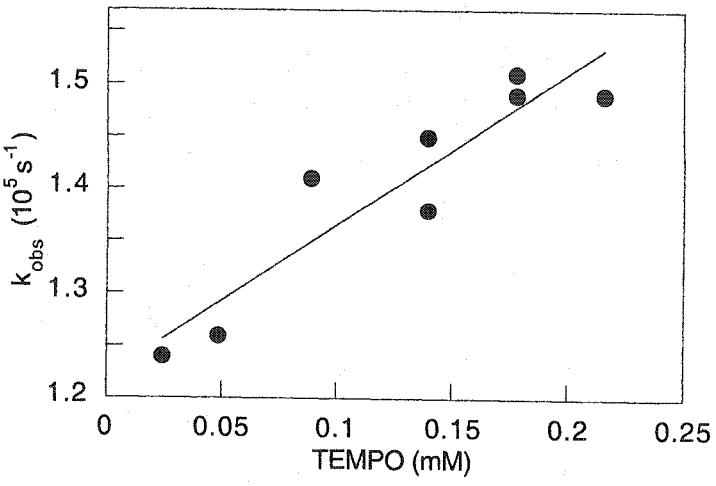

Figure 4-4. Quenching of 1-phenylethyl radical with TEMPO monitored at 319 nm in acetonitrile with the single cell method.

The values of k_3 obtained by both methods are given in Table 4-2 and lead to an average of 1.34 x 10^8 M^{-1} s^{-1} for the 1-phenylethyl radical reacting with TEMPO. For the related benzyl radical, reported values are 4.8 x 10^8 $M^{-1}s^{-1}$ and 9.5 x 10^7 M^{-1} s^{-1} in isooctane and acetonitrile, respectively.[2,3] It should be noted that in Ingold's work,[1] which reported values of 1.6 and 1.9 x 10^8 M^{-1} s^{-1} for the same system in isooctane, the radicals were generated by reaction of *tert*-butoxyl radical with toluene or the corresponding alkyl aromatic compound (*vide infra*). These reactions are not 'instantaneous' sources of the radical[30] and may lead to somewhat slower apparent rate constants. We have previously determined[31] the rate of TEMPO trapping for the benzylic system in acetonitrile to be 2.1 x 10^8 M^{-1} s^{-1} derived from an essentially instantaneous source of benzyl radicals. The measured rate constant supports the fact that the values derived from reactions of *tert*-butoxyl radicals lead to inherently slower rate constants. The rate constant obtained here is somewhat slower partly because of the solvent polarity, as the solvent for the study is slightly more polar than that used by Ingold.[2]

Table 4-2. Summary of results obtained by quenching various carbon centered radicals with various nitroxides in acetonitrile.

Initiator	Radical gen. method[a]	k_3 (10^8 $M^{-1}s^{-1}$)	Other information
1	Direct	1.24	multiple cells
	Direct	1.34	single cell
2	Direct	30	multiple cells
	Direct	20	single cell
3	Direct	(1.8)	single cell, value uncertain, see text
	Probe	5.0	single cell
4	H-abstraction	0.95	mixed solvent with acetonitrile
	2,4-diphenyl propanone	2.0	
5	Direct	0.71	
	2,4-diphenyl propanone	0.87	
6	Direct	0.98	

Initiator **2** is an ideal model for probing the polymerization dynamics of acrylates and understanding the overall kinetics of polymerization of this aliphatic system in general. This is of interest because most research has focused primarily on styrene systems.[32,33] The lack of published material on the acrylate systems has been mostly due to the difficulty in obtaining "living" qualities, although recently the Xerox and IBM groups have had some success in polymerizing acrylates.[34-38] Only few examples[39-43] have concentrated on analyzing the kinetics of nitroxides in the polymerization of acrylates. Therefore, **2** represents

an ideal model compound to investigate the capping kinetics of acrylates in order to compare them to the LFRP of styrene-based systems.

The acrylate initiator **2** has no pendant aromatic group; this led us to anticipate that the radical generated by direct photolysis would be invisible to our LFP system. However, direct photolysis of **2** produced the transient spectrum as shown in Figure 4-5 and the maximum at 262 nm is ascribed to the methyl propionate radical.[44] The radical in not resonance stabilized and is therefore expected to be blue shifted compared to benzylic radicals.[29,45] The methyl propionate radical has only a weak absorbance in the 260 nm region, which makes it difficult to analyze given the proximity of this wavelength to that of the intense 266 nm laser. TEMPO itself absorbs at this wavelength, thus effectively attenuating the monitoring beam from a xenon lamp employed in these experiments. In spite of these difficulties, we were able to record the radical lifetime (inset in Figure 4-5) and spectrum with good signal-to-noise ratio. Therefore, quenching of the radical derived from **2** can be observed directly with TEMPO addition.

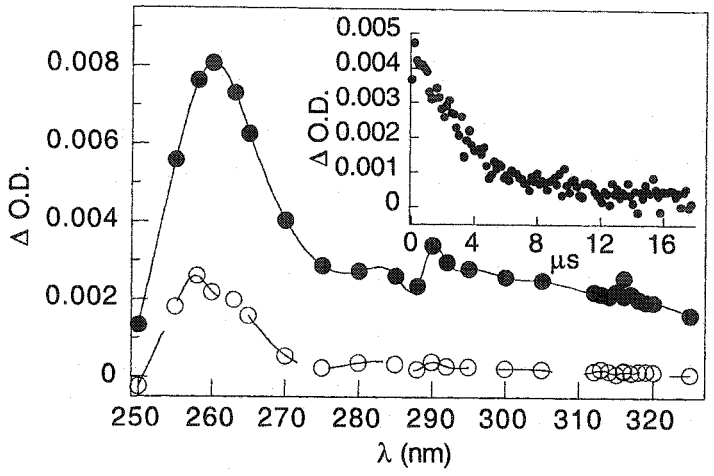

Figure 4-5. Transient spectrum of methyl propionate radical in acetonitrile recorded at 4.16 (●), 17.8 (○) μs after initial laser pulse. Inset: Decay of methyl propionate radical at 260 nm after excitation at 266 nm.

As was the case with **1**, two methods of determining the nitroxide concentration were used for **2**. Two determinations by the multiple cell method were done and led to the rate constant included in Table 4-2. All measurements were carried out under conditions where the decay followed first-order kinetics. However, in the

absence of added nitroxide in fresh samples, the radical decay occurs with a mixture of first and second order kinetics. If the sample is exposed to a number of laser shots, the decay gradually becomes shorter and first-order kinetics dominate as a result of TEMPO accumulation. In a preliminary experiment, a sample in this fashion was examined until we observed that a single exponential could easily fit the decay. HPLC analysis of this sample served to guide us in order to employ adequate concentrations of TEMPO, i.e., high enough to fit first-order kinetics, yet low enough to minimize problems due to competitive light absorption by TEMPO. The results using the multiple cell approach are shown in Figure 4-6 lead to $k_3 = 3.0 \times 10^9$ M^{-1} s^{-1}. These measurements were far more difficult than those were for **1**.

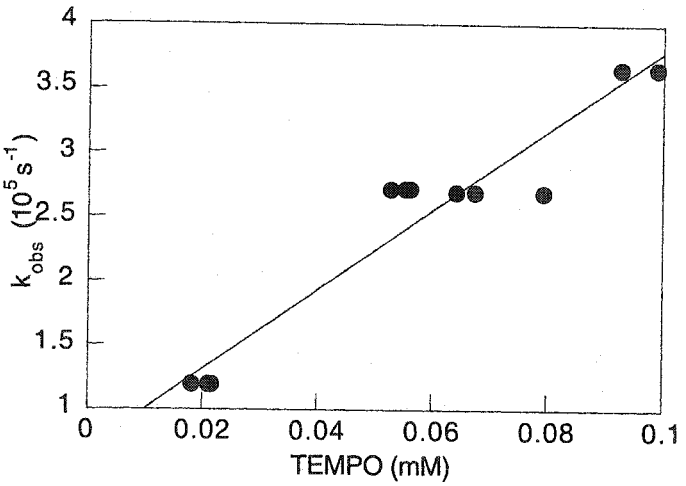

Figure 4-6. Quenching of methyl propionate radical with TEMPO monitored at 260 nm in acetonitrile using the multiple cell method.

Attempts to measure this system with the single cell method led to complications as indicated by systematic negative intercepts in plots such as that of Figure 4-6. The accumulation of nitroxide tends to introduce errors, and possibly some photodecomposition of TEMPO occurs at the shorter wavelengths, with anticipated product accumulation in the single cell method.[46] Overall, the multiple cell method is more reliable in this case.

The typical initiator used for LFRP in the benzoyl peroxide-styrene-TEMPO adduct, **3**, which is structurally similar to **1** with the exception of an additional benzoyl moiety. With this in mind, we anticipated that this system would be easily studied. It was expected that the TEMPO C-O photoinduced cleavage (see

Equation 5) would lead to a benzylic radical with significant absorption in the 320 nm region similar to the spectrum in Figure 4-2 for **1**. However, analysis of this commonly used initiator proved quite difficult and the results of quenching are inconclusive due to the difficulty in assigning the transients in the spectrum obtained.

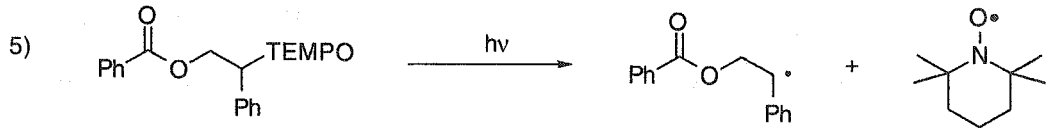

3 8

Scheme 4-3. Anticipated photodecomposition of benzoylbenzoate LFRP initiator.

If the mechanism of Equation 5 was the only important photochemical process, one would expect to observe essentially instantaneous formation of radical **8** followed by its decay. In other words, the study would follow closely the observations for the case of **1**. The spectra recorded upon laser photolysis of **3** are shown in Figure 4-7; note that the two bands at 260 and ~320 nm decay with different kinetics and are appreciably different from **1**. From this figure it is clear that at least two species are involved. In fact, a decay trace at 320 nm follows bi-exponential decay, suggesting that more than one species absorb at this wavelength. This is illustrated in the insert of Figure 4-7 that leads to lifetimes of 0.38 and 5.5 μs, with weights of essentially 50% each. To our surprise, at 260 nm we observe a signal growth in the 1.2 μs time scale. The kinetics for this growth is concurrent with the decay of the fast portion of the decay observed at 320 nm, thus suggesting that the short-lived 320 nm intermediate is the precursor of the 260 nm signal. The growth of the yet unidentified transient is illustrated in the inset of Figure 4-7. In cyclohexane, the kinetics at 260 and 320 nm also agree and both are absent under oxygen saturation, suggesting the involvement of free radicals. The response to TEMPO addition is also different at the two wavelengths. At 320 nm TEMPO quenching leads to a bimolecular rate constant of 2.1 x 10^9 M^{-1} s^{-1} for the fast component and 1.8 x 10^8 M^{-1} s^{-1} quenching for the slow component at this absorption. Meanwhile, the growth at 260 nm gives rise to a rate constant of 9.2 x 10^9 M^{-1} s^{-1} under identical quenching conditions. The slower rate constant for TEMPO quenching at 320 nm is assumed to be the desired rate constant because the order of magnitude is similar to other benzylic radicals. The faster component is probably due to quenching of

an excited state by TEMPO as nitroxides are known to quench triplets with similar rate constants.[47]

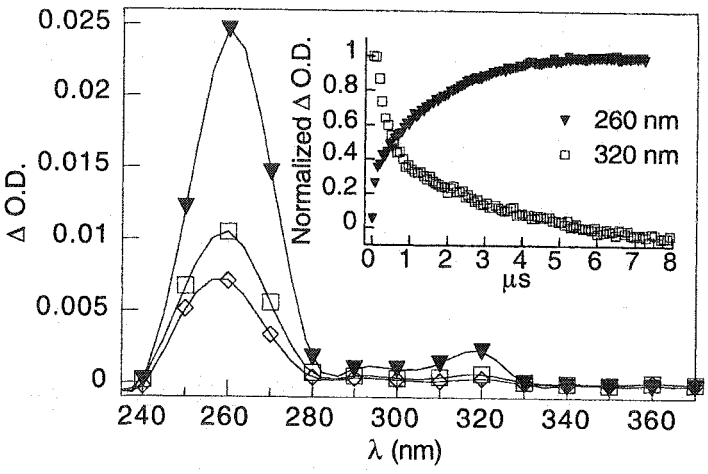

Figure 4-7. Transient spectrum of 3 in acetonitrile recorded 2.08 (▼), 9.04 (□), and 11.9 (◊) μs after initial laser pulse. Inset: Transients recorded after 266 nm excitation pulse with normalized Δ O.D. Growth of transient (▼) monitored 260 nm. Time scale is multiplied by 4. Decay of transient (□) recorded at 320 nm.

Product studies are difficult due to the instability of **3** to GC conditions. In any event, it is clear from HPLC that the products of photodecomposition of **3** include styrene, but not benzoic acid. It is possible that if benzoyloxyl radicals are formed they will decarboxylate almost quantitatively in the inert solvent. At high conversions, the products identified by LC-MS are **1**, hydroxylamine and minor amounts of styrene. The true amount of styrene produced may be greater since the ionization method used for this analysis is not ideal for olefin detection. In general, the photolysis of **3** leads to mixed decomposition and it is uncertain as to what is being quenched by the nitroxide since TEMPO is known to quench triplets,[47] undergo electron transfer,[48,49] radical trapping,[1-3] in addition to hydrogen abstraction,[50,51] albeit slower than the other processes. The unexpected photochemical behavior of **3** is the focus of a full investigation in the chapter treating photoinitiators.

In order to determine the rate constant for TEMPO quenching of **3**, a model compound, **7**, was synthesized. The TEMPO-free analog can give the desired radical by hydrogen abstraction of the α-hydrogen by *tert*-butoxyl radical.[30] Simple photolysis of **7** at 266 nm yields transients that cannot be identified and

implies the participation of the carbonyl group in complex photochemistry. However, 308 or 337 nm excitation gives no detectable transients, as expected, and allows for studies using the hydrogen abstraction method. Reaction of 7 with *tert*-butoxyl yields the desired substituted 1-phenylethyl radical 8 by hydrogen abstraction schematically represented by Equation 6.

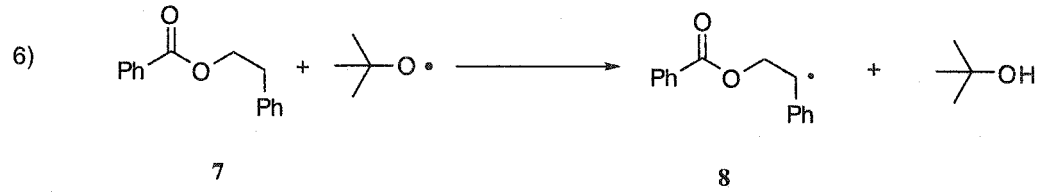

7 8

Scheme 4-4. Hydrogen abstraction of benzoylbenzoate leading to radical 8.

The spectra obtained by reaction with 7 and with ethylbenzene are essentially identical and indicate that the desired benzylic radical is being generated. However, the reaction of 7 shown in Scheme 4-4 does not produce a transient at 260 nm. Since the signal of radical 8 derived from 7 by hydrogen abstraction was weak, it was thought that the abstraction could also occur at the β-position. Steady state irradiation at 300 nm with 1.2 equivalents of TEMPO and 7 dissolved in neat Bu^tOOBu^t gave only 3, confirmed by NMR. Therefore α-abstraction occurs exclusively, albeit with a low efficiency.

The absence of the benzoyl moiety in compound 4 would lead one to anticipate that its direct photochemistry would be less complicated than that experienced with compound 3. The transient absorption spectrum recorded in acetonitrile with 266 nm excitation did not yield the characteristic maxima ca. 319 nm and 305 nm, typical of the 1-phenylethyl radical. In lieu was a broad absorption band spanning from 270 to 350 nm possibly a result of the secondary photochemistry involving the functionalities in the 3, 4, and 5 positions on the nitroxide moiety.

A probe method similar to Ingold et al. was used to determine the desired trapping rate of 8 with TEMPO.[1] The probe used was 1,1-diphenylethylene (10) which forms an adduct with carbon centered radicals (11). The resulting radical shown in reaction 7 is detectable by the LFP apparatus ca. 329 nm.[1,2,52,53] The trapping rate constant of radical 8 with TEMPO can subsequently be determined without the problems discussed above by monitoring the growth of the adduct under various concentrations of added nitroxide.

7)

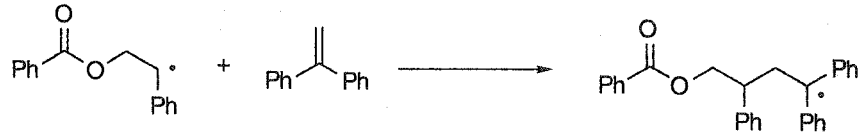

8 10 11

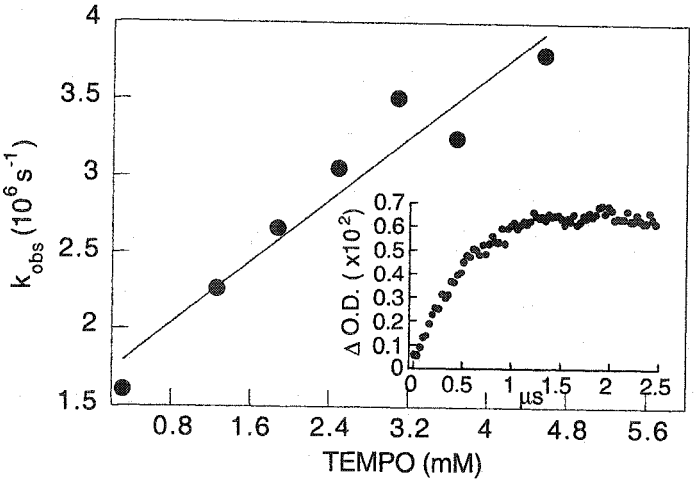

Figure 4-8. Quenching of 8 by TEMPO derived from 7. Inset: Growth of radical 11 monitored at 329 nm.

Similar to compound **3**, **4** seems to produce two transients which are indicated by the bi-exponential decay at 314 nm and a similar growth rate at 250 nm. The kinetics of these two species are identical within experimental error and suggest complex photochemistry. The 314 nm transient is quenched by Bodaz with a rate constant of 2.1 x 10^9 M^{-1} s^{-1}, too fast to involve a benzylic radical.

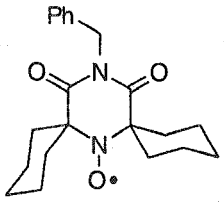

Bodaz

In order to circumvent this problem, the radical can be prepared by two alternate routes: hydrogen abstraction from 1 M solution of ethylbenzene gives the 1-

phenylethyl radical where its decay can be monitored at 319 nm as a function of Bodaz concentration leading to a rate constant of 9.5×10^7 M^{-1} s^{-1}.

The Norrish Type I reaction gives better values than the hydrogen abstraction method because the latter is inherently slower due to the multistep reactions that are required to produce the 1-phenylethyl radical. Photolysis of **9** yields the radical rapidly and efficiently.[54-58] Upon photolysis, α-cleavage occurs giving rise to a 1-phenylethyl radical and an acyl radical that rapidly decarbonylates. The photoinduced decomposition of **9** is represented by Equation 8.

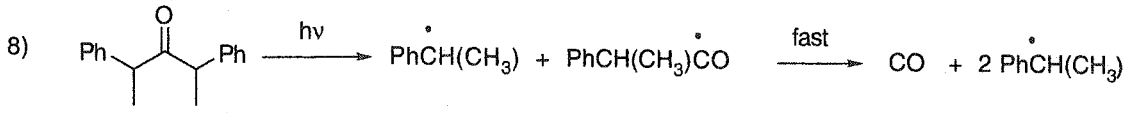

9

Scheme 4-5. Photodecomposition of 1,3-dimethyl-1,3-diphenylpentae-3-one leading to 1-phenylethyl radical.

The Norrish Type I reaction of **9** was used in order to determine accurate quenching constants corresponding to the back reaction leading to compounds **4** and **6**. In contrast with the di-*tert*-butyl peroxide method, the substituted ketone is a fast precursor of two 1-phenylethyl radicals,[56,57] thereby leading to better rate constants for nitroxide trapping.

Compound **5** differed from the previous compounds in that it afforded the typical 1-phenylethyl radical by homolytic C-O bond cleavage by direct 266 nm excitation. The absorption spectrum of the radical gave the characteristic absorptions at 304 and 320 nm and the decay of the latter was monitored as a function of nitroxide concentration. The rate constant obtained is similar to those obtained for related systems (see Table 2). The indirect method, as used for compound **4** using Bu^tOO^tBu with ethylbenzene, was used to verify k_3 for compound **5** and led to a slightly slower rate constant, as usual. A rate constant was determined for the quenching the 1-phenylethyl radical derived from **9** by di-*tert*-butyl nitroxide. This value is identical to that derived from the direct method within experimental error.

The ketone method was also used to determine the rate constants for compound **6** as the benzoyl group on the nitroxide would lead to difficulties as encountered with **3**.

The initiators that have been examined can be grouped into two major classes based on the type of carbon centered radical generated upon decomposition, aliphatic and aromatic. The pseudo-first order experimental conditions used exclusively yield the rate constants for trapping of the carbon centered radical by the nitroxide according to Equation 4-3. The aromatic (1-phenylethyl) radicals are all quenched with rate constants around 10^8 M^{-1} s^{-1}, which are well below the diffusion control limit of 10^{10} M^{-1} s^{-1} for acetonitrile. However, the aliphatic radical derived from **2** reacts faster by an order of magnitude. This is mainly due to the carbon centered radical structure and the nitroxide structure. This is apparent from the rate constants measured for **1** and **2** that differ by an order of magnitude and are different only in their carbon centered radical structure. The rate constant for the trapping of the aliphatic radical is similar to that obtained by Ingold et al.[1-3] for the *n*-nonyl radical and possesses fast kinetics when quenched with TEMPO because it lacks resonance stabilization as compared with its aromatic analogue (*vide supra*). The values measured by Ingold et al., shown in Table 4-1, are slower than our experimentally determined value simply because their analysis method involves the use of a probe that produces a spectroscopically visible transient. This method, similar to the hydrogen abstraction reaction, gives somewhat slower rate constants because two relatively slow steps are required before the observed radical is produced. The rate constant for addition of the aliphatic radical generated upon the decomposition of diacyl peroxide to the probe is approximately four orders of magnitude slower than the trapping rate constant of the propionyl radical by TEMPO.[3] The values measured by direct photolysis are in general more accurate as the radical to be observed is generated instantaneously within the laser pulse (~ 10 ns) and the rate limiting step becomes the desired trapping reaction.

The fast rate of trapping for the acrylate probe provides some insight into the dynamics of the initial polymerization process and the problems in achieving living conditions with acrylate systems in general. This poor behavior is possibly due to a combination of detrimental factors. Typical polymerization temperatures (e.g., 125 °C) are most likely too low to induce de-capping of the nitroxide group for acrylate systems, where the C-O bond is probably stronger than in benzylic systems.[4] Any de-capping that does occur will be rapidly reversed. A balance between polymerization temperature and steady state nitroxide concentration must be found for acrylate systems to sustain living polymerization.

Taking **1** to be the benchmark for the other initiators, there appears to be little variation within the rates for the various nitroxide groups. This holds true when comparing the direct methods, when possible, with the radical derived from **9** which provides a convenient fast radical source. The rate constants observed are all within the upper 10^7 M^{-1} s^{-1} and lower 10^8 M^{-1} s^{-1} region. Comparing different nitroxides, only the rate constants for di-*tert*-butyl nitroxide appear to be marginally lower.

The rates of **6** and **1** are essentially identical within experimental error and suggest that substitution at the 4 position of the nitroxide does not play an important role for the kinetic stabilization or destabilization of the radical. Furthermore, the substituent at C-4, despite its bulkiness, is too far away to influence the kinetics.

The only factor that seems to influence the rate of trapping by nitroxide is the nature of the actual carbon centered radical. This is seen between the rates of **2** compared to the other initiators studied. Also, the fast rate obtained for **3** is nearly 5 times faster than that for **1** and the difference lies only with the type of radical generated.

4.2.2 Organometallic Initiators

The key step in LFRP is the trapping of radicals by nitroxides such as TEMPO and was previously described. In this section, laser flash photolysis (LFP) was equally used to examine the rates of trapping of a series of organometallic radicals with TEMPO. Fast rates, yet slightly slower than the diffusional controlled limit, indicate that the organometallic radical generated is trapped by TEMPO in a fashion similar to conventional initiators and may prove to be a novel stoichiometric initiator. This technique has previously been used by this research group for this purpose.[27,59] As an alternative to this, a series of organometallic based initiators that appear to be potential initiators for LFRP is proposed. It should be noted that organometallic initiators may provide a mechanism to insert specific groups at the polymer terminus, either directly or following workup.

The organometallic radicals of silicon, germanium, and tin have been extensively characterized in terms of their reactivity[60-66] and spectroscopic

properties.[64,67] These radicals are particularly well known for their radical mediated reactions in synthetic organic chemistry.[68-72] Here, this knowledge has been expanded to see whether these metal centered radicals would exhibit the same reactivity towards the persistent nitroxide radical and be useful for polymer initiation. Persistent nitroxide free radicals, such as TEMPO, are known to trap carbon radicals at rates below the diffusion controlled limit.[1-3,14] Unfortunately, monitoring some of the organometallic radicals generated cannot be done directly as with carbon based benzylic initiators[8,9] because aliphatic $R_3M\bullet$ radicals are only weakly absorbing, with the exception of the $R_3Sn\bullet$ radical.[64,67] In order to examine the trapping rates, the metallic radicals must be generated using Bu^tOOBu^t.[30] Direct excitation of the peroxide with 337 nm leads to rupture of the O-O bond giving rise to 2 *tert*-butoxyl radicals that further react by hydrogen abstraction to give the metal centered radical. These two steps are seen in Equations 9 and 10 of Scheme 4-6, respectively, where the rate constants for reaction 10 range from 10^6 to 10^8 M^{-1} s^{-1}, depending on the metal center.[64] In order to produce signals that can be detected in a convenient time scale, relatively high concentrations of the hydride precursors are frequently required. In the case of the aryl substituted metal hydrides, the transients can be directly seen and their lifetimes monitored as a function of nitroxide addition. In the absence of any nitroxide and in neat Bu^tOOBu^t, the signal slowly decays according to second order kinetics, consistent with radical-radical reactions. In the presence of scavenger, the decay follows pseudo-first order kinetics. The reciprocal of the lifetime leads to a first order rate constant under pseudo-first order conditions. A typical decay trace for the triaryl metal system is shown in Figure 4-9.

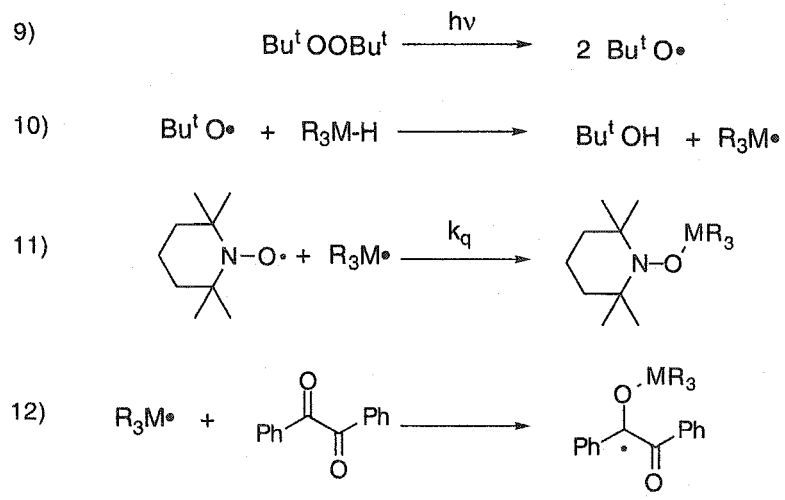

Scheme 4-6. Reaction scheme leading to organometallic radicals visible by the LFRP system.

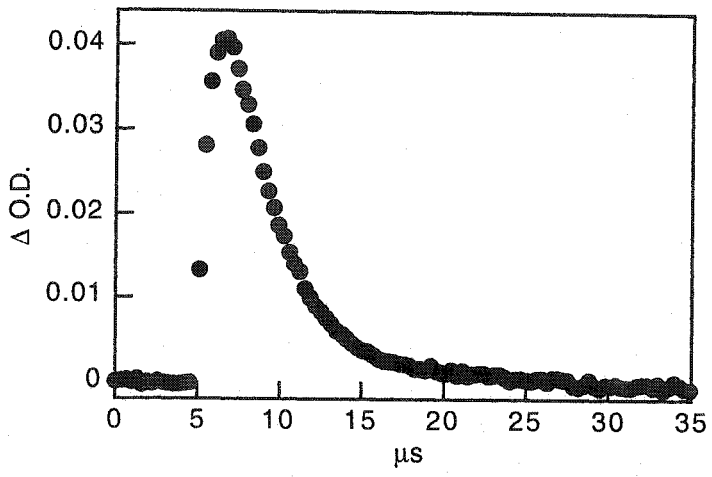

Figure 4-9. Decay of the Ph_3Si• radical monitored at 330 nm in the presence of 0.9 mM TEMPO (note the resolved growth reflecting the reaction of alkoxy radicals with Ph_3SiH.)

While the trialkyl metal radicals have absorptions that are visible with our LFP system,[64] the transients produced by hydrogen abstraction are weak and quenching studies could not be performed. Benzil can be used as a probe permitting quenching studies as the adduct formed has a large extinction coefficient in a region suitable for our system,[60,61] and does not overlap with any

other absorbing species. The adduct formed between the metal centered radical and benzil is represented in Equation 12. This probe technique has been previously used to visualize transients in the case of triethylsilane and to extract kinetic information.[60,62] Germanium and tin radicals also form adducts that are spectroscopically visible. The observed rate constant obtained using the probe technique is expressed in Equation 13 and is concentration dependent upon all the species reacting with the metal-centered radical. Under constant concentration of organometallic precursor and benzil, the rate equation simplifies to Equation 14 and the quenching constant is obtained in the same fashion as for the aryl series. Monitoring the pseudo-first order growth kinetics (k_{obs}) of the adduct for various TEMPO concentrations leads to the trapping constant, k_q. A typical signal for the adduct growth is found in the inset of Figure 4-10.

13) $$k_{obs} = k_o + k_B[\text{Benzil}] + k_q[\text{Nitroxide}]$$

14) $$k_{obs} = k_o' + k_q[\text{Nitroxide}]$$

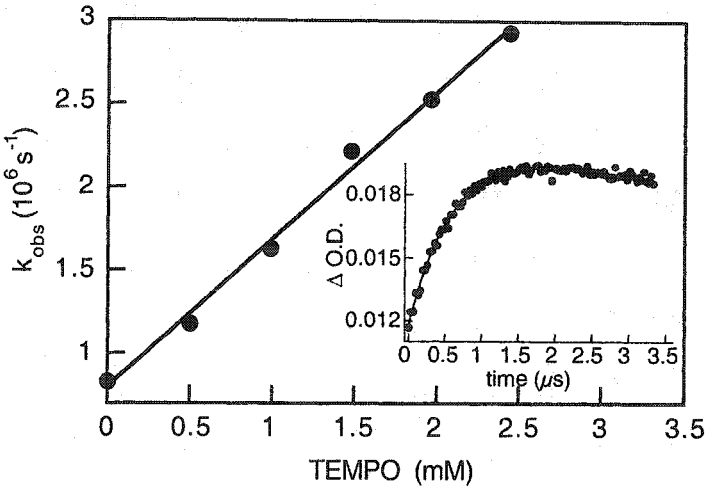

Figure 4-10. Quenching of $Et_3Si\bullet$ radical in the presence of benzil and various amounts of TEMPO done in Bu^tOOBu^t. Inset: Growth of adduct between $Et_3Si\bullet$ radical and benzil in the presence of 0.99 mM TEMPO monitored at 378 nm.

The rate constants obtained for the alkyl and aryl series are summarized in Table 4-3. Also summarized in this table are the conditions of analysis and monitoring

wavelengths. The alkyl series shows only a marginal decrease in the observed trapping rate constant on going from Si to Sn, while all three metal-centered radicals show fast kinetics for nitroxide trapping. In general, the physical properties of group IV compounds do not exhibit any abnormalities when progressing through the family,[73] and would lead one to believe that the reactivity of the radicals equally would follow a similar trend. The trapping kinetics for the organometallic radicals towards TEMPO do indeed follow the trend reflecting the homologous series.

Table 4-3. Summary of observed rates of trapping for various organometallic radicals with TEMPO.

Radical	λ_{max} (nm)	Solvent	Rate Constant (10^7 $M^{-1}s^{-1}$)
[a]$Bu_3C\bullet$	317[b]	Isooctane : Bu^tOOBu^t	76, 88
$Et_3Si\bullet$	378[c]	50% Bu^tOOBu^t	89
$Bu_3Ge\bullet$	480[c]	50% Bu^tOOBu^t	72
$Bu_3Sn\bullet$	478[c]	Bu^tOOBu^t	62
$Ph_3C\bullet$	335[d]	Isooctane : Bu^tOOBu^t	< 0.1
$Ph_3Si\bullet$	330[d]	Bu^tOOBu^t	16
$Ph_3Ge\bullet$	325[d]	4:1 Cyclohexane: Bu^tOOBu^t	34
$Ph_3Sn\bullet$	320[d]	4:1 Cyclohexane: Bu^tOOBu^t	1.9

a) Values taken from Ingold et al. for analogous carbon based systems.[1,3]
b) Refers to monitoring the absorption arising form the adduct between benzil and organometallic radical.
c) A probe method was used to determine the rate constant.
d) The kinetics were determined by directly monitoring the radicals generated.

In general, the rate constants for the trapping of the organometallic radicals by TEMPO are below the diffusion controlled limit. For $Et_3Si\bullet$, the value of $8.9x10^8$ M^{-1} s^{-1} is somewhat slower than that estimated by Lucarini et al.,[74] for $Me_3Si\bullet$. Under similar experimental conditions, the aliphatic organometallic and carbon analogues exhibit much the same kinetic behavior in contrast to the triphenylmethyl case that is 100 times less reactive towards TEMPO than $Ph_3M\bullet$. Substitution by aryl groups at the metal center has a relatively small contribution to resonance stabilization.[64] Unlike the carbon radical that has a planar structure with propeller-like phenyl groups, the metallic radicals are pyramidalized and resonance stabilization does not occur to the same degree as for the carbon radical, and optimal molecular overlap permitting delocalization is achieved to a lesser extent.[64,75-78] The triphenylmethyl radical draws its low reactivity from two origins: resonance stabilization from the phenyl groups, and from steric hindrance by the same groups. Steric hindrance is not as important for the metallic analogues because the atomic radius of the metal center is considerably larger, thus placing the substituents further apart and exposing more the metal center.[79]

Figure 4-11 shows that the aryl metal radicals are quenched by TEMPO; the observed rate constants for these systems are summarized in Table 4-3. The rate constants obtained are well below the diffusion controlled limit and are comparable to rate constants observed for the analogous carbon-centered radicals presented earlier in this chapter.[1-3] A slight trend does exist based upon the stability of the generated radical where the observed rate becomes slower as the organometallic radical trapped becomes larger. This is clear for the case of the tin radical as it is considerably larger than the other metallic centers and for which bond energies tend to be lower. A larger radius also implies the lone electron is distributed over a larger area resulting in somewhat increased stability and reduced reactivity.[48,80-92] Aromatic substitution may also decrease the reactivity even further through some resonance stabilization, contributing to the slow trapping kinetics seen with $Ph_3Sn\bullet$. However, the germanium radical does not fit this trend as the rate is faster than for the silicon analogue; the same rate was determined after repeated purification, and by 308 nm excitation, where only a small amount of peroxide is required. A possible explanation for the observed faster germanium kinetics is a change in quenching mechanism; germanium is known to be slightly more electronegative than silicon and tin, and TEMPO is a

good reducing agent.[73] Thus some contribution from charge transfer, but not a complete shift to electron transfer quenching may be possible.

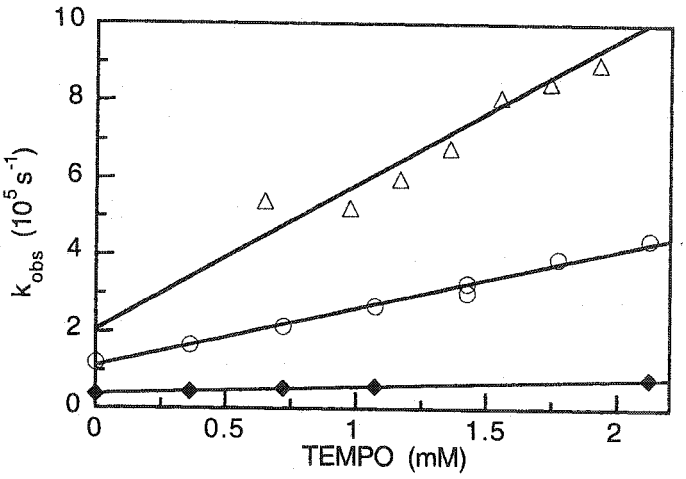

Figure 4-11. Quenching of $Ph_3Si\bullet$ (○), $Ph_3Ge\bullet$ (●), and $Ph_3Sn\bullet$ (Δ) as a function of TEMPO addition.

In general, the trapping of carbon centered radicals by TEMPO shows a dependence on the polarity of the solvent, being slower in polar solvents.[2] The rates obtained in this study can be compared directly without concern for the solvent effect, as identical trapping rate constants were obtained for $Ph_3Ge\bullet$ with acetonitrile or cyclohexane as cosolvents with di-*tert*-butyl peroxide.

The proposed R_3M-TEMPO adduct resulting from radical trapping of the organometallic center by TEMPO has been previously confirmed for the trialkyl and triarylsilyl species[74] and the germanium analogue.[93] It seems reasonable to assume that the remaining adducts can equally be formed, based on the observation of Lucarini coupled with the knowledge that alkoxides are known for all three metal centers studied.[73] Overall, the rate constants obtained for the quenching of the organometallic radicals studied are consistent with radical trapping and are similar to the carbon based radical systems that are known to initiate polymerization.[94,95] From the measured rate constants, the compounds studied would be suitable initiators for the polymerization process, as the rates do not suggest unusual irreversible termination by metal-TEMPO trapping, which is a key property for LFRP. The rate constants are also comparable to the

carbon centered analogues that are known to successfully initiate LFRP for styrene and its derivatives.

The kinetic data obtained reflect only the preference for the formation of an organometallic species capped with TEMPO. However, the ultimate fate of these nitroxide-based organometallic initiators upon thermal decomposition is not known, and is important for determining suitable initiator candidates for LFRP. Theoretical calculations have been used as a preliminary screening tool to determine the best initiator candidates without having to synthesize all of them. The calculation approach also provides a means for predicting the potential thermal decomposition products. Suitable candidates would favorably undergo C-O bond cleavage to yield O-centered nitroxide radicals instead of N-O bond cleavage. The latter gives rise to a reactive oxygen-centered radical and a nitrogen centered radical, neither of which exhibit any LFRP properties. Suitable initiator candidates were determined by calculating the overall heats of reaction (ΔH_{rx}) for the pathways described in Scheme 4-7, by examining the individual heats of formation (ΔH_f) for the various species. A summary of the calculated values is found in Table 4-4.

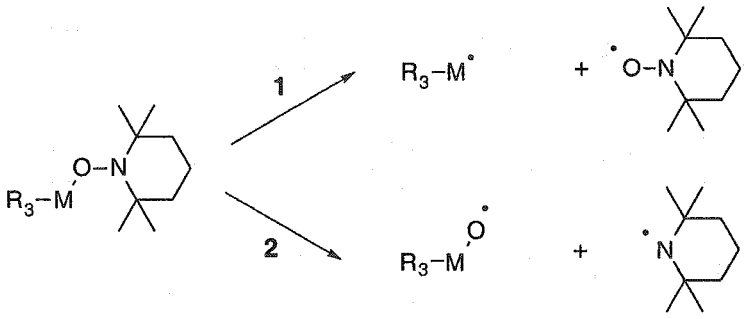

Scheme 4-7. Potential thermal decomposition pathway for organometallic based LFRP initiators.

Absolute values for the decomposition energies derived from semi-empirical calculations cannot be accurately determined. However, the relative values determined within a series of compounds are reliable and trends can be identified within a homologous series.[96-100] There may be slight discrepancies between the two semi-empirical methodologies (AM1 and PM3), but regardless of the method used, the relative values still represent a reasonable tool to

establish trends. This level of theory has previously been used to predict bond dissociation energy orders in a homologous series involving radicals and is a convenient tool to determine relative energies for open shell species.[101,102] The carbon based radical was used as a benchmark test for the decomposition pathway as its fragmentation is known to occur exclusively via path 1 in Scheme 4-7.[4] The values obtained denote that the C-O cleavage (path 1) is the thermodynamically preferred route for only a few compounds within the series investigated.

Table 4-4. ΔH_{rx} results determined semi-empirically for various organometallic-TEMPO initiators where reaction path numbers refer to Scheme 4-7.

Metal center (M)	R_3=(alkyl)$_3$ ΔH_{rx} (kcal/mol)		R_3=(Phenyl)$_3$ ΔH_{rx} (kcal/mol)	
	1	2	1	2
C	14.9	21.2	-0.9	16.8
Si	63.2	33.9	41.3	25.2
Ge	30.1	28.6	18.7	30.1
Sn	19.0	28.4	17.6	31.2

The accuracy of our semi-empirical calculations for predicting the correct decomposition pathway is supported by Lucarini's report that examined the decomposition products of TEMPO-Si adducts. In his work, the products isolated were from N-O bond cleavage for both trialkyl and triaryl silicon adducts. These results, in addition to the carbon benchmark test (see Table 4-4), show our calculations can reasonably predict the strength of M-O bond relative to the N-O bond. These calculations predicted the preferred M-O cleavage occurs for the alkyl and aromatic substitution in the case of tin, reflecting radical stability. As the metal center decreases in size upon going to germanium, the substituents dictate the stability of the decomposition route and the *d* orbitals are less influential. The aryl substituents are sufficiently large to induce a pseudo-

planarity (*vide supra*) and as a result stabilize the metal radical by delocalization onto the aromatic moieties. The O-M bond in the case for germanium is known to be very labile and supports the calculated results.[93,103] In contrast, the Si-O bond is extremely strong; i.e., 30-50 kcal/mol stronger than its carbon analogue.[73,104]

Based on the calculations, the organometallic initiators that appear worthwhile to pursue as candidates for LFRP are Ph_3Ge-T, Ph_3Sn-T and Bu_3Sn-T where T=TEMPO. Since the reactivity of the metallic radicals towards TEMPO and the fragmentation calculated are both similar to their carbon based analogues, we assume their initiation rate constants towards vinyl monomers would also be similar.

4.3 Conclusion

The non-stabilized carbon centered radicals such as that derived from **2** react with nitroxides much faster than do benzylic radicals. Therefore, the nature of this radical determines the rate constants for important radical trapping process in LFRP. Also, the nitroxide structure offers limited control of the reactivity for the trapping of the radical, but electronic effects may be a factor.

Semi-empirical calculations have been coupled with kinetic data arising from the quenching of various organometallic centers with TEMPO. The kinetic data have shown that all the organometallic radicals are rapidly trapped by TEMPO and the rates are comparable to the carbon centered analogues measured in the first section. The experimental kinetic and theoretical calculations have shown three candidates (Ph_3Ge-T, Ph_3Sn-T and Bu_3Sn-T) as potential stoichiometric initiators for LFRP. These may ultimately prove as good candidates for LFRP initiation, but also for incorporating functionality into the polymer terminus for future polymer modification.

4.4 Experimental

All chemicals were used as received from Aldrich unless otherwise stated. Hexanes used for chromatographic purposes were washed and distilled over calcium chloride prior to use. OmnioSolv grade solvents for laser work and HPLC grade solvents for analytic work were used as received from VWR.

4.4.1 Laser Flash Photolysis

Direct photolysis of initiators 1-6: Rate constants were determined using the LFP technique with nanosecond resolution. The laser system and the data processing after acquisition are similar to that reported elsewhere in this thesis.[52,53] Excitation at 266 nm from a Continuum Nd-YAG Surelite laser (fourth harmonic, 10 mJ/pulse, ~6 ns) was used for the direct photolysis of the initiators. The 308 nm pulses from an excimer laser were also used in some experiments with other radical precursors. In general, all samples were dissolved in spectroscopic grade acetonitrile, unless otherwise stated, and fully deareated in a 7 x 7 mm^2 quartz Suprasil cell for a minimum of 20 minutes prior to use. Absorbances of the samples were targeted at 0.3 at the excitation wavelength. Known amounts of nitroxide aliquots were added to the samples for the quenching studies and the total nitroxide present after photolysis was quantified by HPLC analysis.

The rate constants for radical trapping for initiators **1** and **4** were done by monitoring the radical decay from the direct photodecomposition **9** after excitation at 266 nm.

Indirect photolysis: A Molectron UV-24 nitrogen laser for 337 nm was used for work involving radical generation from di-*tert*-butylperoxide and described elsewhere.[1-3] Several methods for determining the rate constants were used.

Organometallic Initiators: Rate constants were determined using the laser flash photolysis technique with nanosecond resolution similar above. A Molectron UV-24 nitrogen laser for 337 nm excitation delivering ca. 7 mJ per pulse was used. In the case of 308 nm excitation, pulse durations were <10 ns and typical pulse energies between 5 and 50 mJ. In general, all samples were dissolved in spectroscopic grade solvents in the proportions described according to Table 4-3 with approximately 0.4 M of the organometallic source. In the case of the aliphatic systems, of doubly recrystallized benzil (4 mg, 8 mM) was added to the

laser cell because the metal radicals add at the oxygen center to form a detectable adduct. This adduct is a carbon centered radical that is spectroscopically visible with our system, and has a much stronger absorption than aliphatic metal radicals.[60,61] TEMPO quencher was dissolved in the appropriate solvent and thoroughly deareated. Aliquots were added to the organometallic samples and the kinetics investigated as a function of nitroxide concentration. The samples were fully deareated in a 7 x 7 mm^2 quartz Suprasil cell for a minimum of 20 minutes prior to use. Some kinetic studies were repeated using 308 nm pulses from an excimer Lumonics E5-510 with less than 10% (v/v) of Bu^tOOBu^t.

Laser Flash Photolysis studies of (7). A solution of 0.5 M of **7** with a 2:1 solution of acetonitrile : di-*tert*-butylperoxide was excited with 337 nm. The peroxide was passed through a plug of alumina oxide prior to use. The probe method[1,30,52,53] was used to determine rate constants for the quenching of radical **8** by TEMPO. This was done by monitoring the change in the growth of 1,1-diphenylethyl-adduct (**11**) radical at ca. 329 nm as a function of nitroxide concentration after excitation with the 337 nm laser. A solution of 2:1 acetonitrile : di-*tert*-butylperoxide was used to dissolve 154 mg (0.58 mmol, 0.2 M) of **7** and 86.5 mg (0.47 mmol, 0.16 M) of 1,1-diphenylethylene. 1,1-Diphenylethylene was purified according to literature procedure immediately prior to use in this system.[2]

4.4.2 Product Quantification

A Varian HPLC instrument equipped with a diode array absorption detector was used to determine the nitroxide concentrations immediately following LFP studies. A Zorbax C-18 reverse phase column (4.6 mm x 25 cm) with 85% methanol / 15% water was used as eluent. Products formed after irradiation studies were analyzed with the same setup using LC-MS and UV absorption at 254 nm coupled with an ESI mass spectrometer. Concentrations were determined by peak area calibration against authentic samples in methanol at 220 and 254 nm. The total volume injected for each sample with the use of an autosampler was 20 µl. Products formed after irradiation studies were analyzed with the same setup using LC-MS yet the detection method was UV absorption at 254 nm coupled with a ESI mass spectrometer giving rise to the molecular ion +1.

4.4.3 Synthesis

Di-*tert*-butyl peroxide (Bu^tOOBu^t) was passed through a plug of neutral aluminum oxide immediately prior to use. Triphenyl germanium hydride was prepared by reduction of the corresponding chloride with lithium aluminum hydride.[105] The initiators used in this work were either the same as in earlier publications, or were prepared using the same methodology. Their identity were confirmed by NMR (^1H and ^{13}C) and mass spectrometry.

1-phenyl-1-(2,2,6,6-tetramethylpiperdine-N-oxide)-ethane (1): A 250 mL UV reactor vessel was charged with ethylbenzene (250 mL), 2,2,6,6-tetramethylpiperidine-N-oxyl (TEMPO) (17.0 g, 109 mmol) and di-*tert*-butyl peroxide (23.0 mL, 18.3 g, 125 mmol). Oxygen was purged from the reaction vessel by bubbling argon through the solution, and then the product was irradiated at room temperature using a Canrad-Hanovia medium pressure mercury vapor lamp with a 220 nm cutoff filter until the orange color of the nitroxide had disappeared (5 days). The reactor was discharged and the residual ethyl benzene was removed by evaporation. Recrystallization from isopropanol afforded colorless crystals in 63% yield. ^1H NMR (500 MHz, $CDCl_3$ TMS) δ 7.05-7.30 (m, 5H), 4.83 (q, 1H), 1.5 (s, 3H), 1.27 (m, 21H). ^{13}C NMR (300 MHz, $CDCl_3$) δ 145.8, 127.9, 126.7, 126.5, 83.0, 59.6, 40.3, 34.4, 34.1, 23.5, 20.3, 17.2. MS (EI) m/z (%)156 (37), 142 (100), 123 (21), 114 (4), 105 (77), 104 (23), 77 (13), 69 (40), 56 (14), 55 (19), 41 (17). MS (ESI) m/z (%) 262 (5, M+1), 157 (95), 126 (100), 125 (55), 121 (30), 105 (14), 82 (16), 69 (85), 57 (10), 42 (13).

2-(2,2,6,6-tetramethylpiperdine-N-oxide)-methylpropionate (2): This compound was synthesized according to the method of Matyjaszewski.[106,107] ^1H NMR (400 MHz, $CDCl_3$ TMS) δ 4.3 (q, 1H), 3.7 (s, 3H), 1.5 (s, 3H), 1.3 (m, 18H). ^{13}C NMR (300 MHz, $CDCl_3$) δ 157.2, 125.3, 83.6, 60.1, 51.4, 40.2, 33.7, 33.6, 20.2, 17.2, 9.4. MS (EI) m/z (%) 243 (4), 177 (2), 156 (100), 140 (8), 123 (20), 105 (27), 83 (21), 69 (37), 57 (43).

***1-benzoyloxy-1-(2,2,6,6-tetramethylpiperidine-N-oxide)-ethane* (3):** This was synthesized according to previous work with a slight modification.[26,108] Distilled styrene (100 mL, 0.87 mol) was added to a round bottom flask where benzoylperoxide (5 g, 20.6 mmol) and TEMPO (6.1 g, 41 mmol) were dissolved. The reaction was placed in an oil bath pre-heated to 125 °C after purging the solution with nitrogen for a minimum of 25 minutes. After the initial orange color faded to pink, typically 7 minutes, the reaction was immediately cooled in

an ice bath. The residual monomer was removed under pressure and the remaining material was purified by flash chromatography with neat dichloromethane to afford the product as a white solid in 5 % yield. ^{1}H NMR (400 MHz, $CDCl_3$ TMS) δ 7.9 (dd, 2H), 7.3 (m, 8H), 5.1 (t, 1H), 4.8-4.4 (m, 2H). ^{13}C NMR (300 MHz, $CDCl_3$) δ 166.1, 140.9, 133.4, 130.7, 129.1, 128.5, 127.8, 127.4, 80.9, 67.0, 53.7, 38.9, 27.2, 25.2, 17.8. MS (EI) m/z (%) 381 (0.1), 276 (0.1), 246 (0.4), 225 (30), 209 (2), 156 (13), 122 (10), 105 (100), 91 (6), 77 (39), 57 (18), 40 (20).

1-Benzyl-3,3,5,5-dicyclohexyl-4-(1-phenyl-ethoxy)-piperazine-2,6-dione (4): Ethylbenzene (25 mL), BODAZ (5) (830 mg, 2.33 mmol) and di-*tert*-butyl peroxide (0.49 mL, 390 mg, 267 mmol) were combined and the same procedure as **1** was followed. After the color had bleached (6 days) the solution was discharged and the residual ethylbenzene was removed by evaporation. Recrystallization from isopropanol afforded colorless crystals in 78% yield. ^{1}H NMR (200 MHz, $CDCl_3$ TMS) δ 7.20-7.32 (m, 10H), 4.82 (q, 1H), 1.5 (d, 3H), 1.08 (s, 9H), 1.05 (s, 9H). ^{13}C NMR (300 MHz, $CDCl_3$) δ 157.2, 132.5, 128.3, 128.1, 127.9, 127.5, 127.1, 90.8, 82.5, 77.4, 77.0, 76.6, 43.8, 33.2, 25.9, 25.5, 22.4, 20.5. MS (EI) m/z (%) 355 (1), 339 (10), 297 (13), 249 (25), 209 (68), 178 (39), 122 (36), 105 (100), 91 (59), 77 (82), 51 (45).

2-N-oxyl-3,3,5,5-dicyclohexyl-4-(1-phenyl-ethoxy)-piperazine-2,6-dione (BODAZ): BODAZ was prepared by a procedure adapted from Ramey and Luzzi.[109] To a solution of 4-N-benzyl-4-azoglutarimide[109] (2.70 g, 8 mmol) in dichloromethane (75 mL) was added 3-chloroperoxybenzoic acid (99%) (2.76 g, 16 mmol). The temperature rose to 28 °C during the course of the addition. After 24h, the precipitate was filtered off and the lemon yellow solution was chromatographed on silica gel using hexane ethyl acetate (3%). The product was isolated as an orange syrup (2.01 g, 71%). MS (EI) m/z (%) 355 (26), 340 (100), 297 (28), 284 (12), 269 (39), 249 (26), 216 (19), 178 (36), 109 (15), 91 (57), 69 (29), 55 (9), 40 (39).

1-phenyl-1-(N-N-di-tert-butyl-N-oxide)-ethane (5): The literature procedure was followed.[37] ^{1}H NMR (200 MHz, $CDCl_3$ TMS) δ 7.24-7.33 (m, 10H), 4.86 (m, 2H), 4.78 (m, 1H), 1.76 (m, 4H), 1.56 (d, 3H), 1.43 (m, 16H). ^{13}C NMR (300 MHz, $CDCl_3$) δ 145.3, 127.9, 127.8, 126.9, 126.8, 82.8, 76.5, 61.9, 61.7, 30.6, 22.7. MS (EI) m/z (%) 169 (1), 145 (25), 120 (2), 105 (80), 91 (5), 77 (15), 57 (100).

1-phenyl-1-(4-benzoyloxy-2,2,6,6-tetramethylpiperdine-N-oxide)-ethane (6): A procedure similar to **1** was followed with ethylbenzene (25 mL), 4-benzoyloxy-2,2,6,6-tetramethylpiperdine-N-oxyl (262 mg, 10 mmol) and di-*tert*-butyl peroxide (2.3 mL, 1.83 g, 12.5 mmol). After bleaching of the nitroxide color upon

irradiation similar to **1** (6 days), the residual ethylbenzene was removed by evaporation followed by flash chromatography with hexane/ethyl acetate (3%) to give a pale yellow syrup (45%). ^{1}H NMR (200 MHz, $CDCl_3$ TMS) δ 8.0 (d, 2H), 7.21-7.97 (m, 8H), 5.24 (m, 1H), 4.79 (q, 1H), 1.50-1.97 (m, 4H), 1.47 (d, 3H), 1.23 (s, 1H), 1.16 (s, 1H), 1.06 (s, 1H), 0.68 (s, 1H). ^{13}C NMR (300 MHz, $CDCl_3$) δ 166.1, 145.3. 132.8, 130.6, 129.5, 128.3, 128.1, 126.9, 126.8, 126.7, 83.4, 76.9, 67.5, 60.3, 44.7, 34.4, 34.0, 23.3, 21.2, 21.0. MS (EI) m/z (%) 381 (26), 277 (35), 262 (17), 246 (10), 154 (17), 140 (143), 124 (77), 105 (100), 91 (8), 77 (51), 69 (11).

1-benzoyl-2-phenyl-ethane (7): Phenylethyl alcohol (1.04 g, 8.5 mmol) was dissolved in 30 mL of dichloromethane and cooled to 0 °C. To this solution was added 1.8 mL of triethylamine (12.9 mmol, 1.5 equivalents) with a catalytic amount of N,N-dimethylaminopyridine. A solution of 1.2 mL of benzoyl chloride (10.3 mmol, 1.2 equivalents) dissolved in dichloromethane was slowly added to the cooled solution. The resulting solution was allowed to warm to room temperature and stirred for three hours. The reaction was judged completed by the disappearance of starting material by TLC. The reaction was quenched with a brine solution and the organic layer was separated and further washed with brine. The organic layer was dried with magnesium sulfate, filtered, concentrated and flash chromatographed with an eluent of 10% ethylacetate/hexanes. This gave 1.95 g of **7** as a colorless oil (86 %). ^{1}H NMR (200 MHz, $CDCl_3$ TMS) δ 8 (m, 2H), 7.4 (m, 8H), 4.5 (t, 2H), 3.1 (d, 2H). ^{13}C (300 MHz, $CDCl_3$) 166.5, 137.9, 132.9, 129.5, 128.9, 128.5, 128.3, 126.6, 118.8, 65.5, 35.2. MS (FAB) m/z (%) 227 (20, M+1), 132 (8), 105 (100), 77 (12), 57 (6). MS (EI) m/z (%) 105 (100), 91 (48), 77 (93), 65 (38), 51 (60).

4.4.4 Semi-Empirical Calculations

Semi-empirical calculations were done on a Silicon Graphics Indigo workstation using Spartan SGI version 4.0.4 GL IRX 5.2. The geometries of the desired compounds were optimized using PM3[96] and their heats of formation (ΔH_f) were calculated based upon these geometries. For all systems, unrestricted Hartree-Fock (UHF) was selected for the calculations, particularly to handle the open shell systems, but it was also applied to closed shell systems for consistency.

4.5 Chapter References

1. Bowry, V. W.; Ingold, K. U. *J. Am. Chem. Soc.* **1992**, *114*, 4992-4996.
2. Beckwith, A. J.; Bowry, V. W.; Ingold, K. U. *J. Am. Chem. Soc.* **1992**, *114*, 4983-4992.
3. Chateauneuf, J.; Lusztyk, J.; Ingold, K. U. *J. Org. Chem.* **1988**, *53*, 1629-1632.
4. Skene, W. G.; Belt, S. T.; Connolly, T. J.; Hahn, P.; Scaiano, J. C. *Macromolecules* **1998**, *31*, 9103-9105.
5. Skene, W. G.; Scaiano, J. C. **2000**, Manuscript in preparation.
6. Skene, W. G.; Scaiano, J. C. *Polym. Prepr.* **2000**, *41*, 163-164.
7. Kothe, T.; Marque, S.; Martschke, R.; Popov, M.; Fischer, H. *J. Chem. Soc., Perkin Trans. 2* **1998**, *7*, 1553-1559.
8. Skene, W. G.; Connolly, T. J.; Scaiano, J. C. *Tetrahedron Lett.* **1999**, *40*, 7297-7302.
9. Skene, W. G.; Scaiano, J. C.; Listigovers, N. A.; Kazmaier, P. E.; Georges, M. K. *Macromolecules* **2000**, In press.
10. Skene, W. G.; Connolly, T. J.; Scaiano, J. C. *Int. J. Chem. Kin.* **2000**, *32*, 238-244.
11. Skene, W. G.; Scaiano, J. C. **2000**, Manuscript in preparation.
12. Skene, W. G.; Martin, A.; Scaiano, J. C. **2000**, Manuscript in preparation.
13. Skene, W. G.; Scaiano, J. C. **2000**, Manuscript in preparation.
14. Beckwith, A. L. J.; Bowry, V. W.; O'Leary, M.; Moad, G.; Rizzardo, E.; Solomon, D. H. *J. Chem. Soc., Chem. Comm.* **1986**, 1003-1004.
15. Laidler, K. J.; Meiser, J. H. *Physical Chemistry*; The Benjamin/Cummings Publishing Company, Inc.: Menlo Park, 1982, pp 919.
16. Lowry, T. H.; Richardson, K. S. *Mechanism and Theory in Organic Chemistry*, 3rd ed.; Harper Collins Publishers: New York, 1987, pp 1090.
17. Fischer, H. *J. Am. Chem. Soc.* **1986**, *108*, 3925-3927.

18. Fischer, H. *Macromolecules* **1997**, *30*, 5666-5672.
19. Catala, J. M.; Bubel, F.; Hammouch, S. O. *Macromolecules* **1995**, *28*, 8441-8443.
20. Georges, M. K.; Veregin, R. P. N.; Kazmaier, P. M.; Hamer, G. K.; Saban, M. *Macromolecules* **1994**, *27*, 7228-7229.
21. Hawker, C. J. *J. Am. Chem. Soc.* **1994**, *116*, 11185-11186.
22. Veregin, R. P. N.; Georges, M. K.; Hamer, G. K.; Kazmaier, P. M. *Macromolecules* **1995**, *28*, 4391-4398.
23. Howell, B. A.; Priddy, D. B.; Li, I. Q.; Smith, P. B.; Kastl, P. E. *Polym. Bull.* **1996**, *37*, 451-456.
24. Steenbock, M.; Klapper, M.; Mullen, K.; Pinhal, N.; Hubrich, M. *Acta. Polymer.* **1996**, *47*, 276-279.
25. Greszta, D.; Matyjaszewski, K. *Macromolecules* **1996**, *29*, 7661-7670.
26. Hawker, C. J.; Barclay, G. G.; Orellano, A.; Dao, J.; Devonport, W. *Macromolecules* **1996**, *29*, 5245-5254.
27. Connolly, T. J.; Baldovi, M. V.; Mohtat, N.; Scaiano, J. C. *Tetrahedron Lett.* **1996**, *37*, 4919-4922.
28. Scaiano, J. C.; Connolly, T. J.; Mohtat, N.; Pliva, C. N. *Can. J. Chem.* **1997**, *75*, 92-97.
29. Chatgilialoglu, C. Electronic Absorption Spectra of Free Radicals. In *Handbook of Organic Photochemistry*; Scaiano, J. C., Ed.; CRC Press: Boca Raton, Florida, 1989; Vol. II; 3-11.
30. Paul, H.; Small, R. D., Jr.; Scaiano, J. C. *J. Am. Chem. Soc.* **1978**, *100*, 4520-4527.
31. Baldovi, M. V.; Mohtat, N.; Scaiano, J. C. *Macromolecules* **1996**, *29*, 5497-5499.
32. Chong, Y. K.; Ercole, F.; Moad, G.; Rizzardo, E.; Thang, S. H. *Macromolecules* **1999**, *32*, 6895-6903.

33. Solomon, D. H.; Rizzardo, E.; Cacioli, P. U.S. Patent 4,581,429, **1986**.
34. Odell, P. G.; Rabien, A.; Michalak, L. M.; Vergin, R. P. N.; Quinlan, M. H.; Moffat, K. A.; MacLeod, P. J.; Listigovers, N. A.; Honeyman, C. H.; Georges, M. K. *Polym. Prepr.* **1997**, *38*, 414-415.
35. Georges, M. K.; Listigovers, N. A.; Odell, P. G.; Hamer, G. K.; Quilan, M. H.; Veregin, R. P. N. *Polym. Prepr.* **1997**, *38*, 454-455.
36. MacLeod, P. J.; Georges, M. K.; Quinlan, M.; Moffat, K. A.; Listigovers, N. A. *Polym. Prepr.* **1997**, *38*, 459-460.
37. Benoit, D.; Chaplinski, V.; Braslau, R.; Hawker, C. J. *J. Am. Chem. Soc.* **1999**, *121*, 3904-3920.
38. Keoshkerian, B.; Georges, M.; Quinlan, M.; Veregin, R.; Goodbrand, B. *Macromolecules* **1998**, *31*, 7559-7561.
39. Goto, A.; Fukuda, T. *Macromolecules* **1999**, *32*, 618-623.
40. O'Neil, G. A.; Torkelson, J. M. *Macromolecules* **1999**, *32*, 411-422.
41. Rizzardo, E.; Serelis, A. K.; Solomon, D. H. *Aust. J. Chem.* **1982**, *35*, 2013-2024.
42. Rizzardo, E.; Solomon, D. H. *Polym. Bull.* **1979**, *1*, 529-534.
43. de Leon, M. E.; Gnanou, Y.; Guerrero, R. *Polym. Prepr.* **1997**, *38*, 667-668.
44. Wojárovits, L.; Takács, E. *Res. Chem. Intermed.* **1999**, *25*, 275-283.
45. Lambert, J. B.; Shurvell, H. F.; Ligtner, D.; Cooks, R. G. *Introduction to Organic Spectroscopy*; Macmillan Publishing Company: New York, 1987, pp 454.
46. Johnston, L. J.; Tencer, M.; Scaiano, J. C. *J. Org. Chem.* **1986**, *51*, 2806-2808.
47. Lissi, E. A.; Encinas, M. V. Representative Kinetic Behavior of Selected Reaction Intermediates: Triplet States. In *Handbook of Organic Photochemistry*; Scaiano, J. C., Ed.; CRC Press, Inc.: Boca Raton, 1989; Vol. 2; 111-176.
48. Green, S.; Fox, M. A. *J. Phys. Chem.* **1995**, *99*, 14752-14757.

49. Rozantsev, E. G.; Sholle, V. D. *Synthesis* **1971**, 401-414.
50. Scaiano, J. C. *Chem. Phys. Lett.* **1981**, *79*, 441-443.
51. Connolly, T. J.; Scaiano, J. C. *Tetrahedron Lett.* **1997**, *38*, 1133-1136.
52. Scaiano, J. C.; Tanner, M.; Weir, D. *J. Am. Chem. Soc.* **1985**, *107*, 4396-4403.
53. Scaiano, J. C. *J. Am. Chem. Soc.* **1980**, *102*, 7747-7753.
54. Engel, P. S. *J. Am. Chem. Soc.* **1970**, *92*, 6074-6076.
55. Robbins, W. K.; Eastman, R. H. *J. Am. Chem. Soc.* **1970**, *92*, 6076-6077.
56. Turro, N. J.; Gould, I. R.; Baretz, B. H. *J. Phys. Chem.* **1983**, *87*, 531-532.
57. Lunazzi, L.; Ingold, K. U.; Scaiano, J. C. *J. Phys. Chem.* **1983**, *87*, 529-530.
58. Turro, N. J. *Modern Molecular Photochemistry*; University Science Books: Sausalito, 1991, pp 628.
59. Korolenko, E. C.; Cozens, F. L.; Scaiano, J. C. *J. Phys. Chem.* **1995**, *99*, 14123-14128.
60. Chatgilialoglu, C.; Ingold, K. U.; Scaiano, J. C.; Woynar, H. *J. Am. Chem. Soc.* **1981**, *103*, 3231-3232.
61. Chatgilialoglu, C.; Ingold, K. U.; Scaiano, J. C. *J. Am. Chem. Soc.* **1982**, *104*, 5119-5123.
62. Chatgilialoglu, C.; Ingold, K. U.; Scaiano, J. C. *J. Am. Chem. Soc.* **1982**, *104*, 5123-5127.
63. Chatgilialoglu, C.; Ingold, K. U.; Scaiano, J. C. *Organometallics* **1982**, *1*, 466-469.
64. Chatgilialoglu, C.; Ingold, K. U.; Lusztyk, J.; Nazran, A. S.; Scaiano, J. C. *Organometallics* **1983**, *2*, 1332-1335.
65. Ingold, K. U.; Lusztyk, J.; Scaiano, J. C. *J. Am. Chem. Soc.* **1984**, *106*, 343-348.
66. Lusztyk, J.; Maillard, B.; Lindsay, D. A.; Ingold, K. U. *J. Am. Chem. Soc.* **1983**, *105*, 3578-3580.
67. Scaiano, J. C. *J. Am. Chem. Soc.* **1980**, *102*, 5399-5400.
68. Chatgilialoglu, C. *Acc. Chem. Res.* **1992**, *25*, 188-194.

69. Neumann, W. P. *Synthesis* **1987**, *8*, 665-683.

70. Ding, Y. *Huaxue Shiji* **1992**, *14*, 355-358.

71. Bennett, R. F. *Cambridge Environ. Chem. Ser.* **1996**, *8*, 21-61.

72. Yamazaki, O.; Togo, H.; Mogami, G.; Yokoyama, M. *Bull. Chem. Soc. Jap.* **1997**, *70*, 2519-2523.

73. Cotton, F. A.; Wilkinson, G. *Advanced Inorganic Chemistry: A Comprehensive Text*, 5 ed.; John Wiley & Sons: New York, 1988, pp 1455.

74. Lucarini, M.; Marchesi, E.; Pedulli, G. F.; Chatgilialoglu, C. *J. Org. Chem.* **1998**, *63*, 1687-1693.

75. Griller, D.; Ingold, K. U. *Acc. Chem. Res.* **1976**, *9*, 13-19.

76. Cotton, J. D.; Cundy, C. S.; Harris, D. H.; Hudson, A.; Lappert, M. F.; Lednor, P. W. *J. Chem. Soc., Chem. Comm.* **1974**, 651-652.

77. Bennet, J. E.; Howard, J. A. *Chem. Phys. Lett.* **1972**, *15*, 322-324.

78. Lloyd, R. V.; Rogers, M. T. *J. Am. Chem. Soc.* **1973**, *95*, 2459-2464.

79. Jackson, R. A. Group IVB Radical Reactions. In *Advances in Free-Radical Chemistry*; William, G. H., Ed.; Logos Press Limited: London, 1969; Vol. 3; 231-288.

80. Atkins, P. W. *Physical Chemistry*, 5th ed.; W.H. Freeman and Company: New York, 1994, pp 1031.

81. Rychnovsky, S. D.; Vaidynanathan, R. *J. Org. Chem.* **1999**, *64*, 310-612.

82. Doa, J.; Benoit, D.; Hawker, C. J. *J. Polym. Sci. A. Polym. Chem.* **1998**, *36*, 2161-2167.

83. Semmelhack, M. F.; Chou, C. S.; Cortes, D. A. *J. Am. Chem. Soc.* **1983**, *105*, 4492-4494.

84. Einhorn, J.; Einhorn, C.; Ratajczak, F.; Durif, A.; Averbuch, M.-T.; Pierre, J.-L. *Tetrahedron Lett.* **1998**, *39*, 2565-2568.

85. Summermann, W.; Deffner, U. *Tetrahedron* **1975**, *31*, 593-596.

86. Fish, J. R.; Swarts, S. G.; Sevilla, M. D.; Malinski, T. *J. Phys. Chem.* **1988**, *92*, 3745-3751.

87. Limoges, B.; Degrand, C. *J. Electroanal. Chem.* **1997**, *422*, 7-12.

88. Yamauchi, Y.; Maeda, H.; Ohmori, H. *Chem. Pharm. Bull.* **1996**, *44*, 1021-1025.

89. Yoshida, E.; Takata, T.; Endo, T. *Macromolecules* **1992**, *25*, 7282-7285.

90. Faucitano, A.; Buttafava, A.; Martinotti, F. *J. Phys. Chem.* **1984**, *8*, 1187-1190.

91. Bolm, C.; Fey, T. *J. Chem. Soc., Chem. Comm.* **1999**, *18*, 1795-1796.

92. de Nooy, A. E. J.; Besemer, A.; van Bekkum, H. *Tetrahedron* **1995**, *51*, 8023-8032.

93. Kobayashi, S.; Iwata, S.; Abe, M.; Shoda, S.-i. *J. Am. Chem. Soc.* **1995**, *117*, 2187-2200.

94. Georges, M. K.; Veregin, R. P. N.; Kazmaier, P. M.; Hamer, G. K. *Macromolecules* **1993**, *26*, 2987-2988.

95. Veregin, R. P. N.; Georges, M. K.; Kazmaier, P. M.; Hamer, G. K. *Macromolecules* **1993**, *26*, 5316-5320.

96. Stewart, J. J. P. *J. Comput. Chem.* **1989**, *10*, 209-220.

97. Stewart, J. J. P. *J. Comput. Chem.* **1989**, *10*, 221-264.

98. Stewart, J. J. P. Semiempirical Molecular Orbital Methods. In *Reviews in Computational Chemistry I*; Lipkowitz, K. B., Boyd, D. B., Eds.; VCH:, 1990; 45-81.

99. Dewar, M. J. S.; Zoebisch, E. G.; Healy, E., F.; Stewart, J. J. P. *J. Am. Chem. Soc.* **1985**, *107*, 3902-3909.

100. Zerner, M. C. Semiempirical Molecular Orbital Methods. In *Reviews in Computational Chemistry II*; Lipkowitz, K. B., Boyd, D. B., Eds.; VCH:, 1991; 313-359.

101. Kazmaier, P. M.; Moffat, K. M.; Georges, M. K.; Veregin, R. P. N.; Hamer, G. K. *Macromolecules* **1995**, *28*, 1841-1846.

102. Cogen, J. M. *Polymer Degrad. Stab.* **1994**, *44*, 49-53.

103. Armitage, D. A. *Comprehensive Organometallic Chemistry*; Pergamon Press: Oxford, 1982; Vol. 2, pp 1-203.

104. Walsh, R. *Acc. Chem. Res.* **1981**, *14*, 246-252.

105. Clark, K. B.; Griller, D. *Organometallics* **1991**, *10*, 746-750.

106. Matyjaszewski, K. *Macromolecules* **1999**, *31*, 4710-4717.

107. Matyjaszewski, K. "Overview: Fundamentals of Controlled/Living Radical Polymerization"; Controlled Radical Polymerization, 1998, San Francisco, CA.

108. Hawker, C. J.; Barclay, G. G.; Dao, J. *J. Am. Chem. Soc.* **1996**, *118*, 11467-11471.

109. Ramey, C. E.; Luzzi, J. J. U.S. Patent 3,936,456, **1976**.

5. Formation of Disproportionation Products

5.1 Introduction

The alkoxyamine based unimolecular initiators examined in a previous chapter are useful for probing the kinetics and thermodynamics of the LFRP process. These initiators produce a stoichiometric amount of nitroxide upon their decomposition and have been taken advantage of by many groups[1-5] including the current work as they lead to living type polymers.[6-13] The use of these initiators as a polymeric mimetic probe is of convenience since experimental procedures involving bulky polymers are experimentally challenging in terms of solubility, viscosity, and handling.

It would appear as though the unimolecular initiators are excellent mimetics for the processes occurring during LFRP. However, a minor side reaction was identified while examining the decomposition kinetics of these initiators in a preceding chapter. A substantial amount of disproportionation products, hydroxylamine and olefin (See Scheme 5-1), were identified during the previous analyses. The formation of the hydroxylamine does not have the direct effect of destroying the living properties of the polymer by reducing the free nitroxide concentration in the polymerization reaction. Rather, the reaction is spontaneous giving vinyl terminated oligomers of different length that subsequently undergo uncontrolled chain elongation. This ultimately leads to polymers of variable lengths and high polydispersities, hence a lack of living properties. Even though the quantified amounts of the disproportionation products are relatively low (~ 3 %), 1 in 29 initiator decomposition events of **3a** would give disproportionation products leading to large molecular weight distributions for the polymerization of styrene and subsequently an absence of desired living properties. However, the nitroxide based polymerization with the styrene monomer is known to give extremely low polydispersities (< 1.2) with high conversions.[14-16] The objective of this chapter is to examine the origins of the disproportionation products arising from the unimolecular initiators by comparing their formation kinetics and thermodynamic properties.

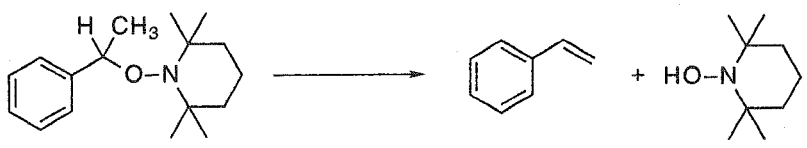

Scheme 5-1. Decomposition of LFRP initiator leading to disproportionation products.

From the numerous reports[17-26] achieving narrow polydispersity with TEMPO capped polymer termini done with nitroxide mediated LFRP, the disproportionation reaction must not be present during typical living polymerization. These results would lead one to believe that the undesired reaction reported in Scheme 5-1 is suppressed in the presence of monomers under polymerization conditions for styrene. To confirm the detrimental effect of additional monomer repeating units upon forming disproportionation products, the dimer like compound **2** known as the 'penultimate' initiator (see Figure 5-1) was synthesized. The structure of this compound is similar to a nitroxide-capped styrene dimer or a polystyrene oligomer (**1**) with the exception of one less methyl group. The penultimate initiator was examined for its mimetic properties and to gain knowledge concerning the origins of disproportionation product formation in the actual polymerization process. The methyl-less analogue was selected because of its synthetic ease relative to a true nitroxide capped styrene dimer. Investigation of the origins of disproportionation products for this study focused primarily on comparing the initiator **3a**, known to give these products, and **2** that does not. Reasons leading to the different observed amounts of disproportionation products for these two initiators were examined in terms of the their kinetic and thermodynamic properties.

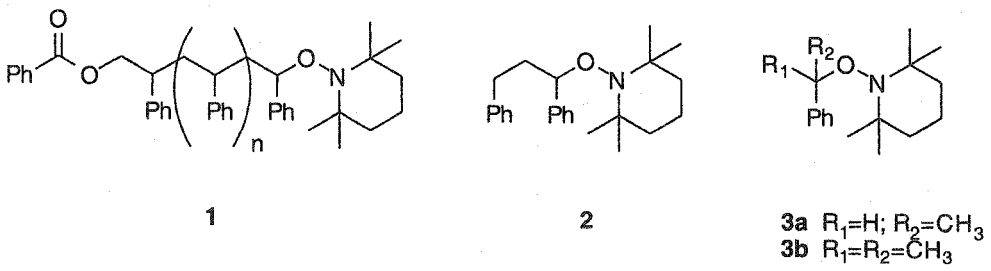

1 **2** **3a** R_1=H; R_2=CH_3 **3b** R_1=R_2=CH_3

Figure 5-1. Unimolecular LFRP initiators used to investigate the origins of disproportionation products.

5.2 Results and Discussion

5.2.1 Synthesis

The initial strategy for the synthesis of the desired 'penultimate' initiator **2** was thermally based. It involved the synthesis of 1,3 diphenylpropane (**5**) from dibenzyl ketone as shown in Scheme 5-2. This route was chosen as the commercial source of this hydrocarbon is limited and extremely expensive. The synthesis of the hydrocarbon and its subsequent bromination are effected in high yields. However, the photochemical bromine displacement and subsequent trapping by nitroxide gives the target molecule in such low yield that sufficient material for subsequent studies could not be obtained. The predominant reaction route leading to low yields of **2** is by electron transfer between the Br• and TEMPO to give the contact ion pair as they have similar redox properties.[27-30] Any product **2** that is formed photochemically efficiently undergoes N-O bond cleavage to give 1,3-diphenylpropan-1-ol (**10**) and a hindered amine with the irradiation wavelengths used. Irradiation at longer wavelengths eliminates N-O bond cleavage, but also does not promote the homolytic cleavage of the C-Br bond. This reaction is identical to that encountered in the PAC studies examined in the chapter treating the initiator thermodynamics.

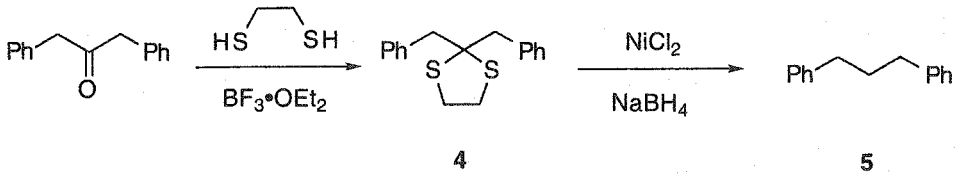

4 5

Scheme 5-2. Original strategy for the synthesis of 1,3-diphenylpropane.

In light of the difficult preliminary photochemical synthesis, a complete thermal synthetic route was adopted. The primary step involved addition of the nitroxide in the correct α-position via enolization of dibenzyl ketone followed by electrophilic addition to the TEMPO nitroxonium salt. The yield for this reaction, shown in Scheme 5-3, is extremely high, but the subsequent steps leading to the desired target compound could not be done. Protection of the ketone group by 1,2 ethanedithiol followed by its reductive cleavage to give **2** could not be successfully done. However, the protection reaction simply regenerated the starting material regardless of the Lewis acid employed for the coupling reaction. The reaction temperature also did not have a substantial

effect of pushing the reaction to the desired products. In lieu, was the formation of the dione (7) when the reaction was run at room temperature. Increasing the temperature further resulted in the formation of more dione product.

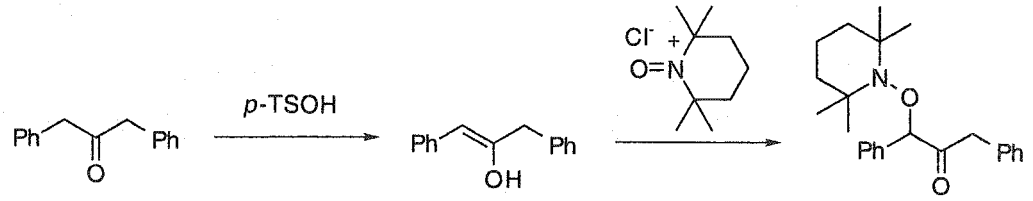

6

Scheme 5-3. Alternative synthetic approach of the target 'penultimate' initiator 2.

The formation of the dione is reminiscent of the reaction encountered by Barton who reported the decomposition α-nitroxide-carbonyls to give 1,2-dicarbonyl products.[31] This reaction was shown to proceed via an ionic mechanism by protonation of the piperidine nitrogen. The decomposition reaction observed here for **6** (see Scheme 5-4) is also identical to the ionic decomposition of benzoins discussed in the LFRP Photoinitiators chapter. The suppression of the desired reaction is therefore a result of preferential Lewis acid assisted ionic decomposition of the N-O bond. The formation of the diketone product also epitomizes the sensitivity of the nitroxide functionality.

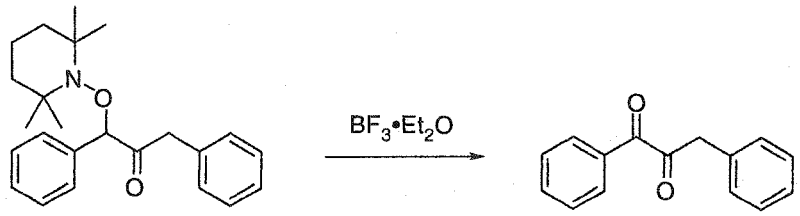

6 7

Scheme 5-4. Lewis acid induced decomposition of the nitroxide functionality to 1,2-diketone.

Other thermal based synthetic approaches proceeding through an organo-zinc intermediate[32-34] were met with marginal success, but the product could not be readily purified and was heavily contaminated with unreacted nitroxide.

Coupling of the benzylic center with TEMPO mediated by samarium diiodide[34-36] resulted only in the cross-coupled carbon centered radical product.

Due to the lack of thermal based synthetic success, an alternative photochemical method was employed. The method of Connolly[37] was adopted in which di-*tert*-butyl peroxide is photochemically decomposed generating two *tert*-butylalkoxyl radicals. These subsequently abstract a hydrogen from the parent hydrocarbon leading a carbon centered radical (see Equation 4 of Scheme 5-5). The carbon centered radical is consequently trapped by TEMPO giving the desired product. The yields of this reaction are quantitative when the hydrocarbon undergoing hydrogen abstraction is used as the solvent. The hydrocarbon **5** is expensive, exhibits a high viscosity, and high boiling point which precludes its use as a solvent, and therefore was used in stoichiometric amount with the nitroxide. This led to extremely poor yields of the desired initiator **2**, typically < 5 %. The poor yield stems primarily from the known β-cleavage reaction of *tert*-butylalkoxyl (see Equation 2) and the subsequent trapping of the methyl radical by TEMPO in the absence of solvent.[38,39] This has a two fold influence on the results. Firstly, the *tert*-butylalkoxyl concentration is reduced during the reaction by the β-cleavage reaction and subsequently there is insufficient oxygen centered radicals to promote hydrogen abstraction. This suppresses the formation of the desired carbon centered radical. Secondly, the amount of nitroxide is effectively reduced through trapping of the methyl radical. This is apparent from the characteristic nitroxide orange color that dissipates upon irradiation without the formation of **5**. These two reactions do not predominate when the hydrocarbon is used as the solvent. Instead, the hydrogen abstraction reaction occurs. The rate constant for the latter is extremely slow at ~ 10^5 M^{-1} s^{-1},[40] but the overall rate of the reaction can be accelerated by increasing the concentration of the hydrocarbon. This is the case when the hydrocarbon is used as the solvent. However, reducing the concentration of the hydrocarbon decreases the rate of the abstraction reaction and leads to a competition with the β-cleavage reaction. The rate of β-cleavage is known to be influenced by the solvent polarity being faster in polar solvents.[41] However, the yields of the desired reaction are moderately increased with *tert*-butanol as a solvent, most likely because of its inertness.

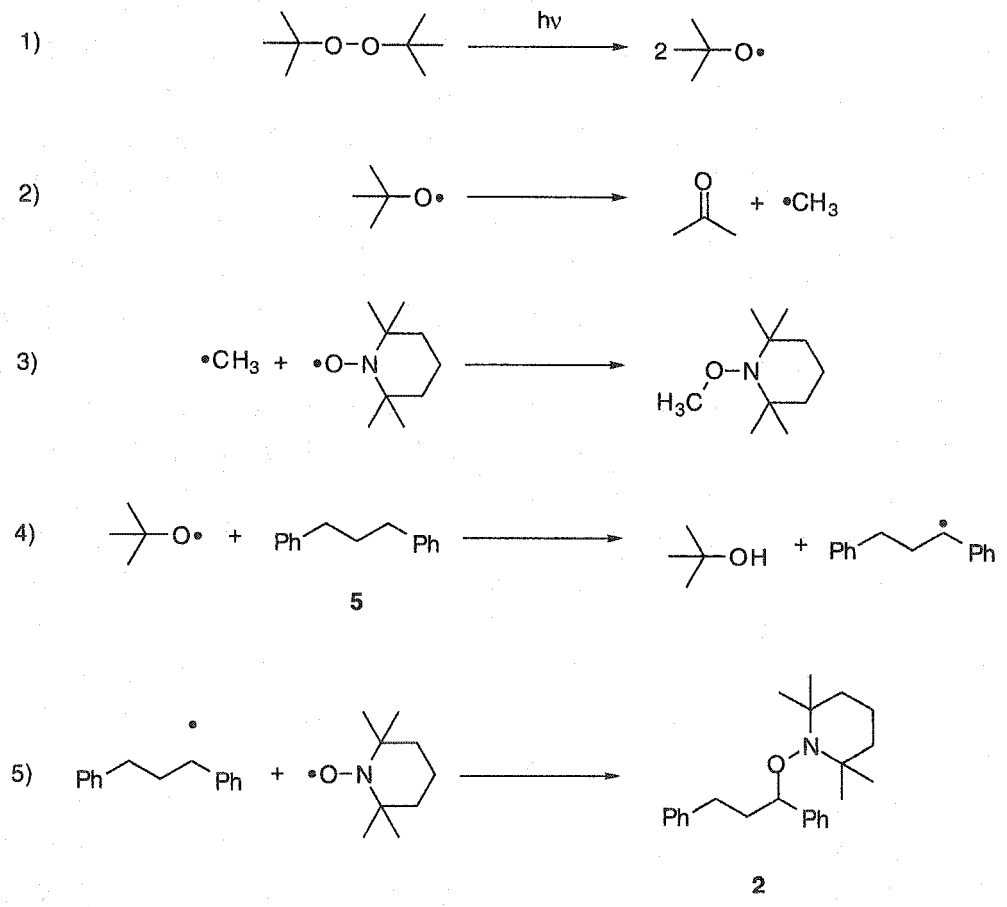

Scheme 5-5. Photochemical pathway for the synthesis of the 'penultimate' initiator 2.

5.2.2 Polymerization Studies

Preliminary polymerization investigation with the two unimolecular initiators, 2 and 3a, done in the presence of 100 equivalents of styrene at 115 °C yield polymers with identical properties. This study was done to verify that both initiators possessed similar, if not identical, initiation properties. The properties determined by gel permeation chromatography are represented in Table 5-1. The conversions for both initiators are greater than 95 % and have the expected DP. There is no apparent difference in the initiation properties of the two initiators based upon the polymerization results. The preliminary results suggest the addition of the extra styrene group does not influence the initiation capabilities of these compounds.

Table 5-5. Comparison of polymerization results of different macroinitiators at 115 °C for 22 hours.

Initiator	PD	M_n
2	1.12	8688
3a	1.16	8615

5.2.3 Thermodynamic Studies

The preliminary polymerization studies showed little behavioral difference between the two initiators investigated, suggesting their decomposition properties are identical. To confirm this, thermal decomposition studies of the Arrhenius type were done similar to these reported in the Initiator Decomposition chapter. This involved decomposition of the initiator at elevated temperatures to generate the nitroxide and carbon centered radicals. In the absence of any scavenger, the back reaction involving these two radicals occurs quite fast (see Equation 6 in Scheme 5-6), on the order of 10^8 M^{-1} s^{-1}.[6,42,43] An external trap, typically another nitroxide, is added to ensure the suppression of the back reaction. If the reaction is allowed to proceed, i.e. absence of trap, the thermodynamic parameters measured would appear different than the true value simply due to analytical difficulties in quantifying the amount of reagent decomposition. The formation of another nitroxide trapped product that can easily be resolved by analytical methods is the other benefit of using an external trap. This method, referred to as the cross-over or nitroxide exchange experiment, has been successfully used to determine the decomposition parameters of other unimolecular initiators, as seen in Initiator Decomposition chapter.[6]

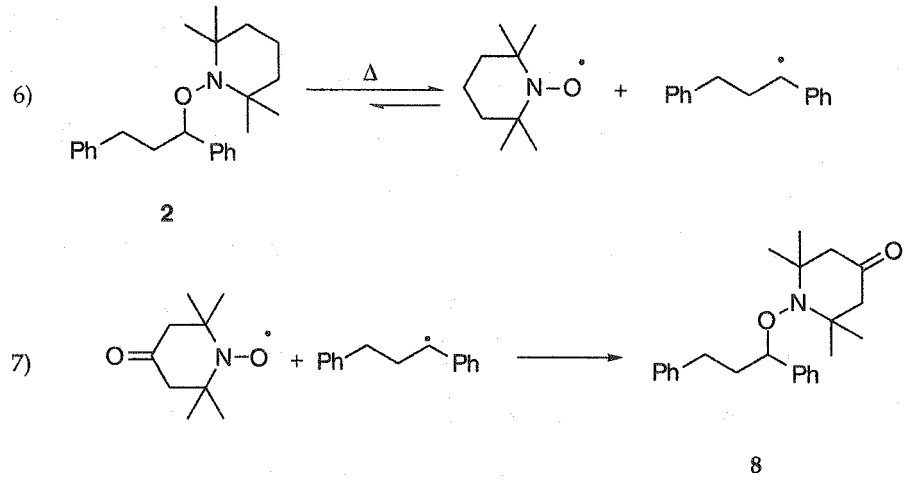

Scheme 5-6. Thermal decomposition of 2 in the nitroxide cross-over experiment.

The inset of Figure 5-2 shows the concentration increase of the trapped product during the nitroxide exchange upon thermal decomposition. Effectively, the slope refers to the rate constant of product formation which is also equal to the rate of reagent decomposition. Performing the decomposition nitroxide-exchange experiment over a series of temperatures gives the temperature dependent rate constants. The Arrhenius equation (Equation 5-1) can then be used to extrapolate the pre-exponential factor (log A) and the activation energy (E_a) from the intercept and slope, respectively. Figure 5-2 graphically represents the decomposition parameters required for Equation 5-1.

$$\log k = \log A - 2.303 \cdot \left(\frac{E_a}{RT} \right)$$

Equation 5-1. Arrhenius equation leading to the pre-exponential factor and activation energy.

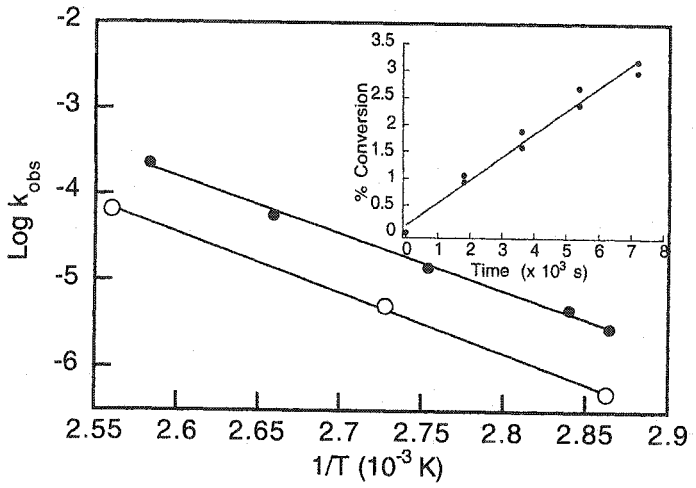

Figure 5-2. Arrhenius plot of 3a (●) and 2 (○) from thermolysis leading to the activation energy and pre-exponential factor. Inset: Rate constant for 2 obtained at 93.5 °C in the presence of 4-oxo-TEMPO.

The calculated decomposition values for the two initiators are reported in Table 5-2. The activation energy (E_a) reported refers only to the barrier that must be overcome for homolytic bond scission leading to the two radicals. This is referred to as E_a forward. The back reaction (Equation 6) involving the two radicals is not void of an activation energy (E_a back) and is approximately 1.5-2 kcal/mol for compounds of similar structures.[42,43] Therefore, the bond dissociation energy for the C-O bond fragmentation is the difference between the activation energies of the forward and back reactions.

It can be seen from Table 5-2 that the properties of the two structurally similar initiators are quite close. The only difference is the amount of disproportionation products generated upon their thermal decomposition. The addition of the styrene type unit in **2** successfully suppresses the amount of detectable disproportionation products **9** and the corresponding hydroxylamine (see pathway a in Scheme 5-7). The compound **9** was also not observed during thermal decomposition of **2** in the absence of any external trap. Normally in the absence of radical scavengers, the general reaction depicted in Scheme 5-1 is the main pathway for the decomposition for other alkoxyamines. In the presence of radical scavengers, such as monomers,[44] oxygen,[45] or other nitroxides,[6] irreversible decomposition of alkoxyamines typically occurs with faster observed rates and gives other products, indicative of scavenging of carbon centered radicals, along with small amounts of disproportionation products.[6,45,46] The

difference in behavior, particularly the relative thermal stability of alkoxyamines in the absence of scavengers can be readily explained with the Fischer-Ingold persistent free radical effect, which in this case favors cross combination of the radicals to regenerate the starting material.[47-49]

Table 5-6. Activation parameters of various macroinitiators.

Initiator	log A (s^{-1})	E_a (kcal/mol)	BDE[a] (kcal/mol)	Disproportionation (%)
2	13.3	30.3	28.0	0
3a	13.7	30.7	28.4	3

a) Refers to bond dissociation energy.

The unusual decomposition behavior of **2** was also observed during photochemical studies. Under typical nitroxide exchange conditions (see experimental section), irradiation of the initiators of the like of **3a**, decompose via all three pathways reported in Scheme 5-7. However, the photochemical decomposition of **2** proceeds only by pathways a and c arising from C-O and N-O homolytic bond fragmentation, respectively. No unsaturated disproportionation products were observed in the presence and absence of an external nitroxide trap further confirming the role of the additional styrene-type unit for deterring the formation of these disproportionation products. However, thermal and photochemical studies do not shed much light into the modes of suppression for disproportionation products. Rather, these preliminary studies only show the incorporation of a second styrene type unit in the initiator successfully suppresses the reaction leading to disproportionation products. Therefore, the second bulky styrene group plays an active role in suppressing this reaction. Further investigation involving kinetic and solid state studies were done to find the answer to the origins of disproportionation product suppression in **2**, which ultimately leads to living polymers.

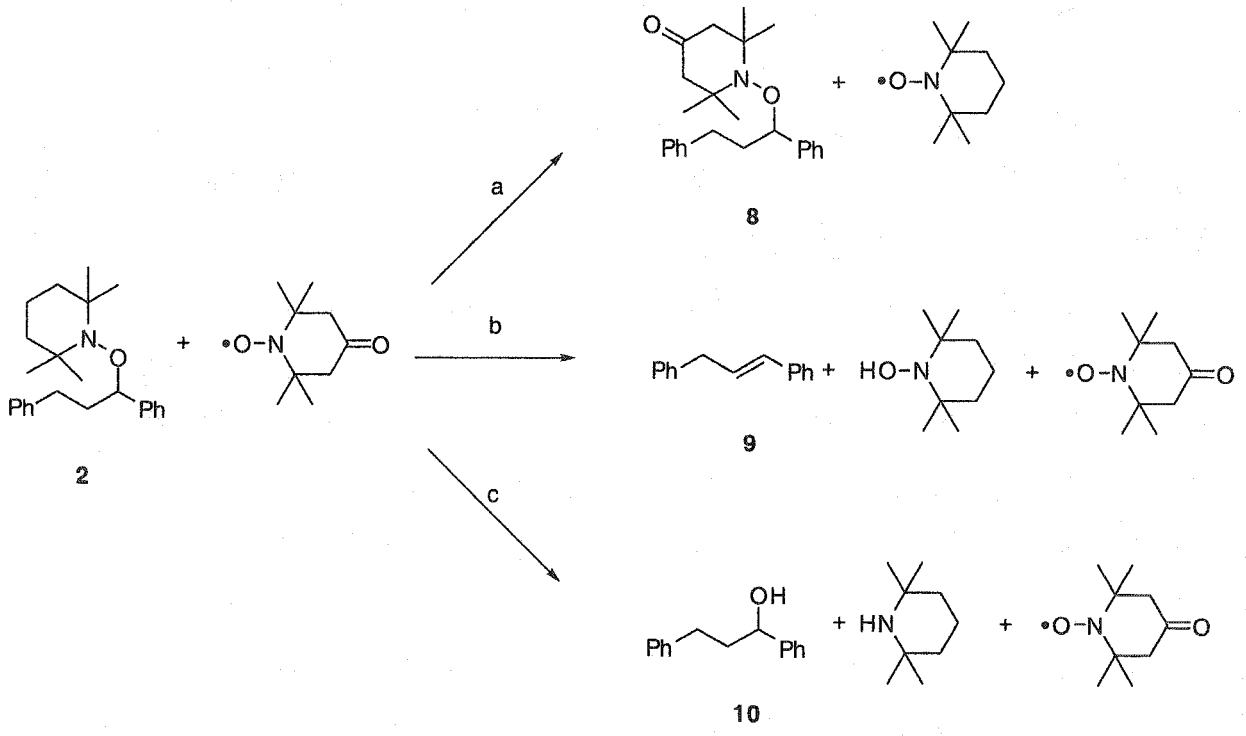

Scheme 5-7. Potential decomposition pathways of the 'penultimate' LFRP initiator.

5.2.4 Disproportionation Mechanism

In order to discuss the differences in the observed disproportionation products between **2** and **3a** it is important to understand the type of mechanism by which the products of the reaction in Scheme 5-1 are formed. This is not a facile question to resolve as little work has focused on determining the origins of disproportionation products for alkoxyamines such as **2** and **3a-b**.[45] Interestingly, **2** does not form disproportionation products, while **3b** (5 %) forms them slightly more efficiently than **3a**. The number of available β-hydrogens cannot be exclusively responsible for the amount of disproportionation products. No such products are observed for **2**, while doubling the number of abstractable β-hydrogens from **3a** to **3b**, only marginally increases (1.5%) the amount of disproportionation products observed. This is opposite to previous reports concerning disproportionation findings.[50] Other factors such are orientation and steric hindrance (*vide infra*) must also play a role in determining whether disproportionation occurs for the compounds of this study.

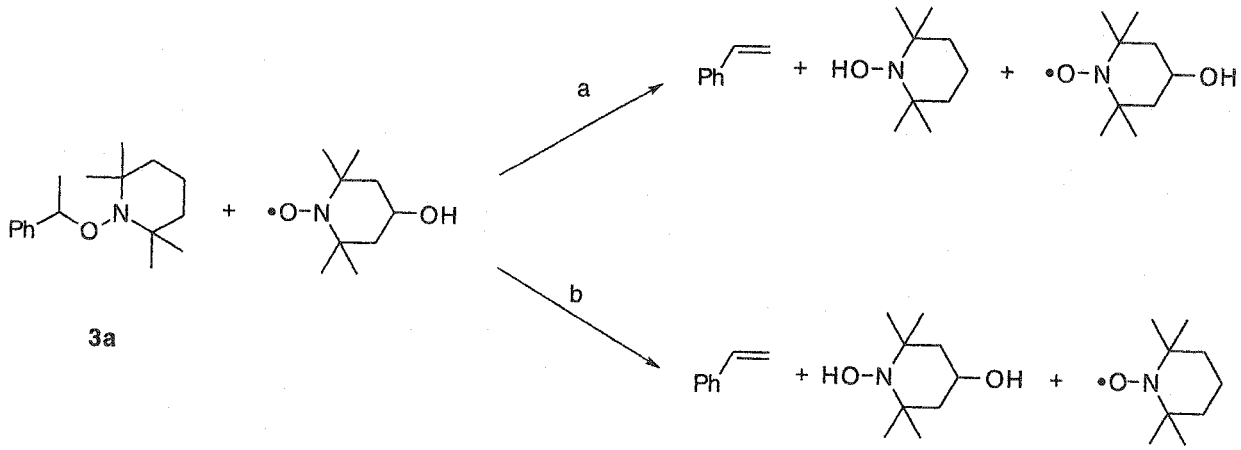

Scheme 5-8. Decomposition of 3a in the presence of an additional trap by in-cage (a) and out-of-cage (b) disproportionation mechanism.

In principle, there are three mechanisms by which disproportionation products can be formed: (i) by a concerted four-center elimination; (ii) by in-cage reaction within the radical pair formed by C-O cleavage; and (iii) by out-of-cage disproportionation between true free radicals. Thermal decomposition of **3a** under nitroxide exchange conditions exclusively gave the products shown by pathway a in Scheme 5-8.[51] The hydroxylamine of the external trap was not observed at all even at long decomposition times. This precludes the out-of-cage disproportionation mechanism, at least as a significant pathway for the formation of disproportionation products. An in-cage mechanism generates two radicals that are confined within a solvent cage and then undergo disproportionation according to Scheme 5-9.[46] Strict orientation for *p* orbital overlap of the geminate radicals, configuration, and steric requirements are important for achieving disproportionation products.[50,52,53] A recent report by Georges et al.[51] found that disproportionation involving nitroxide based unimolecular initiators was step-wise in nature and not concerted.

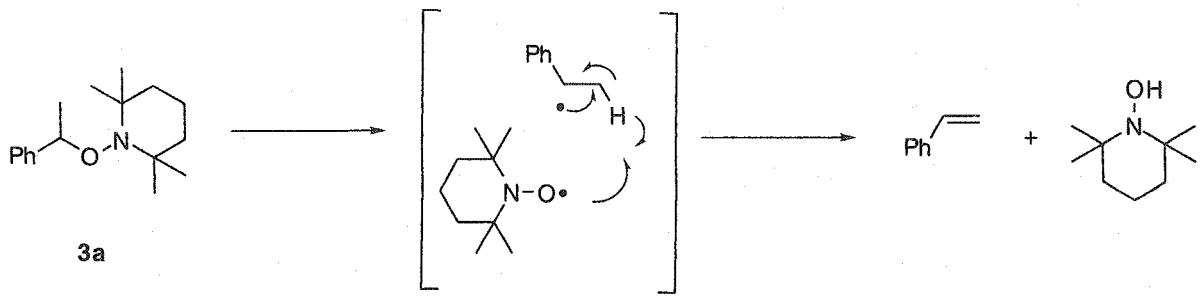

Scheme 5-9. In-cage radical process leading to disproportionation products.

Unlike the in-cage process, the concerted mechanism does not involve the formation of radicals. Rather, the mechanism leading to disproportionation products requires correct alignment of the orbitals through bond rotation. The correct orientation anticipated to lead to disproportionation products is a syn-periplanar conformation of the H-C-C-O moiety and an increase in the rotational barrier of this bond would have the effect of reducing the amount of observed disproportionation products. Schematically, the correct configuration required for concerted mechanism leading to disproportionation products is represented in Figure 5-3.

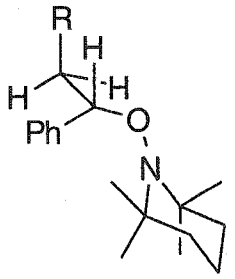

Figure 5-3. Required conformation for four center concerted elimination.

There is no practical experiment that can distinguish between the other two mechanisms, i.e., concerted or an in-cage radical disproportionation. Even today's ultrafast spectroscopic techniques are unlikely to yield conclusive results. Thus, differentiation between the two mechanisms must be largely based on a critical analysis of the data obtained being kinetic and rotational studies.

5.2.5 Kinetic Studies

Preliminary kinetic work was undertaken to probe the origins of different amounts of disproportionation formation between the two initiators 2 and 3a. This involved the use of 1,3-diphenylpropane (5) using indirect LFP work because of the difficulties involving the synthesis of the target molecule 2. The indirect LFP method involves photodecomposition of di-*tert*-butyl peroxide generating two *tert*-butylalkoxyls that subsequently abstract a hydrogen from the hydrocarbon. In the case of aromatic hydrocarbons, such as 1,3-diphenylpropane (5), the abstraction leads to a carbon centered radical that is visible on the laser system and its decay can be monitored as a function of nitroxide concentration. Under pseudo-first order conditions, this gives the desired trapping rate constant (k_q, see Equation 10 in Scheme 5-10). The overall reaction sequence of this process is represented in Scheme 5-10. Typical rate constants (k_{RH}) for the hydrogen abstraction reaction of Equation 9 are in the range of 10^5 to 10^7 M^{-1} s^{-1} for different hydrocarbons.[40]

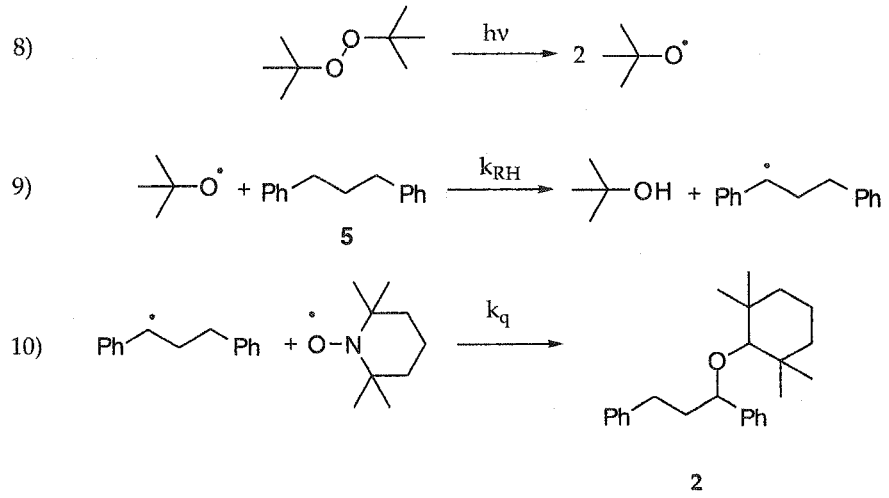

Scheme 5-10. LFP indirect method for determining the trapping rate constant of 1,3-diphenyl-1-propyl radical by TEMPO.

The indirect LFP method was originally used as an easy approach for determining the rate constant for radical trapping by TEMPO since this method has been successfully used previously to produce the desired radical without difficult synthesis of the target molecule.[40,42,43] The drawback to this approach is that high concentrations of the hydrocarbon are required to produce a signal within the time resolution of the LFP setup. The hydrocarbon solvent 5 is

extremely viscous and its use in high concentration was of concern as the rate constants for TEMPO trapping are known to be solvent and viscosity dependent.[43,54] The yield of the 1,3-diphenyl-1-propyl radical derived from hydrogen abstraction of **5** (Equation 9) was quite low as the observed LFP signal was extremely weak. Increasing the concentration of the hydrocarbon normally boosts the signal, however this had no effect with **5** and resulted only in an extremely viscous solution with the same poor signal to noise ratio. Regardless, the correct radical was generated as confirmed by the characteristic absorption maximum centered at 320 nm.[55] Product studies from steady state irradiation confirmed by NMR and HPLC do not show any sign of TEMPO addition occurring at the β-position, but rather exclusive α-position addition. Addition at the β-position was not expected since statistically there are fewer abstractable hydrogens at this position. Also, the BDE for the hydrogen atom at this position is expected to be considerably higher than that of the α-position due to the reduced stability of the subsequently generated radical. Therefore, the low efficiency in generating the correct 1,3-diphenyl-1-propyl radical (**2**•) was the predominant cause for the weak signal and was further confirmed by the steady state irradiation that gives low yields for product formation of **2** (*vide supra*).

The rate constant for the trapping reaction (k_q) of **2**• generated by hydrogen abstraction of **5** by *tert*-butylalkoxyl (Scheme 5-10) was found to be 4.0×10^7 M^{-1} s^{-1}. This value is considerably slower than the rate constant for nitroxide trapping of the 1-phenylethyl radical derived from **3a**. This was of concern as the rate was originally thought to be slower due to the high viscosity of the reaction medium as these reactions are known to be viscosity dependent.[54] Also, this method of generating the carbon centered radical is not instantaneous and inherently gives slower trapping rate constants because of the steps required to generate the desired radical to be observed. Therefore, direct photolysis of **2** was done to determine the true rate constant because the radical is instantaneously generated within the laser pulse (~ 10 ns) by this method.

Direct photolysis of **2** at 266 nm gave the characteristic absorption spectrum expected for the 1,3-diphenyl-1-propyl radical (**2**•) with maximum absorptions at 308 and 320 nm (see Figure 5-4).[56] Subsequent quenching of this radical as a function of TEMPO concentration under pseudo-first order conditions led to the trapping rate constant, k_q (direct), being 4.7×10^7 M^{-1} s^{-1} shown in Table 5-1 and Figure 5-5. The direct method generates an instantaneous source of the carbon centered radical upon irradiation and reflects the true rate constant for radical

trapping, unlike the indirect method of Ingold et al. that gives slower observed rate constants.[42,43,57] The k_q value obtained by this method is well below the diffusional controlled limit and roughly four times slower than the value expected for the 1-phenylethyl radical derived from **3a** under similar experimental conditions.[12,42,43] However, there is little difference between the rate constants measured for the direct and indirect methods implying the high viscosity condition of the indirect method does not greatly influence the trapping kinetics. Also, it can be concluded that the hydrogen abstraction method does give fairly accurately trapping rate constants providing these values are slower than 10^8 M^{-1} s^{-1}. Furthermore, the measured rate constant of k_q for **2** is truly slower than **3a** (*vide infra*).

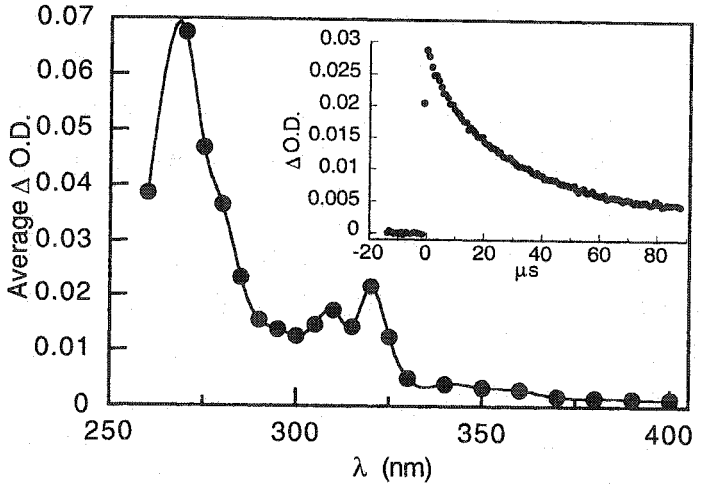

Figure 5-4. Transient absorption spectrum of 1,3-diphenyl-1-propyl radical (2•) recorded 10.4 μs after the 266 nm laser pulse. Inset: Decay of the radical in the absence of any quencher recorded at 320 nm.

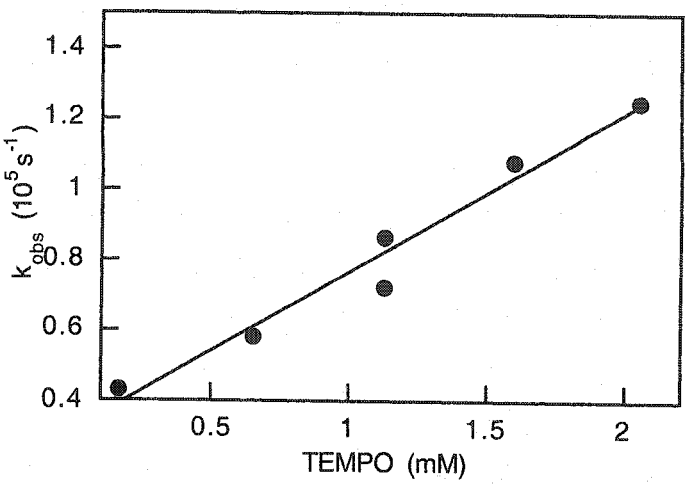

Figure 5-5. Quenching of 1,3-diphenyl-1-propyl radical (2•) in the presence of various amounts of TEMPO recorded at 320 nm after 266 nm photolysis.

The radical structures formed from **2** and **3a** are essentially similar, with the exception of the extended chain in **2**, suggesting their trapping reactivity by TEMPO would also be similar. However, the kinetics obtained are different implying the elongated chain of **2** somehow influences the reactivity of the carbon centered radical. The rate constant of hydrogen abstraction (k_{RH}, Equation 9, Scheme 5-10) from the parent hydrocarbon does not give much insight into differences between the two initiators because the measured k_{RH} from Equation 9 measured for **5** (1.1×10^6 M^{-1} s^{-1}) is identical to ethylbenzene.[40] Other factors, such as steric elements, are responsible for the different k_q observed between **2** and **3a**.

Table 5-1. Representative rate constants for quenching of various radicals by TEMPO.

Radical	k (10^7) (M^{-1} s^{-1})
	49[a]
	19[a]
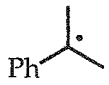	12[a]
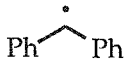	4.6[a]
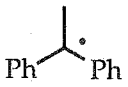	4.5[a]
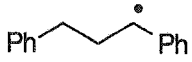	5.1[b]
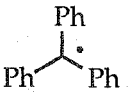	< 0.1[a]

a) Values from literature measured in iso-octane.[57]
b) Experimentally determined value.

At first glance, the rate constants of TEMPO trapping, as seen in Table 5-1, are similar for the radicals from **2** and diphenylmethane suggesting similar stability. The slow trapping constant of $(Ph)_2HC\bullet$ is not entirely from resonance stabilization from the additional aromatic group, but mainly from steric factors as the phenyl groups act like propellers around the central planar radical.[58,59] Substitution by additional phenyl groups increases the stability of the radical through major steric and minor resonance means as seen in the reduced trapping constant for $(Ph)_3C\bullet$.[57] The slower observed rate constant for **3a** is not from resonance or electronic stabilization as the additional aromatic group is

located 2 σ bonds from the radical center. The efficiency of any electronic stabilization is minimized over this distance. Also, the lifetime of the radical is too short to be stabilized by folding of the secondary aromatic group closer to the radical center. Therefore, the difference in the observed k_q for **2** and **3a** stems from steric contributions and not electronic or thermodynamics. The rate constant measured is more representative of the true trapping constant found in the LFRP process as the radical trapped in our studies is structurally similar to a bulky styrene dimer responsible for propagation encountered in the polymerization process.

The slow rate constant for the reaction of the 1,3-diphenyl-1-propyl radical with TEMPO means that approximately one in 500 radical encounters leads to radical termination, since the rate constant for diffusion controlled process in acetonitrile is around 2×10^{10} $M^{-1} s^{-1}$. Even taking into account spin configuration statistics, less than 1% of the singlet encounters lead to a reaction. Thus, the vast majority of the encounters are unreactive. One can usually assume that in-cage pairs are not dramatically different form those produced by random encounters of free radicals. On this basis, reaction of a geminate radical pair before exit from the original solvent cage must be a rare event. As applied to the disproportionation reaction, one would have to argue that geminate pairs are intrinsically different from random pairs. This is an uncommon, but not impossible argument for a straight recombination reaction, since the radical-pair must be born with the perfect orientation for back reaction.[60,61] But this is not true for disproportionation that requires a radical pair orientation different from the nascent one. Thus, one is forced to the conclusion that this must be a concerted elimination, not involving free or geminate radicals.

5.2.6 Rotational Barriers

The evidence previously presented for the two initiators **2** and **3a** supports a concerted mechanism responsible for disproportionation product formation. The rotational barriers of the initiators were examined with different techniques to seek further evidence for a concerted mechanism responsible for the observed disproportionation products. An increase in the rotational barrier height for **2** relative to **3a** would support the presence of a concerted mechanism. The specific bond rotation investigated is shown in the Newman projection in Figure 5-6. The eclipsed formation of the α,β-hydrogens leading to the syn-periplanar

configuration of the H-C-C-O bond is required for the four center concerted elimination leading to the formation of disproportionation products.

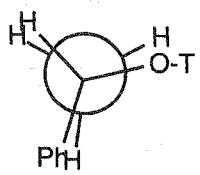

Figure 5-6. Newman projection of required conformation for disproportionation product formation.

5.2.6.1 Semi-Empirical Calculations

Even though sufficient evidence has been presented to support a concerted process, theoretical rotational barriers for the two initiators **2** and **3a** were examined for supporting evidence. Semi-empirical calculations were used to determine the barrier heights associated with the C-C bond rotation shown in Figure 5-6. This method involves locking the H-C-C-H dihedral angle at a given value and calculating the lowest energy of the system for the lowest given energy conformation. The angle is changed and the new heat of formation (ΔH_f) for the rotamer is subsequently calculated after the lowest energy geometry has been found. The series of ΔH_f values as a function of the H-C-C-H dihedral angle lead to the plot of the type shown in Figure 5-7. The lowest energy rotamer for each initiator studied was taken as 0 kcal/mol and all other rotamers are relative to this value for ease and direct comparison of the calculated barrier heights.

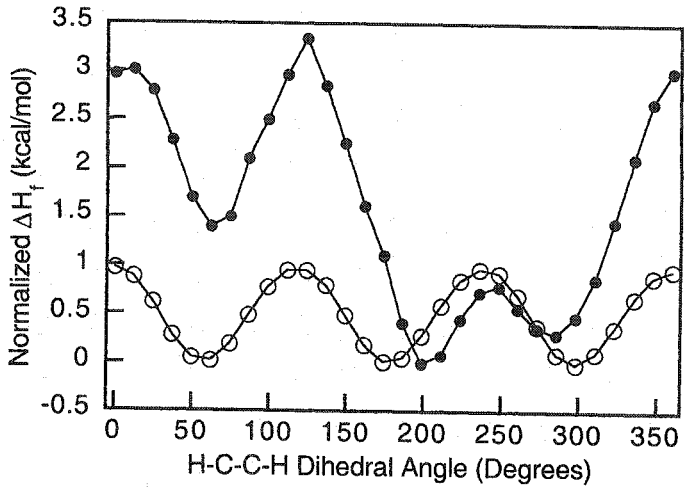

Figure 5-7. Rotational barrier height for compounds 2 (●) and 3a (○) calculated from semi-empirical AM1 coordinate driving with Spartan. The heat of formation (ΔH_f) of each rotamer has been normalized to the lowest energy rotamer.

The absolute values derived from these calculations do not afford any information. However, the relative values can be used with a high degree of accuracy to predict any trend because the errors associated with the calculations are largely systematic.[62-66] These types of semi-empirical calculations normally fail with radical systems, but are well suited for the closed shell initiators studied here. The relative accuracy of the values was exploited to calculate the height of the rotational barriers for the two initiators.

A comparison between **2** and **3a** was done because the latter is known to give significant amounts of disproportionation products. The difference between the rotamers of **3a** seen in Figure 5-7 and Table 5-2 is relatively small suggesting the rotational barrier ($E_{rotational}$) is quite small. However, the calculated values of **2** are considerably higher relative to **3a**, regardless of the semi-empirical method selected. This implies substitution of the CH_2-Ph group increases the rotational barrier for the C-C bond shown in Figure 5-6. The correct syn-periplanar conformation of the H-C-C-O moiety necessary for the formation of disproportionation products is less energetically favorable for the initiator **2** than for **3a**. The lack of disproportionation products for **2** can then be attributed to the increased height of the rotational barrier due to steric stereoelectronic effects which suppress the correct configuration of a concerted four-center elimination. Further, the C-O rotational barrier placing the oxygen orbitals in correct

alignment of the concerted disproportionation is once again much higher for 2 than 3a.

Table 5-2. Semi-empirical calculations of the rational barriers from dihedral coordinate driving of various macroinitiators.

Initiator	$E_{rotational}$ (AM1) (kcal/mol)	$E_{rotational}$ (PM3) (kcal/mol)
2	3.3	5.8
3a	1.0	2.5

5.2.6.2 Solid State Studies

The initiator 3b was found to thermally decompose in the solid state at room temperature to give an orange solid, characteristic of free TEMPO. The products determined by HPLC were found to be the free nitroxide and not the hydroxylamine anticipated as a disproportionation product. This may have been a result of oxidation of the hydroxylamine to the nitroxide under atmospheric oxygen. However, the irradiation of the initiator in the solid state in the presence and absence of oxygen both fail to provide the hydroxylamine disproportionation product. The importance of these preliminary findings is they provide further support for a concerted disproportionation mechanism. In the solid state, the transients produced upon irradiation cannot rapidly diffuse away from one another as in solution. Therefore, an increase in disproportionation products is anticipated with irradiation in solid state if a step-wise disproportionation mechanism is present. Also, the correct conformation for elimination may be difficult to achieve in the solid state leading to fewer disproportionation products if a concerted process was present. Solid state irradiation leads to little disproportionation products, and as a consequence, give further experimental evidence supporting a concerted mechanism.

Laser flash photolysis measurements of 3b in the solid state lead to the transient absorption spectrum shown in Figure 5-8. The spectrum obtained is

characteristic of the cumyl radical with absorptions at ca. 308 and 320 nm.[67] The recombination of geminate radicals is expected to decay by first order kinetics and is the case with the laser photolysis of **3b**. Analysis of the products by HPLC after irradiation once again show no sign of the hydroxylamine further supporting the claim of a concerted mechanism for disproportionation product formation.

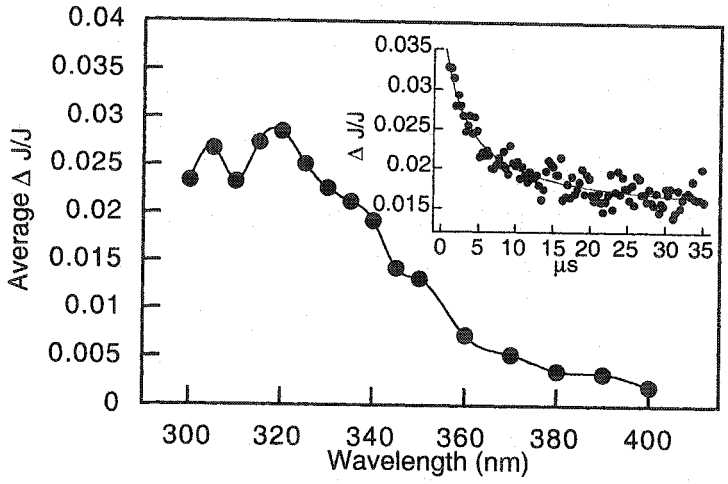

Figure 5-8. Diffuse reflectance transient absorption spectrum of 3b over silica gel recorded 3.36 μs after the laser pulse at 266 nm. Inset: Decay of 1-phenylpropyl radical monitored at 320 nm.

5.2.6.3 X-Ray Crystallography

In general, the lowest energy form is adopted in the crystal form and the structures of the two initiators were examined for any differences. The X-ray crystal structures of the two unimolecular initiators are not remarkably different as shown in the ORTEP diagrams in Figure 5-9. The lowest energy conformer for **2** is the expected staggered conformation because of the anticipated high energy barrier for rotation.[68] Conversely, **3a** may have an eclipsed form because its rotational barrier was found to be quite low, therefore the energy difference between the eclipsed and staggered conformers are expected to be equally small. However, this is not the case as both initiators exhibit the lowest energy staggered conformation and no concrete conclusion can be drawn from this study.

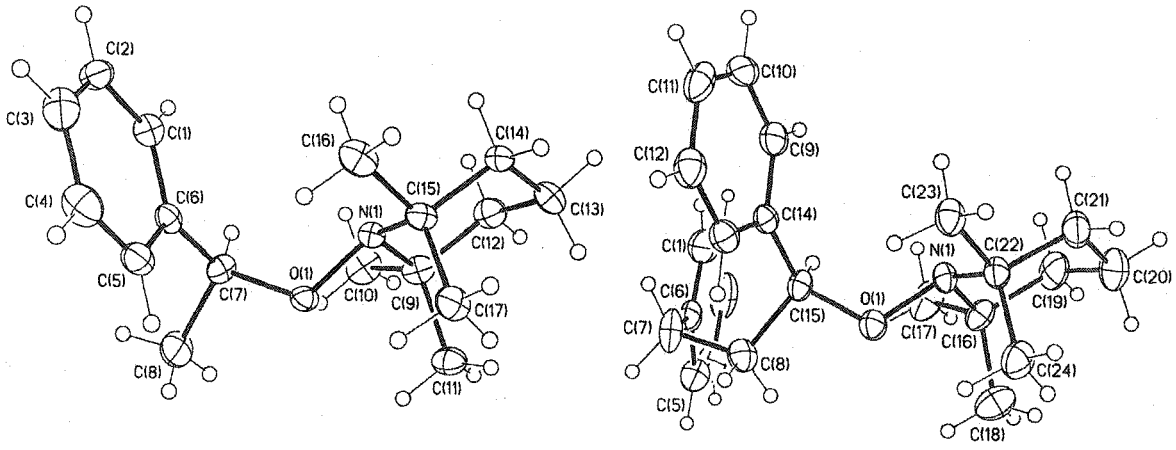

Figure 5-9. ORTEP diagram of initiators 3a (left) and 2 (right).

5.2.6.4 NMR Studies

Temperature dependent NMR studies were performed for further experimental evidence. In principle, this method involves building an energetic profile of the desired process through a series of NMR spectra taken at different temperatures. Importantly, the protons observed during this study must be chemically nonequivalent in order to provide any information. Alkoxyamines represent a class of stereochemical compounds that posseses chemically nonequivalent protons.[69] This is in part due to the non-planar nitrogen and the non-linear oxygen center shown in Figure 5-10. The initiators **2** and **3a** give four methyl groups in the 2 and 6 positions lead to 4 discrete singlets integrating for 3 protons each in the ^{1}H-NMR spectrum.

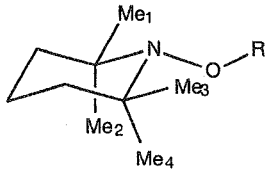

Figure 5-10. Illustration of non-equivalent methyl protons in alkoxyamines.

Here we are concerned with the barrier involved in bond rotation for the exocyclic bond N-O not directly involved in the proposed concerted elimination reaction. This study was taken on to investigate if other factors than the ones examined are responsible for the difference in observed amounts of

disproportionation products between these two initiators. The bond rotation was easily measured by monitoring the change in the four methyl singlets as a function of temperature. At room temperature, the rotational processes are quite slow compared to the time resolution of the NMR spectrometer. This results in a snap-shot giving an NMR spectrum with four discrete methyl groups. With increasing temperature, the rate of the dynamic process being bond rotation or inversion increases and becomes faster than the time resolution of the spectrometer. This results in an *average* spectrum being recorded and the chemically different protons are no longer nonequivalent. The temperature at which the discrete peaks combine into one is known as the coalescence temperature (T_c) from which the energetics of the desired process can be calculated. T_c is proportional to the activation energy ($\Delta G^{\neq}$) of the studied process and the difference in chemical shifts between the different peaks in frequency units ($\Delta\nu$) as shown by Equation 5-2. This equation is valid only for singlets of equal population, which is the case for the study involving the initiators **2** and **3a**. Typical ^{1}H-NMR spectra used to calculated T_c for **3a** are shown in Figure 5-10.

$$\Delta G^{\neq} = 4.56 \cdot RT_c\left[10.32 + \log\left(\frac{T_c}{\Delta\upsilon}\right)\right]$$

Equation 5-2. Rotational barrier equation for NMR studies involving the coalescence temperature (T_c).

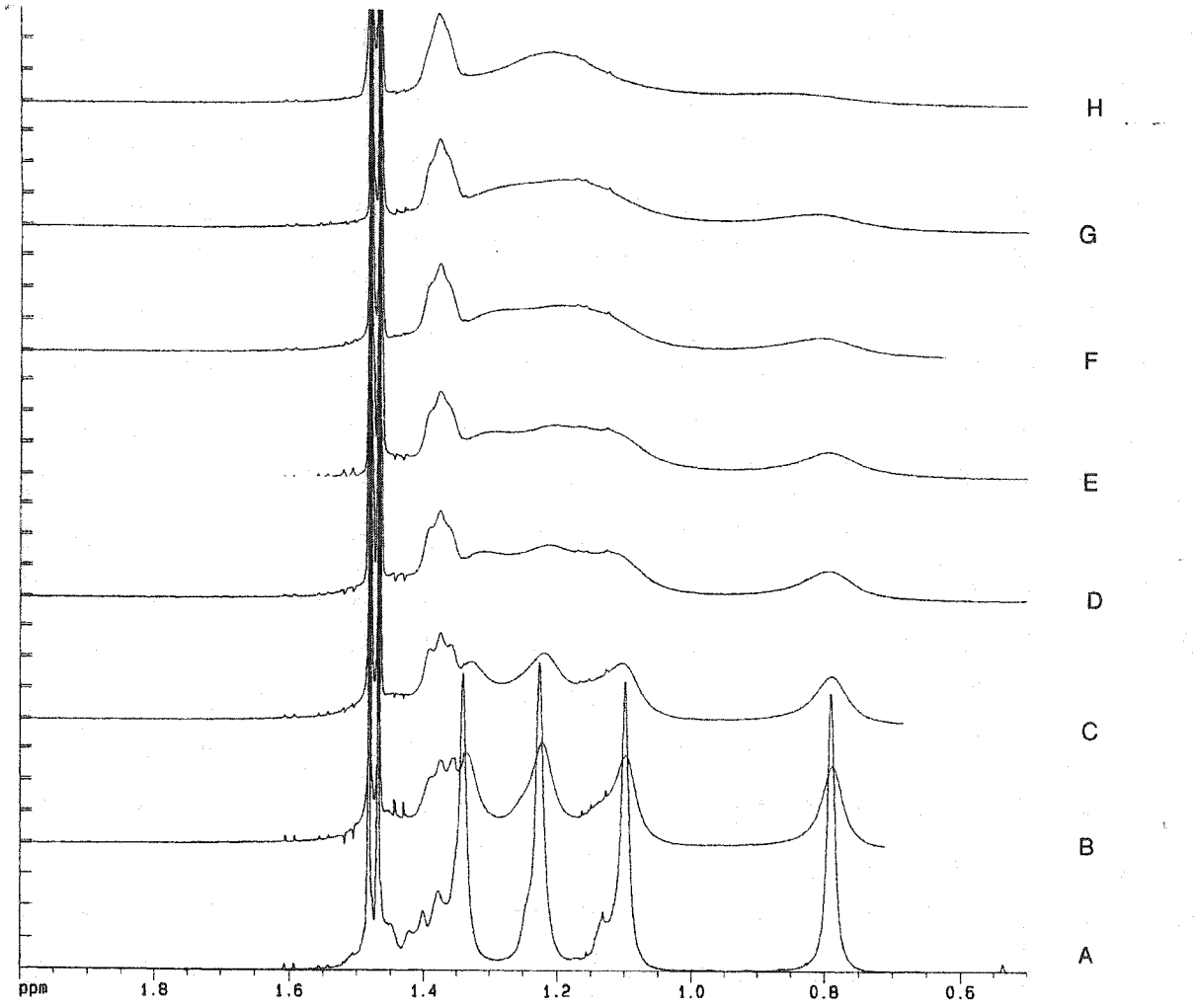

Figure 5-11. ^{1}H-NMR spectra of **3a** from 298 - 348 K to determine the coalescence temperature for Equation 5-2. The letters denote the temperature at which the spectra was recorded in K: A = 312; B = 320; C = 330; D = 330; E = 332; F = 335; G = 337; H = 342 K.

The coalescence temperature measurements gave energy barriers of 16.7 and 16.3 kcal/mol for **2** and **3a**, respectively. These values suggest that there is an increase in the rotational barrier possibly as a result in increase due to steric factors. A similar study involving different substituted alkoxyamines was done by Anderson et al. who found the barrier for a benzyl-nitroxide analogue to be slightly lower.[70] This is consistent with the rationale that the rotational barrier

height increases with substitution. The results obtained here are outside the range of experimental error, but the value for **2** is not as high implying the steric effect discussed previously does not drastically influence the N-O barrier height. The lower than expected value may be due to a ground state effect where the rotational barrier is actually higher. This effect was previously seen for crowded compounds that showed lower barriers than less substituted ones.[70] It is assumed that the rate determining step for these measurements is the exocyclic N-O bond rotation shown in Figure 5-11 and does not include any other processes such as Walden inversion or ring flipping (*vide infra*).[71] Typical values for these other processes are considerably lower than the exocyclic rotation energy.[70,72]

The DNMR studies do not provide any additional evidence for a concerted mechanism. The measured values for the two initiators studied by this method are quite small and would suggest only a slight increase in the N-O rotational barrier due to the additional substitution found in **2**. The major disadvantage of this method is its incapability of resolving each discrete rotation process. Instead, only the highest energy barrier, hence the rate determining step, is recorded regardless of the pathway selected, providing the stable species formed are detectable by NMR. This is shown in Scheme 5-11 where the interconversion from stable species **a** to **b** is not a direct route, but involves a three step process, regardless of the route selected. The three steps involved are any combination of N-O bond rotation (BR), Walden or nitrogen inversion (NI), and ring inversion (RI). The specie **Z** indicates a meta-stable species that cannot be resolved by NMR because its lifetime is outside the resolution of the instrument. It becomes extremely difficult to assign the measured energetics to one specific step since all three steps are involved and any one of them may be the rate determining step.

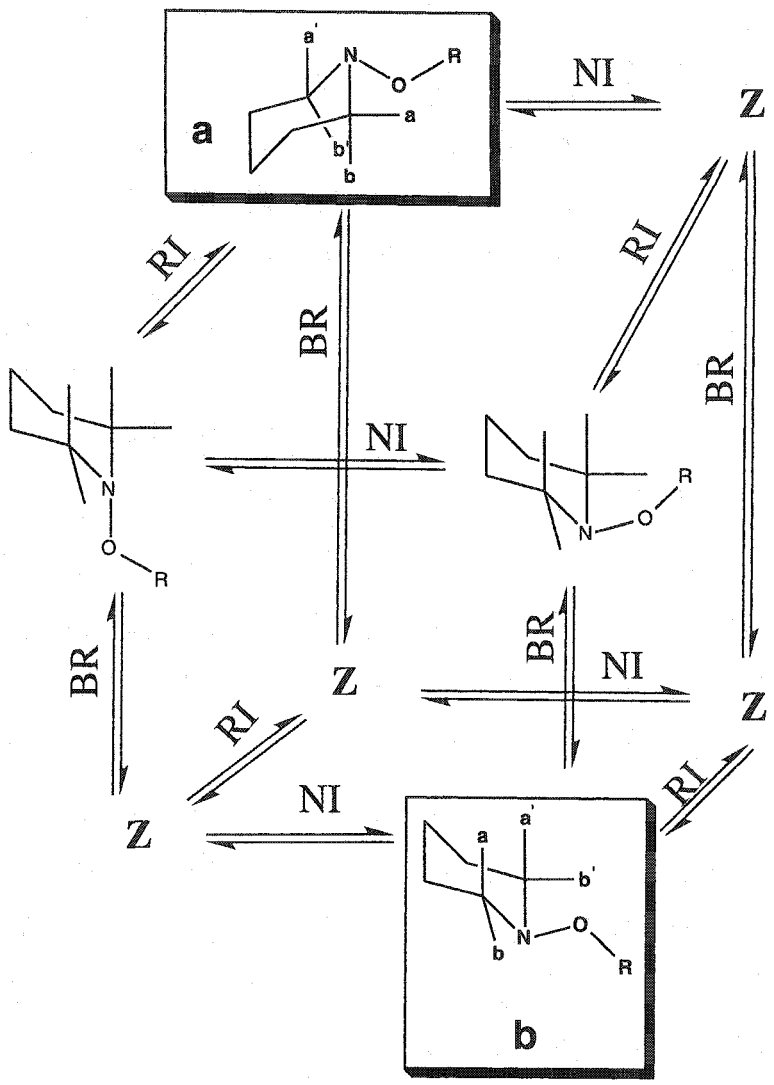

Scheme 5-11. Conformational scheme illustrating stepwise interconversion to NMR detectable products. BR = N-O bond rotation; NI = nitrogen inversion; RI = ring inversion.

Anderson and Lunazzi have investigated various alkoxyamines with different substituents in order to assign the energetics associated with BR, NI, and RI.[70,72,73] There is no easy solution or general trend that can be predicted since O-substitution inconsistently changes the energetics for NI and BR through changes in the ground state barrier and steric factors. By in large, the only conclusion that can be made is the observed 0.4 kcal/mol difference between the two initiators **2** and **3a** is due to a slight steric effect in the rotation barrier for the N-O exocyclic bond. No real information concerning the desired C-C bond

rotation can be extrapolated from this analysis because the individual rotation processes cannot be isolated on the NMR time frame.

5.3 Conclusion

The difference in the amount of detected disproportionation products for the LFRP initiators **2** and **3a** were found to be a result of the low rotational barrier. Semi-empirical and solid state studies confirm that the mechanism leading to disproportionation products is a concerted process and does not involve the formation of radicals. The insertion of an additional styrene type unit in the initiator, such as with **2**, increases the height of the rotational barrier for correct orbital alignment required for the four-center elimination. This in turn suppresses the disproportionation reaction by stereoelectronic means. Under typical polymerization conditions, decomposition of the initiator **3a** gives the 1-phenylethyl radical that is trapped by styrene leading to a dimer with similar structure to **2**. Upon thermal decomposition of the dimer under polymerization conditions, the reaction leading to disproportionation products is suppressed. This is due to the additional styrene unit that increases the height of the rotational barrier for the H-C-C-O bond and the correct syn-periplanar alignment is more difficult to attain. The ultimate result for the suppression of this pathway is polymers with narrow molecular weight distributions and high conversions.

5.4 Experimental

5.4.1 Synthesis

All chemicals used were from Aldrich and were used as received unless otherwise stated. Dry THF and diethyl ether for reactions were obtained by distillation over sodium-potassium wire with benzophenone. Hexanes used for flash chromatography purposes was first washed and distilled over calcium chloride.

1-(2,2,6,6-tetramethylpiperidine-N-oxide)-1,3-diphenylpropane (2)
Photochemical method A. Typical conditions consisted of dissolving of 1,3-diphenyl propane (Lancaster) (500 mg, 2.55 mmol) and TEMPO (500 mg, 3.20 mmol) in di-*tert*-butyl peroxide (5 g, 7.2 mmol) purified through a plug of neutral aluminum oxide. The orange solution was further diluted in 30-35 mL of *tert*-butanol and placed in a pyrex test tube, capped, deaerated for a minimum of 20 minutes with a stream of nitrogen, and irradiated at 300 nm till the orange color no longer persisted, typically 3 days. The lightly colored yellow solution was concentrated under vacuum and the resulting oil was purified by flash chromatography with 5% (v/v) ethylacetate/hexanes mixture to afford 1 in 40% yield. ^{1}H NMR (500 MHz, $CDCl_3$ TMS) δ 7.4-7.1 (m, 10H), 4.72-4.40 (m, 1H), 2.51-2.41 (m, 2H), 2.30-2.16 (m, 2H), 1.58 (m, 6H), 1.31 (s, 3H), 1.23 (s, 3H), 1.05 (s, 3H), 0.69 (s, 3H). ^{13}C NMR (300 MHz, $CDCl_3$) δ 143.3, 142.1, 129.6, 128.3, 128.2, 127.97, 127.86, 127.82, 127.04, 125.7, 125.6, 86.9, 59.8, 40.3, 39.5, 37.4, 34.3, 34.2, 33.9, 31.5, 20.2, 17.2. MS (EI) m/z (%) 194.1 (18.1), 179 (8.2), 156 (50.7), 142.1 (100), 140 (12.2), 123 (13.3), 117 (37.6), 105 (13.3), 91.1 (96.7), 83.1 (12.4), 69 (42.3), 55 (28.7), 41 (18.8). MS (FAB) m/z (%) 352 (12, M+1), 268 (2), 193 (5.7), 157 (61.6), 142 (100), 126 (26), 117 (52), 91 (99.8), 69 (44).

Photochemical method B. This method consisted of dissolving 1,3-diphenyl-1-bromopropane (250 mg, 0.91 mmol) in spectroscopic grade acetonitrile with TEMPO (141 mg, 0.91 mmol) and dearated for 20 minutes in a quartz test tube. The sample was irradiated at either 254 nm or 300 nm to afford a black colored solution where the color did not dissipate with continuous irradiation. Only trace amounts of the desired product were detected after removing the solvent

under vacuum and purifying by flash chromatography. Major products isolated were from N-O bond cleavage and nitroxonium salt formation.

Thermal method A. A modified procedure based upon literature was used.[32,74] Dry zinc dust (76.4 mg, 1.17 mmol) was added to approximately 25 mL dry THF with the addition of a couple of drops of 1,2-dibromoethane. The solution was refluxed for 2 hours and then cooled to 0 °C. 1,3-Diphenyl-1-bromopropane (220.6 mg, 0.81 mmol) in THF was added to the activated zinc solution and stirred at 0 °C for three hours. TEMPO (128.4 mg, 0.82 mmol) in dry THF was added to the cooled solution and allowed to warm to room temperature and stir for three hours. The reaction was quenched with water, filtered, and THF solvent removed. Dichloromethane was added and the organic layer extracted then dried over anhydrous magnesium sulfate. The orange solid was purified by flash chromatography with 10 % ethylacetate/hexanes mixture to afford < 5% yield of the target compound.

Thermal method B. 0.1 M Samarium diiodide (6 mL, 0.6 mmol) and hexamethylphosphoramide (HMPA) (1 mL, 1.1 mmol) were added to 20 mL dry THF under a nitrogen environment. 1,3-Diphenyl-1-iodopropane (193 mg, 0.59 mmol) was added to the samarium solution and the green/blue color immediately disappeared. TEMPO (206 mg, 1.32 mmol) was subsequently added and the solution was allowed to stir at room temperature for 2 hours. Water was added and the organic layer extracted with dichloromethane and subsequently dried over anhydrous magnesium sulfate. The crude product was subjected to flash chromatography with 10 % ethylacetate/hexanes to afford < 5 % yield of the desired product.

2,2,6,6-Tetramethyl-1-(1-phenyl-ethoxy)-piperidine (3a): The synthesis and characterization of the compound was presented in a previous chapter.

2,2,6,6-Tetramethyl-1-(1-phenyl-1-methyl-ethoxy)-piperidine (3b): The synthesis and characterization of the compound was presented in a previous chapter.

2,2-Dibenzyl-[1,3]dithiolane (4): Dibenzyl ketone (480 mg, 2.28 mmol) was dissolved in 35 mL dichloromethane and cooled to 0 °C. After 10 minutes 1,2 dithioethane (210 μL, 2.5 mmol) was added along with boron trifluoroetherate (310 μL, 2.5 mmol). The solution was allowed to warm to room temperature and stirred for five hours. The reaction was quenched with aqueous potassium hydroxide and the organic layer was separated with dichloromethane and dried

over anhydrous magnesium sulfate. The solvent was removed under vacuum and the product isolated by flash column chromatography with 10 % ethylacetate/hexanes in 98 % yield as a white waxy solid. ^{1}H NMR (200 MHz, $CDCl_3$ TMS) δ 7.25 (m, 10H), 3.21 (s, 4H), 2.75 (s, 4H). ^{13}C NMR (300 MHz, $CDCl_3$) δ 139.3, 130.5, 128.2, 66.5, 49.0, 47.0, 38.8.

1,3-Diphenyl-propane (5): 2,2-Dibenzyl-1[1,3]-dithiolane (169 mg, 0.59 mmol) was dissolved in 30 mL of a 3:1 methanol/THF solution and cooled to 0 °C. Nickel (II) chloride hexahydrate (1.03 g, 4.3 mmol) was then added followed by sodium borohydride (530 mg, 14.0 mmol) and the green solution was stirred till the color faded. The solvent was removed under vacuum and then dichloromethane was added and then washed with 10 % aqueous sodium bicarbonate. The organic layer was separated, dried with anhydrous magnesium sulfate and purified by flash chromatography with neat hexanes to afford an oil in 75 % yield. ^{1}H NMR (200 MHz, $CDCl_3$ TMS) δ 7.54-7.70 (m, 10H), 3.01 (t, 4H), 2,31 (m, 2H). ^{13}C NMR (300 MHz, $CDCl_3$) δ 142.1, 128.4, 128.2, 125.7, 35.4, 32.9. MS (EI) m/z (%) 196 (78), 117 (22), 115 (16), 104 (100), 91 (92), 89 (20), 79 (27), 78 (26), 77 (42), 65 (44), 63 (25), 51 (29), 50 (16).

1,3-Diphenyl-1-(2,2,6,6-tetramethyl-piperidin-1-yloxy)-propan-2-one (6): Dibenzyl ketone (1.3 g, 6.18 mmol) was dissolved in 30 mL of acetonitrile followed by a catalytic amount of *p*-toluenesulfonic acid and nitroxonium TEMPO salt (1.2 g, 6.26 mmol). The orange colored solution was allowed to stir at room temperature overnight after which the color turned yellow/green. The acetonitrile was removed under vacuum and dichloromethane was added. The organic layer was washed with 10% aqueous sodium bicarbonate solution, separated, and dried over anhydrous magnesium sulfate. The product was isolated as a yellow oil in 66 % yield after purification by flash column chromatography with 30:1 ethylacetate/hexanes. ^{1}H NMR (200 MHz, $CDCl_3$ TMS) δ 7.31-7.44 (m, 10H), 5.27 (s, 1H), 3.80 (dd, 2H), 1.48 (m, 4H), 1.40 (q, 2H), 1.28 (s, 3H), 1.13 (s, 3H), 1.04 (s, 3H), .067 (s, 3H). ^{13}C NMR (300 MHz, $CDCl_3$) δ 180.2, 137.6, 133.6, 131.1, 129.7, 128.8, 128.5, 128.1, 127.9, 127.8, 127.6, 127.0, 126.6, 95.2, 59.9, 59.6, 44.1, 40.2, 39.8, 35.2, 34.1, 33.6, 33.3, 27.5, 20.2, 16.9, 16.5. MS (EI) m/z (%) 327 (11), 210 (14), 180 (11), 179 (12), 156 (57), 141 (11), 126 (19), 105 (24), 91 (100), 90(29), 77 (13), 74 (13), 70 (23), 65 (16), 58 (10), 56 (41), 55 (36), 41 (34), 39 (16). MS (FAB) m/z (%) 365 (15, M+1), 210 (12), 209 (25), 131 (20), 126 (95), 91 (100), 69 (72), 65 (63).

1,3-Diphenyl-propane-1,2-dione (7): 1,3-Diphenyl-1-(2,2,6,6-tetramethyl-piperidin-1-yloxy)-propan-2-one (60 mg, 0.16 mmol) was dissolved in 25 mL dichloromethane with ethane dithiol (20 μL, 0.24 mmol) and boron trifluoride acetic acid (4 mL, 28.8 mmol). The black solution was stirred overnight and worked-up with 10 % aqueous sodium bicarbonate. The black organic layer was separated with dichloromethane from the aqueous red layer and dried over anhydrous magnesium sulfate. The product was isolated by flash column chromatography with 10 % ethylacetate/hexanes to afford the product in 20 % yield. ^{1}H NMR (200 MHz, $CDCl_3$ TMS) δ 8.15 (d, 1H), 7.89 (d, 1H), 7.35-7.55 (m, 8H), 3.65 (s, 2H). ^{13}C NMR (300 MHz, $CDCl_3$) δ 199.0, 192.9, 135.5, 134.6, 131.2, 129.7, 128.4, 127.4, 48.4.

1-(4-oxo-2,2,6,6-tetramethylpiperidine-N-oxide)-1,3-diphenylpropane (8): was synthesized similarly to **2**, but substituting 4-hydroxy-TEMPO for TEMPO. Under these conditions, the oxidation of the alcohol to the oxo function cannot be controlled. Work-up and purification were done similar to **2**. Product yields were identical to **2**. ^{1}H NMR (200 MHz, $CDCl_3$ TMS) δ 7.34-7.08 (m, 10H), 4.65 (t, 1H), 3.68-2.34 (m, 4H), 2.32-2.10 (m, 4H), 1.88-1.02 (m, 12H). ^{13}C NMR (300 MHz, $CDCl_3$) δ 210, 142.4, 141.9, 128.5, 128.4, 128.4, 128.2, 127.9, 126.0, 64.93, 63.4, 62.7, 53.9, 53.7, 37.1, 33.9, 33.8, 31.9, 26.6, 22.8, 22.6. MS (FAB) m/z (%) 366 (57, M+1), 268 (40), 185 (10), 156 (15), 132 (29), 117 (77), 91 (100), 67 (31)

1,3-diphenyl-propan-1-ene (9): was synthesized from **6**. To a round bottom flask was added 1,3 diphenylpropan-1-ol (**6**) (148 mg, 0.53 mmol) in a 50:50 mixture of methanol/water and was allowed to reflux overnight with sodium hydroxide (63 mg, 15.68 mmol). The sample was separated with dichloromethane, the organic layer dried with anhydrous magnesium sulfate, and concentrated under vacuum. The oil was purified by flash chromatography with 20:1 ethylacetate/hexanes to afford 30 mg (29%) of **7**. ^{1}H NMR (200 MHz, $CDCl_3$ TMS) δ 7.40-7.14 (m, 10H), 6.63 (d, 10 Hz, 1H), 6.28 (dd, 1H), 4.08 (m, 2H). ^{13}C NMR (300 MHz, $CDCl_3$) δ 142.3, 138.2, 130.7, 128.7, 128.4, 127.3, 127.4, 126.8, 126.5, 38.9. MS (EI) m/z (%) 194 (100), 165 (5), 121 (73), 115 (32), 103(100), 91 (93), 77 (100), 65 (55), 51 (41).

1,3-diphenyl-propan-1-ol (10): 3-Phenylpropionaldehyde (530 mg, 3.93 mmol) was dissolved in dry THF (distilled over potassium and benzophenone) and cooled to 0 °C. Phenylmagnesium bromide (1.5 mL, 4.5 mmol) dissolved in dry THF was added drop wise to the 3-phenylpropionaldehyde solution to give

another white precipitate that cleared up with time. The reaction was stirred at 0 °C for 5 minutes then ice and water were added to give a white precipitate. The organic layer was washed with a brine solution and then separated with diethyl ether. The organic layer was dried over anhydrous sodium sulfate, concentrated under vacuum, and purified by flash chromatography with 20 % ethylacetate/hexanes to afford 530 mg of the target compound (64 %). ^{1}H NMR (200 MHz, $CDCl_3$ TMS) δ 7.36-7.15 (m, 10H), 4.67 (dd, 2H), 2.72 (m, 2H), 2.11 (t, 2H). ^{13}C NMR (300 MHz, $CDCl_3$) δ 144.5, 141.8, 128.7, 128.6, 128.5, 128.4, 125.9, 73.9, 40.8, 32.1. MS (EI) m/z (%) 212 (25), 194 (100), 179 (10), 107 (86), 91 (14), 77(13), 65 (3), 51 (3), 32 (2).

1,3-diphenyl-propan-1-one: This compound was synthesized by pyridinium dichromate (PDC) oxidation of **4** by dissolving 1,3-diphenyl-propan-1-ol (**10**) (73 mg, 0.343 mmol) in dichloromethane and PDC (270 mg, 0.748 mmol). The resulting organic mixture was stirred at room temperature and 1:1 mixture of silica gel and Celite was added after the reaction was complete. The resulting slurry was filtered and washed with diethyl ether and concentrated under vacuum then purified by flash chromatography with 10% ethylacetate/hexanes mixture to afford 51 mg of product in 71% yield. M.p. 65-66 °C. ^{1}H NMR (200 MHz, $CDCl_3$ TMS) δ 7.96 (m, 2H), 7.55-7.4 (m, 3H), 7.3-7.19 (m, 5H), 3.34-3.26 (t, 2H), 3.1-3.03 (t, 2H). MS (EI) m/z (%) 210 (88), 194 (4), 134 (14), 117 (6), 105 (100), 91 (33), 77 (21), 57 (4). ^{13}C NMR (300 MHz, $CDCl_3$) δ 198.2, 140.3, 135.8, 132.1, 127.6, 127.5, 127.4, 127.3, 127.0, 126.9, 125.1, 39.4, 29.1. MS (EI) m/z (%) 210 (88), 134 (14), 105 (100), 91 (33), 77 (21).

1,3-diphenyl-1-bromopropane: A solution of triphenylphosphine (1.21 g, 4.61 mmol) was dissolved in dichloromethane and bromine (0.25 mL, 4.85 mmol) was added to give a colorless solution. In dichloromethane, 1,3-diphenylpropan-1-ol (**10**) (869 mg, 4.09 mmol) was dissolved and of triethylamine was added (0.76 mL, 5.45 mmol). The bromine solution was added dropwise to the alcohol solution and allowed to stir at room temperature for two hours. After the solution was washed with saturated brine, separated with dichloromethane, concentrated, and purified by flash chromatography with 5% ethylacetate/hexanes mixture to afford 791 mg (71%) of the title compound as a colorless oil. Bromination with N-bromosuccinimide leads to an isomer mixture of 1- and 2-bromo-1,3-diphenylpropane substitution (3 : 1) that cannot be easily separated. ^{1}H NMR (200 MHz, $CDCl_3$ TMS) δ 7.41-7.14 (m, 10H), 4.8 (t, 2H), 2.8 (m, 2H), 2.4 (3, 2H). ^{13}C NMR (300 MHz, $CDCl_3$) δ 128.8, 128.6, 128.4, 127.3,

126.2, 54.7, 41.3, 34.2. MS (EI) m/z (%) 276 (1), 274 (1), 195 (77), 179 (12), 165 (7), 117 (75), 104 (50), 91 (100), 77 (10), 63 (5), 50 (7), 39 (6).

1,3-diphenyl-1-iodopropane: Sodium iodide (183 mg, 1.22 mmol) was dissolved in OmniSolv acetone and allowed to stir for 5 minutes. 1,3-Diphenyl-1-bromopropane (238 mg, 0.87 mmol) dissolved in acetone was added to the sodium iodide solution was allowed to stir for 30 minutes at room temperature where the solution turned yellow The solution was then refluxed resulting in a white precipitate which turned to orange with time. Upon cooling, the solution was filtered, concentrated under vacuum, and purified by flash chromatography with 5 % ethylacetate/hexanes. The resulting pink colored solid was washed with sodium thiosulfate to afford the desired product in 69 % yield. ^{1}H NMR (200 MHz, $CDCl_3$ TMS) δ 7.15-7.45 (m, 10 H), 5.05 (3, 1H), 2.65 (m, 2H), 1.47 (3, 1H). MS (EI) m/z (%) 321 (12), 217 (43), 194 (30), 193 (100), 178 (12), 171 (30), 149 (21), 117 (11), 115 (21), 104 (13), 91 (53), 77 (5).

5.4.2 NMR Studies

^{1}H-DNMR of **2** and **3** were done in C_6D_6 and $CDCl_3$ on a 500 MHz Brüker NMR in the temperature range of 298 - 348 K. The rotational barrier was determined from the coalescent temperatures according to previous methods.[70,72]

5.4.3 Semi-Empirical Calculations

Semi-empirical calculations were done on a Silicon Graphics Indigo workstation using Spartan SGI version 4.0.4 GL IRX 5.2. The rotational barriers were calculated using the coordinate driving option with the PM3[63] and AM1[75] semi-empirical level of theory on the N-O-CH-CH_2 dihedral angle that calculated the optimized geometries and heats of formation (ΔH_f) for the particular dihedral angle. Restricted Hartree-Fock (RHF) was selected for the calculations for all systems and the σ value was set to 100.

5.4.4 X-Ray Crystallography

Suitable crystals were selected, mounted on thin, glass fibers using paraffin oil by Dr. Glenn Yap and cooled to the data collection temperature. Data were collected on a Brüker AX SMART 1k CCD diffractometer using 0.3° ω-scans at 0, 90, and

180° in ϕ. Unit-cell parameters were determined from 60 data frames collected at different sections of the Ewald sphere. No absorption corrections were required.

Systematic absences in the diffraction data and unit-cell parameters were uniquely consistent with the reported space group. The structure was solved by direct methods, completed with difference Fourier syntheses and refined with full-matrix least-squares procedures based on F^2. All non-hydrogen atoms were refined with anisotropic displacement parameters. Phenyl groups were treated as idealized, rigid, flat hexagons. Hydrogen atoms on carbon atom C(8) in **2** were initially located from the difference map and refined with a riding model. All other hydrogen atoms were treated as idealized contributions. All scattering factors and anomalous dispersion factors are contained in the SHEXTL 5.10 program library (Sheldrick, G. M., Brüker AS, Madison, WI, 1997).

5.4.5 Laser Flash Photolysis Studies

The indirect[57] laser flash photolysis (LFP) method was done using a Molectron UV-24 nitrogen laser for 337 nm for work involving radical generation from di-*tert*-butylperoxide. All pulse duration's are < 10 ns and typical pulse energies are around 7 mJ. To a 2 : 1 solution of acetonitrile/di-*tert*-butyl peroxide (purified with neutral alumna oxide) was added (659 mg, 3.36 mmol) of **2** in a total of 3 mL of solvent in a 7 x 7 mm^2 quartz Suprasil laser cell. The growth of the radical resulting from hydrogen abstraction from *tert*-butylalkoxyl was monitored at 320 nm. Quenching studies were subsequently done by monitoring the decay of the 1,3-diphenyl-1-propyl radical at 320 nm in the presence of various amounts of TEMPO under pseudo-first order conditions.

The rate constant for hydrogen abstraction from 1,3-diphenylpropane was determined by an approach similar to the method of Scaiano et al.[40] A 0.23 M solution of recrystalized and doubly sublimed benzhydrol in 4:1 acetonitrile/di-*tert*-butyl peroxide was dearated and then irradiated with pulses from a 337 nm laser. The growth of the subsequently generated ketyl radical from hydrogen abstraction by *tert*-butylalkoxyl was observed at 535 nm. Its growth was monitored under pseudo-first order conditions in the presence of various concentrations of 1,3-diphenylpropane leading to the desired rate constant.

The samples for LFP spectroscopic and kinetic studies were excited with any of the following excitation sources dependent upon their ground state absorption. The wavelength of 266 nm was generated from the fourth harmonic of a Nd-

YAG Surelite laser from Continuum with 15 mJ in 6 ns pulses. The 337 nm pulses were from a Molectron UV-24 nitrogen laser delivering circa 7 mJ per pulse. In the case of 308 nm excitation, pulse durations were < 19 ns and typical pulse energies between 5 and 50 mJ from an Excimer 550 laser were also used. The 355 nm wavelength was generated from the third harmonic of a Nd-YAG Surelite laser from Continuum with 15 mJ in 6 ns pulses. Other details for the laser setup can be found elsewhere.[76,77] Quenching studies were done similarly to those stated above.

All samples for laser flash photolysis were made up using OmniSolv grade solvents in a Suprasil 7 x 7 mm^2 quartz cell and fully deaerated with nitrogen for a minimum or 20 minutes prior to use. Solutions were made such that the absorbance at the irradiation wavelength ranged from 0.3 - 0.4. The continuous flow of 1 drop/second was used for actinometry purposes to avoid product build-up. The number of laser shots taken varied from sample to sample, but a satisfactory number was chosen that produced a consistent maximum absorption.

Laser power measurements were done using a calibrated power meter and roughly 30 - 40 shots were averaged. Neutral densities filters were used to vary the laser power for excitation wavelengths at 308 and 337 nm. The same effect was achieved for 266 and 355 excitation sources by changing the delay gate of the laser output. The subsequent change in laser power was measured with each such change by averaging about 20 - 30 shots per power reading.

The digitized kinetic data from the laser flash studies is stored as a text file. The data is subsequently fit using the commercially available Kaleidagraph software the kinetic information obtained by numerical iteration of the rate equations.

Diffuse reflectance studies were done with the same general experimental set-up as with transmission methods. The solid sample was prepared by placing it in a 7 x 3 mm^2 Suprasil quartz cell and purging with nitrogen for 30 minutes prior to use. Either neat solid or the solid mixed with silica gel was used for diffuse reflectance measurements. The irradiation wavelength used was 266 nm and the scattered light was recorded and digitized in the same manner as transmission work. The absorbance data are represented as $\Delta J/J$, where ΔJ is the change in reflectance after excitation and J is the pre-laser flash voltage level. This is used to calculate the change in reflectance values.

5.4.6 Activation Energies

Determination of the activation energies were done similarly to that previously reported,[6] where 2 mL of a solution of 18.4 mM of **2** and 51 mM of 4-oxo TEMPO in cyclohexanol were deaerated and flame sealed in 7 cm x 7 mm test tubes. The samples were heated in a thermostated aluminum block and were removed at given intervals. The samples were then analyzed for product concentrations by HPLC with a Zorbax® C-18 reverse phase column with a flow rate of 0.5 mL/min and 85% methanol / 15% water as eluent. The retention times and peak areas were calibrated against authentic samples. The rate constants were derived from product formation as a function of time over a series of temperatures. The subsequently generated Arrhenius plot represents the average of at least two trials per temperature.

5.4.7 Polymer Studies

The polymerization reactions were carried out using freshly distilled styrene. The initiators, **2** or **3a**, were dissolved in 100 equivalents of styrene/reactant and flame sealed in 7 mm glass tubing after two cycles of freeze-pump-thaw. They were then heated in a thermostated aluminum block at 115 °C for 22 hours. The samples were cooled and any residual styrene was evaporated under vacuum and the resulting oil was dissolved in THF and then analyzed by GPC-HPLC equipped with a Waters Styragel® HR3 column and RI detector. The molecular weights and polydispersity were determined relative to polystyrene molecular weight standards.

5.5 Chapter References

1. Scaiano, J. C.; Connolly, T. J.; Mohtat, N.; Pliva, C. N. *Can. J. Chem.* **1997**, *75*, 92-97.
2. MacLeod, P. J.; Georges, M. K.; Quinlan, M.; Moffat, K. A.; Listigovers, N. A. *Polym. Prepr.* **1997**, *38*, 459-460.
3. Goto, A.; Fukuda, T. *Macromolecules* **1999**, *32*, 618-623.
4. de Leon, M. E.; Gnanou, Y.; Guerrero, R. *Polym. Prepr.* **1997**, *38*, 667-668.
5. Braslau, R.; Burrill, L. C. I.; Siano, M.; Naik, N.; Howden, R. L.; Mahal, L. K. *Macromolecules* **1997**, *30*, 3445-6450.
6. Skene, W. G.; Belt, S. T.; Connolly, T. J.; Hahn, P.; Scaiano, J. C. *Macromolecules* **1998**, *31*, 9103-9105.
7. Skene, W. G.; Connolly, T. J.; Scaiano, J. C. *Tetrahedron Lett.* **1999**, *40*, 7297-7302.
8. Skene, W. G.; Connolly, T. J.; Scaiano, J. C. *Int. J. Chem. Kin.* **2000**, *32*, 238-244.
9. Skene, W. G.; Scaiano, J. C. *Polym. Prepr.* **2000**, *41*, 163-164.
10. Skene, W. G.; Scaiano, J. C.; Yap, G. P. A. *Macromolecules* **2000**, *33*, 3536-3542.
11. Skene, W. G.; Scaiano, J. C.; Yap, G. P. A. *Polym. Prepr.* **2000**, *41*, 119-120.
12. Skene, W. G.; Scaiano, J. C.; Listigovers, N. A.; Kazmaier, P. E.; Georges, M. K. *Macromolecules* **2000**, *33*, 5065-5072.
13. Skene, W. G.; Scaiano, J. C. **2000**, Manuscript in preparation.
14. Malmström, E. E.; Hawker, C. J. *Macromol. Chem. Phys.* **1998**, *6*, 923-935.
15. Davis, T. P.; Haddleton, D. M.; Richards, S. N. *J. Macromol. Sci. Rev. Macromol. Chem. Phys.* **1994**, *C34*, 243-324.
16. Matyjaszewski, K.; Pugh, C. *Makromol. Chem., Macromol. Symp.* **1993**, *67*, 67-82.

17. Kazmaier, P. M.; Moffat, K. M.; Georges, M. K.; Veregin, R. P. N.; Hamer, G. K. *Macromolecules* **1995**, *28*, 1841-1846.

18. Georges, M. K.; Veregin, R. P. N.; Kazmaier, P. M.; Hamer, G. K. *Macromolecules* **1993**, *26*, 2987-2988.

19. Georges, M. K.; Veregin, R. P. N.; Kazmaier, P. M.; Hamer, G. K.; Saban, M. *Macromolecules* **1994**, *27*, 7228-7229.

20. Mardare, D.; Shigemoto, T.; Matyjaszewski, K. *Polym. Prepr.* **1994**, *35*, 557-558.

21. Veregin, R. P. N.; Georges, M. K.; Kazmaier, P. M.; Hamer, G. K. *Macromolecules* **1993**, *26*, 5316-5320.

22. Veregin, R. P. N.; Odell, P. G.; Michalak, L. M.; Georges, M. K. *Macromolecules* **1996**, *29*, 2746-2754.

23. Veregin, R. P. N.; Georges, M. K.; Hamer, G. K.; Kazmaier, P. M. *Macromolecules* **1995**, *28*, 4391-4398.

24. Fukuda, T.; Goto, A. *Macromol. Rapid Commun.* **1997**, *18*, 683-688.

25. Patten, T. E.; Xia, J.; Abernathy, T.; Matyjaszewski, K. *Science* **1996**, *272*, 866-868.

26. Zaremskii, M.; Stoyachenko, Y.; Plutalova, A.; Lachinov, M.; Golubev, V. *Vysokomol. Soed. Ser. A & Ser. B* **1999**, *41*, 398-398.

27. Hunter, D. H.; Racok, J. S.; Rey, A. W.; Ponce, Y. Z. *J. Org. Chem.* **1988**, *53*, 1278-1281.

28. Rychnovsky, S. D.; Vaidyanathan, R.; Beauchamp, T.; Lin, R.; Farmer, P. J. *J. Org. Chem.* **1999**, *64*, 6745-6749.

29. Semmelhack, M. F.; Chou, C. S.; Cortes, D. A. *J. Am. Chem. Soc.* **1983**, *105*, 4492-4494.

30. Stain-Aman, E.; Serve, D. *New J. Chem.* **1989**, *13*, 121-130.

31. Hunter, D. H.; Barton, D. H. R.; Motherwell, W. J. *Tetrahedron Lett.* **1984**, *25*, 603-606.

32. Berk, S. C.; Knochel, P.; Yeh, M. C. P. *J. Am. Chem. Soc.* **1988**, *53*, 5789-5791.
33. Kim, S.; Oh, C. H.; Ko, J. S.; Ahn, K. H.; Kim, Y. J. *J. Org. Chem.* **1985**, *50*, 1927-1932.
34. Nagashima, T.; Curran, D. P. *Synlett.* **1996**, *4*, 330-332.
35. Nomura, R.; Endo, T. *Chem. Eur. J.* **1998**, *4*, 1605-1610.
36. Yacovan, A.; Hoz, S. *J. Am. Chem. Soc.* **1996**, *118*, 261-262.
37. Connolly, T. J.; Baldovi, M. V.; Mohtat, N.; Scaiano, J. C. *Tetrahedron Lett.* **1996**, *37*, 4919-4922.
38. Tsentalovich, Y. P.; Kulik, L. V.; Gritsan, N. P.; Yurkovskaya, A. V. *J. Phys. Chem. A* **1998**, *102*, 7975-7980.
39. Mekarbane, P. G.; Tabner, B. J. *Macromolecules* **1999**, *32*, 3620-3625.
40. Paul, H.; Small, R. D., Jr.; Scaiano, J. C. *J. Am. Chem. Soc.* **1978**, *100*, 4520-4527.
41. Wagner, P. J. *J. Am. Chem. Soc.* **1967**, *89*, 5898-5901.
42. Bowry, V. W.; Ingold, K. U. *J. Am. Chem. Soc.* **1992**, *114*, 4992-4996.
43. Beckwith, A. J.; Bowry, V. W.; Ingold, K. U. *J. Am. Chem. Soc.* **1992**, *114*, 4983-4992.
44. Hawker, C. J.; Barclay, G. G.; Orellano, A.; Dao, J.; Devonport, W. *Macromolecules* **1996**, *29*, 5245-5254.
45. Howard, J. A.; Tait, J. C. *J. Am. Chem. Soc.* **1978**, *43*, 4279-4283.
46. Li, I.; Howell, L.; Matyjaszewski, K.; Shigemoto, T.; Smith, P. B.; Priddy, D. B. *Macromolecules* **1995**, *28*, 6692-6693.
47. Fischer, H. *J. Am. Chem. Soc.* **1986**, *108*, 3925-3927.
48. Kothe, T.; Marque, S.; Martschke, R.; Popov, M.; Fischer, H. *J. Chem. Soc., Perkin Trans. 2* **1998**, *7*, 1553-1559.
49. Fischer, H. *J. Polym. Sci., Part A: Polym. Chem.* **1999**, *37*, 1885-1901.
50. Weiner, S. A.; Hammond, G. S. *J. Am. Chem. Soc.* **1969**, *91*, 986-991.

51. Moffat, K. A.; Hamer, G. K.; Georges, M. K. *Macromolecules* **1999**, *32*, 1004-1012.

52. Gibian, M. J.; Corley, R. C. *J. Am. Chem. Soc.* **1972**, *94*, 4178-4183.

53. Benson, S. W. *J. Phys. Chem.* **1985**, *89*, 4366-4369.

54. Gratton, D. W.; Carlsson, D. J.; Howard, J. A.; Wiles, D. M. *Can. J. Chem.* **1979**, *57*, 2834-2842.

55. Chateauneuf, J.; Lusztyk, J.; Ingold, K. U. *J. Am. Chem. Soc.* **1988**, *110*, 2877-2885.

56. Chatgilialoglu, C.; Ingold, K. U.; Scaiano, J. C. *J. Am. Chem. Soc.* **1982**, *104*, 5123-5127.

57. Chateauneuf, J.; Lusztyk, J.; Ingold, K. U. *J. Org. Chem.* **1988**, *53*, 1629-1632.

58. Chatgilialoglu, C.; Ingold, K. U.; Lusztyk, J.; Nazran, A. S.; Scaiano, J. C. *Organometallics* **1983**, *2*, 1332-1335.

59. Griller, D.; Ingold, K. U. *Acc. Chem. Res.* **1976**, *9*, 13-19.

60. Benson, S. W. Some Problems of Structure and Reactivity in Free Radical and Molecule Reactions in the Gas Phase. In *Advances in Photochemistry*; Noyes, W. A. J., Hammond, G. S., Pitts, J. N. J., Eds.; John Wiley & Sons: New York, 1964; Vol. 2; 1-23.

61. Tanner, D. D.; Rahimi, P. M. *J. Am. Chem. Soc.* **1982**, *104*, 225-229.

62. Fabian, W. M. F. *J. Comput. Chem.* **1988**, *9*, 369-677.

63. Stewart, J. J. P. *J. Comput. Chem.* **1989**, *10*, 209-220.

64. Stewart, J. J. P. *J. Comput. Chem.* **1989**, *10*, 221-264.

65. Feigel, M.; Strassner, T. *Theochem.* **1993**, *283*, 33-48.

66. Burke, L. A.; Krishnan, P. N.; Morris, R. E.; Famini, G. R. *J. Org. Chem.* **1992**, *5*, 614-616.

67. Chatgilialoglu, C. Electronic Absorption Spectra of Free Radicals. In *Handbook of Organic Photochemistry*; Scaiano, J. C., Ed.; CRC Press: Boca Raton, Florida, 1989; Vol. II; 3-11.

68. March, J. *Advanced Organic Chemistry: Reactions, Mechanisms, and Structure*, 3rd ed.; John Wiley and Sons: New York, 1985, pp 1346.

69. Raban, M.; Kost, D. *Tetrahedron* **1984**, *40*, 3345-3381.

70. Anderson, J. E.; Casarinin, D.; Corrie, J. E. T.; Lunazzi, L. *J. Chem. Soc., Perkin Trans. 2* **1993**, *7*, 1299-1304.

71. Riddell, F. G. *Tetrahedron* **1981**, *37*, 849-858.

72. Anderson, J. E.; Corrie, J. E. T. *J. Chem. Soc., Perkin Trans. 2* **1992**, *7*, 1027-1031.

73. Lunazzi, L.; Macciantelli, D. *J. Chem. Soc. Perkin 2* **1981**, 604-609.

74. Nagaoka, S.-I.; Kshihara, K. *J. Am. Chem. Soc.* **1996**, *118*, 7361-7366.

75. Dewar, M. J. S.; Zoebisch, E. G.; Healy, E., F.; Stewart, J. J. P. *J. Am. Chem. Soc.* **1985**, *107*, 3902-3909.

76. Scaiano, J. C. *J. Am. Chem. Soc.* **1980**, *102*, 7747-7753.

77. Scaiano, J. C.; Tanner, M.; Weir, D. *J. Am. Chem. Soc.* **1985**, *107*, 4396-4403.

6. Acrylate Polymerization

6.1 Introduction

The seminal work by Georges et al. from the Xerox group presented the first successfully nitroxide mediated polymerization of styrene leading to polymers with living properties.[1] Subsequently, this caused a flood of research interest resulting in optimized experimental conditions[2-4] and new polymer architectures[4-7] not previously achieved by radical means. Nitroxide based living free radical polymerization (LFRP) has flourished with every type of styrenic based monomer, but has failed when applied to other non-styrenic vinyl monomers. Commercially viable polymers such as acrylates have proven nearly impossible to yield polymers with LFRP properties when polymerized by standard nitroxide techniques. Polymerization of these vinyl monomers with similar experimental conditions to those of styrene typically give polymers with poor properties such as low molecular weights, relatively high polydispersities, and low conversions.

Several strategies have been adopted to try and transfer the desired living properties to acrylate monomers. A popular approach is the chemical destruction of some of the excess nitroxide produced during the course of the polymerization reaction through the use of additives such as organic acids,[8,9] phosphates,[10] or other electron acceptors,[11] and acylating agents.[12] This controls the nitroxide concentration during the polymerization process, resulting in marginally increased molecular weight. Another approach, met with some success, is through the design of new nitroxides that exhibit slower trapping rate constants.[13,14] This has improved the living properties of acrylate polymers somewhat; however, they are still not comparable to styrene based LFRP in terms of kinetics and living properties. A new generation of nitroxides containing a hydrogen adjacent to the nitroxide functionality have resulting in LFRP of various monomers other than styrene, but living polymerization of acrylates is still elusive.[15-21]

Trapping the propagating carbon centered radical by various nitroxides is bimolecular in nature as the rate is determined by the concentration of the two radicals. This combination reaction is pivotal for controlling the concentration of propagating radicals for polymerization, which in turn, is responsible for controlling the molecular weight distribution. In the chapter dealing with initiator kinetics, the trapping rate constant for an acrylate analogue radical was shown to be an order of magnitude faster than for the styrenic radical. It was also

shown that little influence on the trapping kinetics was observed with different nitroxide structures. For simplicity and direct relative comparison, assuming the C-O bond dissociation energy for nitroxide capped acrylates is the same, then the equilibrium is shifted more in favor of the capped or "dormant" species for the acrylates, shown in Figure 6-1. This leads to fewer carbon radicals for polymerization resulting in lower molecular weight polymers and other poor LFRP properties. Overall this appears as a shift to a conventional free radical polymerization mechanism. Reducing the amount of free nitroxide during the polymerization process should shift the equilibrium in favor of uncapped or "active" radicals, and in turn, give rise to polymers with improved desirable properties; higher molecular weights and narrow polydispersities compared to conventional acrylate based LFRP. The focus of this chapter will present results concerning two original strategies for controlling the amount of free nitroxide leading to successful living polyacrylates.

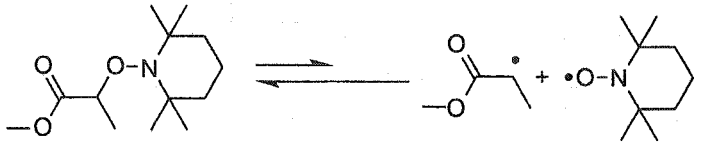

Figure 6-1. Equilibrium reaction responsible for LFRP control as applied to acrylates.

6.1.1 Biphasic Polymerization

The initial approach to controlling the nitroxide concentration was through the use of a second medium not miscible with the bulk phase, such as water or ethylene glycol. The amount of nitroxide present during polymerization after decomposition of a unimolecular initiator is a function of the nitroxide's solubility in the second phase in addition to the amount of aqueous layer used. Therefore, partitioning of the nitroxide into the second phase would act as a means of absorbing a sufficient amount of the free nitroxide and reducing its bulk concentration. This in turn would influence the initial LFRP bi-molecular kinetics by slowing the trapping rate. This directly controls the equilibrium between "dormant" and "active" radicals which is crucial for controlling the polymerization process and subsequently the polymer properties, leading to living polymers with desirable lower polydispersities, higher molecular weights, and higher conversions. Figure 6-2 is a schematic representation of the biphasic approach where upon initiator thermal decomposition, a portion of the nitroxide is absorbed by the aqueous layer.

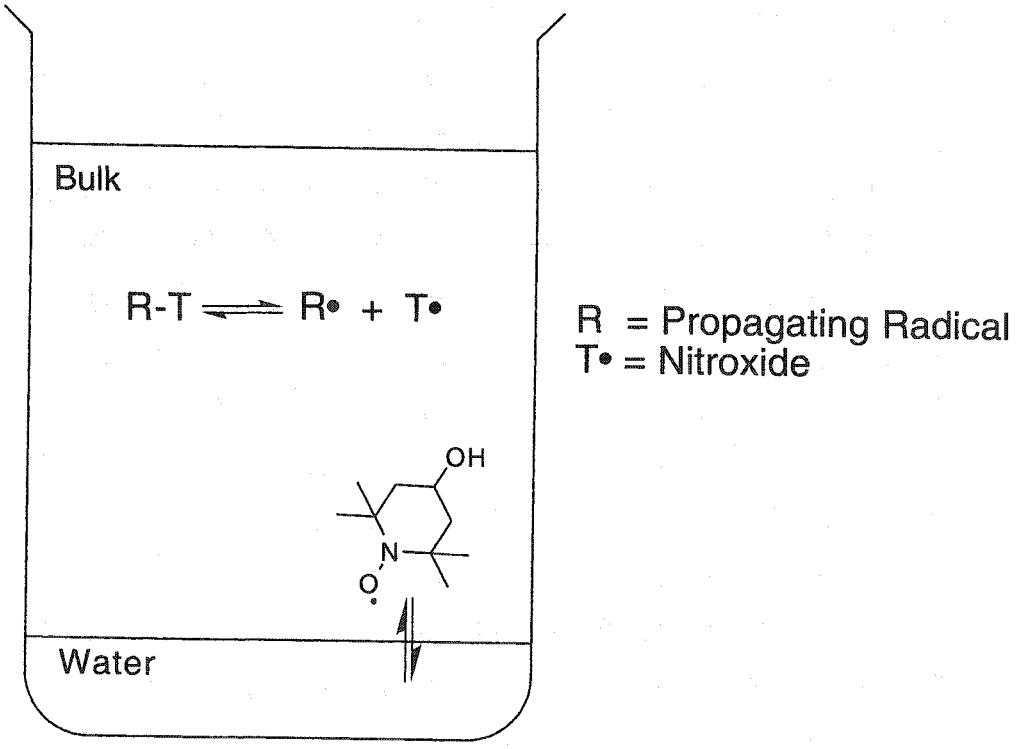

Figure 6-2. Schematic of biphasic approach for controlling nitroxide concentration.

With the second phase present at all times, the amount of nitroxide during the polymerization is originally regulated at the onset of the reaction and its concentration is relatively constant using this approach. This is of importance since an excess of nitroxide exerts a greater negative effect on the polymer properties during the initial period of polymerization. A build-up of nitroxide during the polymerization at higher molecular weights has less of an influence than earlier during the polymerization process. The series of initiators examined is shown in Figure 6-3.

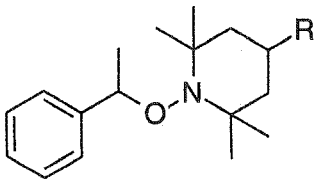

1 R=H
2 R=OH
3 R=(O)
4 R=COOH

Figure 6-3. Unimolecular initiators studied for biphasic acrylate polymerization.

6.2 Results and Discussion

6.2.1 Biphasic Polymerization

The affinity of various nitroxides for different solvents is only qualitatively known.[22] Therefore quantitative determination of the nitroxide partitioning as a function of substitution in their 4 position with different amounts of monomer analogue solvents was undertaken. This work was originally done by Ivan Piletic, a summer student under the direction of this author. Toluene was used as a model for styrene, while methyl propionate was used as a saturated analogue of methacrylate. These solvents were used as analogues to facilitate analytical GC analysis and avoid polymerization on the GC column. The saturated solvents were also used to minimize the exposure to the toxic monomers. Table 6-1 clearly shows the affinity of different nitroxides for the monomer analogous solvents. TEMPO and di-*tert*-butyl nitroxide show little partitioning into the aqueous layer, as expected. Increasing the polarity of the functional group at the 4 position increases the partitioning into the aqueous layer according to chemical intuition. Also, increasing the amount of aqueous layer increases the amount of nitroxide that it can partition. From the nitroxides studied, 4-hydroxy-TEMPO is readily dissolved into the aqueous layer in substantial amounts regardless of the organic or aqueous layers used. These analyses were done at room temperature for convenience sake and for analysis of any noticeable trends. Only the amount of nitroxide partitioned and not the trend is expected to change at higher temperatures comparable to those for polymerization.

Table 6-1. Partitioning of various nitroxides in different two solvent mixtures at room temperature.

Solvents	Ratios (org:aq)[b]	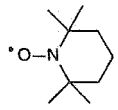	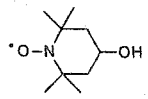	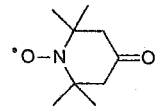	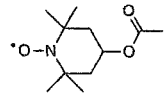	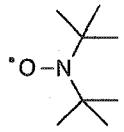
Toluene[a]	1:2	0.24	0.97	0.32	-	0.05
	2:1	0	0.25	0.07	0.20	-
Methyl Propionate	1:1	0	0.44	0.14	0.03	-
	1:2	0	0.55	0.20	0.01	-
n-butyl acrylate	3:1	0	0.29	0.04	0.02	-

a) Aqueous layer was composed of a 3:1 mixture by volume of ethylene glycol and water.
b) Aqueous layer is water.
*Values denote partition coefficients of nitroxides in the organic layer determined by analytical methods.

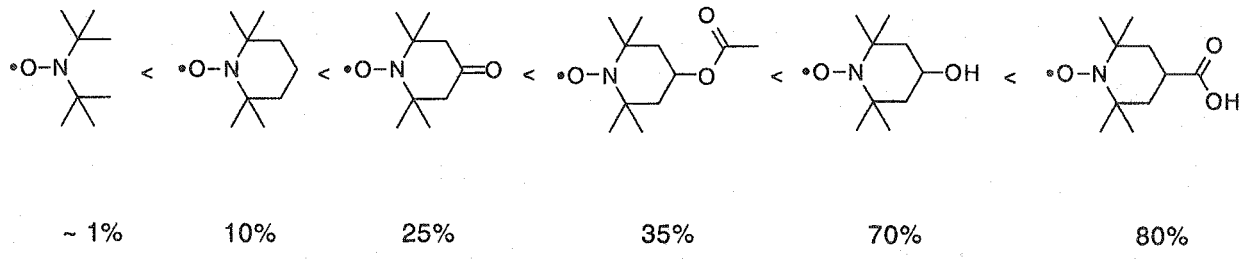

Figure 6-4. Experimentally determined order of nitroxide affinity for ethylene glycol in biphasic system with *n*-butyl acrylate at room temperature.

The general trend of nitroxide affinity for the aqueous layer is summarized in Figure 6-4 above. From this list, the 4-oxo-TEMPO initiator was chosen as an ideal nitroxide for preliminary biphasic polymerization studies of methyl methacrylate (MMA) since it shows a marginal affinity for the aqueous layer. Upon thermal decomposition, compound **3** gives the desired nitroxide and was therefore selected as the choice initiator for biphasic studies. Conducting the polymerization of MMA with **3** according to method 1 (see experimental section)

gives the results summarized in Table 6-2. Here, only a relatively small amount of water was added compared to the bulk phase to observe the effect of partitioning only a minute amount of nitroxide. It is clear that even the addition of this small amount of second phase is sufficient to partition enough nitroxide and to influence the polymer properties. The molecular weight is increased compared to the bulk control experiment and the biphasic approach, but the polydispersity has been sacrificed. This is most likely due to an insufficient amount of nitroxide being partitioned.

Table 6-2. Methyl methacrylate polymerization (436 equivalents relative to the initiator) initiated by 3 at 110 °C.

Time	Condition[a]	M_n	M_w	PD
4.2 hrs	no water	15500	22200	1.4
4.2 hrs	water	18100	37500	2.1
5.3 hrs	no water	8900	14800	1.7
5.3 hrs	water	13300	31200	2.3

a) Water denotes biphasic experiments with 6:1 monomer to water ratio by volume.

The use of the biphasic method as applied to acrylates appears to work during the initial stages of the polymerization and gives low conversions. The biphasic polymerization method was applied to styrene to ensure the observed acrylate results were inherent to this monomer and not because of the polymerization method. Biphasic experiments using styrene were run in tandem with bulk polymerization of this monomer under standard LFRP conditions. Styrene was selected as the benchmark monomer because LFRP is known to be achieved with great success when it is mediated by nitroxides.[1,2,4,7,9,11,23-31] Table 6-3 shows the polymerization conditions used give rise to a LFRP process with high conversions for styrene regardless of the method. This validates the preliminary biphasic results and implies the selected method may be capable of inducing acrylate LFRP. Close examination of the results in this table show the PD decreases for bulk polymerization, which have been previously observed.[1,24,28,30,32,33] However, the polydispersity for the biphasic polymerization is relatively low at the onset of the reaction suggesting

partitioning of excess nitroxide into the organic layer is beneficial even for the proven LFRP of styrene. Decreasing the amount of free nitroxide at the early stages of polymerization through nitroxide partitioning gives rise to higher molecular weights and lower polydispersities. The proof of concept for nitroxide partitioning by biphasic polymerization occurs here and its application to acrylates is examined herein.

Table 6-3. Polymerization of styrene (861 equivalents relative to the initiator) at 120 °C initiated by 2.

Time	Condition[a]	M_n	M_w	PD
1 hr	no water	9400	15800	1.7
1 hr	water	18600	26500	1.4
2.75 hrs	no water	24300	29500	1.2
2.75 hrs	water	25900	35000	1.4
4 hrs	no water	26600	32100	1.2
4 hrs	water	28000	37300	1.3
7.5 hrs	no water	37600	44600	1.2
7.5 hrs	water	33100	43000	1.3
19.5 hrs	no water	45100	53000	1.2
19.5 hrs	water	50000	59000	1.2

a) Water denotes biphasic experiments with 2:1 monomer to water ratio by volume.

The biphasic concept proven by styrene polymerization implied the poor results obtained for **3** were from insufficient nitroxide partitioning. The 4-oxo-TEMPO nitroxide was subsequently replaced by 4-hydroxy-TEMPO to examine the influence of nitroxide concentration on the polymer properties. This was achieved through the use of initiator **2**. The results, summarized in Table 6-4, show a dramatic improvement over the initiator **3**, where the effects of this hydroxy based initiator are more pronounced during the initial polymerization

stages. Similarly to the previous experiment, there is a slight improvement in the polydispersities, while the molecular weights are consistently higher in the case of the biphasic polymerization. The improved difference between the two systems decreases with longer polymerization times. This suggests that nitroxide build-up occurs during prolonged polymerization subsequently influencing the polymer's properties.

Table 6-4. Methyl methacrylate polymerization (745 equivalents relative to the initiator) at 120 °C initiated by 2.

Time	Condition[a]	M_n	M_w	PD
1.25 hrs	no water	13800	26500	1.9
1.25 hrs	water	34600	55700	1.6
2.25 hrs	no water	14600	27800	1.9
2.25 hrs	water	29600	49900	1.7
3.25 hrs	no water	14200	28600	2.0
3.25 hrs	water	32600	59100	1.8

a) Water denotes biphasic experiments with 6.25:1 monomer to water ratio by volume.

Pictorially, the difference between the two polymers obtained via bulk and biphasic polymerization in the gel permeation chromatograph (GPC) is shown in Figure 6-5. The molecular weight of the polymer derived from the biphasic approach is higher and has less of a bimodal distribution than the bulk polymerization. This strongly suggests the decreased nitroxide concentration positively influences the physical properties through a shift in the equilibrium of capped and uncapped radicals. However, the system is far from ideal as low conversions (< 5 %) are achieved and the molecular weights are insufficiently high to warrant commercial application.

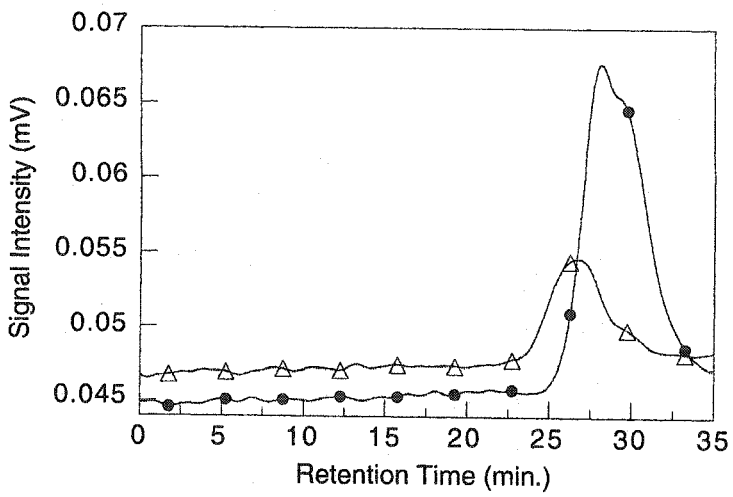

Figure 6-5. GPC chromatograms of bulk (●) and biphasic (Δ) methyl methacrylate polymerization with 3 after 1.5 hours in 1:1 monomer to aqueous volume ration.

Increasing the amount of aqueous phase added to the reactions results in an increased amount of partitioned nitroxide into the aqueous layer. This modification leads to somewhat improved results according to Table 6-5. The molecular weights are consistently higher for the biphasic approach, even at longer polymerization times. The polydispersities are marginally improved, but the lack of conversion apparently cannot be increased by partitioning more nitroxide into the aqueous layer.

Table 6-5. Methyl methacrylate (861 equivalents relative to the initiator) polymerization initiated by 2 at 120 °C.

Time	Condition[a]	M_n	M_w	PD	Conversion
1.5 hrs	no water	17800	24100	1.4	1%
1.5 hrs	water	40200	50800	1.3	2%
8.5 hrs	no water	13300	20100	1.5	4%
8.5 hrs	water	26800	38900	1.5	4%
17.5 hrs	no water	13500	28000	2.1	4%
17.5 hrs	water	23000	36900	1.6	5%
27 hrs	no water	12300	20100	1.7	6%
27 hrs	water	20100	32900	1.6	8%

a) Water denotes biphasic experiments with 2:1 monomer to water ratio by volume.

Comparison of the rates of conversion between styrene and methyl methacrylate, as seen in Figure 6-6, shows the polymerization is incomplete after long polymerization times for methyl methacrylate. Typically, the polymerization of methyl methacrylate does not surpass 10 % conversion with the conditions used in methods 1 and 2. Under these conditions it was found that the initiator did not quantitatively decompose and some water evaporation was noticed. Incomplete initiator decomposition gives rise to a mixture of LFRP and conventional free radical polymerization occurring simultaneously. The lack of control during the polymerization and observed poor polymer properties may possibility be explained by the presence of conventional free radical polymerization mechanism. However, the polydispersities observed would be close to or greater than 2.[34,35] Regardless, a true controlled nitroxide mediated LFRP mechanism similar to styrene is not observed for the biphasic polymerization of acrylates.

It should be noted that the biphasic approach does not affect the polymer properties at longer polymerization times for styrene either (*vide infra*). As with

the case of the acrylate monomers, decreasing the nitroxide concentration at the onset or the initial polymerization period of styrene affects the polymer's properties; higher molecular weight and narrow polydispersity. This suggests the amount of propagating radicals or non-nitroxide capped species must be higher at the initial stages of polymerization or a build-up of free nitroxide.

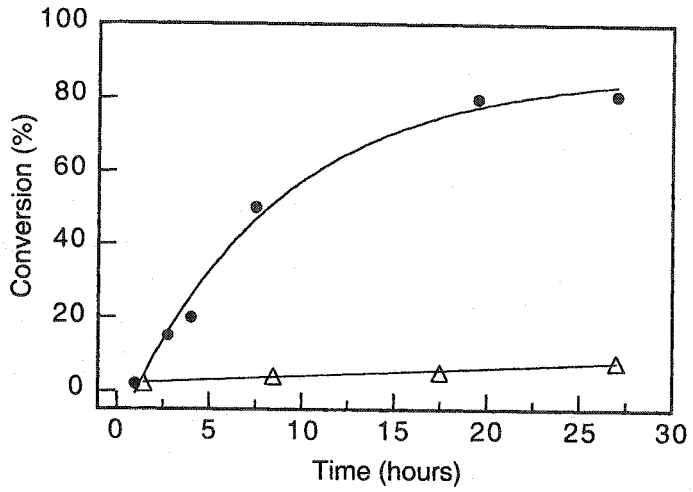

Figure 6-6. Polymerization conversion of styrene (●) and methyl methacrylate (Δ) initiated by 4 at 120 °C under biphasic 2:1 monomer to aqueous volume conditions. Equal ratio of monomer to initiator were used for the samples.

A new protocol was adopted, which called for the polymerization to be done in sealed tubes to prevent water loss and avoid introduction of oxygen into the samples. These experimental difficulties are most likely the cause of inconsistent polymerization results between aliquots observed in the data reported above. In order to induce complete initiator decomposition, the polymerization temperature was increased to 135 °C and a new monomer, *n*-Butyl acrylate (b.p. 145 °C), was used as its boiling point is higher than methyl methacrylate and would not cause the reaction vessel to explode. Also, ethylene glycol (b.p. 197 °C) was used as an aqueous phase replacement not miscible with the organic layer for the same reasons as *n*- butyl acrylate.

Preliminary results with the new protocol (method 3) shown in Table 6-6 suggests complete initiator decomposition and implies the increased temperature is a favorable condition. The resulting polymers from this method have higher molecular weights than achieved with previous methods. Initiator 1 was used a benchmark test as it does not partition into the ethylene glycol (EG)

layer and the results obtained from the bulk and biphasic experiments with this initiator are essentially identical. Under identical experimental conditions, initiator 2 gives higher molecular weights and similar polydispersities and expectantly higher conversions than before (> 50 %). However, repeated polymerization with various initiator concentrations does not lead to lower polydispersities while increasing the ethylene glycol to monomer ratio only slightly improves the results.

Table 6-6. Polymerization results of *n*-butyl acrylate initiated by 2 at 135 °C.

Initiator	Condition[a]	M_n	M_w	PD
1	Bulk	112 000	170 000	1.5
	EG[b]	111 000	174 000	1.6
2	Bulk	103 000	192 000	1.9
	EG[b]	144 000	233 000	1.6

a) Biphasic ratio of 1:1 by volume.
b) EG: ethylene glycol.

The bimodal distribution of molecular weights in Figure 6-7 shows the addition of the second phase controls the polymerization process better than standard bulk polymerization. However, this distribution suggests one of two processes are occurring; either a conventional free radical polymerization is present or a combination of this and the anticipated LFRP process. A typical characteristic of conventional polymerization is the initial formation of high molecular weight polymers in low conversions. Also, there is a total lack of control over the polymerization process leading to broad molecular weight. The conventional free radical process was dismissed after repeated polymerization showed typical LFRP type kinetics and polymers with some living properties.

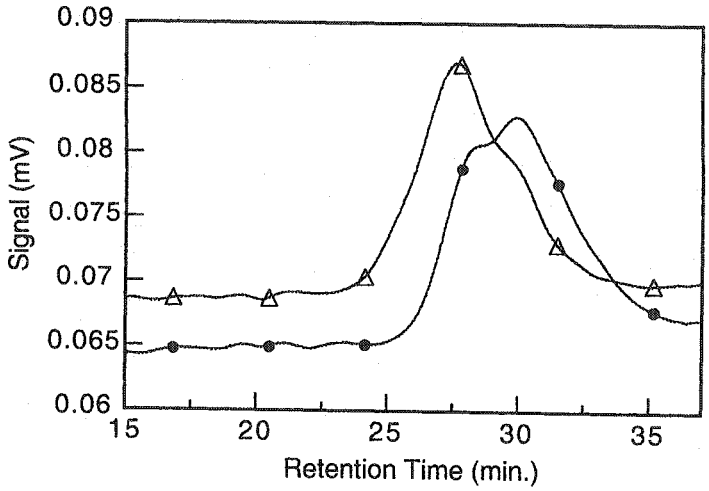

Figure 6-7. GPC traces for poly-*n*-butyl acrylate polymerization in bulk (●) and 1:2 ethylene glycol to monomer per volume (Δ) initiated by 2 at 135 °C in sealed tubes. Equal ratio of monomer to initiator were used for both systems.

Further decreasing the amount of nitroxide in the bulk phase during the polymerization would yield polymers with the desired living properties. This can be achieved through increasing the amount of non miscible layer or through the use of a nitroxide that partitions more. Increasing the amount of ethylene glycol to the point where it is more abundant than the bulk phase is not an attractive option from an industrial point of view. The alternative is to use an initiator that has a lower affinity for the organic layer than **2**, hence partitions more into the non miscible ethylene glycol layer. The 4-carboxy-TEMPO nitroxide is a good candidate as over 85 % of it partitions into the ethylene glycol layer at room temperature. Compound **4** was used as an initiator for the polymerization of *n*-butyl acrylate because upon thermal decomposition it gives the desired nitroxide. Under similar polymerization conditions as **2**, **4** yields polymers with equally high molecular weights (> 120 000) and acceptable polydispersities (~ 1.4). However, the added advantage of this initiator comes in the form of polymer conversions, which are considerably higher than any of the other methods. Conversions as high as 75 % can be achieved with this initiator with the biphasic approach compared to only 20 % conversion with bulk polymerization or biphasic method with other initiators. Figure 6-8 shows the relative conversions achieved for the polymerization of *n*-butyl acrylate using **4** as the initiator. Even though the conversion for the biphasic method is higher than previously achieved it is still considerably less than that for styrene. Also,

its rate of polymerization is nearly four times slower than styrene. This is opposite to that expected since the rate of propagation for *n*-butyl acrylate is nearly three times greater than for styrene at 135 °C.[36] This suggests even though sufficient nitroxide from the bulk has been removed, thereby slowing the rate at which the propagating radical is trapped, another means is present that gives either dormant, dead chains, or uncontrolled polymerization. Also, insufficient amount of nitroxide is drawn into the ethylene glycol phase because low conversions, less than 100 %, are obtained.

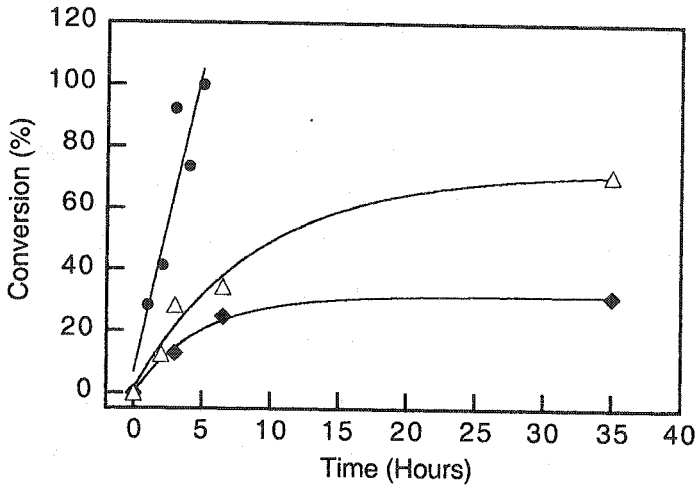

Figure 6-8. Polymerization conversion initiated by 4 at 135 °C in bulk styrene (●), bulk *n*-butyl acrylate (◆), and biphasic *n*-butyl acrylate (Δ) with 1:1 monomer to ethylene glycol ratio by volume.

Figure 6-9 gives some insight for the lack of true control and living properties obtained during the polymerization of acrylates. The peak at 40.5 minutes corresponds to residual monomer, while that at 25.9 minutes is assigned to the polymer. It was originally thought the peak at 39 minutes was that of the nitroxide since the injection of an authentic sample gave relatively the same retention time. This would suggest that free nitroxide builds-up during the course of the reaction and traps any propagating radicals leading to dormant chains. Ultimately, this causes a shift in the equilibrium to account for low conversions, but not the observed poor polydispersities. However, the co-injection of 4-carboxy-TEMPO and its hydroxylamine derivative were resolved with the GPC columns used for analyses. The peak at 39 minutes originally assigned to the free nitroxide was in fact the hydroxylamine. Therefore, a

reaction leading to disproportionation products is present and is similar to that discussed in the previous chapter dealing with disproportionation products. The removal of free nitroxide from the reaction in the form hydroxylamine does not directly account for the lack of control over the polydispersity. Rather, the formation of its complimentary vinylic product means a reduction in the amount of free carbon centered radical formation and a suppression in controlled polymerization (*vide infra*). Hydroxylamine formation will be partitioned into the second phase similar to the free nitroxide, ultimately leading to the same overall reduction in nitroxide concentration.

The presence of hydroxylamine implies the formation of its complimentary vinylic polymer (see Figure 6-10), which is difficult to isolate and identify analytically. The vinyl terminated polymer can add to chain carrying radicals. Since the reaction leading to disproportionation products is not controlled and is inconsistent, the chain length at which this reaction occurs is random. The polymerization of chains of random length with other monomers causes the observed molecular weight broadening and ultimately polymers with poor living properties. Consequently, the disproportionation products are responsible for the lack of polydispersity control and not the build-up of free nitroxide. The removal of excess nitroxide from the bulk phase is more important during the initial stages of the polymerization reaction, but becomes less important when the formation of disproportionation products dominates because the nitroxide cannot influence the rate or the amount of the disproportionation products formed.

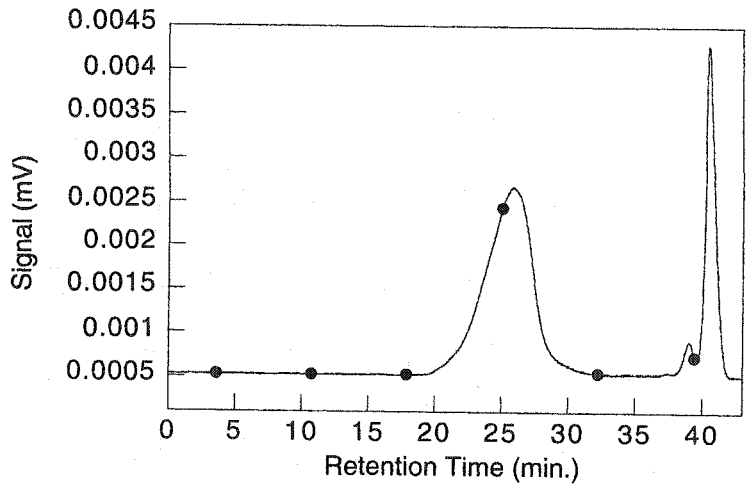

Figure 6-9. GPC of poly-*n*-butyl acrylate polymerization of 1785 equivalents of *n*-butyl acrylate initiated by 4 after 32 hours at 135 °C in 1:1 ethylene glycol to monomer ratio per volume.

The reaction leading to disproportionation products has recently been confirmed by Burguière et al. who examined the polymerization of methyl methacrylate leading to its oligomers and polymers.[37] Their results from polymerization studies lead to the general scheme shown in Figure 6-10 accounting for the formation of hydroxylamine. The formation of disproportionation products is of no surprise since this is the predominant route for polymer termination in conventional free radical polymerization of acrylates.[34] However, it is surprising that this is also the predominant route for polymer termination in nitroxide mediated LFRP. The reported conversion for acrylates with typical LFRP conditions is approximately 3% with low molecular weights.[37] This is expected since the rate of disproportionation was found to be 1.4×10^6 M^{-1} s^{-1},[37] nearly three orders of magnitude greater than the rate of acrylate propagation at 130 °C. Hence, the lack of observed nitroxide control in the polymerization of acrylates at higher molecular weights is from the formation of disproportionation products. The resulting vinyl terminated polymers are of random length and undergo polymerization leading to large polydispersities.

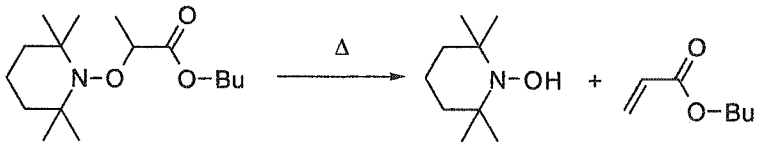

Figure 6-10. Disproportionation products arising from thermal decomposition of poly-*n*-butyl acrylate confirmed here and by others.[37]

6.2.1.1 Section Conclusion

The use of a non miscible second phase can partition the free nitroxide and reduce its concentration in the bulk phase. This in turn is responsible for shifting the equilibrium from "dormant" to a more "active" species during the polymerization. Increasing the amount of propagating radicals shifts the kinetics and polymerization process to that found with styrenic monomers, thereby leading to higher molecular weight polymers. Higher conversions and acceptable polydispersities can be achieved through the removal of excess nitroxide during the initial stages of polymerization. However, this has little effect later on during the polymerization because the formation of disproportionation products dominates which are responsible for the lack of control over the polydispersity.

6.2.2 Sterical Nitroxide Mediated Polymerization

Since the biphasic approach led only to a marginal success in yielding living type polymers when applied to acrylates, a new polymerization approach was investigated. The idea was to find a means by which to eliminate the reaction responsible for disproportionation product formation, and in turn, would give polyacrylates with higher molecular weights and greater conversions. This approach draws upon the knowledge gained from a previous chapter concerning disproportionation products. There it was learned that steric factors arising from the *penultimate* group increased the height of the rotational barrier, where the eclipsed geometry of the α,β hydrogens responsible for the formation of disproportionation products was not possible. The mechanism for disproportion products formation with polyacrylates is essentially the same as that found with the styrene based unimolecular initiators.[37] Therefore, incorporating a steric element into the polymer would decrease the amount of disproportionation products and result in higher conversions. However, this factor must be incorporated into the nitroxide and not the monomer, as modification of the

latter has no effect and would lead to different polymer properties in general. The *penultimate* effect applied to the monomer is not sufficient to suppress the formation of disproportionation products as these products are observed when polymerizing higher molecular weight oligomers when applied to acrylates. The nitroxide **5** previously used as a polymer stabilizer[38-46] is a suitable candidate since it contains two bulky cyclohexyl groups in the 2 and 6 positions, which should increase the rotational barrier. Subsequently, the eclipsed orientation of the α,β hydrogens cannot be attained. The suppression of such products in turn should lead to polyacrylates with high conversions and low polydispersities. Disproportionation product formation of acrylates is assumed to be similar to that of styrene. Recent product and kinetic studies involving TEMPO[37] and a new generation of nitroxides[16,18-21] prove this to be true for acrylates.

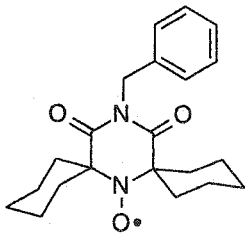

5

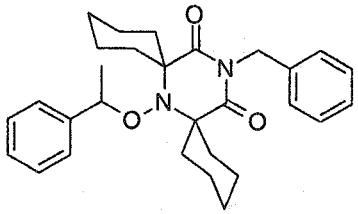

8

Figure 6-11. Piperazine based nitroxide and its unimolecular initiator containing sterically bulky cyclohexyl groups adjacent to the nitroxide functionality.

Preliminary results were obtained using semi-empirical calculations to determine the rotational barrier height to see whether **5** was a viable candidate for suppressing the formation of disproportionation products. This procedure consists of calculating the individual heats of formation for each rotation of the dihedral angle shown by the Newman projection in Figure 6-12. Compound **6** was used as a benchmark test for calculating the barrier height as it is known to give significant amounts of disproportionation products during the polymerization of acrylates.[37] The rotational barrier for **7** was also calculated and the results are graphically represented in Figure 6-13. The lowest energy rotamer for both initiators was taken as zero for easy and direct comparison of their respective rotational barriers. The barrier height for **6** is relative small, which is expected since it gives disproportionation products. Contrary to this, the barrier for **7** is remarkably higher and suggests the correct configuration leading to

disproportionation products cannot be obtained. This is in agreement with the results obtained for the similar study involving the *penultimate* compound. Hence, the initiator **8** would appear to be an ideal candidate for nitroxide based LFRP of acrylates. This approach has previously proven beneficial for predicting the barrier heights and was addressed in a preceding chapter.[47,48] Semi-empirical calculations are not known to give exact or accurate heats of formation. However, the barrier calculated is an accurate representation of the true height as the errors are systematic and their relative values yield small errors.[49-51] The calculated barrier is nearly double the height found for the penultimate compound in an earlier chapter that did not form any disproportionation products. This leads to the belief that **7** would be an ideal nitroxide for suppressing the formation of disproportionation products and in turn promote narrow polydispersities and higher conversions.

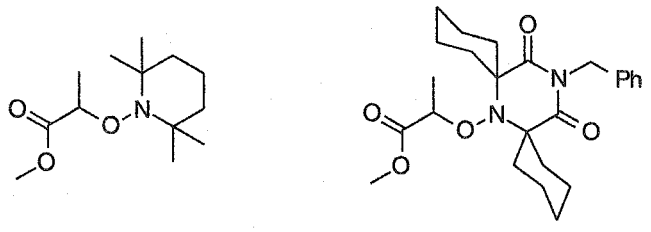

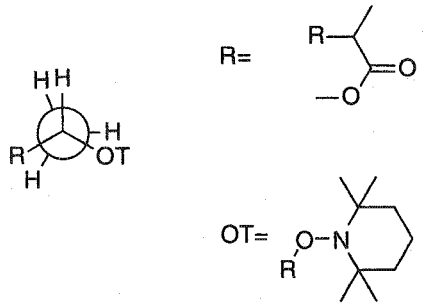

Figure 6-12. Above: Acrylate based models for calculating the rotational height. Below: Newman projection of dihedral angle rotated for calculations.

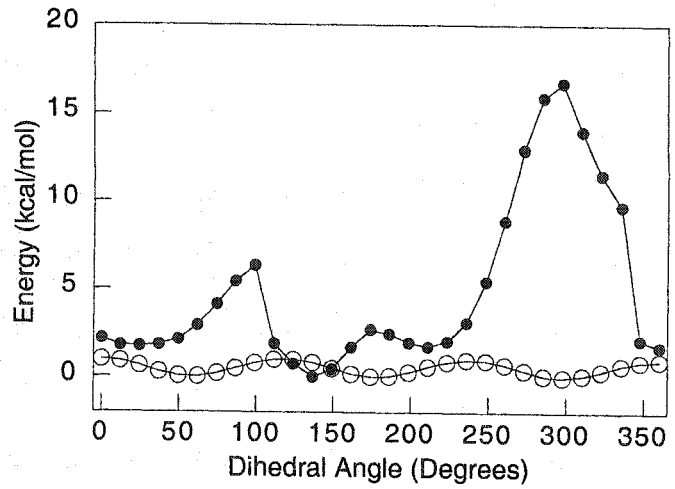

Figure 6-13. Rotational barrier calculated semi-empirically for initiator 6 (○) and 7 (●).

Reasonable results are obtained when applying typical polymerization methods to *n*-butyl acrylate with **8** as an initiator. High molecular weights (> 200 000) are easily achieved and the polydispersities are equally acceptable. The major difference comes in the form of the polymer conversion. Unlike the biphasic method that gave moderate conversions, polymerization with the nitroxide **7** gives exceptionally high yields, > 80 %. Even more remarkable is the small reaction time required to achieve these high conversions as represented in Figure 6-14 showing the polymerization conversion with reaction time. This controlled behavior has not previously been reported in the literature or searchable patents by any other group and represents the first such polymerization control with nitroxides. Under similar conditions, the rate of polymerization using initiator **8** with *n*-butyl acrylate is $5.1 \times 10^{-2} M^{-1} s^{-1}$, and is 2.5 times faster than for styrene.[36] This is the expected trend since the rate of propagation (k_p) of styrene is approximately four and a half times slower than for *n*-butyl acrylate at this polymerization temperature.[36] The formation of disproportionation products is therefore not occurring with the use of the **7** as the trapping nitroxide based upon the faster observed k_p of *n*-butyl acrylate. The GPC chromatograph also did not yield any hydroxylamine derived from **5** further confirming the lack disproportionation products. Therefore, **5** used as the trapping nitroxide suppresses the formation of disproportionation products giving rise to true nitroxide mediated living free radical polymerization.

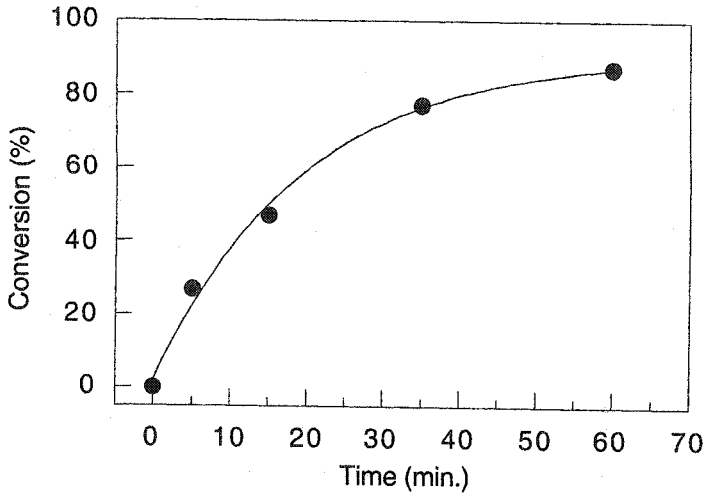

Figure 6-14. Polymerization conversion of *n*-butyl acrylate initiated by 5 at 135 °C.

Nitroxide mediated polymerization of *n*-butyl acrylate with **5** was compared to a typically used initiator, AIBN. It is known that this initiator induces conventional free radical polymerization and exerts no control over the polymers properties. Polymerization of the acrylate monomer with AIBN under identical conditions gave polymers with low molecular weight (< 100 000) and poor polydispersities (PD > 2). This further confirms nitroxide mediated polymerization of acrylate with **8** is able to control the reaction similarly to styrene and give poly-*n*-butyl acrylate with desired low polydispersities, high molecular weights, and high conversions.

6.3 Conclusion

Nitroxide mediated LFRP of acrylates is found to be extremely sensitive to the amount of free nitroxide during the course of the reaction. Reducing its concentration at the initial stages of the reaction by partitioning it into a second medium gives rise to polyacrylates with improved polydispersities and higher molecular weights. However, the living properties of the polymers obtained do not compare to the desirable properties from styrene based LFRP. The major factor responsible for the lack of conversion is attributed to the formation of disproportionation products. The lack of control also stems from the vinyl byproduct that leads to dead polymers when trapped by a propagating radicals. This occurs as a result of termination by cross-coupling and by important free nitroxide removal in the form of hydroxylamine formation. The introduction of steric elements into the nitroxide suppresses the formation of these undesired disproportionation products. The end result is polymers with high molecular weights, narrow polydispersities, and high conversions that rival the styrenic based LFRP.

6.4 Experimental

All chemicals were purchased from Aldrich and were used as received unless otherwise stated. Styrene, methyl methacrylate, and *n*-butyl acrylate were distilled under reduced pressure immediately prior to use. Di-*tert*-butyl peroxide was purified by passing it through a plug of neutral aluminum oxide and used immediately.

6.4.1 Synthesis

1-phenyl-1-(2,2,6,6-tetramethylpiperdine-N-oxide)-ethane (1): The synthesis of this compound was described previously in an earlier chapter according to literature procedures.[52]

1-phenyl-1-(2,2,6,6-tetramethyl-4-hydroxy-piperdine-N-oxide)-ethane (2): The synthesis of this compound was done according to literature procedures and fully described previously in an earlier chapter.[52]

1-phenyl-1-(2,2,6,6-tetramethyl-4-oxo-piperdine-N-oxide)-ethane (3): A 15 cm Pyrex test tube was charged with ethylbenzene (35 mL), 2,2,6,6-tetramethylpiperidine-N-oxyl (350 mg, 2.06 mmol) and di-*tert*-butyl peroxide (2.5 g, 17.1 mmol) that was passed through a plug of neutral aluminum oxide. Oxygen was purged from the reaction vessel by bubbling nitrogen through the solution, and then the product was irradiated at 300 nm at room temperature in a merry-go-round reactor with 6 lamps. The orange solution was irradiated till a light yellow color persisted, normally 2-3 days. The reactor was discharged and the residual ethylbenzene was removed by evaporation with a gentle stream of nitrogen. The yellow solid obtained was purified by flash chromatography with 5% ethylacetate/hexanes to give white needle like crystals in 60% yield. The same product can be obtained under identical experimental conditions and longer irradiation with 4-hydroxy-TEMPO to give the over oxidized product. M.p. 74 °C. ^{1}H NMR (200 MHz, $CDCl_3$, TMS) δ 7.21-7.30 (m, 5H), 4.71 (q, 1H), 3.9 (m, 1H), 1.65-1.79 (m, 4H), 1.48 (d, 3H), 1.31 (s, 3H), 1.19 (s, 3H), 1.05 (s, 3H), 0.65 (s, 3H). ^{13}C NMR (300 MHz, $CDCl_3$) δ 208.4, 144.6, 128.2, 127.3, 126.8, 83.4, 62.9, 62.7, 53.7, 33.9, 33.6, 22.9, 22.8, 22.6. MS (FAB) m/z (%) 276 (22, M+1), 215 (66), 132 (56), 121 (11), 105 (100), 91 (20), 77 (32). MS (EI) m/z (%) 171 (21), 127 (29), 140 (7), 123 (12), 114 (24), 105 (100), 103 (61), 91 (5), 77 (50), 56 (91), 51 (44), 41 (47).

1-phenyl-1-(2,2,6,6-tetramethyl-4-carboxy-piperdine-N-oxide)-ethane (4): A 15 cm Pyrex test tube was charged with ethylbenzene (25 mL), 4-carboxy-2,2,6,6-tetramethylpiperdine-N-oxyl (200 mg, 1.3 mmol) and di-*tert*-butyl peroxide (2.8 g, 1.83 g, 19.2 mmol). Oxygen was purged from the reaction vessel by bubbling nitrogen through the solution, and then the product was irradiated at 300 nm by placing the test tube a merry-go-round apparatus. The yellow color solution was irradiated overnight and the residual ethylbenzene was removed by a gentle flow of nitrogen. The product was isolated is white needle like crystals after double crystallization from hot hexanes in 74 % yield (282 mg). M.p. 122-128 °C. ^{1}H NMR (200 MHz, $CDCl_3$, TMS) δ 7.19-7.31 (m, 6H), 4.76 (q, 1H), 2.64 (m, 1H), 1.61-1.73 (m, 4H), 1.47 (d, 3H), 1.32 (s, 3H), 1.19 (s, 3H), 1.04 (s, 3H), 0.66 (s, 3H). ^{13}C NMR (300 MHz, $CDCl_3$) δ 182.1, 145.4, 128.3, 128.0, 127.9, 126.7, 83.4, 76.6, 42.1, 42.0, 33.9, 33.8, 33.7, 33.6, 23.2, 20.5. MS (EI) m/z (%) 201 (37), 186 (56), 170 (50), 151 (24), 140 (17), 120 (8), 114 (46), 105 (100), 91 (21), 77 (63.4), 67 (309). MS (FAB) m/z (%) 306 (21, M+1), 209 (20), 200 (10), 137 (10), 105 (100), 91 (13), 77 (6).

4-aceto-2,2,6,6-tetramethylpiperdine-N-oxide: 4-Hydroxy-TEMPO (0.43 g, 2.5 mmol) was dissolved in 10 mL of dichloromethane along with 4-dimethylaminopyridine (50 mg, 0.4 mmol). Acetic anhydride (0.3 mL, 3.2 mmol) dissolved in 2 mL dichloromethane was added to the nitroxide mixture and allowed to stir at room temperature overnight. The solvent was removed under vacuum and the organic solid purified by flash chromatography with 2:1 hexanes/ethylacetate as eluent. The nitroxide product was isolated as an orange yellow solid in 70 % yield (0.37 g). M.p. 43-46 °C. MS (EI) m/z (%) 214 (14), 110 (18), 124 (74), 122 (15), 109 (88), 105 (33), 101 (3), 91 (4), 85 (24), 77 (8), 67 (42), 55 (31), 43 (100).

1-Benzyl-3,3,5,5-dicyclohexyl-4-(1-phenyl-ethoxy)-piperazine-2,6-dione (7): A 15 cm Pyrex test tube was charged with ethylbenzene (25 mL), 5 (*vide infra*) (830 mg, 2.33 mmol) and di-*tert*-butyl peroxide (0.49 mL, 390 mg, 267 mmol). Oxygen was purged from the reaction vessel by bubbling argon through the solution, and then the product was irradiated by placing the test tube in ice-water bath containing a Conrad-Hanovia medium pressure mercury vapor lamp. When the orange color of the nitroxide had disappeared (6 days). The test tube was discharged and the residual ethylbenzene was removed by evaporation. Recrystallization from isopropanol afforded colorless crystals in 78% yield. M.p. 110-115 °C. ^{1}H NMR (200 MHz, $CDCl_3$,TMS) δ 7.20-7.32 (m, 10H), 4.82 (q, 1H), 1.5 (d, 3H), 1.08 (s, 9H), 1.05 (s, 9H). ^{13}C NMR (300 MHz, $CDCl_3$) δ 157.2, 132.5, 128.3,

128.1, 127.9, 127.5, 127.1, 90.8, 82.5, 77.4, 77.0, 76.6, 43.8, 33.2, 25.9, 25.5, 22.4, 20.5. MS (EI) m/z (%) 355 (1), 339 (10), 297 (13), 249 (25), 209 (68), 178 (39), 122 (36), 105 (100), 91 (59), 77 (82), 51 (45).

1-Benzyl-3,3,5,5-dicyclohexyl-4-N-oxyl-piperazine-2,6-dione (5, precursor to 7): 5 was prepared by a procedure adapted from Ramey and Luzzi.[53] To a solution of 4-N-benzyl-4-azoglutarimide[53] (2.70 g, 8 mmol) in dichloromethane (75 mL) was added 3-chloroperoxybenzoic acid (99%) (2.76 g, 16 mmol). The temperature rose to 28 °C during the course of the addition. After 24h, the precipitate was filtered off and the lemon yellow solution was chromatographed on silica gel using hexane/ethylacetate (3%). 5 was isolated as an orange syrup (2.01 g, 71%). M.p. 61-64 °C. MS (EI) m/z (%) 355 (26), 340 (100), 297 (28), 284 (12), 269 (39), 249 (26), 216 (19), 178 (36), 109 (15), 91 (57), 69 (29), 55 (9), 40 (39).

6.4.2 Partition Coefficient Determination

10 mg (~ 0.6 mmol) of the nitroxides were dissolved in 10 mL of methylpropionate along with 10 μL of 1,3 diphenylpropane (Lancaster) used as an internal standard. Known amounts of distilled water or ethylene glycol (BDH) were added to the nitroxide samples. The solutions were shaken and upon equilibration, 1 μL of the organic layer was injected into a Fisons GC equipped with a FID detector maintained at 300 °C. The components of the organic layer were separated on a DB-5 25 mm ID column with 0.32 μM coating 50 M in length. The injector temperature was maintained at 220 °C while the initial temperature was 45 °C for 2 minutes then heated to 280 °C at a rate of 10 °C/minute. The ratio of the nitroxide to internal standard was calculated and compared to that of the bulk standard solution.

An HPLC equipped for a diode array detector and a Zorbax® C-18 reverse phase column was used to determine the partition coefficients for the 4-carboxy nitroxide. The eluent was 85% methanol/15 % water with a flow rate of 0.5 mL/minute then increased to 1.5 mL/minute after 12 minutes. Initially 3.5 mg (0.02 mmol) of the nitroxide was dissolved 5 mL of methylpropionate along with 7.9 mg (0.04 mmol) of 1,4 di-*tert*-butylbenzene as internal reference. The data were analyzed in the same manner as with the other nitroxides.

6.4.3 Polymerization Methods

The biphasic polymerizations were done according to the three separate methods listed hereafter.

Method 1 consisted of dissolving the 0.3 mmol of the initiator in 180 equivalents of the monomer charged in a 50 mL round bottom flask. One flask served as a control while water was added to the other to give a ratio of 2:1 monomer/aqueous layer. The systems were degassed with in-house nitrogen for a period of 30 minutes and then placed in an oil bath preheated to 120 °C. Aliquots of 0.5 mL were removed at regular intervals and analyzed as described below.

Method 2 consisted of dissolving 0.3 mmol of the initiator in 800 equivalents of the monomer charged in a 50 mL round bottom flask. Different ratios of monomer to water were measured: 6:1, 3:1 and 2:1. The samples were degassed with in-house nitrogen for a period of 45 minutes and then placed in a preheated oil bath at 120 °C. Aliquots of 0.5 mL were removed at regular intervals and analyzed as described below.

Method 3 involved dissolving 0.8 mmol of the initiator in 25 mL (~ 210 equivalents) of *n*-butyl acrylate. Aliquots of 0.2 mL of this solution was added to 7 mm homemade glass tubes along with 0.2 mL of ethylene glycol (BDH) for the biphasic systems. The tubes were flamed sealed under vacuum after three cycles of freeze-pump-thaw then placed in a thermostated aluminum block preheated to 135 °C. Aliquots were removed at regular intervals for subsequent analysis according to the method below.

A standard test with 2,2'-Azobisisobutyronitrile (AIBN) (36 mg, 0.21 mmol) in 25 mL (842 equivalents) *n*-butyl acrylate was prepared in the same fashion as method 3, but polymerized at 72 °C.

After polymerization the aliquots were immediately cooled in ice water and the contents dissolved in THF and transferred to a round bottom flask. The solvent was removed under reduced pressure and the residual monomer removed under high vacuum. The samples were then weighted and solution concentrations of 2.5 mg/mL were used for GPC analyses.

A volume of 50 µL was injected onto a Waters Styragel® HR4 and HR1 size exclusion columns connected in series. The polymers were detected by a Varian

refractive index detector and the retention times compared to polystyrene molecular weight standards. The molecular weights (M_w and M_n) and polydispersities (PD) were calculated with an in-house program written in the LabVIEW environment and referenced to the calibration curve according to standard techniques.[54,55]

6.4.4 Semi-empirical calculations

Semi-empirical calculations were carried out on a Silicon Graphics Indigo workstation using Spartan SGI version 4.0.4 GL IRX 5.2. The structures were minimized with AM1 and then the energies for the dihedral angle driver were calculated with the respective level of theory and optimized for every angle. The rotational barriers were calculated using the coordinate driving option with the AM1[56] semi-empirical levels of theory that calculated the optimized geometries and heats of formation (ΔH_f) for the particular dihedral angle. Restricted Hartree-Fock (RHF) was selected for the calculations for all systems and the σ value was set at 100.

6.5 Chapter References

1. Georges, M. K.; Veregin, R. P. N.; Kazmaier, P. M.; Hamer, G. K. *Macromolecules* **1993**, *26*, 2987-2988.
2. Hawker, C. J. *Acc. Chem. Res.* **1997**, *30*, 373-382.
3. Matyjaszewski, K. "Overview: Fundamentals of Controlled/Living Radical Polymerization"; Controlled Radical Polymerization, 1998, San Francisco, CA.
4. Malmström, E. E.; Hawker, C. J. *Macromol. Chem. Phys.* **1998**, *6*, 923-935.
5. Fréchet, J. M. J. *Science* **1994**, *263*, 1710-1715.
6. Fréchet, J. M. J.; Hawker, C. J.; Wooley, K. L. *J. Macromol. Pure Appl. Chem.* **1994**, *A31*, 1627-1645.
7. Hawker, C. J.; Fréchet, J. M. J.; Grubbs, R. B.; Dao, J. *J. Am. Chem. Soc.* **1995**, *117*, 10763-10764.
8. Georges, M. K.; Veregin, R. P. N.; Kazmaier, P. M.; Hamer, G. K. *Polym. Prepr.* **1994**, *38*, 870-871.
9. Odell, P. G.; Rabien, A.; Michalak, L. M.; Vergin, R. P. N.; Quinlan, M. H.; Moffat, K. A.; MacLeod, P. J.; Listigovers, N. A.; Honeyman, C. H.; Georges, M. K. *Polym. Prepr.* **1997**, *38*, 414-415.
10. Ogawa, T. U.S. Patent 5,610,249, **1997**.
11. Keoshkerian, B.; Georges, M. K.; Kazmaier, P. M.; Hamer, G. K. U.S. Patent 5,739,229, **1998**.
12. Malmström, E. E.; Miller, R. D.; Hawker, C. J. *Tetrahedron* **1997**, *53*, 15225-15236.
13. Le Mercier, C.; A., G.; Siri, D.; Tordo, P.; Marque, S.; Martschke, R.; Fischer, H. *Polym. Prepr.* **1999**, *40*, 313-314.
14. Le Mercier, C.; Bernard-Henriet, C.; de Sainte-Claire, V.; Le Moigne, F.; Tordo, P. *Polym. Prepr.* **1999**, *40*, 403-404.

15. Grimaldi, S.; Finet, J.-P.; Zeghdaoui, A.; Tordo, P.; Benoit, D.; Gnanou, Y.; Fountanille, M.; Nicol, P.; Pierson, J.-F. *Polym. Prepr.* **1997**, *38*, 651-653.
16. Doa, J.; Benoit, D.; Hawker, C. J. *J. Polym. Sci. A. Polym. Chem.* **1998**, *36*, 2161-2167.
17. Limoges, B.; Degrand, C. *J. Electroanal. Chem.* **1997**, *422*, 7-12.
18. Benoit, D.; Chaplinski, V.; Braslau, R.; Hawker, C. J. *J. Am. Chem. Soc.* **1999**, *121*, 3904-3920.
19. Hawker, C.; Benoit, D.; Rivera, F., Jr.; Piotti, M.; Rees, I.; Hedrick, J. L.; Zech, C.; Maier, G.; Voit, B.; Braslau, R.; Fréchet, J. M. J. *Polym. Prepr.* **1999**, *40*, 315-316.
20. Harth, E.; Benoit, D.; Helms, B.; Hawker, C. J. *Polym. Prepr.* **2000**, *41*, 42-43.
21. Benoit, D.; Harth, E.; Fox, P.; Waymouth, R. M.; Hawker, C. J. *Macromolecules* **2000**, *33*, 363-370.
22. *CRC Handbook of Chemistry and Physics*, 52 ed.; The Chemical Rubber Company: Cleveland, 1995, .
23. Devonport, W.; Michalak, L.; Malmstrom, E.; Mate, M.; Kurdi, B.; Hawker, C. J. *Macromolecules* **1997**, *30*, 1929-1934.
24. Georges, M. K.; Odell, P. G.; Veregin, R. P. N.; Keoshkerian, B. *Polym. Prepr.* **1997**, *38*, 721-722.
25. Veregin, R. P. N.; Odell, P. G.; Michalak, L. M.; Georges, M. K. *Macromolecules* **1996**, *29*, 3346-3352.
26. Hawker, C. J.; Hedrick, J. L. *Macromolecules* **1995**, *28*, 2993-2995.
27. Moffat, K. A.; Saban, M. D.; Veregin, R. P. N.; Georges, M. K.; Hamer, G. K.; Kazmaier, P. M. U.S. Patent 5,449,724, **1995**.
28. Veregin, R. P. N.; Georges, M. K.; Hamer, G. K.; Kazmaier, P. M. *Macromolecules* **1995**, *28*, 4391-4398.
29. Georges, M. K.; Veregin, R. P. N.; Kazmaier, P. M.; Hamer, G. K. *Trends Polym. Sci.* **1994**, *2*, 66-72.

30. Veregin, R. P. N.; Georges, M. K.; Kazmaier, P. M.; Hamer, G. K. *Macromolecules* **1993**, *26*, 5316-5320.
31. Hawker, C. J. *J. Am. Chem. Soc.* **1994**, *116*, 11185-11186.
32. Georges, M. K.; Veregin, R. P. N.; Kazmaier, P. M.; Hamer, G. K.; Saban, M. *Macromolecules* **1994**, *27*, 7228-7229.
33. Georges, M. K.; Veregin, R. P. N.; Daimon, K. The Stable Free-Radical Polymerization Process: Role of Excess Nitroxide. In *Controlled Radical Polymerization*; Matyjaszewski, K., Ed.; American Chemical Society: Washington, 1998; Vol. 685; 170-179.
34. Cowie, J. M. G. *Polymers: Chemistry and Physics of Modern Materials*, 2nd ed.; Blackie and Sons Ltd.: Glasgow, 1991, pp 436.
35. Stevens, M. P. *Polymer Chemistry, An Introduction*, 2nd ed.; Oxford University Press: New York, 1990, pp 633.
36. Berger, K. C.; Meyerhoff, G. Propagation and Termination Constants in Free Radical Polymerization. In *Polymer Handbook*; 3rd ed.; Brandrup, J., Immergut, E. H., Eds.; John Wiley & Sons: New York, 1989; .
37. Burguière, C.; Dourges, M.-A.; Charleux, B.; Vairon, J.-P. *Macromolecules* **1999**, *32*, 3883-3890.
38. Ramey, C. E.; Luzzi, J. J. U.S. Patent 3,928,330, **1975**.
39. Ramey, C. E.; Luzzi, J. J. U.S. Patent 4,007,157, **1976**.
40. Ramey, C. E.; Luzzi, J. J. U.S. Patent 3,968,078, **1976**.
41. Ramey, C. E.; Luzzi, J. J. U.S. Patent 3,992,351, **1976**.
42. Ramey, C. E.; Luzzi, J. J. U.S. Patent 4,007,156, **1977**.
43. Vass, F.; Luston, J. *J. Prakt. Chem./Chem.-Ztg.* **1996**, *338*, 165-168.
44. Luston, J.; Vass, F. *Makromol. Chem., Macromol. Symp.* **1989**, *27*, 231-237.
45. Ramey, C. E.; Luzzi, J. J. U.S. Patent 4,070,335, **1978**.
46. Minagawa, M.; Kubota, N.; Shibata, T. U.S. Patent 4,118,369, **1978**.
47. Skene, W. G.; Scaiano, J. C.; Yap, G. P. A. *Macromolecules* **2000**, *33*, 3536-3542.

48. Skene, W. G.; Scaiano, J. C.; Yap, G. P. A. *Polym. Prepr.* **2000**, *41*, 119-120.
49. Fabian, W. M. F. *J. Comput. Chem.* **1988**, *9*, 369-677.
50. Stewart, J. J. P. *J. Comput. Chem.* **1989**, *10*, 209-220.
51. Stewart, J. J. P. *J. Comput. Chem.* **1989**, *10*, 221-264.
52. Connolly, T. J.; Baldovi, M. V.; Mohtat, N.; Scaiano, J. C. *Tetrahedron Lett.* **1996**, *37*, 4919-4922.
53. Ramey, C. E.; Luzzi, J. J. U.S. Patent 3,936,456, **1976**.
54. Stewart, J. J. P. Semiempirical Molecular Orbital Methods. In *Reviews in Computational Chemistry I*; Lipkowitz, K. B., Boyd, D. B., Eds.; VCH:, 1990; 45-81.
55. Young, R. J.; Lovell, P. A. *Introduction to Polymers*, 2nd ed.; Chapman and Hall: New York, 1991, pp 443.
56. Dewar, M. J. S.; Zoebisch, E. G.; Healy, E., F.; Stewart, J. J. P. *J. Am. Chem. Soc.* **1985**, *107*, 3902-3909.

7. LFRP Photoinitiators

7.1 Introduction

Photoinitiated free radical polymerization is the process of using light to induce a chemical reaction that eventually gives rise to radical centers responsible for initiating the polymerization. The subsequent reactions encountered during photoinitiated based polymerization are identical to its thermal counterparts, i.e., propagation and termination. Since the steps after initiation are identical for the different initiated reactions, the physical properties of the polymers are similar regardless of the type of initiator used. Therefore, light induced free radical polymerization also leads to polymers that exhibit high polydispersities and moderately high molecular weights, similar to the thermal initiated conventional free radical polymerization.[1-8] Photoinitiated radical polymerization is an attractive alternative to thermal induced polymerization for two principal reasons. It primarily generates the propagating radical by photochemical decomposition of the initiator. Unlike its thermal counterpart, the propagation steps are carried out at room temperature, provided the monomer polymerized has a sufficiently high propagation rate constant (k_p) at the reaction temperature. The other benefit of photoinitiated polymerization is the incorporation of a chromophore into the chain terminus. This is advantageous as the polymerization progress can be easily monitored by UV-Vis spectroscopy[9] and it can also be used to examine the polymer's physical properties through the rate and efficiency of quenching of the chromophore's excited state.[10-12]

The most widely employed approach for photoinduced free radical polymerization uses benzophenone as a sensitizer. Direct excitation of benzophenone forms its singlet state which rapidly and efficiently undergoes intersystem crossing (ISC) to its triplet state, which has an n,π^* configuration.[13] This is portrayed by Equations 1 and 2 in Scheme 7-1, respectively. In the absence of any quencher and in inert solvents, the excited benzophenone relaxes to its ground state without any net chemistry. However, in the presence of a good hydrogen atom source, such as an alkane used as a co-solvent, the triplet state abstracts a hydrogen giving rise to the carbon centered ketyl radical shown in Equation 3. This radical and the radical generated from hydrogen donation are responsible for initiating monomer polymerization and the subsequent propagation and termination steps are dark processes, hence do not require any light.

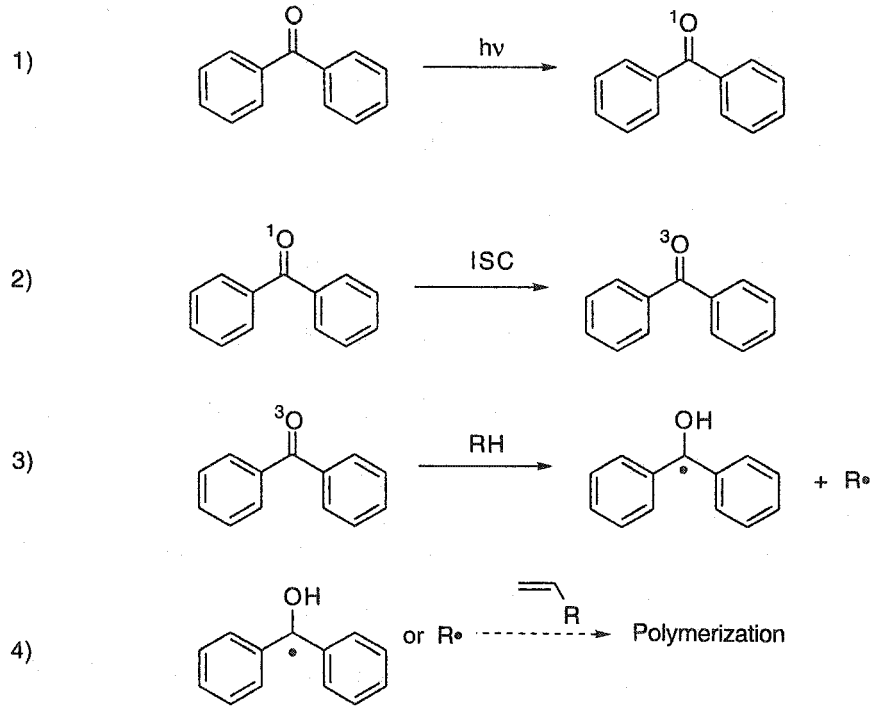

Scheme 7-1. Benzophenone based photoinitiated polymerization.

A major disadvantage of benzophenone initiated polymerization is that a hydrogen source is required. Since the rate constant for hydrogen abstraction leading to the ketyl radical is relative slow (~ 10^6 M^{-1} s^{-1}), a significant amount of hydrogen donor is required.[14] These polymerizations are typically done with a hydrocarbon co-solvent, but the initiation is still slow and not ideal because the reaction conditions are shifted from bulk to solution polymerization.[15,16] The use of an aliphatic amine as an additive increases the polymerization rate by increasing the rate of initiation and the efficiency of chain transfer. The benzophenone triplet is quenched approximately two orders of magnitude faster by an amine compared to a hydrocarbon solvent.[16,17] Since the quenching rate constant is considerably faster with amines, their required concentration can be stoichiometric and eliminates the use of a co-solvent making the reaction conditions similar to those of bulk free radical polymerization. This approach has been advanced by the Neckers group that has successfully promoted photoinduced polymerization by covalently attaching the amine to the chromophore moiety.[18-20] The general mechanism for amine accelerated benzophenone induced polymerization is shown in Scheme 7-2. The amine

quenches the ketone triplet in the order of 10^9 M^{-1} s^{-1},[16] via electron transfer leading to hydrogen abstraction products.

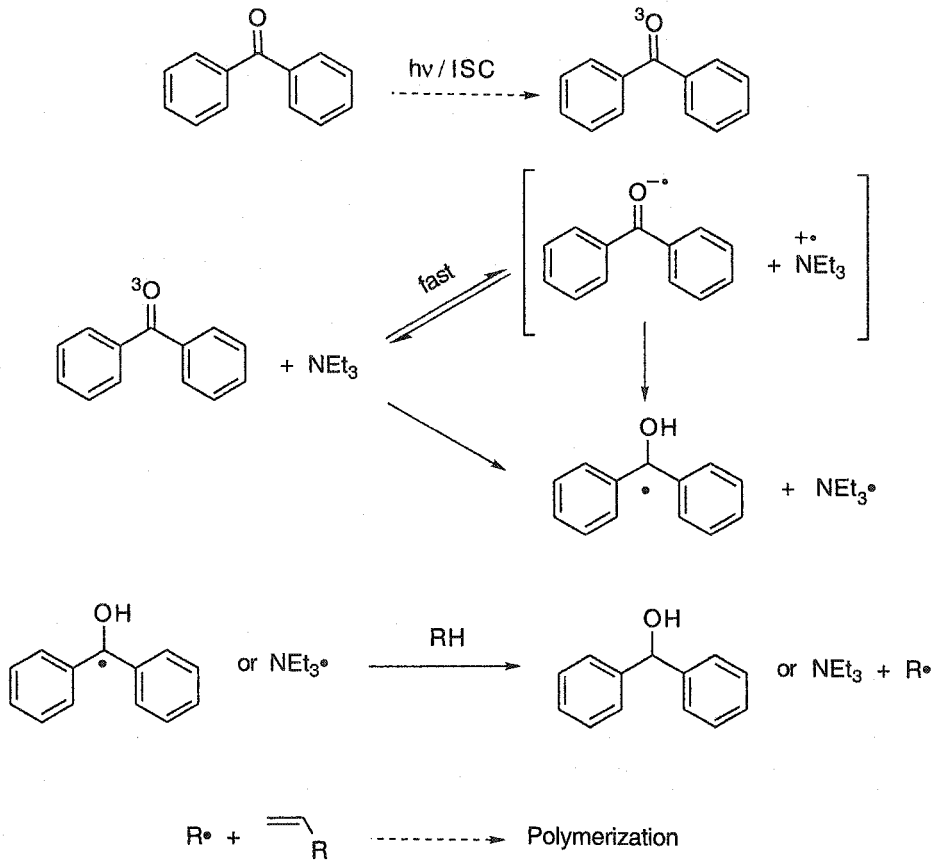

Scheme 7-2. General scheme for amine accelerated photoinitiated polymerization.

The examples presented here are only a few of the chromophores that can be used as photoinitiators for free radical polymerization. Thioxanthone,[3,8] maleimide,[21] benzyl selenides,[22] and peroxypivalate[23] are yet a few other initiators currently used to promote photoinduced free radical polymerization. Regardless of the initiator selected or the addition of additives, photoinduced free radical polymerization suffers from the same lack of control as conventional thermal based free radical polymerization. Therefore, the polymers obtained by this method exhibit poor physical properties such as high polydispersity (PD > 1.5), moderately low molecular weights, and the copolymerization cannot be controlled, contrary to nitroxide based LFRP. The desired living polymer properties could be obtained through controlled radical photopolymerization.

This would involve the introduction of an element, such as a nitroxide, capable of controlling the propagation steps similarly to LFRP.

This idea was originally investigated by Scaiano et al. who examined the sensitized decomposition of typically used thermal unimolecular initiators.[24] The general idea was to photochemically sensitize the C-O bond fragmentation of nitroxide based initiators by energy transfer from a sensitizer to the initiator. This would ultimately lead to the same radicals achieved thermally and result in photochemically controlled living free radical polymerization. The end result would be polymers with the desired living properties without the use of heat, as with conventional LFRP. The general approach is depicted in Scheme 7-3 where the chromophore and nitroxide are covalently bonded. Selective excitation of the chromophore would lead to its excited state. It would then be quenched by the alkoxyamine moiety by energy transfer resulting in the homolytic C-O cleavage. In the presence of monomer, the propagating radical adds to the monomer and is subsequently trapped by the free nitroxide. Continuous excitation of the chromophore leads to a series of constant C-O bond cleavages and trappings analogous to those found in thermal LFRP. The polymer grows with insertion of the monomer between each capping and decapping step.

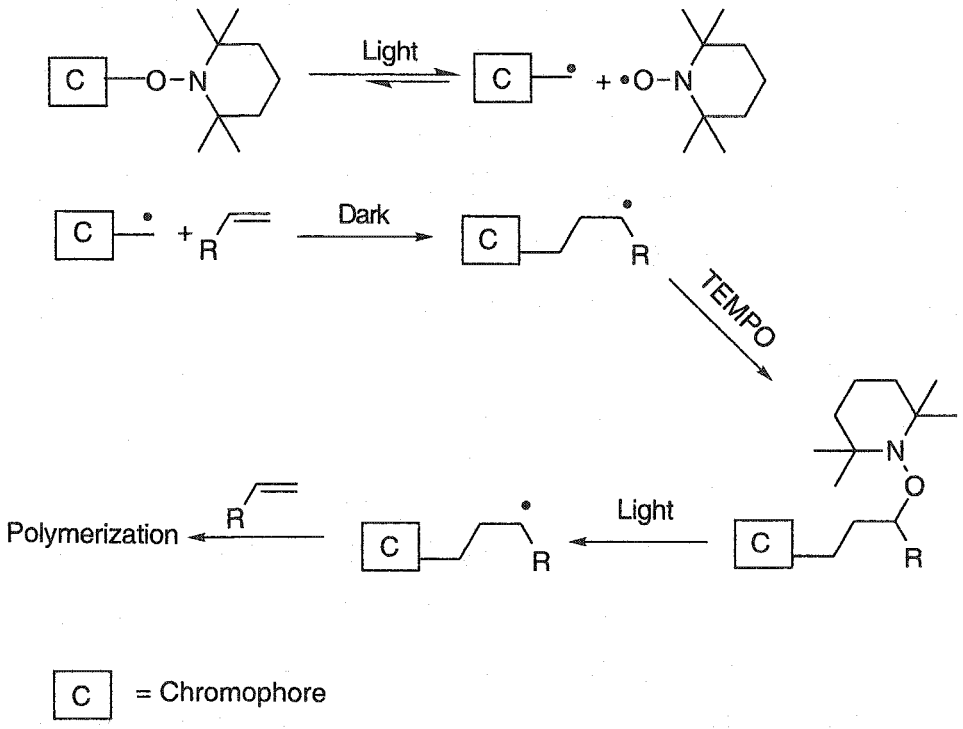

Scheme 7-3. General mechanism of light induced LFRP.

The preliminary study of Scaiano examined a series of triplet sensitizers shown in Figure 7-1. Instead of proceeding with laborious synthesis of nitroxide based photochemical initiators without knowing if they would even control the polymerization, their capability to sensitize the homolytic decomposition of the C-O bond was examined. Similar to the benzophenone initiator previously shown, the sensitizers examined undergo rapid intersystem crossing to their triplet state upon excitation as shown in Scheme 7-3. The excited energy from the triplet is then transferred to the unimolecular initiator. Favorable sensitizers transfer their triplet energy to the unimolecular initiator and induce the desired C-O bond cleavage responsible for LFRP properties. The quenching process is relatively fast if the triplet energy is much greater than the ~ 30 kcal/mol required to cleave the C-O bond. In the case of aromatic initiators, such as those studied in a previous chapter, the benzylic type radical can be spectroscopically seen by laser flash photolysis proving the occurrence of the C-O bond fragmentation.

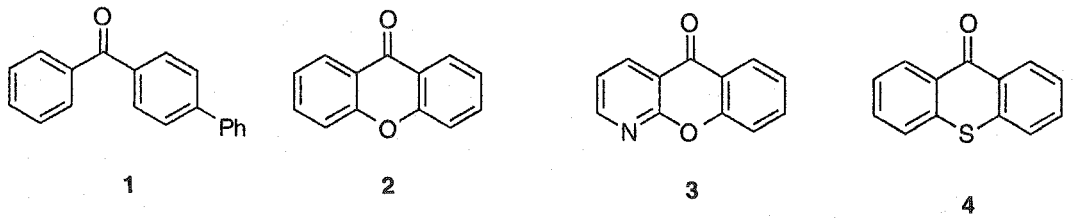

1 2 3 4

Figure 7-1. Sensitizers for photodecomposition of unimolecular initiators.

5) $\text{Sensitizer} \xrightarrow{h\nu} {}^1\text{Sensitizer}$

6) ${}^1\text{Sensitizer} \xrightarrow{ISC} {}^3\text{Sensitizer}$

7) ${}^3\text{Sensitizer} + \text{R-T} \xrightarrow{k_q} \text{Sensitizer} + \text{R}^\bullet + \text{T}^\bullet$

Scheme 7-4. Photosensitized decomposition of unimolecular initiators.

The scope of this chapter will investigate new nitroxide based initiators potentially useful for photocontrolled living free radical polymerization. This will include the synthesis of these new class of compounds in addition to the characterization by their photophysical and photochemical properties. The main focus of this study is concerned with triplet based photoinitiators and the following sections have been further subdivided and dedicated to the different types of photoinitiators examined.

7.2 Benzophenone Based Initiators

The original Scaiano study showed sensitizers **2-4** all gave the desired C-O bond fragmentation determined spectroscopically by laser flash photolysis. However, the benzophenone based sensitizer (**1**) whose triplet energy is approximately 5 to 12 kcal/mol lower than sensitizers **2** and **3**, did not gave any conclusive evidence for C-O bond fragmentation. This was mainly due to the overlapping absorption of the triplet with the benzylic radical in the region of 315 nm. We elected to use the benzophenone moiety as an initial point for our photocontrolled LFRP investigation. The primary reason for this choice was the potential ease of synthesizing the incorporated nitroxide photoinitiator **6** shown in Figure 7-2 leading to an alkoxyamine. Better candidates may contain a xanthone or azaxanthone moiety, but the synthesis of these nitroxide containing compounds are far more laborious than **6**.

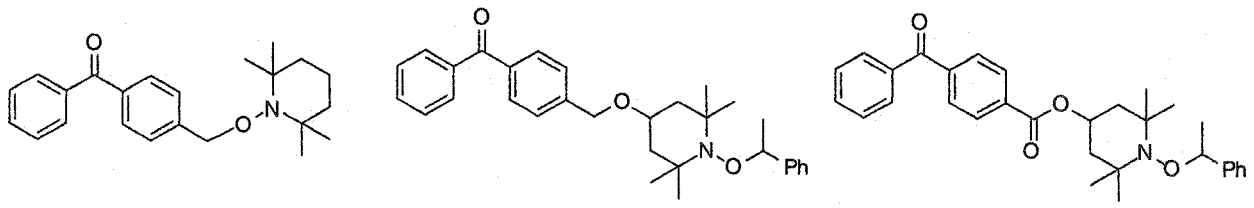

6 **7** **8**

Figure 7-2. Benzophenone based photoinitiators for LFRP examined.

7.2.1 Energy Transfer Efficiency

Even though the photoinitiator **6** can be synthesized in two relatively easily steps, an initial investigation concerning the efficiency of intramolecular energy transfer from the chromophore to the bond to be cleaved was done. The three methyl substituted positional isomers of benzophenone, shown in Figure 7-3, were examined for their efficiency of energy transfer. This was done by selectively exciting the benzophenone chromophore and measuring the amount of bromine produced by homolytic cleavage arising from energy transfer from the benzophenone chromophore to the C-Br bond. The brominated compounds were studied because the 2-, 3-, and 4-methylated isomers are commercially available and the bromination can be readily achieved in one step.

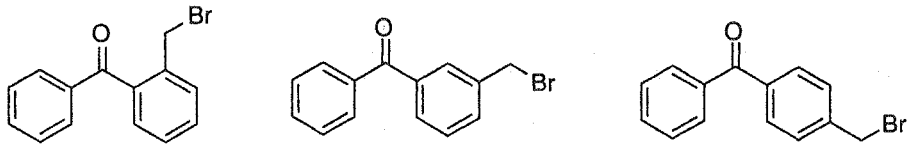

9 10 11

Figure 7-3. Positional isomers used for preliminary study of bromine release efficiency.

The amount of hydrogen bromide (HBr) produced following hydrogen abstraction by the bromine atom can be easily and accurately quantified through the use of an acid sensitive dye. The concept is relatively simple and uses a dye whose absorption spectrum changes upon protonation. This is important as overlapping spectra convolute the analysis. The protonated form must have a large extinction coefficient (ε) allowing for the detection of minute amounts of acid. The candidate selected for this study was coumarin 6 (**13**) as it exhibits a large bathochromic shift of 50 nm upon protonation complimented with an increase in its extinction coefficient (ε = 100 000 M^{-1} cm^{-1} at 519 nm). The long wavelength absorption of the neutral form stems from the charge transfer (CT) transition between the electron rich phenyl moiety and the electron deficient benzothiozole moiety.[25-27] Protonation of the heterocyclic nitrogen increases its electron deficient character and enhances the energy of the CT state. This subsequently causes a red shift in the absorption spectrum and an increase in the extinction coefficient. In the presence of more acid, protonation occurs at the exocyclic nitrogen resulting in a blue shift in the spectrum along with a decrease in intensity. This manifestation occurs as a result in the destruction of the donor ability of the benzyl group and no CT can occur. The ground state absorption spectra of coumarin 6 in the neutral and protonated forms are shown in Figure 7-4.

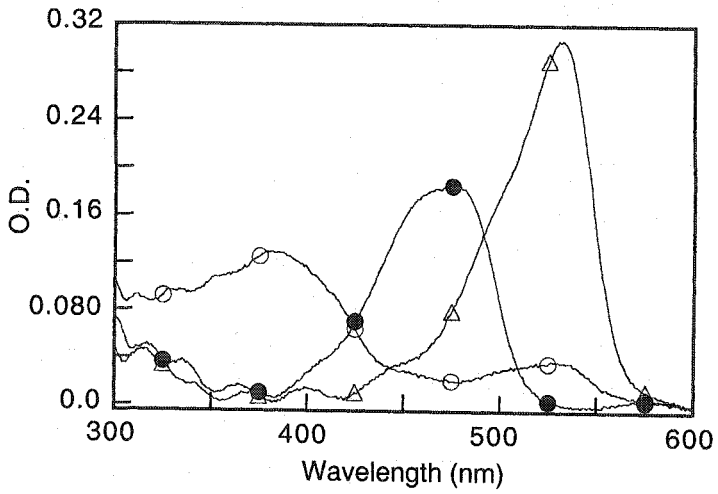

Figure 7-4. Ground state absorption spectra of coumarin 6 (13, ●), mono-cation (14, Δ), and di-cation (O).

The dye approach was originally developed to easily quantify the amount of acid generated by photoacid generators (PAGs) in thin films which are typically used in microlithography resist technology.[28] The PAG Triazine-1 (**12**) generates a chlorine radical upon photoexcitation. It will readily abstract a hydrogen in the presence of a hydrogen source, such as diglyme or dioxane, leading to acid formation. The acid will subsequently protonate the coumarin dye and the absorption at 519 nm, corresponding to the mono-cation (**14**), can be monitored and correlated to the amount of acid produced. The mechanism of acid generation and dye protonation is represented in Scheme 7-5.

Laser flash photolysis (LFP) can be used to determine the amount of acid produced by monitoring the growth of the mono-cation at 519 nm. Under flow conditions, the di-cation (**15**) cannot be produced since the mono-cation is continuously being depleted and the amount of acid generated is typically in the μM concentration.[29,30] LFP studies are conducive to this work since it produces small amounts of transients, hence small amounts of acid. Also, it allows for the time resolved measurements of the mono-cation upon acid protonation. These convey a greater degree of sensitivity, and in turn, a greater degree of accuracy for acid quantification compared to steady state methods and acid titration.

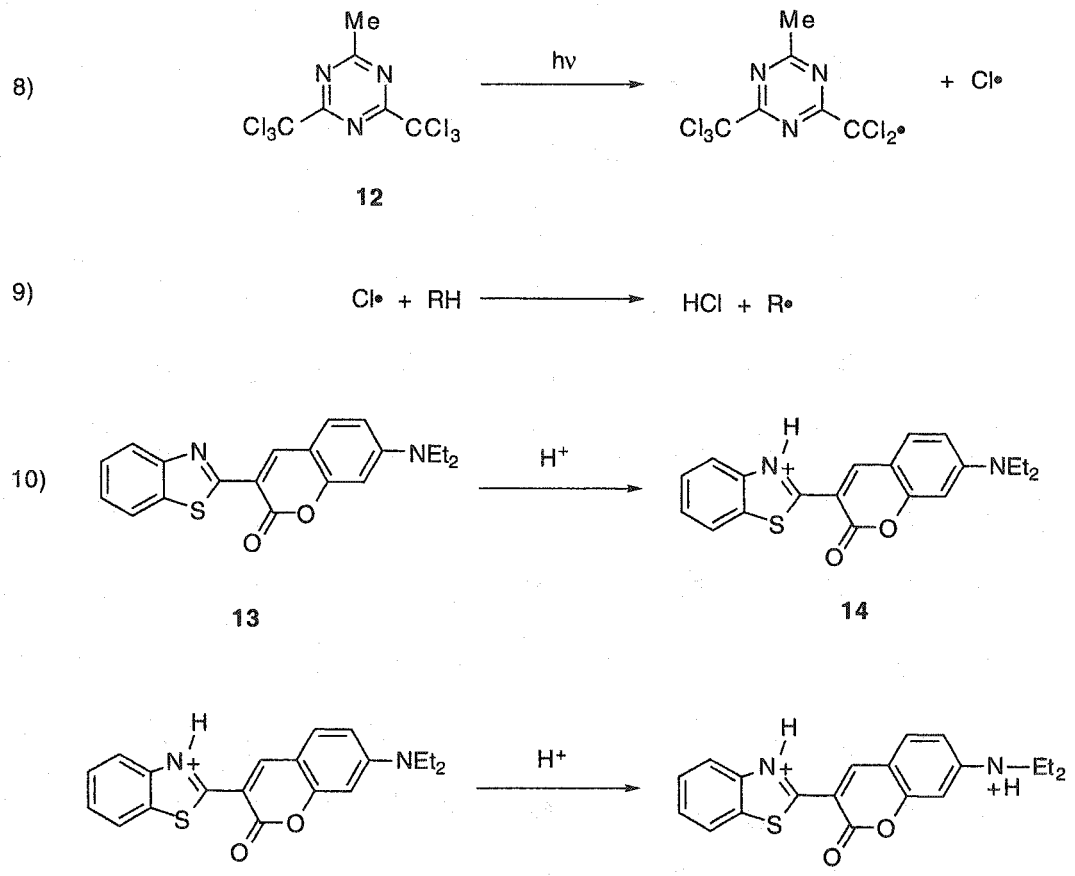

Scheme 7-5. Protonation of coumarin 6 dye by the PAG triazine-1.

The amount of bromine generated upon photolysis of the brominated benzophenone initiators (**9-10**) is done by relative transient actinometry. This involves photolysing the initiators under identical conditions as those of an actinometer that produces a known amount of acid. The amount of **14** produced by a given PAG is proportional to its absorption at 519 nm and the absolute value of acid produced is obtained by comparing the maximum absorption at 519 nm to that of the actinometer. Normally the absorbance of the species monitored is taken over a series of laser powers to minimize the error in the measurements. The efficiency of the brominated benzophenone PAGs photoproduction, hence their quantum yield (Φ) of bromine production, can be calculated by Equation 7-1 relative to the actinometer, triazine-1. The S values in this equation refer to the slope derived from the mono-cation absorbance as a function of laser power. The equation is simplified compared to other transient actinometry measurements because the same mono-cation is monitored for all the PAGs examined. The benefit to this approach is the extinction coefficient is not

accounted for in the equation since the same transient is being observed. This increases the accuracy of the calculated values as there are large discrepancies in the ε values reported in the literature.[31]

$$\Phi_{Br\bullet}^{initiator} = \Phi_{HCl}^{triazine} \cdot \left(S^{initiator} / S^{triazine} \right)$$

Equation 7-1. Equation for calculating quantum yield of acid generation by transient actinometry.

Identical conditions including matched absorbancies at the excitation wavelength of 308 nm were used to measure the amount of bromine formed upon photolysis of the benzophenone PAGs. The absorbance of the mono-cation at 519 nm over a series of laser powers leads to the slope required for the Equation 7-1. The slopes derived are shown in Figure 7-5 where they vary as a function of the brominated isomer. PAG **9** was not examined because it formed the mono-cation immediately once it was added to the stock solution implying spontaneous acid production. This PAG could only be synthesized in low amounts (~ 13 %) and during the bromination reaction it turned orange implying the production of Br_2. Even after repeated purification, **9** immediately produced acid upon dissolving it in the coumarin solution. It is thermally unstable and probably undergoes intramolecular addition forming a five membered ring with the displacement of the bromine similarly to the anomeric effect in sugars.[32,33] Therefore, acid quantification could not be done with this PAG as a result of its thermal instability.

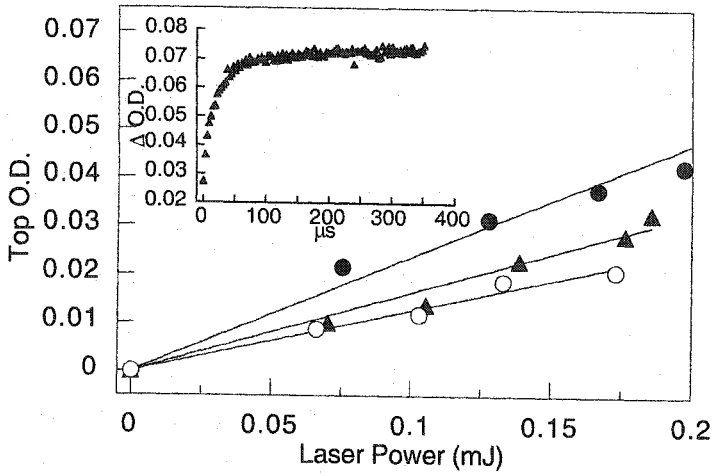

Figure 7-5. Power dependence plots of mono-cation (14) formation with different PAGs, 12 (●), 10 (▲), and 11 (○). Inset: Growth of coumarin 6 mono-cation (14) monitored at 519 nm.

The quantum yields of bromine formation for the benzophenone PAGs are tabulated in Table 7-1 according to Equation 7-1. There is an isomeric dependence on the bromine production being lower when progressing from the 4- to the 3- position. It is assumed that **9** would produce the same amount of bromine as **11** as the amount of resonance species available to this PAG are identical to those shown in Figure 7-6 for the radical derived from **11**, ultimately leading to the formation of a less reactive tertiary radical.

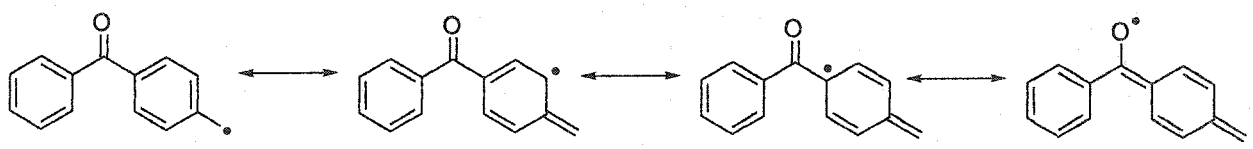

Figure 7-6. Radical resonance stabilization for the radical derived from 11.

The quantum yields of acid formation reported in Table 7-1 are different than expected. Compound **11** was anticipated to generate more bromine since the radical produced upon homolytic cleavage has more canonicals forms available as shown in Figure 7-6. Since there are fewer canonical forms available for **10** than **11** this is anticipated to give a lower quantum yield.

Table 7-1. Quantum yield of photoinduced halogen release.

PAG	Φ^a
12	0.45[b]
11	0.24
10	0.31
9[c]	-

a) Refers to amount of halogen produced upon photodecomposition of the initiator.
b) Value of Φ=0.45 taken from literature.
c) Cannot be determined due to its thermal instability.

Direct laser flash photolysis of **10** and **11** lead to the transient absorption spectra shown in Figure 7-7. These spectra do not show any maxima at 300 or 525 nm ascribed to the benzophenone triplet signifying the triplet is quenched entirely by energy transfer leading to fragmentation of the C-Br bond. Homolytic cleavage of this bond gives a benzylic radical that exhibits typical absorption maxima at 310 and 318 nm[34] that are equally not present in the spectrum. The additional PhCO group in the *para* position may cause a slight change in the absorption of the benzylic radical. However, the addition of nucleophiles such as tetrabutylammonium bromide do not quench the transient proving this transient cannot be the methyl cation originating from photoheterolytic cleavage of the C-Br bond. The signal is also not quenched by methanol when used as the solvent. PAGs that produce ionic transients upon photolysis are known to be quenched by protic solvents and nucleophiles,[35] further suggesting the transient produced here is not ionic in nature.

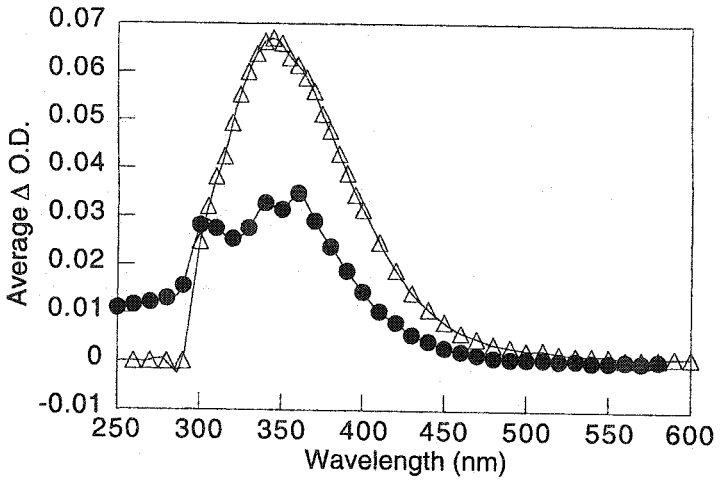

Figure 7-7. Transient absorption spectra from 10 (Δ) and 11 (●) recorded 20 μs after excitation at 308 nm.

The observed transient at 350 nm decays with second order kinetics on the order to 2×10^6 M^{-1} s^{-1} typical of radical decay, but is longer lived than other similar radical systems.[16] This is coupled with mixed kinetics at this wavelength implying the absorption of two species in this region. The addition of the radical trap TEMPO quenches the fast portion of the signal with a rate constant of 7×10^7 M^{-1} s^{-1}. This value is approximately 2 times slower than for similar benzylic radicals, but lies in the acceptable range for radical quenching.[16,36-38] The slower quencher rate is probably due to the slow rate determining release of bromine upon excitation as the signal at 350 nm is not formed within the laser pulse, rather it takes 0.2 μs to completely grow in. The addition of oxygen to the solution quenches the radical portion of the signal, but produces an unknown transient with the same maximum that lives longer than the time resolution of the LFP system.

Substitution on the aromatic ring by electron donating or withdrawing groups causes spectral shifts in the absorption spectrum.[39] The ketone electron withdrawing group stabilizes the benzylic radical and provokes a shift in the absorption spectrum to longer wavelengths, which is observed. However, the mixed kinetics, the presence of the transient after oxygen saturation, and the slow growth imply the long lived transient is from a bromine complexation. This has previously been reported[40-47] and the extinction coefficient of this complex[41,42] is greater than the benzylic radical[48,49] justify the strong signal.

The combination of all these kinetic properties lead to the conclusion that the correct carbon centered radical is produced and ascribed to the transient seen by LFP studies. Selective excitation of the benzophenone group leads to moderately efficient energy transfer to the C-Br group subsequently causing its homolytic cleavage. The absence of any triplet absorption in the transient spectrum denotes the energy transfer process is fast and less than 10 ns, which is the fastest time resolution of the LFP system and the pulse width of the excitation source.[50,51]

7.2.2 TEMPO Incorporated Photoinitiators

The nitroxide containing compound **6** was synthesized as a potential initiator capable of photochemically controlling the polymerization leading to LFRP. In the previous section it was shown that photoexcitation of the benzophenone moiety leads to the desired bond cleavage upon fast energy transfer. The synthesis of the title compound (**6**) is not as straightforward as with the unimolecular initiators previously examined in a preceding chapter. Hydrogen abstraction of methyl-benzophenone by *tert*-butoxyl, similar to the method of Connolly et al., gives **6** in less than 8 % yield. The predominant product is the TEMPO trapped methyl radical arising from the known β-elimination of *tert*-butoxyl.[23,52,53] Alternatively, the organo-zinc approach of Curran was attempted, which equally gave poor yields because the unreacted nitroxide could not be easily separated from the product, even after repeated purification.[54,55] Coupling of the free nitroxide with the brominated methylbenzophenone with lead (IV) oxide,[56-58] manganese (III) oxide,[59,60] or copper adducts[61] are known to give nitroxide coupled products in moderate yields. However, purification proved difficult and subsequently the yields were low. These thermal routes were investigated because direct photochemical displacement of the bromine radical followed by radical trapping with TEMPO equally gave poor yields. Photolysis of **11** in the presence of TEMPO gave a black solution with the formation of many products that were visible by TLC. It was found that a minimum of two equivalents of nitroxide were required for the reaction to progress as the bromine generated upon photolysis underwent electron transfer with the nitroxide giving the nitroxonium salt because nitroxides are known to be easily oxidized and form salt complexes.[62-70] The addition of potassium thiosulfate assisted in absorbing the Br• formed and slightly improves the yields. The wavelength used to induce the photochemical cleavage of the C-Br bond also promotes fragmentation of the C-O bond of the target molecule. The progress of

the reaction must be closely monitored to prevent photochemical decomposition of the desired product once formed.

Laser flash photolysis of **6** at 308 or 355 nm leads to the transient absorption spectrum shown in Figure 7-8. The maximum absorption observed at ca. 315 nm corresponds to the benzylic radical that decays with second order kinetics[34] The absence of any absorption at 525 nm from the benzophenone triplet confirms energy transfer from the selectively excited benzophenone chromophore to the C-O bond is fast and causes this bond to cleave, similar to compounds **11** and **12**. The spectrum is not convoluted as those derived from the photolysis of **11** and **12** denoting cleaner photochemistry, where the benzylic type radical decays either by recombination with itself or with the nitroxide. Unlike the brominated analogues, the transient derived from **6** is completely quenched in the presence of oxygen and radical quenchers further confirming its radical nature.

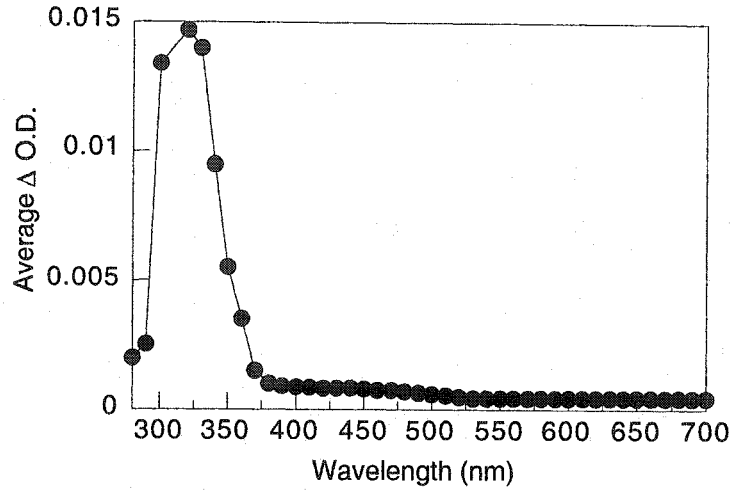

Figure 7-8. Transient absorption spectrum of 6 recorded 48 ns after the laser pulse at 308 nm.

The second order decay kinetics can be described by Scheme 7-6. Upon direct photolysis of the benzophenone moiety, the chromophore is excited to its singlet state. It subsequently undergoes rapid and efficient intersystem crossing to its triplet state from which its energy is transferred to the C-O bond. The bond consequently ruptures from the energy transfer step similar to the C-Br bond previously discussed. These three steps occur within 10 ns because the radical observed by LFP appears as an instantaneously produced signal and not as a growth. The other radical produced upon homolytic C-O bond cleavage is the

nitroxide radical, which is transparent to the laser system. The kinetics of the benzylic type radical can be measured by monitoring the change in its absorbance at 318 nm as a function of time.

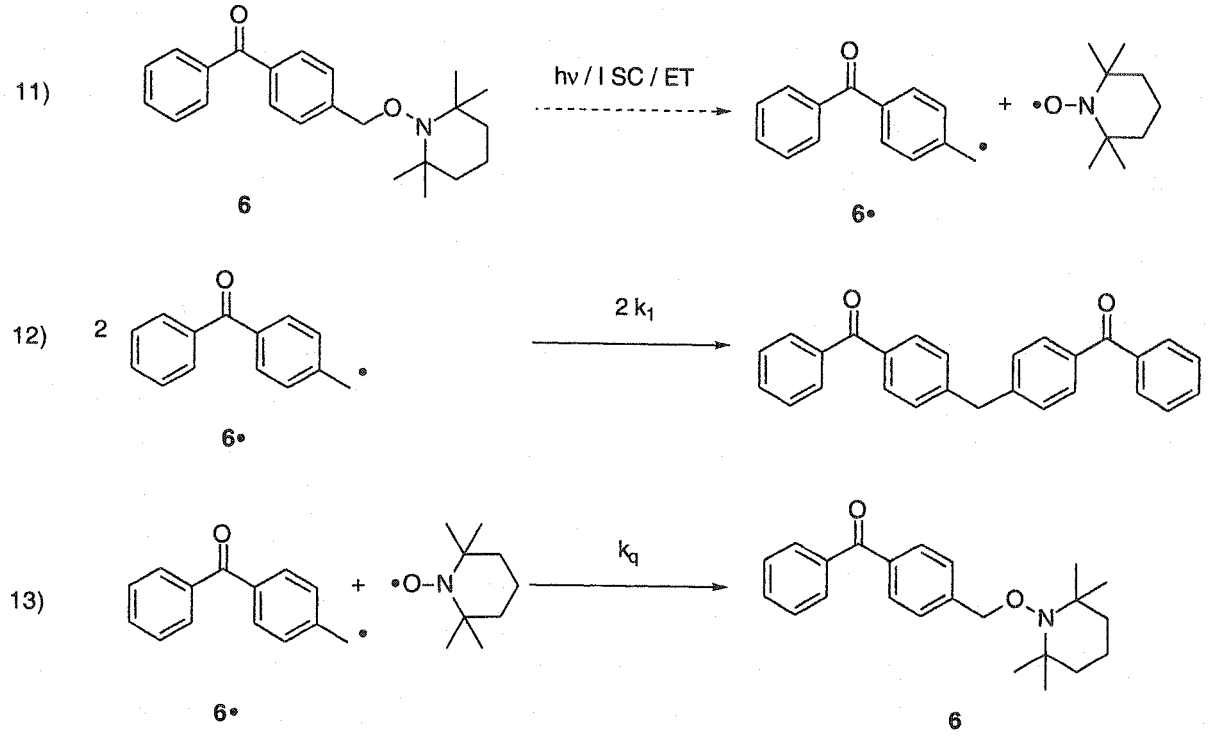

Scheme 7-6. Photochemical decomposition of 6 and the trapping of its generated radicals.

In the absence of any quencher, the observed radical decays by second order kinetics by radical recombination (Equation 12) or by nitroxide trapping (Equation 13). The rate constant for trapping the benzylic radical by TEMPO (k_q) can be obtained by addition of TEMPO. Because the concentration of the radical generated within the pulse of the laser is typically μM, the addition of nitroxide in the order of mM changes the decay kinetics from second order to pseudo-first order. Monitoring the decay of the benzylic radical as a function of the nitroxide concentration leads to the standard Stern-Volmer plot shown in Figure 7-9. The slope of the plot leads to the desired k_q being 2.6×10^8 $M^{-1}s^{-1}$ for the initiator 6. This value is identical to the TEMPO quenching value measured for the benzylic radical derived from the photodecomposition of dibenzylketone.[71] The similarity between the two values implies the ketone moiety does not influence the radical center and will thereby be expected to have similar polymerization properties as its thermal unimolecular analogue.

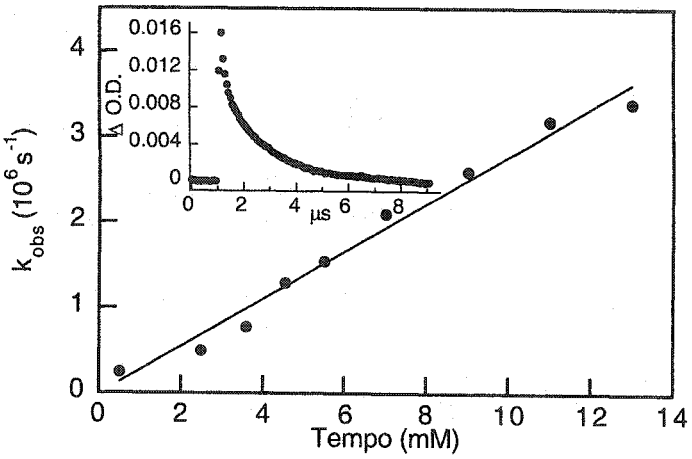

Figure 7-9. Quenching of benzyl radical derived from 6 in the presence of various amounts of TEMPO. Inset: Decay of the benzylic radical monitored at 320 nm after excitation at 308 nm.

Direct photolysis of **6** in the presence of another radical trap such as 4-hydroxy-TEMPO leads to the cross-trapped products as seen in a preceding chapter dealing with the initiator decomposition. Comparing the amount of trapped product formed relative to the Norrish type II decomposition of valerophenone gives the quantum yield of radical formation according to Equation 7-2. Valerophenone is the actinometer which photodecomposes to give a known amount of acetophenone with a known amount of light.[72,73] This general mechanism and steady state actinometry was discussed in a preceding chapter.

$$\Phi_6 = \left(\frac{[Trapped\ Product]}{[Acetophenone]} \right) \cdot \Phi_{actinometer}$$

Equation 7-2. Photodecomposition quantum yield determination for photoinitiator 6.

Steady state irradiation at 254 nm gives a quantum yield of 0.45, which is significantly higher than the amount of acid produced by its brominated analogue. However, the quantum yield of radical formation for the irradiation of **6** at longer wavelengths of 300 nm is 0.87. The lower observed quantum yield for the studies at 254 nm can be explained according to Figure 7-10. The energy of this wavelength is ca. 115 kcal/mol which is sufficient to excite the molecule to the dissociation curve that promotes N-O bond cleavage. A competitive cleavage between N-O and C-O cleavage occurs at this wavelength and is

confirmed by HPLC product studies. This same behavior of dual bond fragmentation at short wavelengths was seen with the PAC studies in the chapter dealing with the initiator decomposition. There must also be a similar dissociation curve for N-O bond cleavage with a gap between the two curves being approximately 18 kcal/mol because no N-O dissociation products are observed with irradiation at longer wavelengths. This is a lower limit value that corresponds to the energy difference between the two irradiation wavelengths.

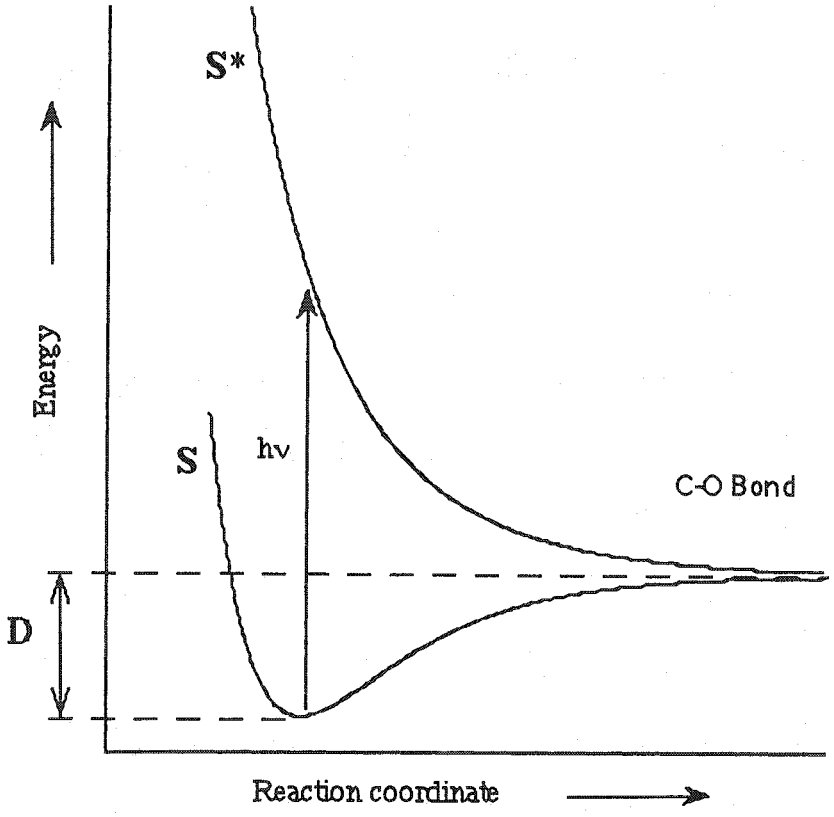

Figure 7-10. Homolytic dissociation curve available for photodecomposition of 6 at 254 nm.

Energy transfer from the excited triplet to cleave the C-O bond is extremely efficient as expressed by the high quantum yield measured at 300 nm for 6. The 13 % energy wastage most likely comes from nonradiative processes such as molecular motion since spectroscopically there is not triplet production or formation of any other products upon photolysis.

The capability of **6** to promote photocontrolled LFRP was investigated using styrene and methyl methacrylate as monomers. The initial bulk photopolymerization at 300 nm yielded no polymerization with irradiation times less than 10 hours. Thermal polymerization was subsequently done to verify whether this initiator was able to undergo LFRP. The polymer isolated showed relatively good LFRP properties with PD = 1.37, 76 % conversion, and the DP = 213, being equal to the equivalents of styrene added. More importantly, the nitroxide group is still pendent at the terminal position, as confirmed by ^{1}H-NMR, making it a true LFRP polymer. Irradiation of **6** for long periods of time at 300 nm leads to polymerization whose properties are listed in Table 7-2. The low conversions, low molecular weights, and high polydispersities obtained are indicative of conventional free radical polymerization with no nitroxide mediation. ^{1}H-NMR shows no triplet at 3.75 ppm characteristic of a TEMPO capped polymer, hence no LFRP polymers. The observed polymers are photochemically formed, as a thermal blank (kept at room temperature in the dark) and a sample protected from the light both did not undergo polymerization.

Table 7-2. Photopolymerization of styrene with 6 at 300 nm.

Irradiation (Hours)	M_w	M_n	PD	DP	Conversion (%)
17.5	28 570	11 510	2.48	107	0.43
46.8	35 660	13 900	2.57	130	0.59
61	24 770	11 160	2.43	104	0.69

The low conversion observed for the photopolymerization of styrene can be explained in terms of its propagation rate constant (k_p). The photopolymerization of styrene was done at room temperature, at which the k_p is approximately 1000 slower than at the typical thermal polymerization temperature of 125 °C.[74] Also, the quenching of the benzophenone triplet by styrene is an exothermic process and as a result exhibits fast values of k_q in the order of 5×10^9 M^{-1} s^{-1}.[5,16,75,76] The value is close to the diffusion controlled limit and appears to compete with energy transfer in spite of the short triplet lifetime.

The end result is predominant ketone quenching by the monomer and little C-O bond cleavage. The moderate molecular weight of the polymers isolated originate from sensitized autopolymerization, which is known to occur thermally,[77-80] and has been observed photochemically as well.[81-84]

The triplet of methyl methacrylate (MMA) is approximately 24 kcal/mol higher in energy than that of benzophenone.[85] This renders the quenching process endothermic and has the effect of a much slower quenching rate constant. The reported values of k_q for benzophenone triplet quenching by MMA are considerably slower than for styrene and are about 7×10^7 M^{-1} s^{-1}.[5,75,76,81] The value of k_p for MMA polymerization is also considerably higher at room temperature and is in the range of 1×10^6 M^{-1} s^{-1}.[76] These properties are better for photopolymerization studies involving triplet **6** since it will not be as readily quenched, thus allowing for C-O bond cleavage to occur. Unfortunately, the polymerization results obtained are similar to those realized with styrene as the monomer and are summarized in Table 7-3. Once again the ^{1}H-NMR shows the lack of any nitroxide-capped polymer.

Table 7-3. Photopolymerization of 374 equivalents of MMA relative to 6 at 300 nm for 4 days.

Sample[a]	M_w	M_n	PD	DP	Conversion (%)
Filtrate	3 701	4 303	1.56	41	25
Solid	20 908	13 017	1.60	127	52

a) The resulting oil mixture after polymerization was precipitated from methanol and the two phases analyzed by GPC.

The lack of any detectable nitroxide capped polymer and the properties shown in Table 7-3 signify that a conventional free radical process is taking place and that the nitroxide group has little influence. Given the kinetic data for MMA, the lack of photocontrol found with this monomer is enigmatic as there should be a considerable degree of nitroxide controlled polymerization. A plausible argument for the lack of control could be due to the relative orientation of the chromophore and the nitroxide found with **6**. The chromophore-nitroxide distance increases with each monomer addition and a critical distance could reduce the efficiency of the energy transfer required for decapping. A series of

oligomers with a different lengths separating the chromophore and the nitroxide were synthesized to verify this hypothesis. A change in the triplet lifetime as a function of oligomer length was expected along with a threshold oligomer length incapable of energy transfer being determined. A decamer oligomer was arbitrarily selected as a starting point and its transient absorption spectrum derived after excitation at 355 nm is shown in Figure 7-11 along the transient absorption spectrum of the 4-methyl benzophenone.

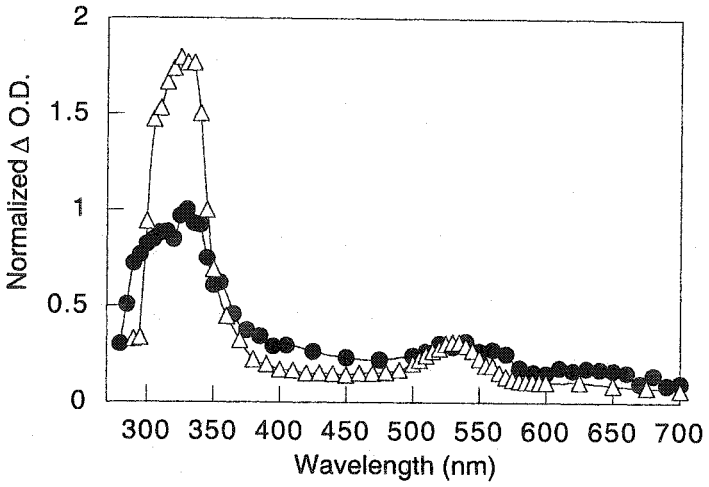

Figure 7-11. Normalized transient absorption spectrum of 4-methyl benzophenone triplet (Δ) and decamer of 6 (●) recorded 0.88 μs after excitation at 308 nm in acetonitrile.

The transient absorption spectrum for the decamer is different from the one derived from **6** with the appearance of absorptions at 530 nm and 550 nm. These correspond to the triplet and the ketyl radical, respectively, assigned by their kinetic decays and quenching properties towards different quenchers.[86] The insertion of the two monomer units between the benzophenone chromophore and the nitroxide of **6** reduces the efficiency of energy transfer to the C-O bond. The appearance of the triplet implies there is no energy being transferred to the C-O bond. In fact, the triplet preferentially undergoes hydrogen abstraction to give the ketyl radical then subsequently decays with second order kinetics without any C-O bond cleavage. Preliminary results involving a series of oligomers ranging in length from one to seven repeating units were synthesized and the influence of the chromophore-nitroxide energy transfer as a function of separation was monitored by the triplet lifetime. The preliminary study was

done by Alan Martin, a summer student under the direction of the thesis author. The rate of triplet decay as a function of degree of polymerization (DP) is graphically depicted in Figure 7-12.

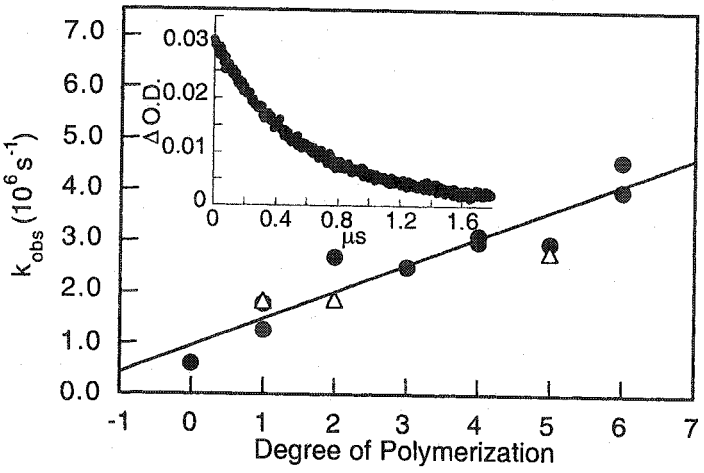

Figure 7-12. Influence of the degree of polymerization upon triplet lifetime in CCl_4 (Δ) and Acetonitrile (●). Inset: Decay of transient DP=4 recorded at 530 nm in acetonitrile.

The decay kinetics at 530 nm were monitored and the fast component fitted with first order kinetics to generate the data for Figure 7-12. The rate constant for triplet decay for DP=0 was taken from the nitroxide-free 4-methyl benzophenone used as a reference since no triplet is seen with **6**. The insertion of one styrene unit in **6** automatically decreases the lifetime of the triplet represented as a faster decay as k_{obs} is the reciprocal of the lifetime for first order processes. The insertion of one monomer completely biases the system from a radical shift in quenching mechanism from energy transfer to hydrogen abstraction, resulting in ketyl radical formation. Therefore, no C-O bond cleavage (Equation 14, Scheme 7-7) occurs and Equation 16 dominates and justifies the observed lack of molecular weight control for the photopolymerization reactions. The intramolecular hydrogen abstraction reaction has previously been reported by Winnik et al. who examined quenching kinetics and hydrogen abstraction rate for different aliphatic chain lengths substituted on benzophenone.[10,12,87-92] Their results paralleled our observations of increased rate constant of decay with an increase in chain length.

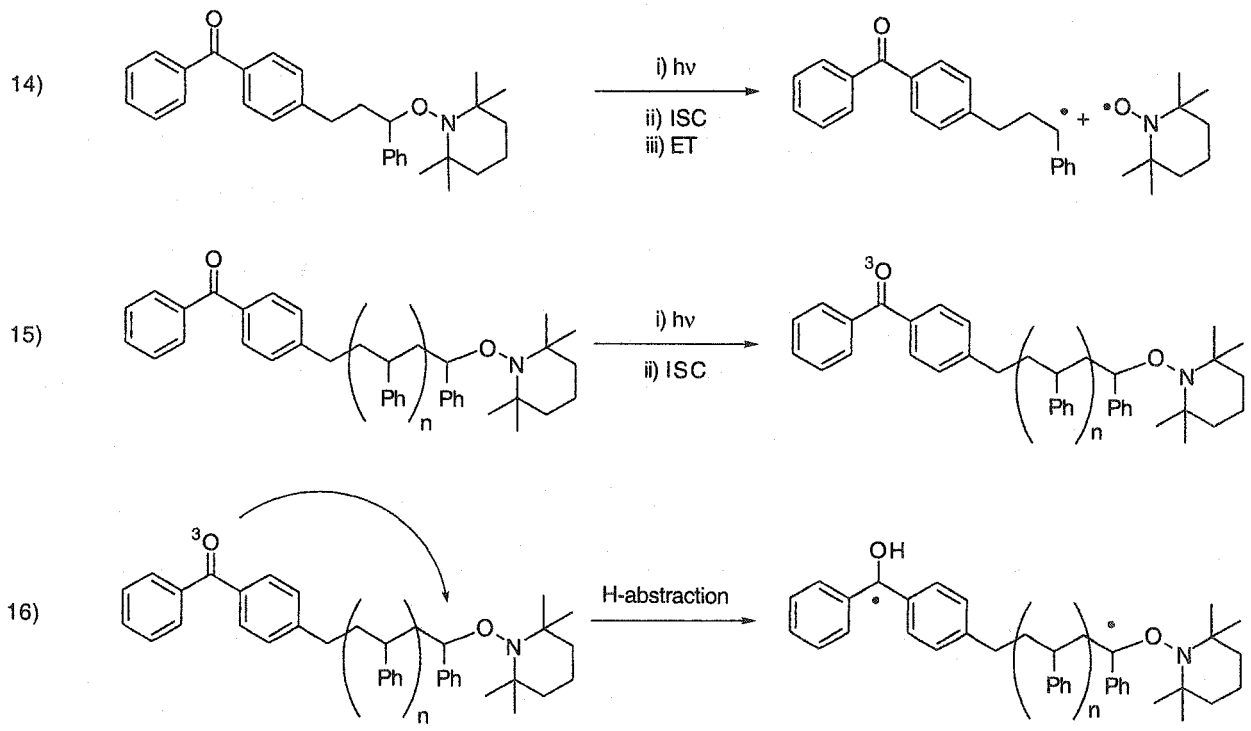

Scheme 7-7. Formation of observed ketyl radical from oligomers of 6.

The synthesis of initiator **7** was attempted in the hope of eliminating the unwanted intramolecular hydrogen abstraction reaction responsible for promoting conventional free radical polymerization. The advantage of this initiator over **6** is the distance between the chromophore and the alkoxyamine bond to be cleaved is fixed and does not vary with polymerization. If efficient energy transfer is observed for **7** then the desired C-O bond would be preferentially cleaved regardless of the polymer chain length thanks to the fixed chromophore-nitroxide distance. However, the synthesis of this initiator proved challenging and sufficient material for photochemical studies and polymerization could not be obtained. Coupling between **11** and 1-phenyl-1-(2,2,6,6,-tetramethyl-4-hydroxy-piperdine-N-oxide) ethane with sodium hydride resulted in less than 2 % product formation regardless of the dry solvent selected to support the anion generated. Different synthetic strategies were undertaken, but the most successful required ketone protection of **11** in the form of an acetal, followed by coupling between the halide and alcohol, then subsequent deprotection. This synthetic route did not increase the overall yield for the synthesis of **7** and was eventually abandoned.

Winnik's previous work concerning the quenching of benzophenone triplets with different lengths of tethered chains showed that an ester group used as a linker did not influence the photochemistry.[10,12,87-92] We took advantage of these findings to synthesize **8** by coupling *p*-benzoylbenzoic acid (**17**, Figure 7-13) 4-hydroxy-TEMPO used in the attempted synthesis of **7**. The condensation reaction works moderately well and sufficient material was produced for subsequent photochemical studies.

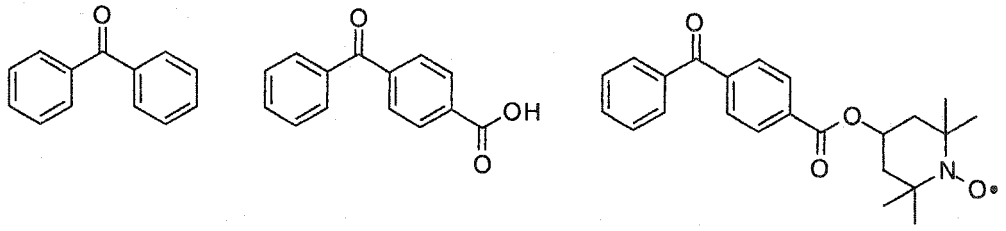

16 **17** **18**

Figure 7-13. Benzophenone and its analogues used in the photochemical characterization of 8.

Direct laser flash photolysis of **8** leads to the transient absorption spectrum shown in Figure 7-14 and shows two maxima at 350 nm and 550 nm. The ketyl radical generated by hydrogen abstraction from 1,4 cyclohexadiene and the triplet derived from **17** are shown in this figure for comparison. The transient at 550 nm for **8** is ascribed to the triplet and is shifted about 25 nm from that of **16** because of the ester moiety that stabilizes the system through electron withdrawing effects. Its maximum at 350 nm is also due to the triplet whose extinction coefficients are known to be about 8 times greater than those for benzylic radicals and subsequently dominates the spectrum.[48-50,93] The triplet at 350 nm overlaps with the absorption of the expected benzylic radical around 320 nm making it difficult to determine if sufficient energy transfer is occurring to cleave the C-O bond is cleaved. The distance separating the chromophore and the C-O bond to be cleaved for initiator **8** is equivalent to three styrene repeating units between the chromophore and C-O bond for initiator **6**. For this separation, **6** undergoes hydrogen abstraction leading to the ketyl radical while **8** does not, as determined by the lack of characteristic absorption at 575 nm corresponding to the ketyl radical.[34] This leads to the assumption that energy from the excited ketone preferentially undergoes energy transfer to the C-O bond instead of hydrogen abstraction for **8**. Irradiation of this initiator under steady state conditions at 300 nm and 350 nm in the presence of TEMPO leads to **18** and

the cross-trapped unimolecular initiator confirmed by LC-MS. At sufficiently long irradiation times, where the TEMPO trap is depleted, **18** undergoes hydrogen abstraction from the solvent acetonitrile forming the hydroxylamine and the methyl cyanide trapped products. Direct excitation of nitroxides are known to under hydrogen abstraction leading to the products observed by LC-MS for **18**.[94-100] Interestingly, the formation of these products confirm energy transfer from the chromophore to the nitroxide moiety occurs as the wavelength used for this study does not directly excite the nitroxide, rather, the energy is selectively localized in the benzophenone moiety.

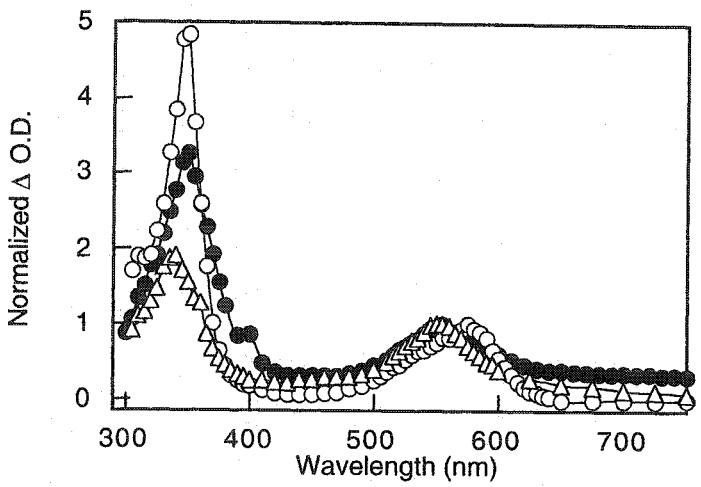

Figure 7-14. Normalized transient absorption spectra of triplet 17 (Δ), ketyl radical of 17 (O), and 8 (●) recorded 1.28 μs after 355 nm excitation.

The phosphorescence spectrum of **8** shown in Figure 7-15, is red shifted by about 10 nm compared to benzophenone (**16**), but is identical to **17**. This is the same phenomenon observed in the transient absorption spectra of the two compounds and can be attributed to stabilization from the ester group. The red shift of 10 nm corresponds to a decrease of 2.5 kcal/mol for the triplet of **8**. The original Scaiano investigation of sensitizer induced C-O bond decomposition concluded a minimum triplet energy of 63 kcal/mol is required for bond fragmentation to occur.[24] However, the decrease in observed triplet energies of **17** and **8** would suggest that the latter cannot undergo the desired C-O bond fragmentation. The photodecomposition of **8** to give **18** was re-investigated and the amount quantified to verify if efficient energy transfer to induce C-O bond cleavage. The quantum yield of radical generation determined by steady state

irradiation through monitoring the growth in concentration of the trapped product is quite high. The value measured (Table 7-4) of 0.83 is only marginally lower than the value measured previously for **6** that was proven to give the desired C-O bond fragmentation. The slight decrease in the quantum yield can be attributed to an increase in the number of degrees of freedom available to the chromophore to dissipate energy by nonradiative processes instead of energy transfer, albeit minimal. This is a common phenomenon in energy transfer systems were energy wastage occurs in non-rigid systems.[101-112] From this, it can be concluded that the chromophore's triplet energy is not crucial for energy transfer leading to the homolytic fragmentation of the C-O bond providing the nitroxide and the chromophore are directly tethered.

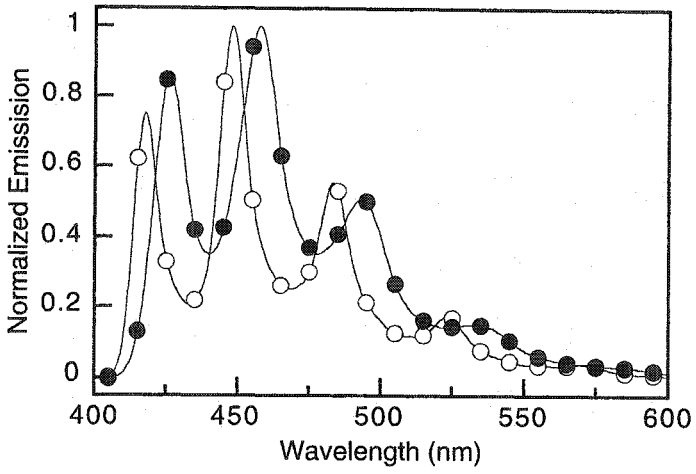

Figure 7-15. Phosphorescence spectra of 16 (O), 17 (●) recorded at 77 K in methylcyclohexane. The phosphorescence spectra 8 and 17 are identical.

Table 7-4. Measured quantum yields for various substituted benzophenones.

Initiator	$\Phi_{radical}$	$\Phi_{triplet}$
6	0.87	-
7	-	-
8	0.83	1.0
17	-	1.0

Steady state phosphorescence measurements do not lead to easy relative determination of the quantum yield of triplet formation unlike other measurements. The triplet quantum yield values for **8** and **17** have not previously been reported and were subsequently determined to complete their photophysical characterization. Since steady state measurements only give qualitative information, relative actinometry using laser flash photolysis was employed to quantify the amount of triplet formation. This method involves quenching the benzophenone-based triplet formed upon laser excitation with the good quencher, 1-methylnaphthalene.[16] The quenching process occurs by energy transfer and subsequently forms the methylnaphthalene triplet that absorbs at 420 nm.[50,51,113] The quenching process is close to the diffusion controlled deactivation limit, where the quenching rate constants measured by laser flash photolysis for **8**, **16**, and **17** are all greater than 9×10^9 M^{-1} s^{-1} as this is an exothermic process. This rate constant allows for easy calculation of known quencher concentration to be added to the samples in order to quench a minimum of 95 % of the triplets formed from the benzophenone compounds. Consequently, the amount of triplet methylnaphthalene produced for each compound can be correlated to the maximum absorbance recorded at 420 nm and linearly correlated over a series of laser powers. The plot derived by this method shown in Figure 7-16 allows for easy determination of the quantum yield of triplet generation through comparison of the slopes to a known actinometer. In this case, we have chosen **16** as the actinometer whose triplet quantum yield is known to be unity.[16,31,113] The triplet quantum yields for **8** and **17** are equally found to be unity through the use of the generic form of Equation 7-1. This is of importance for **8** as it demonstrates the capped nitroxide group (alkoxyamine)

does not directly quench the singlet state of benzophenone allowing for 100 % intersystem crossing to the triplet state.

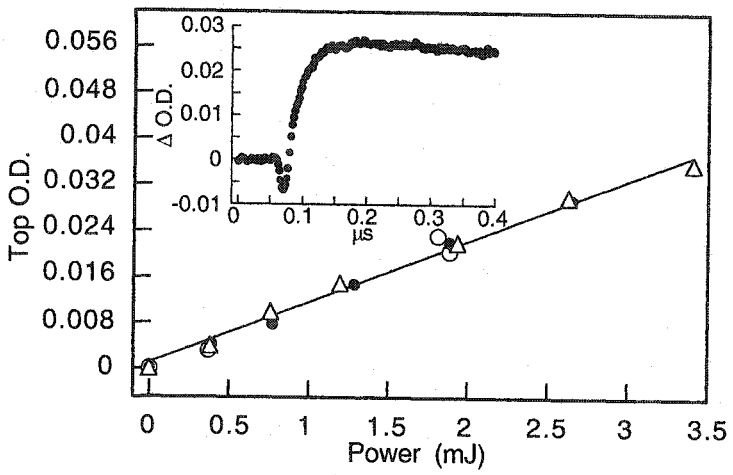

Figure 7-16. Quantum yield of triplet formation of 8 (O), 17 (●), and 16 (Δ). Inset: growth of 1-methylnaphthalene triplet at 420 nm after 355 nm excitation and sensitization.

Photopolymerization of **8** in bulk MMA at 350 nm leads to the formation of polymers in a relatively short period of time. This is a result of the polymerization temperature being increased to ca. 58 °C, the typical polymerization temperature for acrylates. Rapid polymerization leading to high molecular weight polymers occurs at this temperature summarized by the data shown in Table 7-5. Unlike the previous photopolymerization attempts with **6**, the polymers obtained are consistent with LFRP type polymers being high molecular weights, low polydispersities, and acceptable conversions obtained in relatively low polymerization times. Attempted polymerization of MMA in the absence of initiator and with **16** under identical conditions as **8** do not yield any polymers. Therefore, the results obtained stem from the photocontrolled polymerization capabilities of **8**. The properties of the polymer isolated suggest that the desired photocontrolled polymerization is occurring. This is supported by the ^{1}H and ^{13}C NMR data that show the polymer is capped with the desired nitroxide group. The chemical shifts and splitting patterns are consistent with the nitroxide adjacent to a propionate group, rather than the benzyl moiety from the starting initiator, further supporting that photoliving polymerization is

achieved. Further evidence supporting this claim originates from the linear polymer conversion shown in Figure 7-17.

Table 7-5. Photopolymerization of MMA with 8 at 300 nm.

Time (Hours)	M_w	M_n	PD	Conversion (%)
2	397 000	341 500	1.16	5.5
3	405 300	349 300	1.16	17.4
4	323 200	270 900	1.19	29.9
5	377 900	326 00	1.16	-
6	364 800	317 200	1.15	42.7

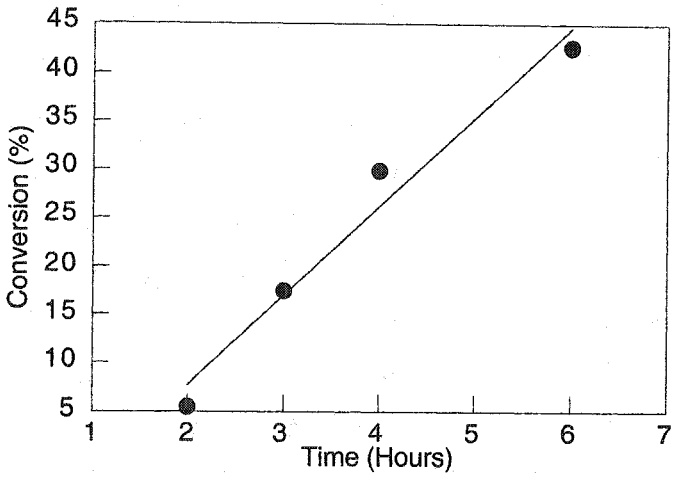

Figure 7-17. Conversion of MMA photopolymerized with 8 at 350 nm and at 58 °C.

7.2.3 Benzophenone Initiator Summary

It was shown that incorporation of the capped nitroxide group (alkoxyamine) to the benzophenone chromophore underwent efficient energy transfer from the chromophore to the nitroxide moiety. This process was found to be extremely

fast and subsequently leads to the desired homolytic cleavage of the C-O bond responsible for controlling the polymerization reaction leading to living polymers. The orientation of the nitroxide group in relation to the chromophore is crucial for obtaining controlled photopolymerization of acrylates. Separation of the chromophore and the nitroxide moiety by repeating monomer units decreases the capacity for energy transfer and promotes the slower process of intramolecular hydrogen abstraction. This reaction can be completely suppressed by the use of triplets that form a π,π^* state where the hydrogen abstraction reaction is forbidden. Rendering the chromophore-nitroxide separation consistent results in homolytic C-O bond fragmentation and consequently photocontrolled LFRP of MMA.

7.3 Benzoin Type Initiator

Substituted benzoins of the general structure of **19** (Figure 7-8) are used as photoinitiators for the polymerization of many vinyl monomers or for their subsequent curing capabilities by photoinduced cross-linking.[114] Upon direct photolysis, they decompose by Norrish-type I cleavage, or α-cleavage giving an acyl and benzylic type radicals as products, according to the mechanism in Scheme 7-8. The pendant R group greatly influences the rate of decomposition.[7,115,116] According to previous studies involving benzoin based structures, no α-cleavage is observed when R=H (**19**), while the rate of deposition is greater than 10^{10} s^{-1} for R=OCH_3 and 5 x 10^7 s^{-1} for R=$OC(O)CH_3$.[7,115]

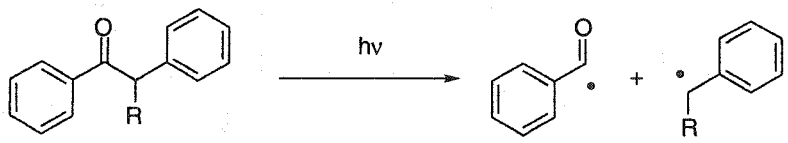

19

Scheme 7-8. Photoinduced α-cleavage of benzoin.

From the knowledge gained from the energy transfer studies of **6-8** compounded with thermal studies, the initiator **20** was synthesized as a potential hybrid LFRP initiator for thermal and photochemical initiation. Upon thermal and photochemical decomposition it is anticipated to give the benzylic type radical responsible for initiation and the nitroxide radical capable of controlling the polymerization, which in turn, would eventually lead to nitroxide mediated LFRP. This section will deal with the thermal and photochemical studies of this hybrid polymer initiator.

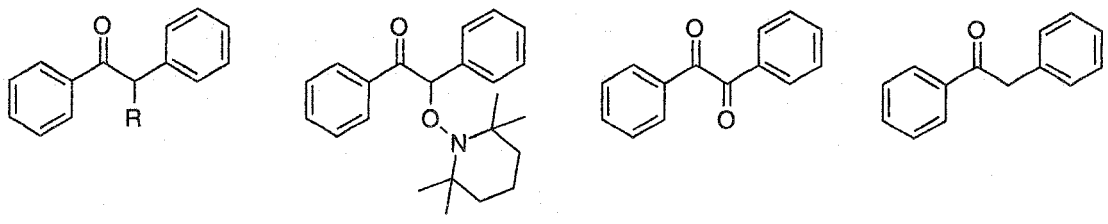

19 **20** **21** **22**

Figure 7-18. Benzoin based photoinitiators.

7.3.1 Photochemical Pathway

Given the photo controlled polymerization results obtained for the benzophenone initiators, the suitability of **20** as a photoinitiator was examined. Irradiation of a solution of this initiator in deaerated acetonitrile at 300 nm leads to a complex mixture of products that were isolated by column chromatography. These were subsequently identified by NMR and compared to authentic samples. All of the identified products are shown in Scheme 7-9 originating from two primary homolytic cleavages. Similar to the substituted benzoins used as photoinitiators, the nitroxide substituted benzoin **20** also undergoes α-cleavage upon irradiation represented by pathway b.

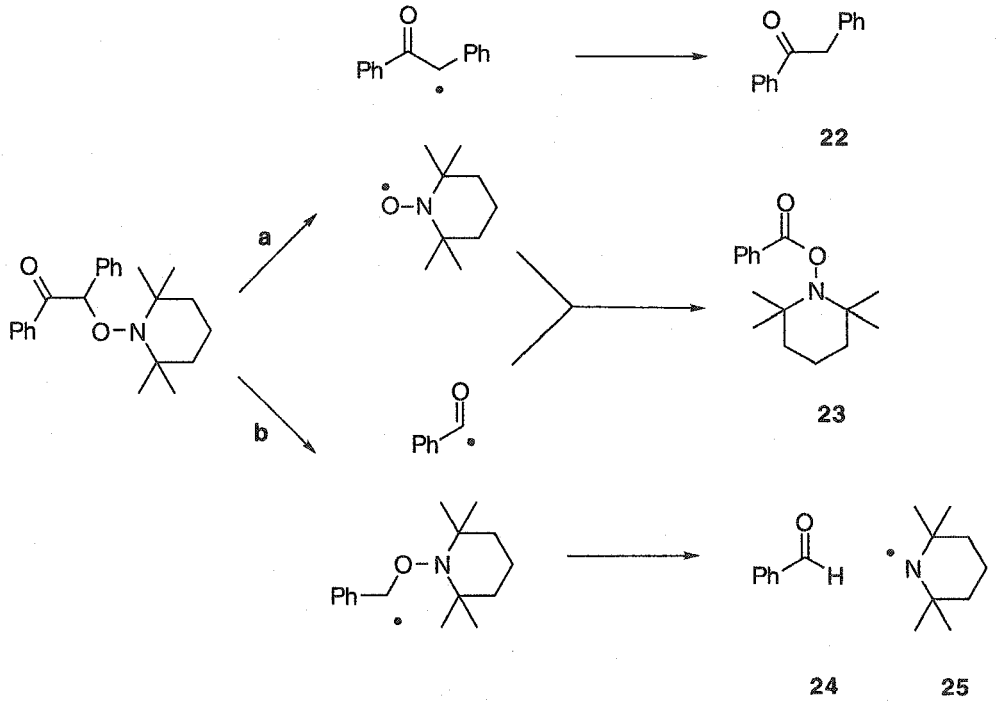

Scheme 7-9. Product distribution arising from the photodecomposition of 20.

The formation of deoxybenzoin (**22**) isolated as a product indicates carbon-oxygen bond cleavage (pathway a) does occur, leading to the deoxybenzoin radical, which can abstract hydrogen from the solvent.[95] The former bond cleavage process was confirmed in a nitroxide exchange experiment in which **20** was irradiated in the presence of 4-hydroxy-TEMPO leading to an exchange of the TEMPO moieties. Products **24** and **25** arise from the known Norrish Type I cleavage (pathway b) typical of substituted benzoin photoinitiators.[7,13,115] Trapping of the acyl radical by TEMPO generated from pathway a leads to compound **23**. A crossover

experiment with 4-hydroxy-TEMPO leads to trapping of the acyl radical, which is known to be formed from nitroxide trapping of the photochemically generated acyl radical.[117-119] Fragmentation of the other part of the radical pair from the Type I reaction leads to benzaldehyde and, presumably, the nitrogen centered radical that can further undergo hydrogen abstraction and is difficult to identify. This pathway is reminiscent of the reaction manifold observed in the reaction of diphenylcarbene and TEMPO.[120] Interestingly, this Norrish Type I cleavage was also observed in the solid state, as noted by the benzaldeyde peak in the NMR spectrum and, more qualitatively, by the smell of benzaldehyde present following irradiation. Unfortunately, the conversions in the solid state were quite low and do not allow for a complete study of the photodecomposition of 3. This low conversion may be due to quenching of the excited state by the generated TEMPO or nitrogen centered piperidine radicals as both are known to quench ketone and aromatic triplets.[16,95,121]

7.3.2 Thermal Pathway

The homolytic scission of carbon-oxygen bonds of O-alkyl alkoxyamines such as those encountered during the LFRP process is not an exclusive reaction. In fact, Barton and Hunter have reported[122] that the thermolysis of compounds containing a nitroxide α to the carbonyl group provides 1,2-dicarbonyl products, as shown in Scheme 7-10, presumably via an ionic mechanism.

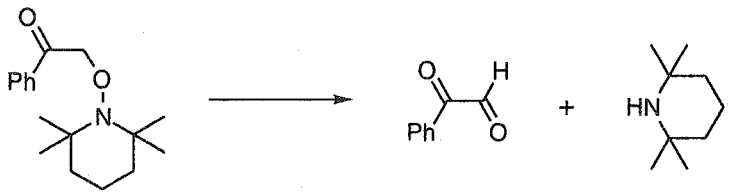

Scheme 7-10. Thermal decomposition products determined by Barton.[122]

The benzoin framework of **20** contains an adjacent carbonyl-nitroxide moiety similar to Barton and Hunter's study. In addition, **20** also contains a benzylic-TEMPO arrangement analogous to the thermal unimolecular initiators previously studied. In connection with the unimolecular initiator thermal studies from a previous chapter[123] and the Barton chemistry, the thermal chemistry of **20** was examined. The benzoin framework of **20** contains the merger of the Barton strategy and the conventional LFRP initiator all in one with both decomposition pathways (ionic and radical) potentially available.

According to the reactions shown in Schemes 7-10 and 7-11, two distinct reaction mechanisms are available to **20**; i.e., radical and ionic. Deoxybenzoin (**22**) arises from homolytic cleavage giving a carbon centered radical followed by hydrogen abstraction. An ionic pathway results in the rupture of the nitrogen-oxygen bond, and ultimately to the formation of benzil (**21**). Preliminary thermal decomposition studies of **20** were done in a sealed tube in the absence of oxygen or any other reagent. Qualitative product studies showed the formation to be predominately **22** and **21** with minor radical cross coupling. The significant formation of these products shows a competition between radical and ionic pathways. The same experiment was repeated in the presence of camphorsulfonic acid (CSA) and a different ratio of decomposition products was obtained being predominately **21** and only trace amounts of **22**. The substantial change in product distribution is indicative of a major change in reaction path. Therefore, experimental conditions were modified to influence the decomposition route and verify our hypothesis.

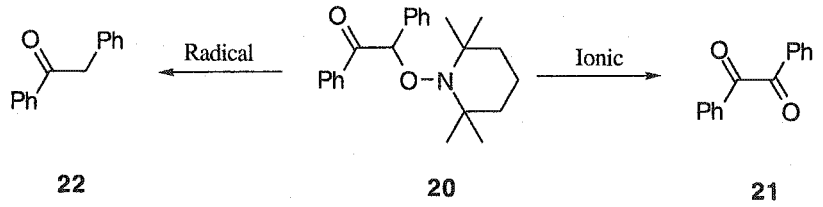

22 **20** **21**

Scheme 7-11. Thermal decomposition pathways of 20.

Refluxing **20** under an inert atmosphere leads to simple homolytic C-O cleavage to give the persistent nitroxide, TEMPO, and carbon centered radicals. The lifetimes of these radicals are sufficiently long and further undergo hydrogen abstraction as seen in Scheme 7-12. The hydrogen abstraction reaction from a good hydrogen donor such as 1,4 cyclohexadiene[124] leads to deoxybenzoin (**22**) as a major product. In sufficiently high concentrations of 1,4 cyclohexadiene, the hydrogen abstraction reaction will be kinetically favored over the back reaction with the nitroxide since both of these are bimolecular reactions;[36,37] in any event, the latter has no chemical consequences as far as products are concerned, and is due to the Fischer-Ingold persistent free radical effect.[125,126] The formation of **22** was observed in a ratio of 2.9:1 over **21** after thermal decomposition of **20** in the presence of 1,4 cyclohexadiene. This follows the conventional radical decomposition pathway shown in Scheme 7-12.

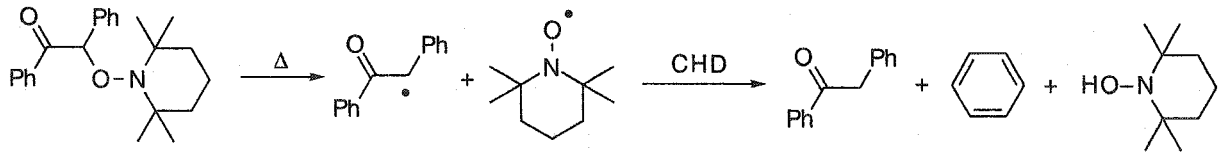

20 22

Scheme 7-12. Radical pathway for thermal induced decomposition of 20 in the presence of cyclohexadiene.

Substituting the organic acid, *p*TsOH, for 1,4 cyclohexadiene followed by the same thermal parameters gave an inverted product ratio of 1:3.5 for **22**:**21**. This indicates suppression of the radical route in favor of the ionic pathway according to Scheme 7-13. Note that even in the absence of 1,4 cyclohexadiene the radical route may involve extensive radical cross-termination to form the starting material. The protonation of the nitroxide nitrogen of **20** is the governing step and subsequently biases the system towards ionic decomposition. Hoffman-type elimination of the amine moiety results in the generation of benzil. The presence of deoxybenzoin suggests that a minor radical mode arising from neutral **20** is still present. This occurs as only a catalytic amount of *p*TsOH was used. Repeating the thermolysis in the presence of one equivalent of *p*TsOH resulted in only a small amount of deoxybenzoin being detected, hence a complete switch to ionic chemistry.

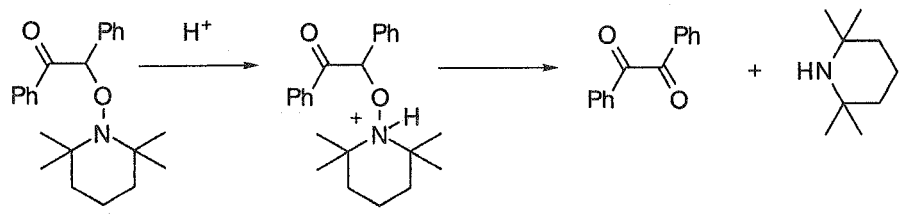

20 21

Scheme 7-13. Ionic pathway for the thermal decomposition of 20.

7.3.3 Benzoin Initiator Summary

Thermolysis of an O-alkylated nitroxide with moieties that favor both radical and ionic cleavage leads to products resulting from both pathways. Although the radical pathway is favored under standard conditions, addition of a proton

source results in a switch to the ionic pathway. Photolysis results in products that appear to be formed via two competitive radical pathways. The products resulting from Norrish Type I cleavage fragment further reacts and leads to benzaldehyde and a piperidine radical similar to the reaction of carbenes with a nitroxide.

7.4 Benzoylbenzoate Based Initiators

Several thermal nitroxide based molecular initiators have been synthesized that are capable of producing polymers with living properties. Among these is the benzoyloxystyrene based initiator (27) popularized by Hawker and extensively used to successfully achieve polymers with desired living properties.[127-134] Thermally this initiator works well for controlling the polymerization, but previous investigation by laser flash photolysis (see Thermal Decomposition chapter) gave results suggesting the presence of photochemical pathways reminiscent of those of the benzoins and other photoinitiators. The combination of these results with the knowledge gained from the investigation of the above photoinitiators prompted the interest to examine the photophysics and photochemistry for this benzoyloxystyrene based initiator. The capability of this initiator to promote photoliving polymerization was investigated in terms of its photophysical properties. This study is the first reported full spectroscopic and kinetic LFP analysis of initiators **26-30**.

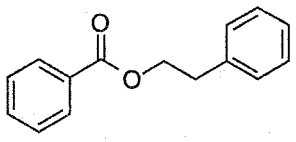

26

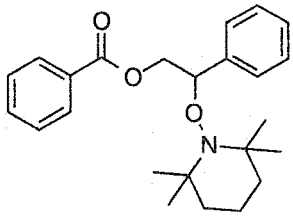

27

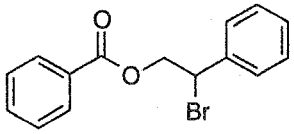

28

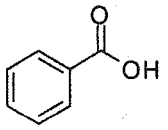

29

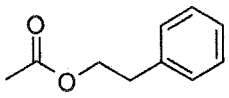

30

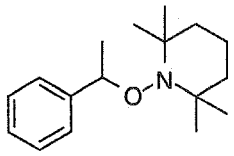

31

Figure 7-19. Benzoyl based structures examined.

It was mentioned in an earlier chapter that the direct photolysis of **27** led to the apparent formation of two or more transients that absorbed at 320 nm in the region of the expected benzylic-type radical. This is evident from the decay monitored at 320 nm (see inset of Figure 7-20), which exhibits a mixture of first

and second order with ca. 50 % contribution from each. There is also the formation of an unknown transient at 260 nm which is quenched by TEMPO (~ 2 x 10^9 M^{-1} s^{-1}) with the same kinetics as the fast decay portion at 320 nm. This indicates the fast decaying transient at 320 nm is the direct precursor for the transient that grows at 260 nm, which possesses a large extinction coefficient. The spectrum from direct photolysis of **27** is difficult to deconvolute and assign all the transients produced. The only conclusion that can be made based upon the preliminary quenching studies is the combination of the benzoyloxy moiety coupled with the nitroxide function leads to complicated photoinduced chemistry. The molecule **26** was used as an analogue to reduce the number of transients produced thereby simplifying the transient spectrum. This would assist in deriving a plausible photochemical reaction mechanism for the decomposition of **27**. The investigation of **27** as a potential photoliving initiator reported here is divided into three major categories: a) transient identification (300 nm), b) quantum yield of observed photochemical processes, and c) transient identification (260 nm).

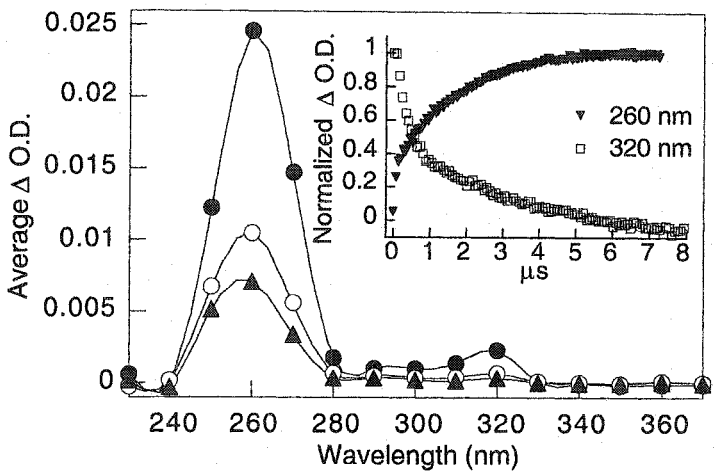

Figure 7-20. Transient absorption spectrum of 27 in acetonitrile recorded 2.08 (●), 9.04 (○), and 11.9 (▲) μs after the initial laser pulse at 266 nm. Inset: Transients recorded after 266 nm excitation pulse normalized for different O.D. Growth of transient (▼) monitored 260 nm, time scale is multiplied by 4. Decay of transient (□) recorded at 320 nm.

7.4.1.1 Transient Assignment (300 nm)

Direct photolysis of **26** leads to the spectrum shown in Figure 7-21 exhibiting a maximum at 300 nm with only one transient. Unlike the transient spectrum for **27**, that of **26** is much cleaner and only one transient is produced, which follows clean first order kinetics. This result combined with signal quenching under oxygen are characteristic of triplet behavior. The same transient and absorption spectra were obtained with **29** and **30** further suggesting the transient at 300 nm is the triplet since its production in moderate efficiency from aromatic esters such as **26** has been reported.[135-138] Upon excitation, the triplet n,π* state is formed and readily undergoes the Norrish type II intramolecular hydrogen abstraction reaction. This gives a 1,4 biradical intermediate (see Scheme 7-14) that either regenerates the starting material or fragments with low efficiency to give benzoic acid and styrene.[135,139-142] The Norrish type II reaction leading to an organic acid and olefin typically does not surpass 10 % efficiency, regardless of the substituent.[139]

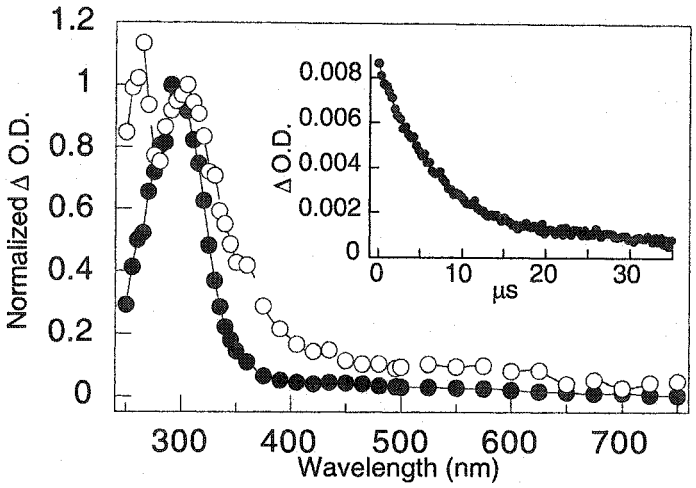

Figure 7-21. Normalized transient absorption spectrum of 26 (○) at 23 ns and 30 (●) at 920 ns after excitation at 266 nm in acetonitrile. Inset: Decay of transient derived from 30 monitored at 316 nm.

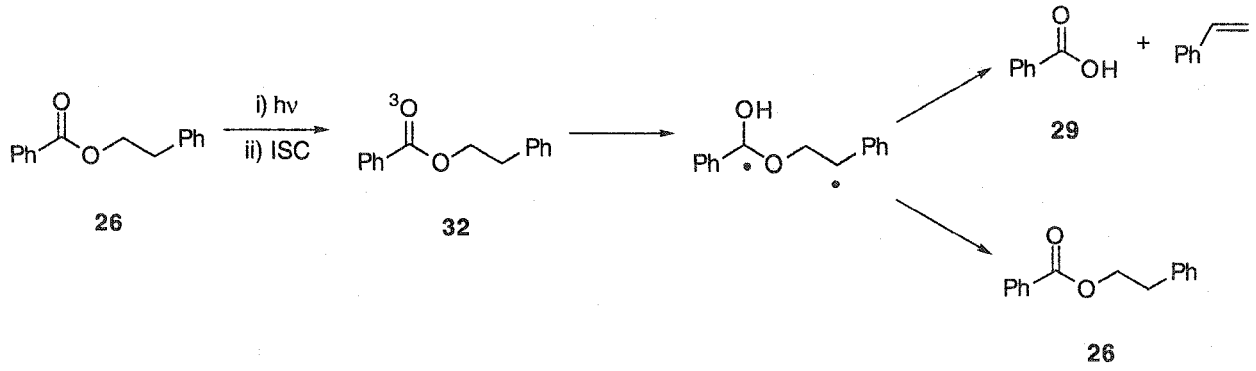

Scheme 7-14. Photodecomposition pathway of 26.

Quenching of the transient derived from **26** was done by monitoring its decay in the presence of known amounts of a quencher. A typical decay of the transient produced upon photolysis of **26** is shown in the inset of Figure 7-22. Each data point within the plot represents the kinetics of the transient decay in the presence of different amounts of quencher under pseudo-first order conditions. For the preliminary quenching study, TEMPO was used and the rate constant is derived from the slope of the plot found in Figure 7-22. The measured quenching with TEMPO is 3×10^9 M^{-1} s^{-1} and is considerably faster than carbon centered radical quenching typically 10^7-10^8 M^{-1} s^{-1}.[36-38,143] Repeating the same experiment with 4-methylbenzophenone, which quantitatively produces its triplet with each excitation, gave a rate constant of triplet quenching of 4.2×10^9 M^{-1} s^{-1} with TEMPO.[13,93,144] This fast quenching rate constant is typical of exothermic energy transfer processes and characteristic of triplet quenching by nitroxides in general.[16,95,121] Other commonly used triplet quenchers were investigated and the measured values are reported in Table 7-6, consistent with triplet quenching. Quenching was also observed with silane and 1,4 cyclohexadiene, both of which are good hydrogen donors. Therefore, the triplet **26** is very similar to the triplet of benzophenone, where both undergo the permitted hydrogen abstraction from the n,π^* state leading to a ketyl type radical.

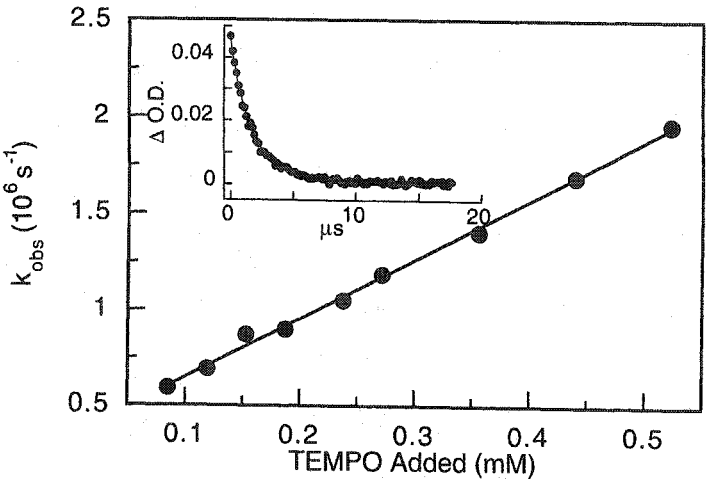

Figure 7-22. Quenching of triplet derived from 26 after excitation at 266 nm in acetonitrile. Inset: Decay of triplet monitored at 318 nm in the presence of 0.085 mM TEMPO.

Table 7-6. Triplet Quenching Rate Constants of 26 with Various Quenchers.

Quencher	k_q (M^{-1} s^{-1})[a]
TEMPO	3.1×10^9
1,3 Cyclohexadiene	1.4×10^9
1,4 Cyclohexadiene	2.6×10^6
Sorbic Acid	8.9×10^9
Bu_3SiH	5.6×10^7

a) Transient decay monitored at 320 nm.

Triplet **26** (**32**) absorbs at 305 nm with a large extinction coefficient.[50,51] Unlike **27**, **26** does not give any transients other than the triplet, as represented by the simple transient absorption spectrum with clean kinetics. The growth shown in Figure 7-20 is not from intramolecular hydrogen abstraction leading to the ketyl-type radical, because the rate constant for this process is too slow to be seen on the time scale of the LFP set-up. Furthermore, the efficiency of this reaction is considerably poor and the observed signal would be dominated by the triplet

absorption since its extinction coefficient is greater than the anticipated ketyl-type and benzylic radicals.[50,51]

Initiator **27** couples two moieties, that is, **29** and the thermal LFRP initiator **31**. Both of these compounds undergo their respective photochemistry upon irradiation at 266 nm, i.e., the formation of TEMPO and a benzylic type radical in the case of **31**, while **29** produces its corresponding triplet. The convoluted spectrum of **27** upon photolysis is not from the concurrent formation from the excited states of the two discrete moieties, **26** and **31**. Photolysis studies of **27** in the presence of a triplet quencher should suppress the triplet formation thereby simplifying the absorption spectrum to that of the carbon centered radical. However, irradiation of **27** with various triplet quenchers gave no LFP signal. This implies the homolytic C-O bond scission is from direct energy transfer from the carbonyl moiety, similar to the photoinitiators previously presented. To confirm this, the ground state extinction coefficients at 266 nm of a few initiators were examined. The extinction coefficient of **31** is approximately eleven times less than that of **26** (see Table 7-7). While typical absorbances used for LFP studies are in the range of 0.3 - 0.4, an absorbance of 0.04 for **31** at 266 nm still produces a signal at 320 nm detectable by the LFP system. This confirms that the observed C-O bond cleavage exclusively comes from energy transfer from the triplet moiety to the nitroxide portion of the initiator. From the previous studies of energy transfer presented and these observations, **26** and **27** appear to have a high efficiency of intersystem crossing and energy transfer. The high degree of energy transfer is supported by the high triplet energy of **26**, which is slightly greater than benzophenone, or about 77 kcal/mol (*vide infra*).[137,145]

Table 7-7. Ground state extinction coefficients at 266 nm measured in acetonitrile.

Compound	ε (M^{-1} cm^{-1})
26	1 882
31	168

7.4.1.2 Quantum Yield and Transient Extinction Coefficient Determination

The efficiency of nitroxide release by energy transfer for **27** was determined by relative transient actinometry. Previously, actinometers producing the same transient as the studied compounds where used eliminating the knowledge of their extinction coefficients. Initiator **27** is more complicated because it produces two transients simultaneously (triplet and carbon centered radical) with overlapping absorptions. Deconvolution of the two transients' kinetics and their extinction coefficients are required in order to calculate their respective concentrations from the observed absorption. Either the triplet quantum yield or the transient extinction coefficient must be known to extrapolate information from the transient measurements. Currently there are no substantial data in the literature for the two desired properties for **26**. The extinction coefficient for **29** is not known with great certainty,[50,51] however the triplet quantum yield 0.7 is reported.[137] Equation 7-3 is a modification of Equation 7-1 and accounts for the different extinction coefficients of the transients. It can be used to determine the triplet extinction coefficient for **29** and subsequently the triplet quantum yield for **26**. Benzophenone was selected as the actinometer because its triplet quantum yield in acetonitrile is well known to be unity with an extinction coefficient in the same order of magnitude as that expected for **32**.[113,146-148] Many values for benzophenone's triplet extinction coefficient have been reported and range from 6000 - 12 000 M^{-1} cm^{-1}.[50,51] The value of 7 800 M^{-1} cm^{-1} was selected as it was measured under similar experimental conditions to those examined here.[31]

$$\varepsilon_{32}^{320nm} = \left(\Phi_{16}/\Phi_{32}\right)\cdot\left(\mathrm{Slope}_{32}/\mathrm{Slope}_{16}\right)\cdot\varepsilon_{16}^{525nm}$$

Equation 7-3. Equation for determining triplet extinction coefficient by relative transient actinometry.

Figure 7-23 shows the required slopes for Equation 7-3 for the triplet extinction coefficient calculation of **29**. The calculated value was 4 655 M^{-1} cm^{-1} (See Table 7-8) and is the same order of magnitude predicted by Acuña et al.[137] Assuming the triplet extinction for **29** and **32** to be identical,[39,149,150] the triplet quantum yield for the latter can be calculated from this equation. The calculated value is identical to that for **29**, within experimental error, confirming the substitution of the acid function for an ester does not influence the yield of intersystem crossing.

In general, literature findings on the physical properties of these two were not found to be dissimilar.[135-139,151,152]

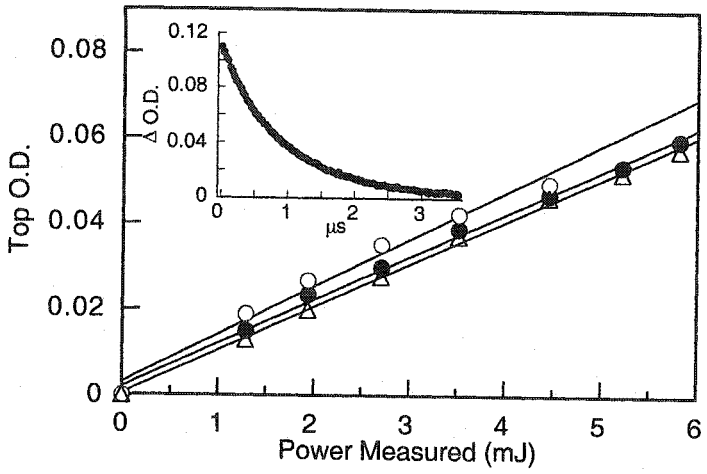

Figure 7-23. Plot used for triplet extinction coefficient determination of 26 (Δ) and 29 (●) both monitored at 320 nm with benzophenone (O) as actinometer monitored at 525 nm. Inset: Decay of triplet derived from 29 monitored at 320 nm in acetonitrile.

Table 7-8. Quantum yield of triplet or carbon centered radical formation of structures from Figure 7-19.

Compound	Φ	ε (M^{-1} cm^{-1})
27[a]	0.53[b]	-
26	0.68[b]	4655
29	0.70[c]	4655
33	0.56[d]	1366
16	1.00[e]	7800

a) Radical formation determined by extrapolating the second order residual.
b) Triplet formation determined against benzophenone.
c) Literature value for triplet formation.[136]
d) Literature value for radical formation.[153,154]
e) Literature value for triplet formation and its extinction coefficient.[31]

The triplet produced from **27** undergoes energy transfer to the nitroxide portion of the molecule and homolytic C-O bond cleavage ensues generating the carbon center radical visible around 320 nm. However, the efficiency of this process is unknown. Only the extinction coefficient of the expected triplet is known, but that of the carbon centered radical and the amount in which it is produced are both unknown. These values are desired for determining whether **27** is a suitable photoliving initiator. An accurate value was measured by relative actinometry using 2,4-diphenyl-pentan-3-one (**33**) as an actinometer, because a large range of values are reported.[48,49,155] The actinometer **33** photochemically decomposes to produce the desired radical according to Scheme 7-15 with a quantum yield of 0.56.[153,156,157] It should be noted that Equation 7-3 must be modified to account for the production of two phenylethyl radicals upon the photodecomposition of **33**, shown in Equation 7-4. The extinction coefficient value measured is 1 366 M^{-1} cm^{-1} at 320 nm (See Table 7-8) and is smaller than the measured triplet value of **26**.

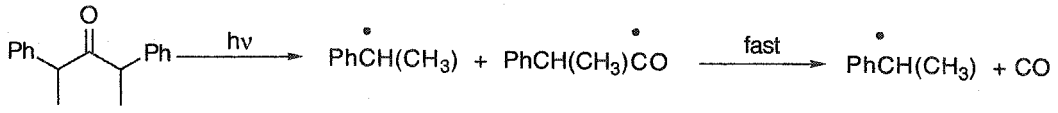

33 **33a**

Scheme 7-15. Photodecomposition of substituted dibenzyl ketone to give the phenylethyl radical.

$$\varepsilon_{33a}^{320nm} = 2 \cdot \left(\Phi_{16} / \Phi_{33a} \right) \cdot \left(\text{Slope}_{33} / \text{Slope}_{16} \right) \cdot \varepsilon_{16}^{525nm}$$

Equation 7-4. Equation for determining the extinction coefficient of the phenylethyl radical (33a) by relative transient actinometry versus the benzophenone triplet.

The amount of carbon centered radical produced upon photolysis of **29** can be determined by combination of all the values measured above. This requires deconvolution of the signal at 320 nm since it is the simultaneous growth of the radical and decaying triplet, schematically represented in Figure 7-24. A simple decay is observed since the extinction coefficient of the radical is considerably smaller than that of triplet (*vide supra*) and is also dependent upon the relative decay rate constants. Using the measured triplet and radical extinction coefficients, the signal can be deconvolutated according to Equation 7-5 and Beer-Lambert's equation to determine the radical concentration produced.[39]

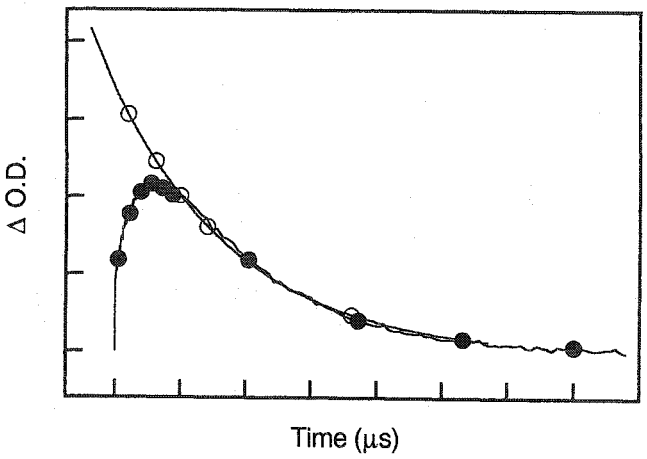

Figure 7-24. Theoretical growth of the phenylethyl radical (●) with simultaneous decay of the ketone triplet (O) and subsequent radical decay at long times.

Equation 7-5 accounts for the mixed first and second order decays for the two transients where the values m_2 and m_4 represent the decay rate constants for the triplet and radical, respectively. The parameter m_3 represents the original maximum absorbance of the triplet without the underlying radical. The parameter m_5 is the desired value and represents the extrapolated maximum radical absorption void of any triplet absorption and is easily obtained by fitting the observed decay trace of **27** (inset of Figure 7-25). Correcting for the differences in the extinction coefficient leads to the phenylethyl radical quantum yield shown in Table 7-8, assuming identical triplet quantum yields for **27** and **26**.[69,158-160] The yield of radical produced is quite high (0.53), but is lower than the triplet of **26**. This is consistent with the studies of other photoinitiators (**6-8**) and implies energy wastage by nonradiative processes such as bond rotation is present, albeit small. Efficient triplet quenching by energy transfer for the alkoxyamine **27** with equally high yield of C-O bond homolysis was observed. The relatively high efficiency of C-O homolysis suggests **27** would be a good candidate for photoliving polymerization. However, the transient growth at 260 nm still cannot be assigned.

$$\Delta \text{ O.D.} = m_3 \cdot \exp\left(-m_2 \cdot \tau\right) + \frac{1}{m_5 + m_4 \cdot \tau}$$

Equation 7-5. First and second order kinetic equation used to extrapolate the maximum absorbance of the phenylethyl radical.

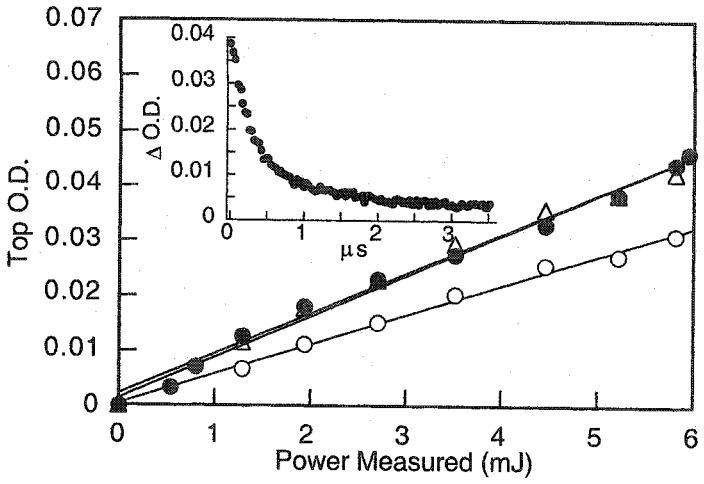

Figure 7-25. Plot used for carbon centered radical quantum yield determination of 27 at 320 nm (Δ) and 320 nm (●) with 33 (O) as actinometer monitored at 320 nm. Inset: Decay of transient derived from 27 monitored at 320 nm in acetonitrile.

7.4.1.3 Transient Assignment (260 nm)

Molecule **28** was used to probe the origins of the growth at 260 nm. Figure 7-26 shows a similar transient absorption to **27** around 300-320 nm including the anticipated intense absorption at 260 nm. The kinetics of this transient, shown in the inset of Figure 7-26, are more convoluted than those of **27**. The fast decay is assigned to the triplet because of its first order decay kinetics and vanishes with oxygen saturation. The slow intense growth is ascribed to the bromine radical (Br•) characteristic of an intense absorption in this region.[41,42] The complicated transient spectrum of **28** and possible charge-transfer complexes do not assist in deconvoluting the spectrum of **28** or assignment of the unknown transient at 260 nm. Triplet quenchers do not quench the signal as with **27**, but give rise to another transient most likely from complexes involving bromine. The transient at 260 nm may tentatively be assigned to styrene which is known to absorb quite strongly in this region (*vide infra*).[161-166]

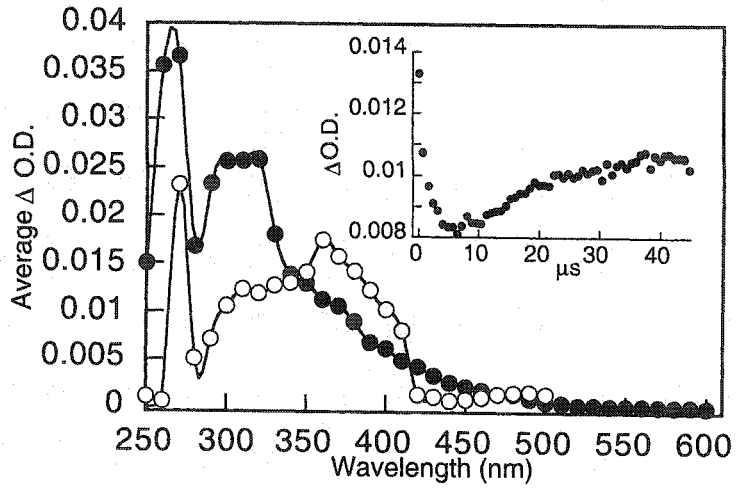

Figure 7-26. Transient absorption spectrum of 28 without sorbic acid (●) at 2.08 μs and 28 with sorbic acid (O) recorded at 1.04 μs after the laser pulse at 266 nm in acetonitrile. Inset: kinetics of transients monitored at 260 nm in the absence of sorbic acid.

Steady state irradiation and subsequent product analysis of **26** and **27** provides insight into the origins of the previously unassigned transient at 260 nm. Irradiation of **26** gives the expected benzoic acid and styrene, albeit in small amounts,[135,139] while irradiation of **27**, regardless of the solvent, generates styrene as a product. The formation of the hydroxylamine (**34**, Figure 7-27) and the hindered amine (**36**) are also observed regardless of the solvent used. The former originates as a result of nitroxide build-up from the decomposition of **27**, which is photochemically excited and subsequently undergoes hydrogen abstraction from the solvent.[80,95] Amine **36** emanates form the homolytic cleavage of the N-O bond as the irradiation wavelength is sufficiently high in energy.

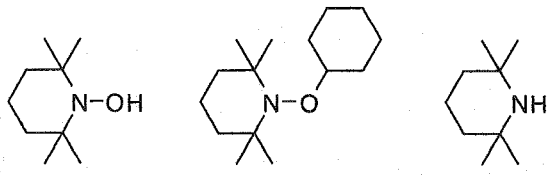

34 **35** **36**

Figure 7-27. Isolated amino based products from the photodecomposition of 27 at 254 nm in cyclohexane.

Decomposition of 27•, produced upon the photolysis of **27**, (see Scheme 7-16) gives styrene in addition to a benzoyloxyl radical. This pathway is confirmed by the formation as benzoic acid from hydrogen abstraction by the benzoyloxy radical isolated only in studies with good hydrogen donor solvents. Studies in acetonitrile do not produce benzoic acid since the precursor radical undergoes quantitative decarboxylation leading to the phenyl radical.[86,161,167] The fate of this radical is shown in Scheme 7-16 where the products were characterized by LC-MS and HPLC.

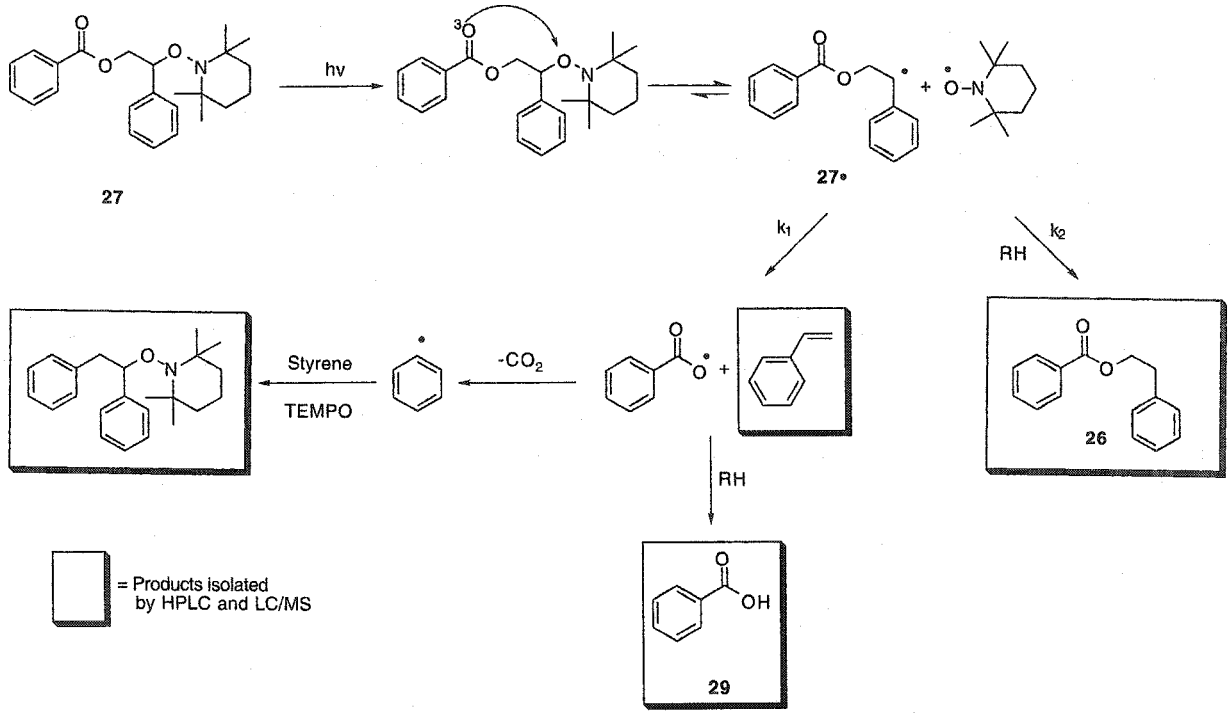

Scheme 7-16. Photochemical decomposition pathway of 27 based upon product isolation by HPLC and LC-MS after irradiation at 254 nm.

The unusual transient absorption spectrum observed for **27** can be explained by product analysis. The transient growth is from the mutual overlap of styrene and the benzoyloxyl radical. These both exhibit strong absorptions in the 260 nm region[161-166] and are expected to show identical kinetics of formation. The benzoyloxyl radical also absorbs in the 320 nm region, but its extinction coefficient is quite weak compared to that of the triplet **32** and consequently would not make a substantial contribution to the signal.[162] Nitroxides are known to quench triplets including those of styrene,[16,95,121] but the styrene

produced upon the decomposition of the radical from Scheme 7-16 is in its ground state. The addition reaction of TEMPO to styrene occurs only at elevated temperatures and not at room temperature.[80] Also, an instantaneous signal at 260 nm would be observed for the triplet styrene if it were produced with styrene build-up. However, the observed quenching kinetics with TEMPO at this wavelength is from trapping of the benzoyloxyl radical. The nitroxide quenching rate constant measured by Ingold et al. for benzoyloxyl radicals is identical to the value of the fast quenching of the growth with TEMPO observed at 260 nm measured here for **27**.[86,161,162]

7.4.2 Benzoylbenzoate Based Initiators Summary

The photophysics of the benzoyloxystyrene compounds were examined and found to generate the triplet state with high efficiency and subsequently undergo relative high efficacy of energy transfer to the alkoxyamine moiety. Like the initiators previously examined, the energy transfer process leads to C-O bond homolysis generating the carbon centered radical responsible for polymer propagation. Also generated, is the nitroxide radical capable of controlling the reaction and ultimately gives rise to LFRP polymers. The convoluted transient absorption spectrum of **27** was found to be a result of several sequential decomposition pathways occurring within the time scale of the LFP instrument. These pathways are ascribed to the triplet and carbon centered radical formation, which exhibited different quenching kinetics towards TEMPO. Selective excitation of the benzoyl moiety leads to the triplet formation followed by energy transfer. The subsequently generated benzylic type radical from C-O bond homolysis further decomposes to give styrene and the benzoyloxyl radical, both of which are visible at 260 nm. The latter is quenched by TEMPO with a fast rate constant. The decomposition to benzoyloxyl radicals renders this compound ineffective as a photoinitiator capable of controlling the LFRP process.

7.5 Photophysics of Benzoylbenzoate Based Initiators

The quantum yield of triplet formation for **26** and **27** were shown to be considerably less than that of benzophenone. Substitution of one of the phenyl groups of benzophenone for OH changes the photophysics of the molecule. The phosphorescence spectrum of **26** and **27** were examined to see whether the addition of the nitroxide group would further change the photophysics or **26**. The spectra obtained in the glass matrix of methylcyclohexane at 77 K are shown in Figure 7-28. Both benzoylbenzoate compounds posses a 0-0 band at 366 nm corresponding to the triplet energy of 78 kcal/mol which is slightly higher in energy than the triplet of benzophenone at 69 kcal/mol.[113] The spectra of the two esters are less ordered than benzophenone consistent with more degrees of freedom in the excited state. Regardless, the addition of the alkoxyamine group does not appear to influence the triplet photophysics.

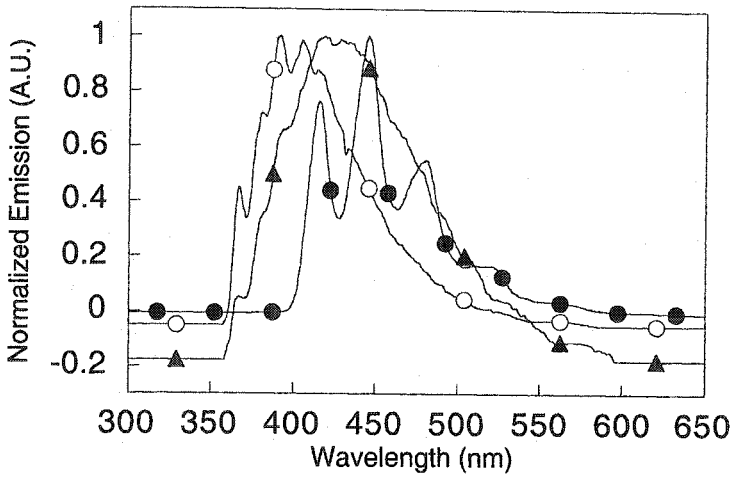

Figure 7-28. Normalized phosphorescence emission of 16 (●), 26 (O), and 27 (▲) recorded after 260 nm excitation in methylcyclohexane glass at 77 K.

There has been much discussion concerning the correct assignment of the triplet character of these compounds with mixed reports assigning it to a n,π* state while others say it is a π,π* state.[140,168] These conclusions are based upon the phosphorescence lifetimes and the emission intensity. Normally, π,π* phosphorescence is 10 to 1 000 times longer lived than the n,π* triplet to ground state transitions.[113,169] The source of confusion stems from benzoic acid that exhibits concentration dependent photophysical properties as a result of dimer

formation at higher concentrations.[136] The monomer has a high phosphorescence quantum yield while the dimer shows a decreased value in addition to fluorescence emission. The shift in photophysical properties represented by fluorescence emission is due to a low lying triplet n,π* state that becomes higher in energy and inaccessible to the dimer. The existence of a n,π* triplet state greatly influences the rate of intersystem crossing and in turn the quantum yield of phosphorescence as a result of symmetry elements.[170] When this state is lower in energy than the singlet π,π* state, the rate of intersystem crossing is fast and no fluorescence is observed. However, when the triplet n,π* is no longer accessible because it is higher in energy, the rate of intersystem crossing is slowed and it competes with fluorescence. The difference between the energy states is schematically represented in Scheme 7-17 for benzoic acid.

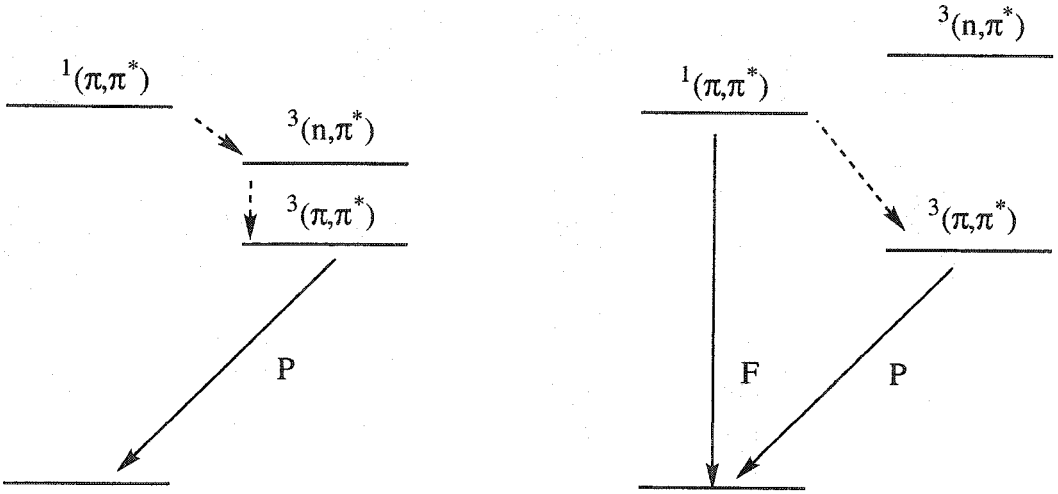

Scheme 7-17. Schematic representation of the different configurations for benzoic acid. P refers to phosphorescence while F denotes fluorescence.

The ratio of the amount of phosphorescence to fluorescence for benzoic acid monomer is quite high because the triplet n,π* is lower in energy than the singlet n,π* state.[136] However, this ratio is smaller (Φ_P/Φ_F = 32) for 27 where considerable amount of fluorescence is observed.[168] From experimentally measured triplet quantum yields for **26** in conjunction with the reported Φ_P/Φ_F ratio, the quantum yield of fluorescence can easily be calculated and is found to be 0.025. The value is quite small and suggests the triplet n,π* state is only

slightly higher in energy than the singlet n,π* state. The fluorescence of **27** was examined relative to **26** to determine its Φ_F and ascertain whether the addition of the alkoxyamine influences the energy gap. The non-normalized fluorescence spectra for **26** and **27** are shown in Figure 7-29 where the peak at 520 nm is an artifact from frequency doubling of the excitation wavelength. The fluorescence quantum yield of **27** is less than **26** illustrated by the decrease in the emission spectrum leading to Φ_F = 0.019. The lower fluorescence value observed is indicative of singlet quenching by the alkoxyamine, but this is not the case, even though nitroxides quench singlet states.[16] The fact that **26** and **27** posses identical phosphorescence quantum yields implies that singlet state of the latter is not quenched by the alkoxyamine. Therefore, the observed decrease in the fluorescence quantum yield must come from either a decrease in the n,π* energy state or by energy dissipation through non-radiative processes. If the former case was valid, the rate of intersystem crossing would increase and an overall augmentation of the phosphorescence quantum yield would be observed. However, Φ_P for **26** and **27** are identical confirming the n,π* triplet state energies for the two are also identical. Thus, the decrease in observed Φ_F must be due to non-radiative deactivation processes such as bond rotation through the increased number of possibilities with the additional alkoxyamine moiety.

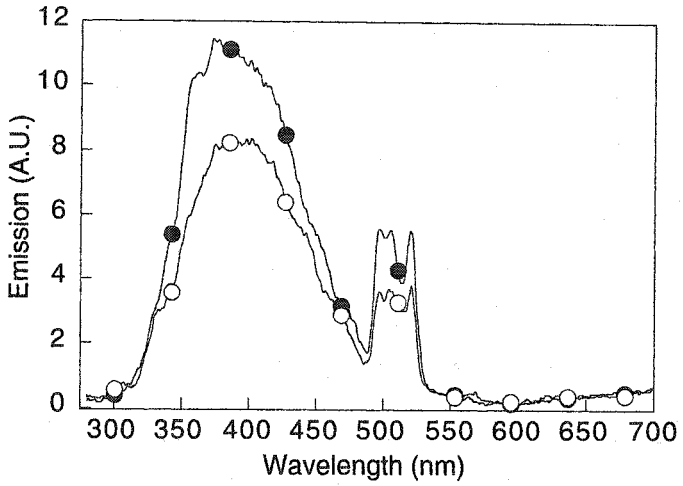

Figure 7-29. Fluorescence emission spectra of 26 (●) and 27 (○) monitored after excitation at 260 nm in methylcyclohexane.

7.6 Other Nitroxide Containing Initiators

Many of the initiators examined suffer a loss of energy transfer efficiency from the selectively excited chromophore to the C-O bond to be cleaved. This is mainly due to less rigid systems that permit energy dissipation through bond rotation or other molecular processes. The knowledge gained through the study of the other initiators were built upon to design and synthesize appropriate compounds potentially capable of promoting LFRP photochemically. Various compounds that produce triplet states when excited were investigated with alkoxyamines covalently linked to them. The series studied vary in triplet energy because our previous studies have shown that a high triplet energy is not required to induce the desired C-O bond homolysis through energy transfer.

7.6.1 Acridone Based Initiators

The essential elements of an ideal target molecule consisted of an invariable chromophore-nitroxide distance since quenching by processes other than energy transfer have been shown to dominate when the distance separating the two is great. Also, a locked geometry between donor and acceptor would be beneficial because reduction in the number of degrees of bond rotation should result in an increase in energy transfer yield. The target initiator **40** based upon acridone (**37**) was chosen because it satisfied the proposed criterion. In addition to this, acridone is commercially available in large quantities and can be used as a precursor for **40**, passing through the nitroxide **39**. Acridone is primarily used as a laser dye.[171,172] It undergoes intersystem crossing with unit efficiency in benzene[173] to form the triplet, which exhibits a large extinction coefficient on the order of 50 000 M^{-1} cm^{-1}.[50,51,113] It is also used as a photoinitiator for radical polymerization proceeding through some yet undetermined mechanism,[82,174-176] and can also serve as an antioxidant.[177] Moreover, the triplet energy of acridone is 57.5 kcal/mol,[171,172] approximately 30 kcal/mol higher than the energy required to cleave the C-O alkoxyamine bond.[123] An attractive advantage of acridone is its ground state absorption that has a band in the 350-400 nm region, which is well outside the longest absorption of any monomer. The photophysics and energy transfer properties of alkoxyamines and their nitroxide-free analogues have previously shown (*vide supra*) not to be drastically changed. The combination of all these physical properties in conjunction with knowledge gained from investigating other photoinitiators led to the belief that the acridone

based initiators (see Figure 7-30) seem likely candidates for photocontrolled LFRP.

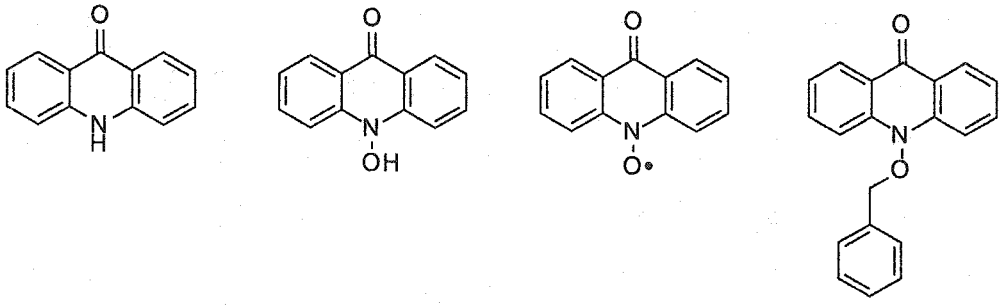

37 38 39 40

Figure 7-30. Series of acridone based molecules examined for potential LFRP initiators.

Energy transfer experiments, similar to Scaiano et al., were undertaken as preliminary studies to avoid laborious synthetic endeavors.[24] Direct excitation of acridone leads to the transient absorption spectrum (see Figure 7-31) with a maximum at 590 nm assigned to the triplet. The triplet decay was monitored as a function of nitroxide concentration giving the bimolecular rate constant of 1.5 x 10^9 M^{-1} s^{-1}, consistent with exothermic triplet quenching by energy transfer.[16] Quenching of the triplet with the thermal LFRP initiator **31** is anticipated to be about 10^8 M^{-1} s^{-1} indicative of energy transfer leading to homolysis of the C-O bond. The desired quenching rate constant with **31** measured from the slope of Figure 7-32 is much slower at 4.1 x 10^7 M^{-1} s^{-1}. This value is similar to that obtained by Scaiano et al. for 4-phenylbenzophenone, which was previously shown to induce the preferred C-O bond homolysis by energy transfer. Direct observation of the phenylethyl radical (**33a**) around 320 nm cannot be done because of its mutual overlap with the triplet in this region. Also, the triplet extinction coefficient is approximately 30 times stronger than **33a** and is expected to dominate the spectrum. Therefore, direct spectroscopic evidence of the desired C-O bond scission by energy transfer cannot be confirmed by indirect LFP studies where the analysis of **40** is necessary.

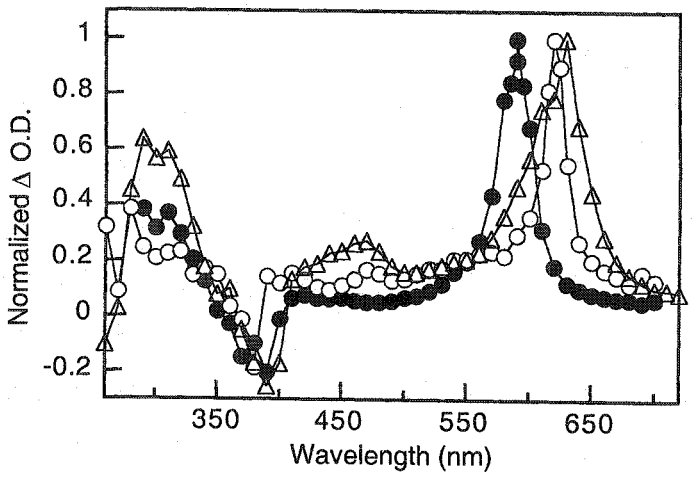

Figure 7-31. Normalized transient absorption spectrum of 37 in acetonitrile (●) and cyclohexane (O) and 40 in acetonitrile (Δ) recorded 2.08 μs after the laser pulse at 355 nm.

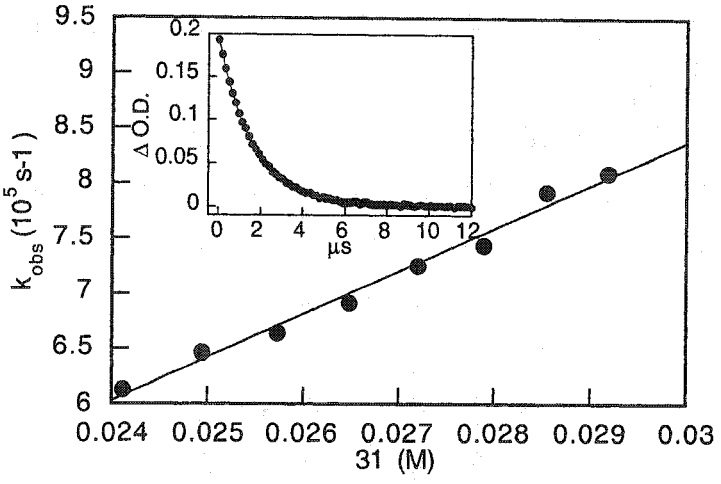

Figure 7-32. Quenching of 37 triplet with 31 by energy transfer. Inset: Decay of triplet monitored at 590 nm after excitation at 355 nm.

Initial synthesis of **39** involved the oxidation of acridone to the desired nitroxide (**39**), previously observed only by ESR.[178] A series of oxidizing agents typically used for nitroxide synthesis were employed under various experimental conditions. All the reagents used (hydrogen peroxide and sodium tungstate

catalyst,[179,180] Oxone,[181,182] and *m*-chloroperbenzoic acid[183]) failed to give the desired nitroxide product. An alternate route consisted of synthesizing the hydroxylamine (**38**) from *o*-nitrobenzaldehyde under harsh acid conditions.[184,185] The desired product was obtained in such low yields (< 3 %) and its photophysical properties could not be analyzed as all the material was used to synthesize the desired alkoxyamine product **40**.

Direct excitation of **40** by laser flash photolysis leads to the transient absorption spectrum shown in Figure 7-31 and represents the first kinetic/spectroscopic investigation of this compound. The region at 320 nm is still dominated by the acridone triplet and excludes direct observation of the benzylic radical from homolytic C-O bond cleavage through energy transfer. Interestingly, the long wavelength triplet absorption is shifted approximately 60 nm from the parent compound **37**. Previous laser flash photolysis studies of similar compounds have shown that N-alkylation of acridone causes slight spectral shifts to longer wavelengths regardless of the type of substituent, although the studies were limited to alkyl species.[186] However, the pronounced shift observed here is considerably larger than those previously reported.

The transient absorption spectrum triplet **37** changes with solvent and is a result of energy level splitting by polar and apolar solvents.[13] The transient at 625 nm in cyclohexane decays with first order kinetics characteristic of triplets and its red shifted maximum is reminiscent of the spectral changes found with triplet benzophenone and its ketyl radical. Quenching of triplet **37** in acetonitrile with the good hydrogen donor 1,4 cyclohexadiene gives an extremely slow rate constant of 2.9 $x10^5$ M^{-1} s^{-1}, considerably slower than for benzophenone.[16] Even though H-abstraction from this triplet occurs from phenols, the slow quenching must occur by some other allowed process as the triplet is π,π^* in character.[187] Also, the spectrum obtained from the photolysis of **37** in cyclohexane does not correlate well with the ketyl type radical (**43**, Figure 7-33) previously observed by laser flash photolysis and characterized by ESR.[187-189] The observed spectra is also not from the nitrogen centered radical (**42**) as its absorption spectrum is less blue shifted (ca. 530 nm) relative to **43** (ca. 560 nm).

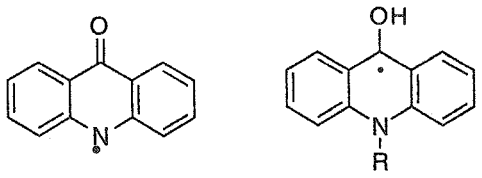

42 43

Figure 7-33. Acridone based radicals previously characterized by ESR and LFP.[187-189]

The observed spectral shifts with solvent polarity are attributed to a net destabilization of the triplet states. The system absorbs energy to be excited to its singlet state (S_1) which rapidly undergoes intersystem crossing to the lowest triplet state (T_1). It is then further excited to a higher triplet state (T_n) and the absorption from T_1 to T_n is the observed triplet transient absorption observed by LFP schematically represented in Scheme 7-18. The energy gap between the two triplet states correlates to the absorption wavelength. Therefore, stabilization of the triplet state results in a smaller energy gap and an observed red shift in the spectrum. The converse is also true and destabilization of the states with polar solvents results in a blue shift in the spectrum. Alkylation of the heteroatomic nitrogen atom causes a red shift of 15 nm implying stabilization of the triplet states.[173,186] The absorption maximum of the transient from **40** does not overlap with that of **42** or **43** and excludes homolytic N-O bond cleavage and hydrogen abstraction. The large red spectral shift of 40 nm from the parent acridone is indicative of triplet stabilization from the alkoxyamine group. The additional heteroatomic oxygen atom acts as an electron donating group to stabilize the system (*vide supra*).[179,180] However, there is still substantial triplet absorption in the region of 320 nm and detection of the benzylic radical production cannot be unequivocally determined.

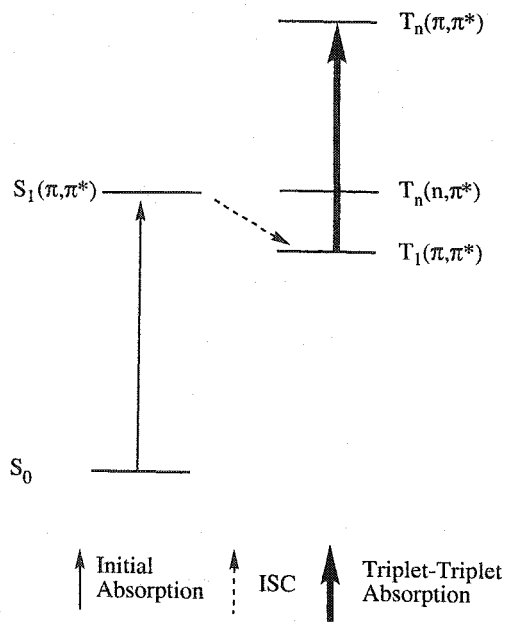

Scheme 7-18. Schematic representation of triplet-triplet absorption spectral shift with solvent polarity.

Direct observation the benzylic radical through C-O bond homolysis by LFP studies cannot be unequivocally done. Therefore, product studies involving the nitroxide exchange experiment were applied to **40**. Initiator irradiation at 350 nm is expected to produce the acridone nitroxide and benzylic radicals. Steady state irradiation at 350 nm did not produce any anticipated product illustrated in Scheme 7-19, even at longer irradiation times. Triplet **40** is probably efficiently quenched by the nitroxide trap suppressing of the C-O bond homolysis. Since the triplet quenching reaction by the nitroxide is by energy transfer, the nitroxide does not degrade and the quenching process can continue indefinitely. Irradiation of **40** in the absence of the external nitroxide trap would lead to the re-trapping reaction between the two radicals (nitroxide and C•) and analytical product determination would be next to impossible. Product studies are therefore equally inclusive and cannot give any insight whether photosensitized C-O bond homolysis occurs.

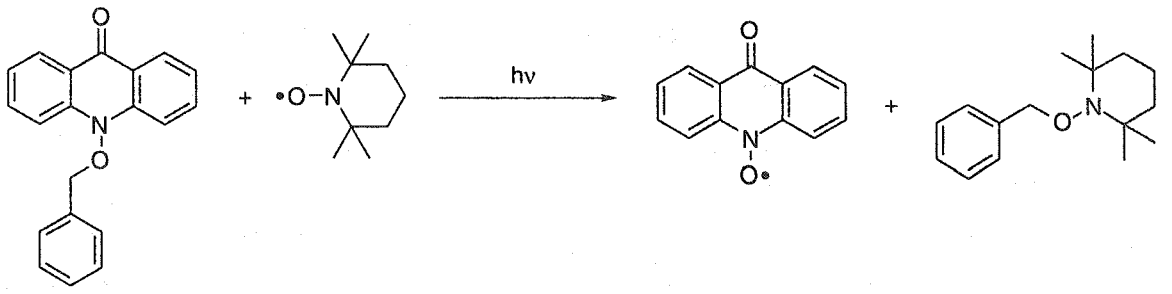

40 39 41

Scheme 7-19. Photoinduced benzylic nitroxide exchange experiment with alkoxymine containing acridone.

The lack of observed photoinduced C-O bond homolysis may be explained by the change in excited state properties of **37** and **40**. The phosphorescence spectrum (see Figure 7-34) of **40** is similar to benzophenone showing a structured emission consistent with a rigid C=O stretching vibration. This is characteristic of n,π* emission different from acridone whose emission is consistent with a π,π* state and is 57 kcal/mol in energy.[171,172] Benzylation of acridone increases the triplet energy by ca. 2 kcal/mol and the singlet energy is simultaneously increased from 65.5 to 69.5 kcal/mol. The combination of change in properties from a π,π* to n,π* character concomitant with a decrease in phosphorescence quantum yield explains the lack of desired properties relative to the other photoinitiators examined.

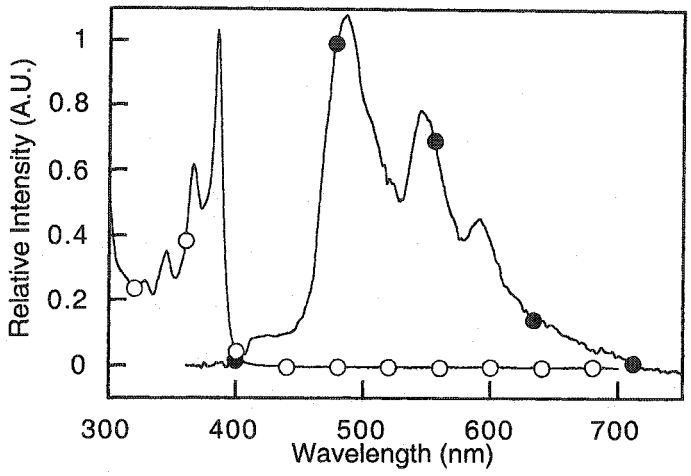

Figure 7-34. Ground state absorption spectrum (O) and phosphorescence emission excited at 350 nm (●) of 40 in methylcyclohexane.

7.6.1.1 Summary of Findings

Time resolved transient studies and steady state irradiation investigation are both inclusive for determining whether selective excitation of the chromophore moiety leads to homolytic C-O cleavage by energy transfer. The incorporation of the alkoxyamine moiety into the rigid chromophore apparently does not promote the energy transfer capabilities. The alkoxyamine moiety stabilizes the excited triplet states, yet increases the energy of the lowest triplet state and the singlet state. These changes are most likely responsible for suppressing the expected energy transfer from the triplet state resulting in C-O bond cleavage generating the benzylic radical.

7.6.2 Naphthalimides

Naphthalimides were selected as another class of potential photoinitiators. This class of compounds consists of naphthalene type chromophores rigidly bound to an alkoxyamine moiety similar to the acridone series. The compounds investigated, located in Figure 7-35, were anticipated to give the desired polymerization results as the general naphthalimide analogue structures are commercially used as photoacid generators.[190-195] The family of analogues has also been successfully employed as photoinitiators for the polymerization of acrylates.[4] The acid generation involves efficient energy transfer from the naphthalene chromophore moiety to the N-O moiety of the molecule, which subsequently cleaves. Here it was anticipated that the same efficient mechanism would proceed resulting in C-O bond homolysis, since this bond is considerably weaker the N-O bond.

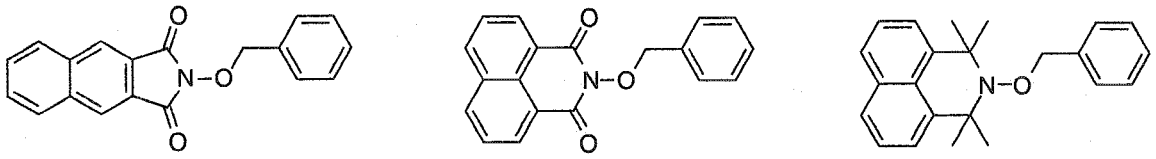

44 45 46

Figure 7-35. Naphthalimides studied as potential LFRP initiators.

The general phthalimide class of compounds are extremely versatile as they exhibit many interesting reaction mechanisms. In addition to their PAG capabilities, they are also useful organic synthesis reagents of which one of their

uses is the catalytic epoxidation of alkenes.[196] The nitroxide (47) plays the role of hydrogen abstractor generating the hydroxylamine (48), which under aerobic conditions, regenerates the nitroxide radical shown in Scheme 7-20. This reaction is of interest because it demonstrates the nature of the phthalimide nitroxide radical in solution. Also, the regeneration of the nitroxide from the hydroxylamine implies a high stability of the former since the O-H bond dissociation energy for this type of family is known to be quite high, approximately 75 kcal/mol.[197]

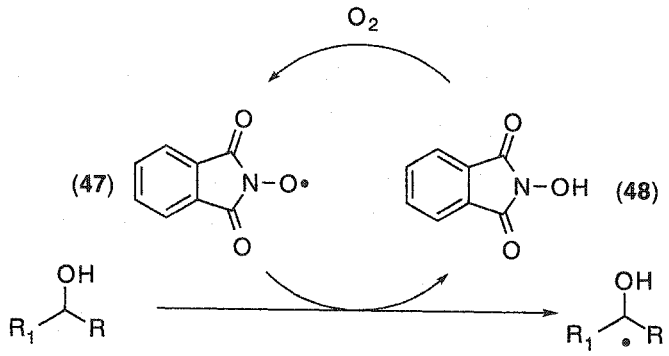

Scheme 7-20. Oxidation cycle of N-hydroxyphthalimide and hydrogen abstraction reaction.

Initial investigation for suitable photocontrol candidates for LFRP involved **44** and **45**. These were easily synthesized in high yields after modification of the literature procedure.[198] Preliminary exploration of the two naphthalimides with laser flash photolysis yielded no unusual results. The transient absorption spectra obtained (Figure 7-36) of the two alkoxyamines resembled those of their parent naphthalimides. The decay kinetics of the observed transients consistently followed first order kinetics and do not suggest any radical formation. Assignment of the desired benzylic radical around 320 nm is difficult because the spectrum shows bleaching at this wavelength due to the strong absorption of the ground state in this region. Also, the observed transient is ascribed to the naphthalimide triplet as the signal is readily quenched by 1,3 cyclohexadiene and sorbic acid, both of which are known triplet quenchers.[34] It was previously shown that triplet extinction coefficients are typically greater than those of the benzylic type radicals (*vide supra*). Therefore, the absence of any growth at 320 nm does not exclude formation of the benzylic radical.

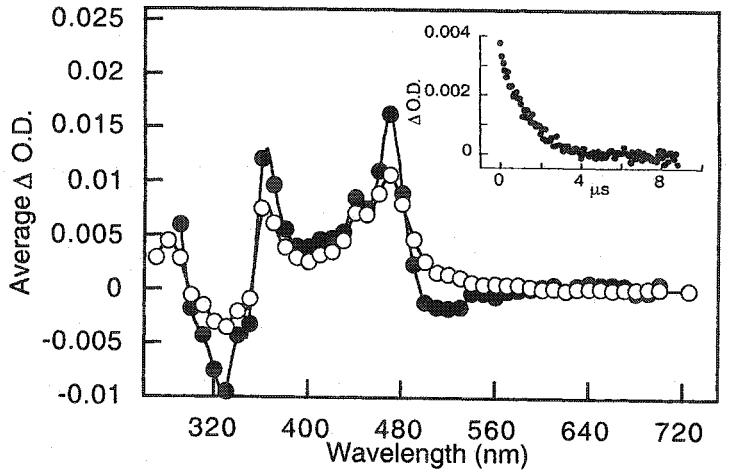

Figure 7-36. Transient absorption spectrum of 46 recorded 2.08 μs after the laser pulse at 355 nm in the absence (●) and presence (○) of 230 mM benzhydrol. Inset: Decay of transient monitored at 530 nm in the presence of benzhydrol.

To simplify the spectrum somewhat, benzhydrol (**49**) was added to the sample prior to analysis. Benzhydrol is reported to be an excellent photoreducing agent in the presence of radicals where it undergoes hydrogen donation.[199,200] The resulting diphenylketyl radical (**50**) has a characteristic absorption at 331 and 545 nm[201] and does not overlap with any region of absorption of the triplets from **44** or **45**. If homolytic C-O bond cleavage did occur from energy transfer, the resulting benzylic radical would undergo hydrogen abstraction leading to an observed growth at 545 nm from **50** at long time scales and also detectable by product analysis. The expected mechanism leading to the growth of **50** is schematically represented in Scheme 7-21. However, irradiation of the alkoxynaphthalimides with benzhydrol leads to the identical triplet absorption spectrum as that in its absence (Figure 7-36). However, the lack of **50** observed does not preclude the formation of the benzylic radical. The formation of **50** is expected to be thermoneutral with the benzylic radical, and as a result, the abstraction reaction may occur on a longer time scale than the time resolution of the LFP system. It can be concluded that the expected bond homolysis reaction may or may not proceed from the triplet state. The same experiment was repeated with the addition of sorbic acid and no signal was observed. This leads to the conclusion that the desired C-O bond homolysis reaction does not occur from the singlet state either. Therefore, the desired reaction leading to a new

photocontrol LFRP initiator candidate cannot be determined within the time resolution of the laser flash photolysis system.

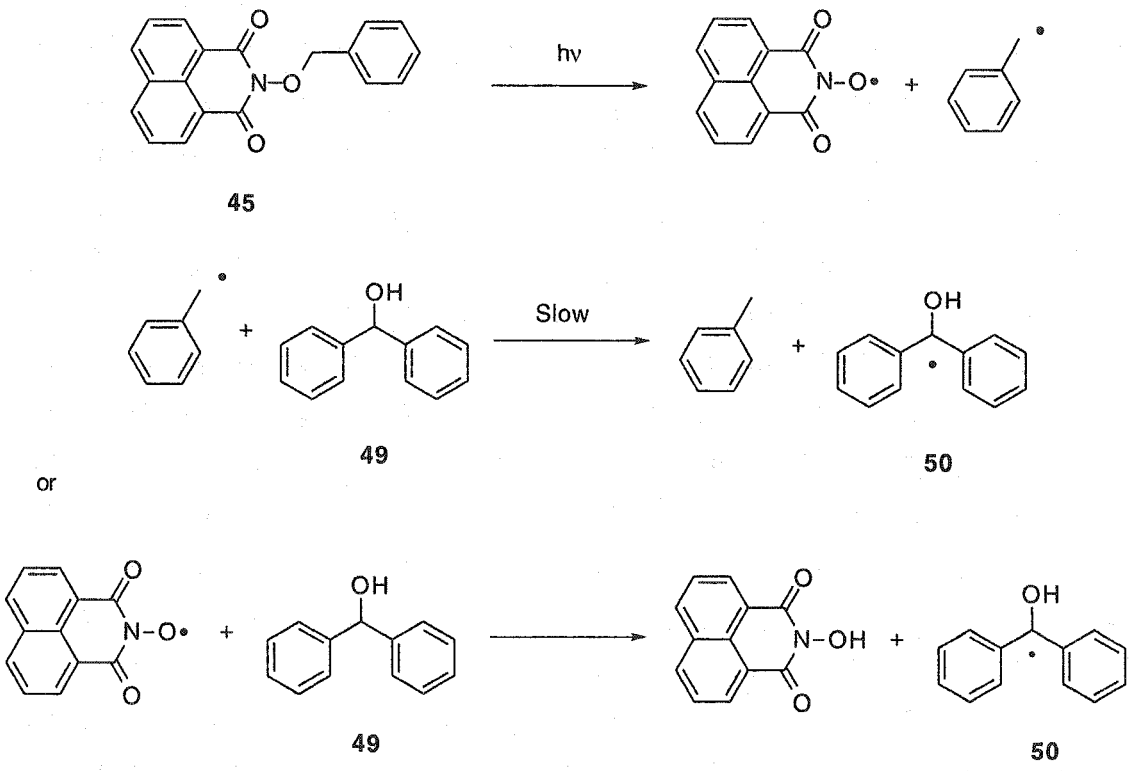

45 49 50 49 50

Scheme 7-21. Anticipated mechanistic pathway leading to diphenylketyl radical (50) by hydrogen abstraction from benzylic radical derived from 45.

Steady state irradiation and subsequent product analysis by HPLC did not provide any evidence for the presence of C-O bond cleavage as the growth of **41** was not observed. These results do not exclude any other decomposition pathways from occurring. The minute amounts of products formed cannot be properly characterized because of a lack of authentic samples and an insufficient amount due to low conversions. A possible decomposition route may be through N-O cleavage either homolytically or heterolytically. The latter dominates in the case of sulfonyl based naphthalimide PAGs.[190] Naphthalimides are essentially amides, which are known to undergo intramolecular hydrogen abstraction leading to a biradical represented by pathway a in Scheme 7-22, albeit with relatively low quantum yields.[13,202] The incorporation of a donor group facilitates electron transfer leading to a radical cation and radical anion pair

illustrated by pathway b. These intramolecular reactions are exploited for the synthesis of heteroatomic cycles by intramolecular cyclization of the radicals.[203]

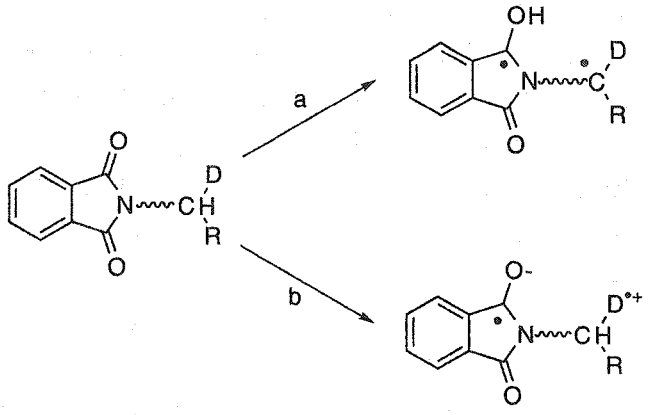

Scheme 7-22. Dual reaction pathway of N-alkylphthalimide.

The amide function appears to play an important role in suppressing the desired C-O bond cleavage by undergoing other preferential deactivation routes such as hydrogen abstraction, N-O cleavage, or bond rotation. An attempt was made to synthesize the tetramethylated analogue **46** that would hopefully mimic the controlling properties of its thermal initiator analogues. The reduction of phthalimide to its tetramethylated analogue has been reported, but in low yields after 6 steps.[204,205] The titanium based Tebbe reagent was used as a more efficient synthetic route. This reagent has previously been used to successfully convert hindered ketones to olefins[206] and the strategy was to subsequently dimethylate the two olefins giving **46** as the expected product. Several attempts were unsuccessful and resulted only in the destruction of the phosphorescent character of the starting material. No identifiable products could be isolated by GC/MS or NMR and the reaction was abandoned for other initiator pursuits.

7.6.2.1 Summary of Findings

Laser flash photolysis studies of the alkoxyamine naphthalimides based initiators are inconclusive as evidence for the correct C-O bond fragmentation is lacking. The triplet of the naphthalimide dominates the transient absorption spectrum, but product studies from steady state irradiation confirm the absence of C-O bond homolysis. Removal of the amide function and substitution with methyl groups should yield the desired photochemical properties with the desired C-O homolysis known for thermal initiators.

7.6.3 Naphthalene

The series of naphthalene based initiators shown in Figure 7-37 were examined for their photochemical nitroxide release capabilities. Unlike the naphthalimides, the new series of initiators do not posses the amide function and would suggest cleaner photochemistry giving rise to the preferred bond cleavage. The triplet energy of naphthalene is 61 kcal/mol[13,113] about 8 kcal/mol less than that of benzophenone whose substituted alkoxyamine analogues were proven to promote the photorelease of the correct radicals.

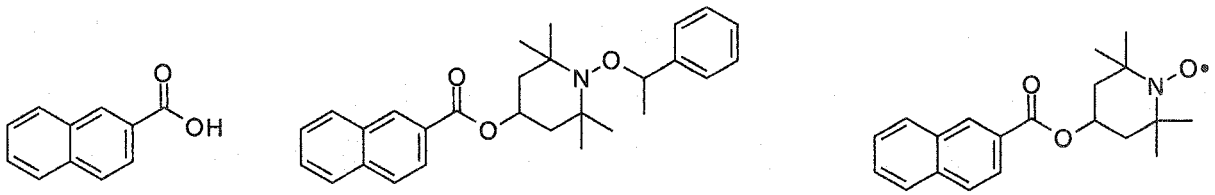

51 52 53

Figure 7-37. Naphthalene based initiators for LFRP.

The transient absorption spectrum derived from the photolysis of **52** is characteristic of the naphthalene triplet and is identical to that of **51**. As was the case with the previous triplet studies, the characteristic signal around 320 nm[34] for the benzylic radical is absent precluding its formation from energy transfer from the triplet state. This is also confirmed by the transient spectra that show nearly identical maximum absorbances and imply no quenching by energy transfer for **52**. The addition of 1,3 cyclohexadiene quenches the triplet signal of **51** and **52** as anticipated. However, the absence of any signal at 318 nm from the benzylic radical under these quenching conditions precludes its formation from the singlet state of naphthalene. There is equally no signal from the laser flash photolysis of **53**, which is expected since it triplet quenching nature is well documented.[16,121,160,207] The results lead to the conclusion that the alkoxyamine does not quench the triplet state and the homolysis of the C-O does not occur from this state. This is of surprise since high efficiencies of homolytic bond scission of C-O in an ester covalently bound to naphthalene have been reported.[208] The cleaved ester bond is higher in energy than that of the C-O bond of the alkoxyamine naphthalenes studied.[57,123,209-212] The only difference between the two systems is the relative orientation of the bond to be cleaved, being similar to that of **6**. Similar results were observed with photoinduced

decomposition of peresters having similar bond decomposition energies to the alkoxyamines.[213,214] The results found showed an increase in efficiency when the bond to be cleaved was directly adjacent to the chromophore and a decrease in radical formation with increasing distance separating the chromophore and the bond to be cleaved.

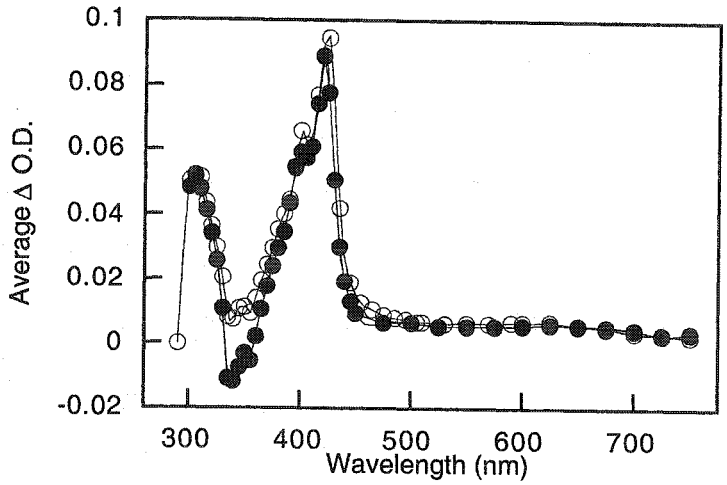

Figure 7-38. Transient absorption spectrum of 51 (●) and 52 (O) recorded 4.16 μs after the laser pulse at 308 nm.

The efficiency of triplet formation of naphthalene is approximate 70 % and it also fluoresces.[13] However, its fluorescence quantum yield is decreased by 50 fold when the paramagnetic nitroxide is covalently bound to it as with **53**,[160] relative to its diamagnetic analogue. This implies the nitroxide promotes efficient singlet quenching by electron exchange in its paramagnetic form.[160] The fluorescence lifetimes of compounds similar to **53** have been reported to be extremely short lived compared to their diamagnetic alkoxyamine analogues.[69,160] There is no energy transfer from the naphthalene moiety to the C-O bond as determined by the lack of singlet quenching from the alkoxyamines. This is not expected since the naphthalene has a relatively high singlet energy (90 kcal/mol)[13] and is nearly three times the amount of energy required to cleave the alkoxyamine bond. The difference in fluorescence intensity has been taken advantage of recently by Moad et al.[159] to determine the radical concentration in polymerization reactions.

7.6.3.1 Summary of Findings

The naphthalene triplet is not quenched by the alkoxyamine when it is covalently attached to the chromophore. Only its triplet state is quenched when the paramagnetic nitroxide is tethered. The lack of quenching by the alkoxyamine also is present for the singlet state of naphthalene, but is readily quenched again by the nitroxide through electron exchange. The lack of quenching by energy transfer to the alkoxyamine moiety is most likely a result of its orientation. A decrease in quantum yield efficiency may be observed if the alkoxyamine were directly attached to the naphthalene chromophore eliminating its use as a potential photocontrolled LFRP initiator.

7.7 Chapter Summary

Several types of N-alkoxyamine coupled triplet sensitizers were examined for their capability to transfer energy from the excited chromophore of the molecule to the C-O bond for subsequent homolytic cleavage. The benzophenone based initiators were shown to undergo the desired bond scission process with high efficiency regardless of the orientation of the chromophore-alkoxyamine relationship. However, the orientation does play a major role for achieving photocontrolled LFRP. The alkoxyamine-chromophore distance must be fixed in order to achieve consistent energy transfer for subsequent bond cleavage and ultimately photopolymerization with living properties. With increasing distance between the two reactive centers, other processes begin to compete with the energy transfer step and eventually dominate. The n,π^* state, accessible by some of the initiators, plays an important role in determining whether energy transfer occurs. The hydrogen abstraction reaction is highly allowed from this state and will compete with energy transfer and eventually prevail. Triplet sensitizers whose states are π,π^* character are an alternative choice as the hydrogen abstraction reaction is forbidden. Xanthone is such a triplet sensitizer and its alkoxyamine analogue is currently being investigated for improved photocontrolled properties over benzophenone based initiators.

The photochemistry from the triplet sensitizer must not be allowed to undergo any competing deactivation processes. Like the benzophenone initiators, the other triplet sensitizers investigated suffered from the same loss of energy transfer due to competing reactions. Primarily, these were in the form of intramolecular quenching or by energy dissipation through nonradiative decay pathways. The orientation of the alkoxyamine-sensitizer is crucial for energy transfer leading to bond homolysis. The alkoxyamine must be directly linked to the chromophore, similar to **6**, in order to promote the desired bond cleavage. Orientation of these two reactive centers in the reverse manner does not undergo energy transfer, rather nonradiative quenching processes dominate precluding their use as potential photocontrolled LFRP initiators.

The energy transfer step from the chromophore to the alkoxyamine moiety must be by a short range exchange mechanism. Poor energy transfer is observed with increasing separation of the two or with change in their relative orientation. However, efficient quenching is observed with the free nitroxide analogue regardless of the degree of separation between the two centers.

The incorporation of the nitroxide function into the conventional benzoin type photoinitiator forming an alkoxyamine was shown to give mixed properties. A competition between the photochemical decomposition pathways of Norrish type I and C-O bond cleavage occurs. This hybrid character is also present with thermal decomposition where an ionic or radical pathway can be achieved based upon the reagent selected.

7.8 Experimental

All chemicals were used as received from Aldrich unless otherwise specified. Styrene, methyl methacrylate, methacrylate, and methacrylic acid were all distilled under reduced pressure prior to polymerization to remove the radical inhibitor. All other solvents were used as received except for dry solvents, which were distilled and dried by conventional methods.[215]

7.8.1 Synthesis

(2-Bromomethylphenyl)-phenylmethanone (16): To a round bottom flask with 40 mL of carbon tetrachloride was added 2-methylbenzophenone (1.0 g, 5.09 mmol), N-bromosuccinimide (1.1g, 6.18 mmol), and a catalytic amount of benzoylperoxide. The colorless solution was refluxed for 4 hours till the color became orange/red. The solid was filtered off and the residual solvent removed under reduced pressure. The resulting oil was purified by flash chromatography with 10% ethylacetate/hexanes to afford 186 mg of the product as an oil in 13 %. ^{1}H NMR (200 MHz, $CDCl_3$, TMS) δ 7.81-7.84 (d, 3H), 7.26-7.78 (m, 6H), 4.68 (s, 2H) ^{13}C NMR (300 MHz, $CDCl_3$) δ 194.6, 138.5, 135.2, 132.5, 131.2, 131.3, 128.3, 125.1, 33.8. MS (EI) m/z (%) 276 (0.3), 274 (1.7), 196 (88), 194 (100), 165 (82), 152 (4), 139 (7), 118 (4), 105 (10), 89 (11), 82(17), 77 (16), 51 (13).

(3-Bromomethylphenyl)-phenylmethanone (17): 3-Methylbenzophenone (0.99g 5.05 mmol) were dissolved in 35 mL carbon tetrachloride followed by N-bromosuccinimide (1.1 g, 6.18 mmol) and a catalytic amount of benzoylperoxide. The mixture was stirred and refluxed overnight. The supernatant material was removed by filtration and washed with dichloromethane. The residual solvent was removed under reduced pressure and the yellow solid was purified by flash chromatography with 5 % ethylacetate/hexanes to afford 1.21 g of white solid as product in 87 % yield. M.p. 45-47 °C. ^{1}H NMR (200 MHz, $CDCl_3$, TMS) δ 7.66-7.81 (d, 4H), 7.45-7.63 (m, 5H), 4.51 (s, 2H). ^{13}C NMR (300 MHz, $CDCl_3$) δ 197.0, 137.7, 136.6, 136.5, 132.2, 130.4, 128.3, 130.3, 129.4, 33.0. MS (EI) m/z (%) 276 (16), 274 (16), 197 (13), 195 (100), 167 (11), 165 (27), 152 (25), 139 (3), 118 (10), 105 (63), 89 (28), 77 (62), 51 (24).

(4-Bromomethylphenyl)-phenylmethanone (18): In a 250 mL round bottom flask was charged 4-methylbenzophenone (5.02 g, 25.6 mmol), N-bromosuccinimide (5.1 g, 28.7 mmol), and a catalytic amount of benzoyl peroxide

all dissolved in approximately 150 mL of carbon tetrachloride. The solution was refluxed overnight, the supernatant removed followed by solvent removal under reduced pressure. The resulting yellow solid was purified by flash chromatography with 5 % ethylacetate/hexanes and recrystalized from 99% ethanol to afford 3.5 g of white solid as product in 50 % yield. M.p. 91-93 °C. ^{1}H NMR (200 MHz, $CDCl_3$, TMS) δ 7.70-7.82 (d, 3H), 7.40-7.58 (m, 6H), 4.51 (s, 2H) ^{13}C NMR (300 MHz, $CDCl_3$) δ 195.9, 141.4, 137.8, 133.0, 129.9, 129.2, 128.2, 128.9, 33.4. MS (EI) m/z (%) 276 (8, M+1), 274 (7), 196 (4), 195 (100), 167 (49), 165 (11), 152 (5), 118 (7), 105 (12), 90 (13), 89 (12), 77 (16), 51 (7).

(4-(2,2,6,6,-tetramethylpiperdine-1-yloxymethyl)-phenyl]-methanone (6): (4-Bromomethylphenyl)-phenylmethanone (1.47 g, 5.37 mmol) and TEMPO (0.92 g, 5.89 mmol) were dissolved in 50 mL acetonitrile in a 15 cm pyrex test tube. The sample was purged with nitrogen for 25 minutes, sealed, and irradiated at 300 nm for 7 days. After the color bleached, the solvent was removed and the resulting yellow solid purified by flash chromatography with 5 % ethylacetate/hexanes to give 1.15 g (25 %) of the product, which solidifies upon resting for 2 weeks. M.p. 36-41 °C. ^{1}H NMR (200 MHz, $CDCl_3$, TMS) δ 7.75-7.81 (d, 2H), 7.24-7.57 (m, 7H), 4.90 (s, 2H), 1.49 (m, 6H), 1.23 (s, 6H), 1.16 (s, 6H). ^{13}C NMR (300 MHz, $CDCl_3$) δ 187.3, 143.2, 137.8, 136.4, 1302.3, 130.2, 130.1, 129.9, 129.6, 128.2, 126.8, 126.7, 78.2, 60.1, 39.7, 33.0, 32.9, 20.3, 17.1. MS (EI) m/z 351 (1), 281 a918), 216 (19), 207 (55), 191 (16), 173 (54), 159 (68), 156 (2), 145 (89), 135 (18), 105 (47), 91 (17), 77 (20), 57 (79), 56 (41), 41 (75). MS (FAB) m/z (%) 352(2, M+1), 344 (8), 20 (19), 199 (10), 159 (100), 156 (5), 144 (12), 143 (16), 105 (8), 91 (2), 77 (4), 68 (10),

[4-(4-Hydroxy-2,2,6,6,-tetramethyl-piperdin1-yloxymethyl)-phenyl]-phenyl-methanone : (4-Bromomethylphenyl)-phenylmethanone (3.54 g, 12.9 mmol) and 4-hydroxy-TEMPO (2.18 g, 12.7 mmol) were dissolved in 50 mL acetonitrile in a 15 cm pyrex test tube and sonicated for 10 minutes, after which was added 2 g of potassium thiosulfate. The sample was purged with nitrogen for 25 minutes, sealed, and irradiated at 300 nm for 5 days. After the color bleached, the solvent was removed and the resulting yellow solid purified by flash chromatography with 10 % ethylacetate/hexanes to give 1.15 g (25 %) of the product. M.p. 72-74 °C. ^{1}H NMR (200 MHz, $CDCl_3$, TMS) δ 7.76-7.81 (m, 2H), 7.24-7.58 (m, 7H), 4.90 (s, 1H), 4.05 (m, 1H), 1.84 (m, 4H), 1.33-1.56 (m, 12). ^{13}C NMR (300 MHz, $CDCl_3$) δ 196, 132.3, 132.1, 130.3, 130.0, 129.9, 128.1, 126.7, 78.1, 63.1, 60.2, 48.1, 32.9, 21.1. MS (EI) m/z (%) 210 (48), 172 (28), 142 (42), 140 (15), 133 (35), 116 (21), 105 (97). 98 (23), 91 (3), 77 (58), 56 (88), 40 (100). MS (FAB) m/z (%) 368 (34, M+1), 268 (13), 196 (34),

195 (36), 172 (84), 167 (25), 156 (16), 142 (12), 133 (100), 124 (12), 116 (14), 105 (29), 77 (16), 57 (13).

4-Benzoyl-benzoic acid 2,2,6,6-tetramethyl-1-(1-phenyl-ethoxy)-piperdidin-4-yl ester (8): 4-Benzoyl benzoic acid (56.2 mg, 0.25 mmol), 1-phenyl-1-(2,2,6,6-tetramethyl-4-hydroxy-piperdine-N-oxide)-ethane (61 mg, 0.22 mmol), 1,3-dicyclohexylcarbodiimide (74.5 mg, 0.36 mmol) were charged into a round bottom flask and dissolved in 50 mL acetonitrile followed by the addition of a catalytic amount of DMAP. After 2 hours, the supernatant was filtered off and the solvent removed followed by purification by flash chromatography with 10 % ethylacetate/hexanes to afford 33 mg (33 %) of the product as a white solid. M.p. 75-78 °C. ^{1}H NMR (200 MHz, $CDCl_3$, TMS) δ 7.80 (d, 2H), 7.75-7.83 (m, 4H), 7.43-7.62 (m, 3H), 7.22-7.32 (m, 5H), 5.39 (q, 1H), 4.88 (q, 1H), 1.59-1.99 (m, 4H), 1.49 (d, 3H), 1.39 (s, 3H), 1.32 (s, 3H), 1.17 (s, 3H), 0.58 (s, 3H). ^{13}C NMR (300 MHz, $CDCl_3$) δ 195.9, 165.3, 145.2, 141.1, 136.9, 133.6, 132.8, 130.0, 129.6, 129.3, 128.4, 128.4, 128.0, 126.9, 126.6, 83.3, 68.0, 60.2, 59.9, 44.6, 34.3, 34.0, 23.2, 21.1. MS (EI) m/z (%) 381 (7), 321 (8), 180 (43), 154 (10), 140 (18), 124 (100), 109 (24), 105 (55), 104 (37), 91 (3), 77 (30), 58 (17), 41 (15). MS (FAB) m/z (%) 486 (2, M+1), 209 (31), 141 (9), 132 (100), 105 (17), 77(5).

4-Benzoyl-benzoic acid 2,2,6,6-tetramethyl-1-(1-phenyl-ethoxy)-piperdidin-4-oxyl : 4-Benzoyl benzoic acid (82.1 mg, 0.36 mmol), 4-hydroxy-TEMPO (65 mg, 0.37 mmol), 1,3-dicyclohexylcarbodiimide (90.6 mg, 0.44 mmol) were charged into a round bottom flask and dissolved in 50 mL THF followed by the addition of a catalytic amount of DMAP. The reaction was monitored by GC and the supernatant filtered after maximum completion. The solvent was removed and the solid purified by flash chromatography with 15 % ethylacetate/hexanes to afford 21 mg (16 %) of product as an orange solid. MS (EI) m/z (%) 380 (2), 154 (120), 124 (100), 105 (17), 91 (2), 77 (9), 58 (13).

Phenyl {4-[2,2,6,6-tetramethyl-1-(1-phenyl-ethoxy)-piperdidin-4-yloxymethyl]-phenyl}-methanone (7): 1-phenyl-1-(2,2,6,6-tetramethyl-4-hydroxy-piperdine-N-oxide)-ethane (470 mg, 1.69 mmol) was dissolved in 10 mL of dry DMF and cooled to 0 °C followed by the addition of sodium hydride (190 mg, 7.9 mmol). After a few minutes, tetrabutylammonium iodide (11.4 mg, 0.03 mmol) and potassium thiosulfate (few mg) was added followed by (4-bromomethylphenyl)-phenylmethanone (460 mg, 1.68 mmol). The reaction was allowed to warm to room temperature and an orange color formed. After two days the reaction was

quenched with water, separated with dichloromethane, the solvent was removed and the product purified by flash chromatography with 10 % ethylacetate/hexanes to give 70 mg (10 %) of product. ^{1}H NMR (200 MHz, $CDCl_3$, TMS) δ 7.75-7.85 (d, 4H), 7.39-7.57 (m, 5H), 7.20-7.38 (m, 5H), 4.75 (q, 1H), 4.58 (s, 2H), 3.65 (q, 1H), 2.15-1.79 (m, 4H), 1.48 (d, 3H), 1.33 (s, 3H), 1.19 (s, 3H), 1.06 (s, 3H), 0.68 (s, 3H). ^{13}C NMR (300 MHz, $CDCl_3$) δ 195.9, 128.2, 127.3, 126.8, 123.2, 77.5, 53.7, 33.9, 33.6, 22.9, 22.7. MS (EI) m/z (%) 254 (1), 210 (31), 181 (11), 177 (31), 165 (19), 153 (16), 149 (39), 133 (29), 105 (100), 91 (26), 86 (21), 77 (60), 57 (37), 43 (56). MS (FAB) m/z (%) 472 (17, M+1), 368 (13), 352 (16), 239 (15), 195 (32), 178 (13), 172 (12), 167 (20), 156 (20), 149 (13), 140 (14), 133 (60), 105 (100), 91 (7), 77 (10), 74 (29).

Phenyl {4-[2,26,6-tetramethyl-1-(1-phenyl-ethoxy)-piperdidin-4-yloxymethyl]-phenyl}-methanone (7): 2,2,6,6-Tetramethyl-4-[4-2-(phenyl-1[1,3]dioxolan-2-yl)-benzyloxy]-1-(1-benzyl-ethoxy)-piperdidine (255 mg, 0.51 mmol) was dissolved in 20 mL normal THF and 10 mL of 10 % HCl was added and allowed to stir at room temperature. Dichloromethane was added and the organic layer separated and the solvent removed. The oil was purified by flash chromatography with 10 % ethylacetate/hexanes to give 70 mg (30 %) of product. ^{1}H NMR (200 MHz, $CDCl_3$, TMS) δ 7.75-7.85 (d, 4H), 7.39-7.57 (m, 5H), 7.20-7.38 (m, 5H), 4.82 (s, 1H), 4.61 (s, 2H), 3.71 (q, 1H), 1.95 (d, 2H), 1.61(t, 2H), 1.30 (s, 6H), 1.18 (s, 6H). ^{13}C NMR (300 MHz, $CDCl_3$) δ 195.9, 158.6, 145.2, 141.1, 136.9, 133.6, 132.8, 130.0, 129.6, 129.3, 128.4, 128.4, 128.0, 126.9, 126.6, 83.3, 75.5, 60.2, 59.9, 44.6, 34.3, 34.0, 23.2, 21.1. MS (EI) m/z (%) 210 (31), 205 (31), 196 (7), 181 (11), 177 (31), 165 (19), 153 (16), 149 (39), 133 (29), 105 (100), 104 (14), 91 (16), 84 (31), 77 (59), 69 (17), 57 (37), 43 (56), 41 (32). MS (FAB) m/z 458 (7, M+1), 366 (18), 246 (5), 196 (15), 195 (33), 167 (20), 164 (15), 147 (11), 132 (36), 107 (14), 105 (28), 97 (30), 91 (52), 83 (48), 77 (17), 71 (48), 69 (70), 57 (100).

(4-Bromomethyl-phenyl)-2-phenyl-[1,3]dioxolane: (4-Bromomethylphenyl)-phenylmethanone (1.18 g, 4.3 mmol), ethylene glycol (0.3 mL, 5.3 mmol) and a catalytic amount of *p*-toluenesulfonic acid were refluxed in toluene overnight and the water removed by azeotrope distillation by a Dean-Stark trap. After complete reaction, the solvent was removed and the product was purified by flash chromatography with 5 % ethylacetate/hexanes to give 0.92 g (67 %) of the product as a yellow oil. ^{1}H NMR (200 MHz, $CDCl_3$, TMS) δ 7.42-7.49 (m, 4H), 7.23-7.35 (m, 5H), 4.45 (s, 2H), 4.05 (s, 4H). ^{13}C NMR (300 MHz, $CDCl_3$) δ 137.5, 130.6, 130.4, 130.2, 130.0, 129.3, 129.2, 129.1, 128.9, 128.8, 128.6, 128.4, 128.3, 128.2, 126.9, 126.6, 126.4, 126.2, 126.0, 64.9, 33.1. MS (EI) m/z (%) 320 (2), 318 (2), 243 (12), 241

(13), 176 (1), 165 (12), 149 (24), 118 (24), 05 (37), 91 (6), 90 (58), 89 (71), 77 (100), 63 (22).

2,2,6,6-Tetramethyl-4-[4-2-(phenyl-1[1,3]dioxolan-2-yl)-benzyloxy]-1-(1-benzyl-ethoxy)-piperdidine: (4-Bromomethyl-phenyl)-2-phenyl-[1,3]dioxolane (2.32 mg, 0.73 mmol) was dissolved in 30 mL of dry DMF and cooled to 0 °C then sodium hydride (200 mg, 0.73 mmol), and 1-phenyl-1-(2,2,6,6-tetramethyl-4-hydroxy-piperdine-N-oxide)-ethane (200 mg, 0.73 mmol) were added. The solution was warmed to room temperature and allowed to stir overnight. The reaction was quenched with saturated brine solution, separated with dichloromethane, the solvent removed, and purified by flash chromatography with neat toluene to give 260 mg (69 %) of product as white crystals. ^{1}H NMR (200 MHz, $CDCl_3$, TMS) δ 7.42-7.49 (m, 4H), 7.23-7.35 (m, 10H), 4.81 (q, 1H), 4.49 (s, 2H), 4.05 (s, 4H), 3.63 (m, 1H), 1.76-1.97 (m, 4H), 1.49 (d, 3H), 1.35 (s, 3H), 1.21 (s, 3H), 1.07 (s, 3H), 0.69 (s, 3H). ^{13}C NMR (300 MHz, $CDCl_3$) δ 165.3, 145.2, 141.1, 136.9, 133.6, 132.8, 130.0, 129.6, 129.3, 128.4, 128.4, 128.0, 126.9, 126.6, 109.0, 83.3, 68.0, 65.9, 60.2, 59.9, 44.6, 34.3, 34.0, 23.2, 21.1. MS (EI) m/z (%) 173 (23), 172 (10), 158 (52), 142 (14), 116 (10), 106 (11), 105 (100), 91 (7), 77 (30), 57 (23), 41 (39). MS (FAB) m/z (%) 516 (15, M+1), 278 (38), 239 (21), 174 (13), 172 (34), 158 (33), 156 (25), 149 (17), 132 (41), 105 (100), 91 (7), 74 (22), 57 (14).

2-Phenylethyl benzoate (26): Phenylethyl alcohol (1.04 g, 8.5 mmol) was dissolved in 30 mL of dichloromethane and cooled to 0 °C. To this solution was added 1.8 mL of triethylamine (12.9 mmol, 1.5 equivalents) with a catalytic amount of DMAP. A solution of 1.2 mL of benzoyl chloride (1.45 mg, 10.3 mmol) dissolved in dichloromethane was slowly added to the cooled solution. The resulting solution was allowed to warm to room temperature and stirred for three hours. The reaction was quenched with a brine solution and the organic layer was separated and further washed with brine. The organic layer was dried with magnesium sulfate, filtered, concentrated and flash chromatographed with an eluent of 10 % ethylacetate/hexanes. This gave 1.95 g of the product as a colorless oil (86 %). ^{1}H NMR (200 MHz, $CDCl_3$, TMS) δ 8.0 (m, 2H), 7.4 (m, 8H), 4.5 (t, 2H), 3.1 (d, 2H). ^{13}C (300 MHz, $CDCl_3$) δ 166.5, 137.9, 132.9, 129.5, 128.9, 128.5, 128.3, 126.6, 118.8, 65.5, 35.2. MS (EI) m/z (%) 105 (100), 91 (48), 77 (93), 65 (38), 51 (60). MS (FAB) m/z (%) 227 (20, M+1), 132 (8), 105 (100), 77 (12), 57 (6).

2-Bromo-2-phenylethyl benzoate (28): 3-Bromo-3-phenyl-1-propanol (535 mg, 2.7 mmol) was dissolved in dichloromethane and cooled to 0 °C. Benzoyl

chloride (0.37 mL, 3.2 mmol) was added along with triethylamine (0.6 mL, 4.3 mmol) and then warmed to room temperature and stirred for 2 hours. A brine solution was added and the organic layer removed with dichloromethane. The solution was concentrated and then purified by flash chromatography with 5 % ethylacetate/hexanes to give 279 mg (63 %) of the product as a colourless oil. ^{1}H NMR (200 MHz, $CDCl_3$, TMS) δ 7.95-7.99 (m, 2H), 7.24-7.55 (m, 8H), 5.25 (m, 1H), 4.77 (m, 2H). ^{13}C (300 MHz, $CDCl_3$) δ 165.8, 138.1, 133.2, 130.5, 129.7, 129.5, 129.4, 129.3, 128.9, 128.8, 128.6, 128.5, 128.4, 128.1, 128.0, 127.8, 127.6, 125.3, 67.9, 49.9, 10.9. MS (EI) m/z (%) 225 (21), 184 (6), 171 (1), 169 (5), 105 (100), 91 (18), 77 (59), 51 (32). MS (FAB) m/z (%) 305 (2, M+1), 225 (34), 185 (140), 183 (15), 105 (100), 104 (19), 83 (22).

1-Bromo-2-phenylethanol: Phenethyl alcohol (0.5 mL, 4.2 mmol) and N-bromo succinimide (0.89 g, 5.0 mmol) were dissolved in 125 mL of carbon tetrachloride and refluxed for 5 hours in the presence of a catalytic amount of benzoyl peroxide. The supernatant was filtered off and the solvent removed. The oil was purified by flash chromatography with 20 % ethylacetate/hexanes to afford 54 mg (64 %) of a colourless oil. ^{1}H NMR (200 MHz, $CDCl_3$, TMS) δ 7.24-7.44 (m, 5H), 5.55 (t, 1H), 4.89 (m, 2H). ^{13}C (300 MHz, $CDCl_3$) δ 128.99, 128.9, 127.92, 67.5, 57.0. MS (EI) m/z (%) 202 (3), 200 (3), 171 (12), 169 (8), 122 (10), 120 (41), 103 (46), 91 (100), 77 (21), 65 (37), 51 (22), 39 (24).

Benzoic acid 2-phenyl-2-(2,2,6,6,-Tetramethylpiperdin-1-yloxy)-ethyl ester (27): The synthesis and characterization of this compound was previously been described in a proceeding chapter.

Acetic acid phenethyl ester (30): Phenethyl alcohol (900 g, 7.4 mmol) was dissolved in 50 mL of dichloromethane and cooled to 0 °C. Acetic anhydride (1.2 mL, 12.8 mmol) and triethylamine (1.3 mL, 9.3 mmol) were subsequently added and the solution was allowed to warm to room temperature and stir for two hours. A brine solution was added and the organic layer removed with dichloromethane and concentrated. The oil was purified by flash chromatography 10 % ethylacetate/hexanes to afforded 1.04 g (86 %) of the product as a colourless oil. ^{1}H NMR (200 MHz, $CDCl_3$, TMS) δ 7.18-7.33 (m, 5H), 4.26 (t, 2H), 2.89 (t, 2H), 1.99 (s, 3H). ^{13}C (300 MHz, $CDCl_3$) δ 179.8, 128.9, 128.8, 128.5, 126.5, 112.4, 64.9, 21.2. MS (EI) m/z (%) 164 (0.5), 105 (20), 104 (100), 91 (31), 65 (13), 43 (73), 40 (17).

2-Bromo-2-phenylethyl ethanoate: 2-Phenylethyl ethanoate (1.04 g, 6.33 mmol) was dissolved in 150 mL of carbon tetrachloride along with N-bromo succinimide (1.36 g, 7.6 mmol), and a catalytic amount of benzoyl peroxide then allowed to reflux overnight. The supernatant was filtered off and the solvent removed. The oil was subjected to flash chromatography with 5 % ethylacetate/hexanes to give a colourless oil as the product in 1.36 g (89 %). ^{1}H NMR (200 MHz, $CDCl_3$, TMS) δ 7.24-7.93 (m, 5H), 5.10 (t, 1H), 4.54 (m, 2H), 0.86 (s, 3H). ^{13}C (300 MHz, $CDCl_3$) δ 179.8, 128.9, 128.8, 128.5, 126.5, 112.4, 64.9, 21.2.

2-(2,2,6,6,-Tetramethylpiperdine-N-oxide)-2-phenylethyl ethanoate: 3-(2,2,6,6-tetramethylpiperdine-N-oxide)-3-phenyl-1-propanol (100 mg, 0.36 mmol) was dissolved in 15 mL of dichloromethane and cooled to 0 °C followed by the addition of triethylamine (50 μL, 0.54 mmol), acetic anhydride (72 μL, 9.51 mmol), and a catalytic amount of DMAP. The solution was allowed to warm to room temperature and stirred for 2 hours. A brine solution was added and the organic layer separated with dichloromethane and then concentrated under vacuum. The oil was purified by flash chromatography with 10 % ethylacetate/hexanes mixture to give an oil that crystallized upon standing overnight. A mass of 94 mg (82 %) of the white needles was collected. M.p. 37-39 °C. ^{1}H NMR (200 MHz, $CDCl_3$, TMS) δ 7.24-7.33 (m, 5H), 4.90 (t, 1H) 4.57 (m, 1H), 4.23 (m, 1H), 1.93 (s, 1H), 1.24-1.93 (m, 6H), 1.93 (s, 3H), 1.17 (s, 3H), 1.01 (s, 3H), 0.66 (s, 3H). ^{13}C NMR (300 MHz, $CDCl_3$) δ 170.6, 140.4, 127.8, 127.6, 127.5, 83.7, 66.1, 59.9, 40.3, 33.8, 20.7, 20.2, 16.9. MS (EI) m/z (%) 163 (100), 156 (48),126 (16), 120 (70), 105 (14), 104 (26), 91 (65), 83 (12), 77 (8), 56 (31). MS (FAB) m/z (%) 320 (34, M+1), 163 (100), 156 (83), 140 (75), 77 (16), 69 (30).

1,2-Diphenyl-2-(2,2,6,6-tetramethyl-piperidin-N-oxyl)-ethanone (20): Typical synthesis involved dissolving deoxybenzoin (250 mg, 1.28 mmol) with TEMPO oxonium salt (268 mg, 1.4 mmol) in acetonitrile with a catalytic amount of *p*-toluenesulfonic acid and stirring at room temperature till judged complete by TLC. The solution was poured into water and extracted with dichloromethane followed by column flash chromatography with 20:1 ethylacetate/hexanes to give a white solid in 85% yield (379 mg). ^{1}H NMR (200 MHz, $CDCl_3$) δ 0.78-1.55 (18H, m), 5.97 (1H, s), 7.21-7.38 (3H, m), 7.42-7.49 (5H, m), 8.04 (2H, d). ^{13}C (300 MHz, $CDCl_3$) δ 16.9, 20.2, 20.3, 33.3, 33.5, 40.2, 59.8, 59.9, 93.1, 127.2, 127.5, 128.3, 129.4, 132.8, 135.2, 137.8, 198.3. MS (EI) m/z (%) 285 (34), 283 (15), 268 (39), 196 (40), 195 (31), 178 (22), 165 (71), 156 (28), 152 (43), 122 (16), 118 (30), 105 (100), 91 (31), 77 (91),

56 (26), 51 (51). MS (FAB) m/z (%) 351 (0.9, M+1), 285 (8.3), 268 (15.9), 195 (16.8), 167 (39.7), 156 (92.9), 141 (37.5), 105 (100), 91 (39.4), 77 (93.2), 56 (87.5), 41(71.2).

N-Hydroxy-Acridine (38): 2-Nitrobenzaldehyde (5.02 g, 33.2 mmol) was dissolved in 25 mL of benzene and cooled to 0 °C where 30 mL of concentrated sulfuric acid was slowly added and then allowed to stir at room temperature. After 2 hours the orange solution turned black. After 6 days of stirring at room temperature the solution was cooled to 0 °C and 120 mL of water was added. Residual benzene was removed under reduced pressure and the product extracted with 2 N sodium hydroxide. The solid was filtered, washed with concentrated sulfuric acid, the green solid was filtered again and purified by flash chromatography with 100 % chloroform to give 169 mg (2.5 %) of the product as an orange solid. ^{1}H NMR (200 MHz, $CDCl_3$, TMS) δ 8.28 (m, 2H), 7.45 (d, 2H), 7.38 (m, 8H). ^{13}C (300 MHz, $CDCl_3$) δ 206.4, 143.9, 137.3, 134.9, 127.9, 126.7, 122.3, 116.7.

Benzyl-N-oxyl acridone (40): N-Hydroxy-acridone (40 mg, 0.19 mmol) was dissolved in dry THF and cooled to 0 °C then sodium hydride (80 mg, 2 mmol) was added. After the initial bubble formation ceased, benzyl bromide (30 μL, 0.25 mmol) was added and the solution allowed to warm to room temperature and stirred for two days. The reaction was quenched with a brine solution, the organic layer separated with dichloromethane then dried with anhydrous magnesium sulfate, and the solvent removed. The solid product was purified by flash chromatography with 20 % ethylacetate/hexanes to give 16 mg (28 %) ^{1}H NMR (500 MHz, $CDCl_3$, TMS) δ 8.44-8.48 (m, 2H), 7.68-7.74 (m, 2H), 7.58 (d, 2H), 7.24-7.34 (m, 7H), 5.6 (s, 2H). ^{13}C (500 MHz, $CDCl_3$) δ 206.4, 143.9, 137.3, 135.1, 134.9, 131.8, 129.1, 128.3, 127.9, 126.7, 122.3, 116.7. MS (EI) m/z (%) 301 (2), 290 (14), 224 (2), 210 (2), 194 (7), 180 (6), 165 (12) 151 (18), 135 (11), 111 (60), 107 (15), 105 (18), 97 (95), 91 (18), 67 (53), 55 (100), 43 (95).

N-benzyl-1,8-Naphthalimide: 1,8-Naphthalimide (438 mg, 2.22 mmol) was dissolved in 60 mL dry THF and cooled to 0 °C then sodium hydride (190 mg, 4.75 mmol) was added. Benzyl bromide (0.35 mL, 2.94 mmol) was added then the solution was refluxed for 2 days. To the yellow solution was added aqueous sodium bicarbonate and the orange solution was separated with dichloromethane, dried with anhydrous magnesium sulfate, and the solvent removed. The solid was purified by flash chromatography with 20 % ethylacetate/hexanes to give 320 mg (50 %) of the product as a yellow solid. ^{1}H NMR (200 MHz, $CDCl_3$, TMS) δ 8.50 (d, 2H), 8.08 (d, 2H), 7.66-7.50 (m, 2H), 7.21-

7.31 (m, 5H), 5.33 (s, 2H). ^{13}C NMR (300 MHz, $CDCl_3$) δ 203.6, 163.9, 137.2, 133.8, 133.6, 131.1, 131.7, 128.7, 128.0, 127.7, 127.2, 126.7, 126.5, 122.2, 43.3. MS (EI) m/z (%) 287 (48), 269 (20), 258 (14), 180 (61), 152 (21), 126 (94), 107 (36), 105 (12), 104 (39), 91 (44), 77 (100), 65 (23), 51 (45).

Benzyl-N-oxide-1,8-Naphthalimide (45): N-Hydroxy-1,8-naphthalimide, sodium salt (443 mg, 1.89 mmol) was dissolved in 50 mL of an acetone water mixture followed by the addition of benzyl bromide (0.25 mL, 2.1 mmol). After one hour the milky white precipitate that formed was filtered, dried under vacuum, and recrystalized from 99% ethanol to afford 525 mg (92%) of product as an off white solid. M.p. 130 °C. ^1H NMR (200 MHz, $CDCl_3$, TMS) δ 8.65 (d, 2H), 8.24 (d, 2H), 7.65-7.82 (m, 4H), 7.24-7.42 (m, 3H), 5.29 (s, 2H). ^{13}C NMR (300 MHz, $CDCl_3$) δ 163.9, 137.2, 133.8, 133.6, 131.1, 131.7, 128.7, 128.0, 127.7, 127.2, 126.7, 126.5, 122.2, 78.9. MS (EI) m/z (%) 197 (93), 153 (25), 127 (29), 105 (11), 91 (100), 77 (18), 65 (7), 51 (7). MS (FAB) m/z (%) 304 (63, M+1), 214 (9), 198 (9), 154 (8), 137 (9), 91 (100).

N-benzyl-2,3-Naphthalimide: 2,3-Naphthalimide (1678 mg, 0.84 mmol) was dissolved in 50 mL dry THF and cooled to 0 °C then sodium hydride (150 mg, 3.75 mmol) was added. Benzyl bromide (0.8 mL, 6.72 mmol) was added then the solution was stirred at room temperature for four days. It was then worked up with 10 % aqueous sodium bicarbonate solution and the organic layer separated with dichloromethane, dried with magnesium sulfate, and the solvent removed followed by purification by flash chromatography with 15 % ethylacetate/hexanes to afford 63 mg (26 %) of the product as a white powder. M.p. 196-204 °C. ^1H NMR (200 MHz, $CDCl_3$, TMS) δ 8.02 (q, 2H), 7.66 (q, 2H), 7.45 (t, 2H), 4.90 (s, 2H). ^{13}C NMR (300 MHz, $CDCl_3$) δ 167.7, 136.4, 135.5, 130.3, 129.1, 128.7, 127.9, 127.8, 124.7, 41.8. MS (EI) m/z (%) 287 (100), 270 (45), 241 (8), 210(5), 183 (11), 181 (55), 153 (59), 140 (12), 127 (50), 91 (22), 77 (46), 63 (12), 51 (19).

4-((1-phenylethyl)-2,2,6,6 tetramethylpiperdine-N-oxide)-2-naphthoate (52): 2-Naphthoic acid (94 mg, 0.34 mmol) was dissolved in 35 mL of dichloromethane and cooled to 0 °C followed by the addition of 1-phenyl-1-(2,2,6,6-tetramethyl-4-hydroxy-N-oxide)-ethane (85 mg, 0.44 mmol), 1,3-dicyclohexylcarbodiimide (59 mg, 0.34 mmol), and a catalytic amount of DMAP. The solution was stirred at room temperature for three hours, and the unreacted 1,3-dicyclohexylcarbodiimide removed by filtration. The solvent was removed and the solid purified by flash chromatography with 5 % ethylacetate/hexanes to give 35 mg (23 %) of product. ^1H NMR (200 MHz, $CDCl_3$, TMS) δ 8.55 (s, 1H), 7.83-7.99

(m, 4H), 7.51-7.62 (m, 2H), 7.23-7.33 (m, 5H), 5.33 (q, 1H), 4.83 (q, 1H), 1.68-2.03 (m, 4H), 1.50 (d, 3H), 1.34 (s, 3H), 1.38 (s, 3H), 1.26 (s, 3H), 0.75 (s, 3H). ^{13}C NMR (300 MHz, $CDCl_3$) δ 166.3, 145.3, 135.5, 132.5, 130.9, 129.3, 128.1, 128.0, 127.8, 127.7, 126.9, 126.7, 126.6, 125.2, 83.4, 67.6, 60.3, 44.8, 34.4, 34.1, 23.5, 21.2. MS (FAB) m/z (%) 432 (5, M+1), 221 (10), 207 (14), 155 (38), 147 (22), 140 (21), 127 (14), 124 (15), 105 (53), 77 (9), 73 (100), 56 (8).

4-(2,2,6,6 tetramethylpiperdine-N-oxide)-2-naphthoate (53): 2-Naphthoic acid (144 mg, 0.84) was dissolved in 35 mL of dichloromethane and cooled to 0 °C followed by the addition of 4-hydroxy-TEMPO (140 mg, 0.81 mmol), DCC (212 mg, 1.06 mmol), and a catalytic amount of DMAP. The solution was stirred at room temperature for three hours, and the unreacted 1,3-dicyclohexylcarbodiimide removed by filtration. The solvent was removed and purified by flash chromatography with 10 % ethylacetate/hexanes to give 165 mg (60 %) of product. MS (EI) m/z (%) 326 (5), 296 (22), 172 (55), 155 (45), 127 (80), 124 (100), 105 (12), 77 (10), 55 (15), 42 (21).

2-(4-Methylphenoxy) benzoic acid: *o*-Chlorobenzoic acid (14.08 g, 89 mmol), *p*-cresol (9.8 g, 91 mmol), copper (II) chloride (1.59 g, 16 mmol), potassium carbonate (6.8g, 49 mmol) and tris [2-(2-methoxyethoxy)ethyl]amine (TDA-1, 5 mL, 16 mmol) were charged into a 500 mL round bottom flask and refluxed for a day in toluene till the blue color faded and the water byproduct removed with the use of a Dean-Stark trap. The organic layer was washed with aqueous 10% HCl and then separated with dichloromethane. The organic layer was removed, washed with 2 N sodium hydroxide, re-acidified, then the organic oil was taken up in dichloromethane. Upon removal of the solvent, a yellow solid 5.12 g (20%) was left. ^1H NMR (200 MHz, $CDCl_3$, TMS) δ 8.18 (d, 2H), 7.44-7.49 (m, 2H), 7.20-7.27 (m, 3H), 7.00-7.17 (m, 1H), 2.36 (s, 3H). ^{13}C NMR (300 MHz, $CDCl_3$) δ 168.1, 153.2, 136.7, 134.8, 133.5, 131.8, 39.9. MS (EI) m/z (%) 228 (12), 158 (26), 156 (80), 139 (100), 121 (26), 120 (63), 111 (26), 105 (22), 91 (33), 77 (18), 75 (15), 50 (11).

2-Methyl xanthone: 2-(4-Methylphenoxy) benzoic acid (5.19 g, 18 mmol) was dissolved in 80 % sulfuric acid and heated to 100 °C for 5 hours and then cooled. The white crystals were filtered off and the precipitate was washed with sodium bicarbonate to give 2.70 g (74 %) of product. ^1H NMR (200 MHz, $CDCl_3$, TMS) δ 8.31 (d, 1H), 8.11 (s, 1H), 7.75 (t, 1H), 7.31-7.55 (m, 4H), 2.46 (s, 3H). ^{13}C NMR (300 MHz, $CDCl_3$) δ 178.1, 136.1, 134.7, 126.7, 126.0, 123.7, 117.9, 117.7, 112.8, 20.9. MS (EI) m/z (%) 210 (100), 181 (28), 162 (10), 105 (3), 91 (3), 77 (7), 76 (11), 63 (7), 40 (13).

2-Methylbromo xanthone: 2-Methyl xanthone (2.79 g, 13 mmol) and N-bromosuccinimide (2.03 g, 1 mmol) were dissolved in 115 mL of carbon tetrachloride along with a catalytic amount of benzoyl peroxide and refluxed for five hours. The supernatant was filtered off and the solvent removed. The solid was recrystallized from hexanes to give 1.82 g (49 %) of yellow crystals as product. M.p. 108-115 °C. ^{1}H NMR (200 MHz, $CDCl_3$, TMS) δ 8.33 (d, 2H), 7.70-7.79 (m, 2H), 7.24-7.51 (m, 3H), 4.59 (s, 2H). ^{13}C NMR (300 MHz, $CDCl_3$) δ 178.1, 136.1, 134.7, 126.7, 126.0, 123.7, 117.9, 117.7, 112.8, 33.0. MS (EI) m/z (%) 290 (2, M+2), 288 (2), 211 (21), 210 (100), 181 (57), 152 (20), 127 (5), 105 (13), 77 (11), 76 (17), 63 (12), 40 (13).

7.8.2 Flash Photolysis Studies

All samples for laser flash photolysis were made up using OmniSolv grade solvents in a Suprasil 7 x 7 mm^2 quartz cell and fully deaerated with argon for a minimum or 20 minutes prior to use. Solutions were made such that the absorbance at the irradiation wavelength ranged from 0.3 - 0.4. A continuous flow of 1 drop/second was used for actinometry purposes to avoid product build-up. The number of laser shots taken varied from sample, but a satisfactory number was chosen that produced a consistent maximum absorption.

The samples were excited with any of the following excitation sources dependent upon their ground state absorption. The wavelength of 266 nm was generated from the fourth harmonic of a Nd-YAG Surelite laser from Continuum with 15 mJ in 6 ns pulses. The 337 nm pulses were from a Molectron UV-24 nitrogen laser delivering ca. 7 mJ per pulse. In the case of 308 nm excitation, pulse durations were ~ 5 ns and typical pulse energies between 5 and 50 mJ from an Excimer 550 laser were also used. Generation of the 355 nm wavelength was generated from the third harmonic of a Nd-YAG Surelite laser from Continuum with 15 mJ in 6 ns pulses. Other details for the laser setup can be found elsewhere.[216,217]

Laser power measurements were done using a calibrated power meter and the roughly 30 - 40 shots were averaged. Neutral densities filters or a change in the lasing delay were employed to vary the power. The subsequent change in laser power was measured with each such change.

The digitized kinetic data from the laser flash studies is stored as a text file. The data is subsequent fit using the commercially available Kaleidagraph software the kinetic information obtained by numerical iteration of the rate equations.

7.8.3 Quantification of Bromine Production

The photoacid generator triazine-1 was purchased from Panchim. and was recrystalized twice from methanol for subsequent use as an actinometer. Sufficient amount of it was dissolved in 250 mL OmniSolv acetonitrile and 11 mL dioxane to give an absorption of 0.4 at 308 nm in a 10 x 10 mm^2 cuvette. Coumarin-6 (3.7 mg, 0.011 mmol) was also added to this solution and charged into a 250 mL flow tank covered with a layer of aluminum foil and purged with nitrogen for 35 minutes. A flow rate of 1 drop/second was used and the sample excited at 308 nm from an Excimer 505 laser. Laser excitation induces photodecomposition of the acid generator producing acid according to Scheme 7-5. The acid produced subsequently protonates the mono-cation of the Coumarin-6 dye which is monitored. Approximately 40-50 shots were taken to determine the growth the of the dye's cation monitored at 519 nm. Neutral density filters were used to decrease the laser power and monitor the subsequent effect on the cation's top absorbance. Solutions of compounds **10** and **11** were made in the same fashion and their absorbancies matched to within 5% at 308 nm to the triazine solution. The top absorbance of the dye cation was also monitored in the same fashion.

7.8.4 Quantum Yield Determination

7.8.4.1 Fluorescence (Φ_F)

Fluorescence quantum yields were determined though the use of the steady state luminescence spectrometer. The emission spectra of the compound of study and the actinometer were measured under matched optical densities at the excitation wavelength. The area under the emission curves of the two samples were calculated and the ratio gives the desired value. Selected actinometers typically fluoresce in the same region as the compounds of study.

7.8.4.2 Phosphorescence (Φ_P)

Phosphorescence quantum yields cannot be measured under the steady state approach as with the fluorescence quantum yield. Relative transient actinometry is used to determine the amount of triplet formation. One method involves monitoring the maximum absorbance of the benzophenone triplet at 525 nm versus the triplet of study over a series of laser dosages. The ratio of the

slopes gives the amount of triplet produced, providing the extinction coefficient of the studied triplet is known. An alternative is to quench the triplet of study and benzophenone with 1-methylnaphthalene within the laser pulse. The desired value is derived from the slope of the maximum absorption of the 1-methylnaphthalene triplet at 425 nm over a series of laser dosages. This approach does not require knowledge of any extinction coefficients. Regardless of the method used, actinometer and sample are optically matched within 2 % at the excitation wavelength.

7.8.4.3 Radical Actinometry

The amount of radicals produced per photon of energy absorbed is done by relative transient actinometry similar to the triplet quantum yield measurements. The actinometer **33** was chosen as it exhibits a strong absorption at 318 nm[34] and use a high quantum yield of radical generation.[153,156]

7.8.4.4 Product Quantum Yields

The choice of actinometer for these studies were either valerophenone[72,73] or dibenzylketone,[114,153,156,218-221] both of which decompose in known amounts upon irradiation to give different products. Either of these actinometers are irradiated in tandem with the sample of study at 254 nm or 300 nm and their respective product concentrations are determined analytical by HPLC (*vide infra*). Typical conversions did not surpass 8 % and only 2 lamps were used to increase the irradiation times. Quantum yield determination of the initiators were done with the cross-over technique[123] which employs an external nitroxide trap. The concentration of the trap was kept below 0.4 mM for irradiations at 254 nm to avoid direct excitation of the nitroxide. Special care was taken not to exhaust the nitroxide trap by over irradiation. Higher concentrations of the nitroxide were use for irradiations at longer wavelengths.

7.8.5 Photopolymerization

Preliminary photopolymerization experiments of **6-8** were done in bulk with 7 mm Pyrex cuvettes in which the solutions were added, purged with nitrogen for 20 minutes and sealed. The samples were irradiated in a merry-go-round type photoreactor at either 300 or 350 nm with 8 lamps where the temperature was

maintained at 30 °C. The residual monomer was removed under reduced pressure and the samples dissolved in THF and characterized as described below.

Photopolymerization of **8** was also done in bulk with methylmethacrylate and styrene. The prepared samples were placed in 7 mm glass tube about 5 cm in height and subjected to three cycles of freeze-pump-thaw. The samples of 0.2 mL in volume were then flame sealed under vacuum. Irradiation was done at 350 nm with 6 lamps placed horizontally at the temperature regulated between 58-63 °C with an aluminum heating block and circulating fan. At specific intervals the samples were removed, cracked opened, and subjected to the analytical methods described below.

7.8.6 Thermal Polymerization

Typical polymerization conditions consisted of dissolving the unimolecular initiator (**31**) in styrene and transferring 0.2 mL to 7 mm glass tubing 5 cm in height. The samples were then subjected to three cycles of free-pump-thaw and flame sealed under reduced pressure. They were subsequently placed in a thermostated aluminum block at 125 °C and heated for 12 - 16 hours. The samples were then cooled and the vials cracked opened and the samples characterized. For preparative work, the target degree of polymerization was set at DP = 5 and the various oligomers separated by means of a preparative recycling HPLC. The recycling HPLC used consisted of a L9-908 instrument from Japan Analytical Industry Co. Ltd. equipped with a Jordi Gel DVB 100 Å column 500 mm in length and ID of 22 mm. Chloroform was used as the eluent and each oligomer of discrete length was separated and removed after each cycle lasting approximately 45 minutes in length and was detected in combination of with RI detector and UV absorption at 254 nm.

7.8.7 Polymer Characterization

After polymerization, the solvent was removed under reduced pressure and the residual monomer removed under high vacuum. THF was used to dissolve the gel like polymers and methanol was slowly added. The white precipitate was filtered, and thoroughly dried. The samples were then weighted and solution concentrations of 2.5 mg/mL were used for GPC analyses.

A volume of 100 µL was injected onto a Waters Styragel® HR3 size exclusion column using stabilized THF as the mobile phase at a flow of 0.5 mL/minute.

The polymers were detected by a Varian refractive index detector and the retention times compared to polystyrene molecular weight standards. The molecular weights (M_w and M_n) and polydispersities (PD) were calculated with an in-house program written in the LabVIEW environment and referenced to the calibration curve according to standard techniques.[222,223]

Some of the polymers were also characterized by standard NMR techniques using $CDCl_3$ as solvent.

7.8.8 Spectroscopic and Analytical Methods

7.8.8.1 Spectroscopy

Absorption spectra were recorded on a Varian Cary 1E spectrophotometer with 10 x 10 mm^2 Suprasil cuvettes and zeroed against the appropriate solvent. Phosphorescence and fluorescence measurements were done using a Perkin-Elmer LS-50 luminescence spectrometer with the excitation energy close to that used for laser flash experiments. For excitation measurements, the scan speed selected was 240 nm/minute with the emission and excitation slits set to 5.0. The same parameters were also used for emission measurements. Suprasil quartz 10 x 10 mm^2 cuvette cells with four windows were used for fluorescence measurements. The samples were purged with nitrogen for a minimum of 20 minutes prior to use and sealed. Phosphorescence measurements were done in a solid matrix of either methylcyclohexane or 4:1 methanol/ethanol at 77 K in a quartz 7 mm NMR tube.

NMR studies were done with $CDCl_3$ as solvent unless otherwise stated and the ^1H spectra collected on a Varian Gemini 200 MHz instrument. ^{13}C spectra were collected on a Varian 300 MHz instrument.

7.8.8.2 HPLC

An autosampler HPLC equipped with a diode array detector from Varian was used for product and concentration studies. The column used for all analyses was a SB-C18 Zorbax reverse phase column. The eluent of choice was 85 % methanol and 15 % water with a flow rate of 0.5 mL/min and subsequently increased to 1.5 mL/min after 12 minutes of run time. The product concentrations and identification were done against authentic samples and

characterized by their respective absorption spectra. LC-MS analyses were done using the same column and same eluent with the exception of 0.1 % formic acid was used in the aqueous solvent. MS detection was done using an ESI coupled spectrometer from Varian.

Thermal decomposition studies involving **20** were done with the same HPLC setup with the exception of solvent composition. The ideal mixture was 55% methanol and 45 % water with a flow rate of 0.5 mL/min.

7.8.8.3 Benzoin Studies

Typical experimental conditions for the thermal investigation of **20** consisted of refluxing it in decalin (bp 189 °C) overnight in the presence of one of the two following reagents: two equivalents of freshly distilled 1,4-cyclohexadiene or 10 mole percent amount of *p*-toluene-sulfonic acid (*p*TsOH). These were added prior to refluxing followed by deaeration of the solution with nitrogen for 20 minutes. Refluxing in an inert solvent such as acetonitrile had no effect as its boiling point is most likely too low for the energy required to induce C-O or N-O bond cleavage.[123] An aliquot of the reaction mixture was analyzed by reverse phase analytical HPLC and the products were identified by their retention times and absorption spectra compared to subsequently injected authentic samples. The HPLC response factors of the products were also calibrated against authentic samples.

7.9 Chapter References

1. Allen, N. S.; Catalina, F.; Green, P. N.; Green, W. A. *Eur. Polym. J.* **1986**, *22*, 49-56.
2. Barton, J.; Capek, I.; Krdlovic, P. *J. Polym. Chem., Phys. Chem. Ed.* **1975**, 2671-2680.
3. Catalina, F.; Tercero, J. M.; Peinado, C.; Sastre, R.; Mateo, J. L.; Allen, N. S. *J. Photochem. Photobiol. A.* **1989**, *50*, 249-258.
4. Clark, S. C.; Hoyle, C. E.; Jönsson, S.; Morel, F.; Decker, C. *Polymer* **1999**, *40*, 5063-5072.
5. Kuhlmann, R.; Schnabel, W. *Angew. Makromol. Chem.* **1977**, *57*, 195-210.
6. Lecamp, L.; Youssef, B.; Bunel, C.; Lebaudy, P. *Polymer* **1999**, *40*, 1403-1409.
7. Rudolph, H.; Rosenkranz, H. J.; Heine, H.-G. Aromatic Ketones as Initiators for Photopolymerizations. In *Polymerization of Polycondensation Processes*; Platzer, N. A. J., Ed.; John Wiley and Sons:, 1975; Vol. 26; 157-164.
8. Yang, J.; Zeng, Z.; Chen, Y. *J. Polym. Sci. A. Polym. Chem.* **1998**, *69*, 2563-2570.
9. Stevens, M. P. *Polymer Chemistry, An Introduction*, 2nd ed.; Oxford University Press: New York, 1990, pp 633.
10. Loutfy, R. O.; Winnik, M. A. *J. Phys. Chem.* **1978**, *82*, 1304-1307.
11. *Photophysical and Photochemical Tools in Polymer Science: Conformation; Dynamics, Morphology*; Winnik, M. A., Ed.; D. Reidel Publishing Company: Boston, 1985; Vol. 182, pp 642.
12. Winnik, M. A.; Lemire, A.; Saunders, D. S.; Kwong, C. *J. Am. Chem. Soc.* **1976**, *98*, 2000-2002.
13. Turro, N. J. *Modern Molecular Photochemistry*; University Science Books: Sausalito, 1991, pp 628.

14. Andrzejewska, E.; Hug, G. L.; Andrzejewski, M.; Marciniak, B. *Macromolecules* **1999**, *32*, 2173-2179.

15. Lougnot, D. J.; Fouassier, J. P. *J. Polym. Sci. Part A: Polym. Chem.* **1988**, *26*, 1021-1033.

16. Lissi, E. A.; Encinas, M. V. Representative Kinetic Behavior of Selected Reaction Intermediates: Triplet States. In *Handbook of Organic Photochemistry*; Scaiano, J. C., Ed.; CRC Press, Inc.: Boca Raton, 1989; Vol. 2; 111-176.

17. Topp, M. R. *Chem. Phys. Lett.* **1975**, *32*, 144-149.

18. Zhang, W.; Kesheng, F.; Wu, X.; Martin, D.; Neckers, D. C. *J. Org. Chem.* **1999**, *64*, 458-463.

19. Sarker, A. M.; Lungu, A.; Mejiritski, A.; Kaneko, Y.; Neckers, D. C. *J. Chem. Soc., Perkin Trans. 2* **1998**, *2*, 2315-2321.

20. Hu, S.; Sarker, A. M.; Kaneko, Y.; Neckers, D. C. *Macromolecules* **1998**, *31*, 6476-6480.

21. Hoyle, C. E.; Viswanathan, K.; Clark, S. C.; Miller, C. W.; Nguye, C.; Jönsson, S.; Shao, L. *Macromolecules* **1999**, *32*, 2793-2795.

22. Kwon, T. S.; Ochiai, H.; Kondo, S.; Takgi, K.; Kunisada, H.; Yuki, Y. *Polym. Journal* **1999**, *31*, 411-417.

23. Nakamura, T.; Suyama, S.; Busfield, W. K.; Jenkins, I. D.; Rizzardo, E.; Thang, S. H. *Polymer* **1999**, *40*, 1395-1402.

24. Scaiano, J. C.; Connolly, T. J.; Mohtat, N.; Pliva, C. N. *Can. J. Chem.* **1997**, *75*, 92-97.

25. Abdel-Mottaleb, M. S. A.; Loutfy, R. O.; Lapouyade, R. *J. Photochem. Photobiol. A. Chem.* **1989**, *48*, 87.

26. Abdel-Mottaleb, M. S. A.; Antonious, M. S.; Ali, M. M. A.; Ismail, L. F. M.; El-Sayed, B. A.; Sherief, A. M. K. *Proc. Indian Acad. Sci.* **1992**, *104*, 185.

27. Osman, A.-M.; Youssef, M. S. K. *Spectrochim. Acta* **1981**, *37A*, 811.

28. Pohlers, G.; Scaiano, J. C. *Chem. Mater.* **1997**, *9*, 3222-3230.
29. McGimpsey, W. G. Spectroscopic Properties of Excited Reaction Intermediates and Upper Excited States in Solution. In *Handbook of Organic Photochemistry*; Scaiano, J. C., Ed.; CRC Press: Boca Raton, 1989; Vol. 1; Chapter 18.
30. Hadel, L. M. Laser Flash Photolysis. In *Handbook of Organic Photochemistry*; Scaiano, J. C., Ed.; CRC Press: Boca Raton, Florida, 1989; Vol. I; 279-292.
31. Wintgens, V.; Johnston, L. J.; Scaiano, J. C. *J. Am. Chem. Soc.* **1988**, *110*, 511-517.
32. Khadem, H. S. *Carbohydrate Chemistry: Monosaccharides and Their Oligomers*; Academic Press, Inc.: New York, 1988, pp 256.
33. Davidson, E. A. *Carbohydrate Chemistry*; Hot, Rinehardt and Winston, Inc.: New York, 1967, pp 441.
34. Chatgilialoglu, C. Electronic Absorption Spectra of Free Radicals. In *Handbook of Organic Photochemistry*; Scaiano, J. C., Ed.; CRC Press: Boca Raton, Florida, 1989; Vol. II; 3-11.
35. Pohlers, G.; Scaiano, J. C.; Step, E.; Sinta, R. *J. Am. Chem. Soc.* **1999**, *121*, 6167-6175.
36. Beckwith, A. J.; Bowry, V. W.; Ingold, K. U. *J. Am. Chem. Soc.* **1992**, *114*, 4983-4992.
37. Bowry, V. W.; Ingold, K. U. *J. Am. Chem. Soc.* **1992**, *114*, 4992-4996.
38. Skene, W. G.; Scaiano, J. C.; Listigovers, N. A.; Kazmaier, P. E.; Georges, M. K. *Macromolecules* **2000**, *33*, 5065-5072.
39. Lambert, J. B.; Shurvell, H. F.; Ligtner, D.; Cooks, R. G. *Introduction to Organic Spectroscopy*; Macmillan Publishing Company: New York, 1987, pp 454.
40. Alfassi, Z. B.; Huie, R. E.; Mittal, J. P.; Neta, P.; Shoute, L. C. T. *J. Phys. Chem.* **1993**, *97*, 9120-9123.

41. Lindeman, T. G.; Wiesenfeld, J. R. *Chem. Phys. Lett.* **1977**, *50*, 364-367.
42. Maric, D.; Burrows, J. P.; Moortgat, G. K. *J. Photochem. Photobiol. A: Chem.* **1994**, *83*, 179-192.
43. Mohan, H.; Mittal, J. P. *J. Photochem. Photobiol. A. Chem.* **1999**, *124*, 119-125.
44. Nagarajan, V.; Fessenden, R. W. *J. Phys. Chem.* **1985**, *89*, 2330-2335.
45. Scaiano, J. C.; Barra, M.; Krzywinski, M.; Sinta, R.; Calabrese, G. *J. Am. Chem. Soc.* **1993**, *115*, 8340-8344.
46. Shoute, L. C. T.; Neta, P. *J. Phys. Chem.* **1990**, *94*, 2447-2453.
47. Treinin, A.; Hayon, E. *J. Am. Chem. Soc.* **1975**, *97*, 1716-1721.
48. Bromberg, A.; Meisel, D. *J. Phys. Chem.* **1985**, *89*, 2507-2513.
49. Mittal, L., J.; Mittal, J. P. *Radiat. Phys. Chem.* **1986**, *28*, 363-371.
50. Carmichael, I.; Helman, W. P.; Hug, G. L. *J. Phys. Chem. Ref. Data* **1987**, *16*, 239-260.
51. Carmichael, I.; Hug, G. L. *J. Phys. Chem. Ref. Data* **1986**, *15*, 1-250.
52. Tsentalovich, Y. P.; Kulik, L. V.; Gritsan, N. P.; Yurkovskaya, A. V. *J. Phys. Chem. A* **1998**, *102*, 7975-7980.
53. Mekarbane, P. G.; Tabner, B. J. *Macromolecules* **1999**, *32*, 3620-3625.
54. Berk, S. C.; Knochel, P.; Yeh, M. C. P. *J. Am. Chem. Soc.* **1988**, *53*, 5789-5791.
55. Nagashima, T.; Curran, D. P. *Synlett.* **1996**, *4*, 330-332.
56. Braslau, R.; Burrill, L. C. I.; Siano, M.; Naik, N.; Howden, R. L.; Mahal, L. K. *Macromolecules* **1997**, *30*, 3445-6450.
57. Stipa, P.; Greci, L.; Carloni, P.; Damiani, E. *Polymer Degrad. Stab.* **1997**, *55*, 323-327.
58. Yamada, B.; Miura, Y.; Nobukane, Y.; Aota, M. "Styrene Polymerization Mediated by Five-Membered Cyclic Nitroxides"; Controlled Radical Polymerization, 1998, San Francisco, CA.
59. Root, K. S.; Hill, C. L.; Lawrence, L. M.; Whitesides, G. M. *J. Am. Chem. Soc.* **1989**, *111*, 5405-5412.

60. Doa, J.; Benoit, D.; Hawker, C. J. *J. Polym. Sci. A. Polym. Chem.* **1998**, *36*, 2161-2167.

61. Matyjaszewski, K.; Woodworth, B. E.; Zhang, X.; Gaynor, S. G.; Metzner, Z. *Macromolecules* **1998**, *31*, 5955-5957.

62. Stain-Aman, E.; Serve, D. *New J. Chem.* **1989**, *13*, 121-130.

63. Kobayashi, S.; Iwata, S.; Abe, M.; Shoda, S.-i. *J. Am. Chem. Soc.* **1995**, *117*, 2187-2200.

64. Semmelhack, M. F.; Chou, C. S.; Cortes, D. A. *J. Am. Chem. Soc.* **1983**, *105*, 4492-4494.

65. Yamauchi, Y.; Maeda, H.; Ohmori, H. *Chem. Pharm. Bull.* **1996**, *44*, 1021-1025.

66. Yoshida, E.; Takata, T.; Endo, T. *Macromolecules* **1992**, *25*, 7282-7285.

67. Bordwell, F. G.; Liu, W.-Z. *J. Am. Chem. Soc.* **1996**, *118*, 10819-10823.

68. Hunter, D. H.; Racok, J. S.; Rey, A. W.; Ponce, Y. Z. *J. Org. Chem.* **1988**, *53*, 1278-1281.

69. Blough, N. V.; Simpson, D. J. *J. Am. Chem. Soc.* **1988**, *110*, 1915-1917.

70. Rychnovsky, S. D.; Vaidyanathan, R.; Beauchamp, T.; Lin, R.; Farmer, P. J. *J. Org. Chem.* **1999**, *64*, 6745-6749.

71. Baldovi, M. V.; Cozens, F. L.; Fornes, V.; Garcia, H.; Scaiano, J. C. *Chem. Mater.* **1996**, *8*, 152-160.

72. Barltrop, J. A.; Coyle, J. D. *J. Am. Chem. Soc.* **1968**, *90*, 6584-6588.

73. Wagner, P. J. *Tetrahedron Lett.* **1967**, *1*, 1753-1756.

74. Berger, K. C.; Meyerhoff, G. Propagation and Termination Constants in Free Radical Polymerization. In *Polymer Handbook*; 3rd ed.; Brandrup, J., Immergut, E. H., Eds.; John Wiley & Sons: New York, 1989; .

75. Kuhlmann, R.; Schnabel, W. *Polymer* **1976**, *17*, 422.

76. Lissi, E. A.; Encina, M. V. *J. Polym. Sci., Polym. Chem. Ed.* **1979**, *17*, 2791-2803.

77. Devonport, W.; Michalak, L.; Malmstrom, E.; Mate, M.; Kurdi, B.; Hawker, C. J. *Macromolecules* **1997**, *30*, 1929-1934.

78. Georges, M. K.; Veregin, R. P. N.; Kazmaier, P. M.; Hamer, G. K. *Polym. Prepr.* **1994**, *38*, 870-871.

79. Georges, M. K.; Kee, R. A.; Veregin, R. P. N.; Hamer, G. K.; Kazmaier, P. M. *J. Phys. Org. Chem.* **1995**, *8*, 301-305.

80. Connolly, T. J.; Scaiano, J. C. *Tetrahedron Lett.* **1997**, *38*, 1133-1136.

81. Timpe, H.-J.; Kronfeld, K.-P. *J. Photochem. Photobiol. A.* **1989**, *46*, 253-267.

82. Ghosh, A.; Biswas, S.; Banerjee, A. N. *J. Macromol. Sci. Chem.* **1983**, *A20*, 927-940.

83. Sandner, M. R.; Osborn, C. L.; Trecker, D. J. *J. Polym. Sci.* **1972**, *10*, 3173.

84. Baumann, H.; Lammel, U.; Timpe, H.-J. *Eur. Polym. J.* **1986**, *22*, 305.

85. Schafer, O.; Allan, M.; Haselbach, E.; Davidson, R. S. *Photochem. Photobiol.* **1989**, *50*, 717-719.

86. Chateauneuf, J.; Lusztyk, J.; Ingold, K. U. *J. Am. Chem. Soc.* **1988**, *110*, 2877-2885.

87. Mar, A.; Winnik, M. A. *Chem. Phys. Lett.* **1981**, *77*, 73-76.

88. Winnik, M. A.; Wang, G. C.; Schaefer, H. J.; Schmidt, W. *J. Photochem.* **1986**, *34*, 281-287.

89. Wang, G. C.; Winnik, M. A.; Schaefer, H. J.; Schmidt, W. *J. Photochem.* **1986**, *33*, 291-296.

90. Winnik, M. A. *Chem. Phys. Lett.* **1977**, *46*, 283-289.

91. Wang, G.; Chen, L.; Winnik, M. A. *Macromolecules* **1990**, *23*, 381-287.

92. Mar, A.; Winnik, M. A. *J. Am. Chem. Soc.* **1985**, *107*, 5376-5382.

93. Bensasson, R.; Gramain, J.-C. *J. Chem. Soc., Faraday I* **1980**, *76*, 1801-1810.

94. Johnston, L. J.; Tencer, M.; Scaiano, J. C. *J. Org. Chem.* **1986**, *51*, 2806-2808.

95. Scaiano, J. C. *Chem. Phys. Lett.* **1981**, *79*, 441-443.

96. Bailie, A. G., Jr.; Wilson, T. D.; O'Brien, R. K.; Beebe, J. M.; Stuart, J. D.; McCosh-Lilie, E. J.; Hill, D. W. *J. Chromatogr. Sci* . **1982**, *20*, 466-470.

97. Hill, D. J. T.; O'Donnell, J. J.; O'Sullivan, P. W. *Prog. Polym. Sci.* **1982**, *8*, 215-276.

98. Cais, R. E.; Hill, D. J.; O'Donnell, J. H. *J. Macromol. Sci ., Chem.* **1982**, *A17*, 1437-1467.

99. Wedzicha, B. L.; Hill, D.; Cockshott, J. B. *J. Sci . Food Agric.* **1982**, *33*, 306-308.

100. Hankin, L.; Hill, D. E. *Soil Sci* . **1982**, *134*, 193-197.

101. Watkins, D. M.; Fox, M. A. *J. Am. Chem. Soc.* **1994**, *116*, 6441-6442.

102. Stewart, G. M.; Fox, M. A. *Chem. Mater.* **1998**, *10*, 860-863.

103. Stewart, G. M.; Fox, M. A. *J. Am Chem. Soc.* **1996**, *118*, 4354-4360.

104. Nowakowska, M.; B., W.; Guillet, J. E. *J. Am. Chem. Soc.* **1988**, *21*, 3430-3437.

105. Li, W.; Fox, M. A. *J. Am. Chem. Soc.* **1996**, *118*, 11752-11758.

106. Kiserow, D. J.; Itoh, Y.; Webber, S. E. *Macromolecules* **1997**, *30*, 2934-2940.

107. Kiserow, D. J.; Itoh, Y.; Webber, S. E. *Macromolecules* **1996**, *29*, 7847-7852.

108. Hong, B.; Fox, M. A. *Can. J. Chem.* **1995**, *73*, 2101-2110.

109. Hargreaves, J. S.; Webber, S. E. *Can. J. Chem.* **1985**, *63*, 1320-1327.

110. de Padua, A.; Miranda-Neto, J. A.; Xavier, I. M. J.; Moraer, F. *J. Math. Chem.* **1997**, *22*, 97-106.

111. Batchelder, T. L.; Fox, R. J. I.; Meier, M. S.; Fox, M. A. *J. Org. Chem.* **1996**, *61*, 4206-4209.

112. Bar-Haim, A.; Klafter, J.; Kopelman, R. *J. Am. Chem. Soc.* **1997**, *119*, 6197-6198.

113. Carmichael, I.; Hug, G. L. Spectroscopy and Intramolecular Photophysics of Triplet States. In *Handbook of Organic Photochemistry*; Scaiano, J. C., Ed.; CRC Press: Boca Raton, Florida, 1989; Vol. I; 369-403.

114. Lewis, F. D.; Lauterbach, R. T.; Heine, H.-G.; Hartmann, W.; Rudolph, H. *J. Am. Chem. Soc.* **1975**, *97*, 1519-1525.

115. Heine, H.-G. *Justus Liebigs Ann. Chem.* **1970**, *56*, 735.

116. Heine, H.-G.; Rosenkranz, H. J.; Rudolph, H. *Angew. Chem. Int. Ed. Engl.* **1972**, *11*, 974.

117. Rabek, J. J. *Mechanisms of Photophysical Processes and Photochemical Reactions in Polymers*; John Wiley & Sons: New York, 1987, pp 756.

118. Faucitano, A.; Buttafava, A.; Martinotti, F. *J. Phys. Chem.* **1984**, *8*, 1187-1190.

119. Zaremskii, M.; Stoyachenko, Y.; Plutalova, A.; Lachinov, M.; Golubev, V. *Vysokomol. Soed. Ser. A & Ser. B* **1999**, *41*, 398-398.

120. Casal, H. L.; Werstiuk, N. H.; Scaiano, J. C. *J. Org. Chem.* **1984**, *49*, 5214-5217.

121. Step, E. N.; Buchachenko, A. L.; Turro, N. J. *J. Am. Chem. Soc.* **1994**, *116*, 5462-5466.

122. Hunter, D. H.; Barton, D. H. R.; Motherwell, W. J. *Tetrahedron Lett.* **1984**, *25*, 603-606.

123. Skene, W. G.; Belt, S. T.; Connolly, T. J.; Hahn, P.; Scaiano, J. C. *Macromolecules* **1998**, *31*, 9103-9105.

124. Lusztyk, J.; Kanabus-Kaminska, J. M. Representative Kinetic Behavior of Selected Reaction Intermediates: Free Radicals. In *Handbook of Organic Photochemistry*; Scaiano, J. C., Ed.; CRC Press Inc.: Boca Raton, 1989; Vol. II; 177-209.

125. Kothe, T.; Marque, S.; Martschke, R.; Popov, M.; Fischer, H. *J. Chem. Soc., Perkin Trans. 2* **1998**, *7*, 1553-1559.

126. Fischer, H. *J. Am. Chem. Soc.* **1986**, *108*, 3925-3927.

127. Hawker, C. J. *J. Am. Chem. Soc.* **1994**, *116*, 11185-11186.

128. Moffat, K. A.; Hamer, G. K.; Georges, M. K. *Macromolecules* **1999**, *32*, 1004-1012.

129. Schmidt-Naake, G.; Drache, M.; Taube, C. *Angew. Makromol. Chem.* **1999**, *265*, 62-68.

130. Veregin, R. P. N.; Georges, M. K.; Kazmaier, P. M.; Hamer, G. K. *Macromolecules* **1993**, *26*, 5316-5320.

131. Georges, M. K.; Veregin, R. P. N.; Kazmaier, P. M.; Hamer, G. K. *Macromolecules* **1993**, *26*, 2987-2988.

132. Zhu, Y.; Li, I. Q.; Howell, B. A.; Priddy, D. B. "Nitroxide-Mediated Radical Polymerization: End-Group Analysis"; Controlled Radical Polymerization, 1998, San Francisco, CA.

133. Fukuda, T.; Goto, A.; Ohno, K.; Tsujii, Y. "Mechanism and Kinetics of Nitroxide-Controlled Free-Radical Polymerization"; Controlled Radical Polymerization, 1998, San Francisco, CA.

134. Goto, A.; Fukuda, T. *Macromolecules* **1999**, *32*, 618-623.

135. Coyle, J. D.; Kingston, D. H. *J. Chem. Soc., Perkin Trans 2.* **1976**, 1475-1479.

136. Baba, H.; Kitamura, M. *J. Mol. Spectrosc.* **1972**, *41*, 302-309.

137. Acuña, A. U.; Ceballos, A.; Molera, M. J. *Anal. Quim.* **1977**, *73*, 1262-1265.

138. Acuña, A. U.; Ceballos, A.; Garcia Dominguez, J. A.; Molera, M. J. *Anal. Quim.* **1975**, *71*, 22-27.

139. Coyle, J. D.; Kingston, D. H. *Tetrahedron Lett.* **1975**, *12*, 1021-1024.

140. Viegut, T. R.; Pisano, P. J.; Mueller, J. A.; Kenney, M. J.; Hossenlopp, J. M. *Chem. Phys. Lett.* **1992**, *195*, 568-573.

141. Ouissi, D.; Mokrini, A.; Chamoarro, E.; Esplugas, S. *Environ. Tech.* **1998**, *19*, 955-960.

142. Wagner, P. J.; Thomas, M. J.; Harris, E. *J. Am. Chem. Soc.* **1976**, *98*, 7675-7679.

143. Chateauneuf, J.; Lusztyk, J.; Ingold, K. U. *J. Org. Chem.* **1988**, *53*, 1629-1632.

144. Poston, P. E.; Harris, J. M. *J. Am. Chem. Soc.* **1990**, *112*, 644-650.

145. Arnold, D. R.; Bolton, J. R.; Pedersen, J. A. *J. Am. Chem. Soc.* **1972**, *94*, 2872-2874.

146. Murov, S. L. ; Dekker, Marcel: New York, 1973, pp 272.

147. Khan, J.; Casey, D.; Linschitz, H.; Cohen, S. G. *J. Org. Chem.* **1991**, *56*, 6080-6083.

148. Darmanyan, A. P.; Foote, C. S. *J. Phys. Chem.* **1993**, *97*, 5032-5035.

149. Eaton, D. F. Luminescence Spectroscopy. In *Handbook of Organic Photochemistry*; Scaiano, J. C., Ed.; CRC Press: Boca Raton, Florida, 1989; Vol. I; 231-239.

150. Lambert, J. B.; Shurvell, H. F.; Verbit, L.; Cooks, R. G.; Stout, G. H. *Organic Structural Analysis*; Macmillan Publishing Co., Inc.: New York, 1976, pp 596.

151. Stroh, C.; Romero, F. M.; Kyritsakas, N.; Catala, L.; Turek, P.; Ziessel, R. *J. Mater. Chem.* **1999**, *9*, 875-882.

152. Shibamoto, T. "Photochemistry of a Major Essential Oil Constituent, Benzyl Benzoate"; 4th International Flavor Conference, 1985, Rhodes, Greece.

153. Skene, W. G.; Scaiano, J. C. **2000**, Manuscript in preparation.

154. Skene, W. G.; Scaiano, J. C. *Polym. Prepr.* **2000**, *41*, 163-164.

155. Wojárovits, L.; Takács, E. *Res. Chem. Intermed.* **1999**, *25*, 275-283.

156. Baretz, B. H.; Turro, N. J. *J. Am. Chem. Soc.* **1983**, *105*, 1309-1316.

157. Gould, I. R.; Baretz, B. H.; Turro, N. J. *J. Phys. Chem.* **1987**, *91*, 925-929.

158. Gerlock, J. L.; Zacmanidis, P. J.; D.R., B.; Simpson, D. J.; Blough, N. V.; Salmeen, I. T. *Free Rad. Res. Comms.* **1990**, *10*, 119-121.

159. Moad, G.; Shipp, D. A.; Smith, T. A.; Solomon, D. H. *Macromolecules* **1997**, *30*, 7627-7630.

160. Green, S. A.; Simpson, D. J.; Zhou, G.; Ho, P. S.; Blough, N. V. *J. Am. Chem. Soc.* **1990**, *112*, 7337-7346.

161. Chateauneuf, J.; Lusztyk, J.; Ingold, K. U. *J. Am. Chem. Soc.* **1988**, *110*, 2886-2893.

162. Avila, D. V.; Lusztyk, J.; Ingold, K. U. *J. Am. Chem. Soc.* **1992**, *114*, 6576-6577.

163. Avila, D. V.; Ingold, K. U.; Di Nardo, A. A.; Zerbetto, F.; Zgierski, M. Z.; Lusztyk, J. *J. Am. Chem. Soc.* **1995**, *117*, 2711-2718.

164. Brede, O.; David, F.; Steenken, S. *J. Photochem. Photobiol., A* **1996**, *97*, 127-131.

165. Brede, O.; David, F.; Steenken, S. *J. Chem. Soc., Perkin Trans. 2* **1995**, 23-32.

166. Brede, O.; David, F.; Steenken, S. *J. Inf. Rec. Mater.* **1994**, *21*, 613-614.

167. Hilborn, J. W.; Pincock, J. A. *Can. J. Chem.* **1992**, *70*, 992-999.

168. Ghoshal, S. K.; Sarkar, S. K.; Misra, T. N.; Kastha, G. S. *Chem. Phys. Lett.* **1979**, *62*, 503506.

169. Gilbert, A.; Baggott, J. *Essentials of Molecular Photochemistry*; CRC Press: Boca Raton, 1991, pp 229-284.

170. El-Sayed, M. A. *J. Chem. Phys.* **1963**, *38*, 2834.

171. Math, N. N.; Mulla, A. D.; Savadtti, M. I. *Pramana* **1991**, *36*, 429-434.

172. Mulla, A. D.; Math, N. N.; Savadatti, M. I. *Pramana* **1991**, *36*, 639-645.

173. Kikuchi, K. *Triplet-Triplet Absorption Spectra*; Bunshin Publishing Co.: Tokyo, 1989, pp 189.

174. Timpe, H.-J.; Kronfeld, K.-P. *Acta Polym.* **1991**, *42*, 197-203.

175. Timpe, H. J.; Kronfeld, K. P.; Lammel, U.; Fouassier, J. P.; Lougnot, D. J. *J. Photochem. Photobiol., A* **1990**, *52*, 111-122.

176. Chakrabarti, K. P. *J. Polym. Sci., Polym. Chem. Ed.* **1975**, *13*, 2051-2059.

177. Carloni, P.; Greci, L.; Mar'in, A.; Stipa, P. *Polym. Degrad. Stab.* **1994**, *44*, 201-209.

178. Neugebauer, F. A.; Bamberger, S. *Chem. Ber.* **1974**, *107*, 2362-2382.

179. Rozantsev, E. G.; Sholle, V. D. *Synthesis* **1971**, 401-414.

180. Rozantsev, E. G.; Kagan, E. S.; Sholle, V. D.; Ivanov, V. B.; Smirnov, V. A. Discovery, Chemistry, and Application of Hindered Amines. In *Polymer Stabilization and Degradation*; Klemchuk, P. P., Ed.; American Chemical Society: Washington, 1985; Vol. 280; 1-10.

181. Brik, M. E. *Tetrahedron Lett.* **1995**, *36*, 5519-5522.

182. Murray, R. W.; Singh, M. *Tetrahedron Lett.* **1988**, *29*, 4677-4680.

183. Cella, J. A.; Kelley, J. A.; Kenehan, E. F. *Tetrahedron Lett.* **1975**, *33*, 2869-2872.

184. White, E. H.; Roswell, D. F.; Dupont, A. C.; Wilson, A. A. *J. Am. Chem. Soc.* **1987**, *109*, 5189-5196.

185. Acheson, R. M.; Adcock, B.; Glover, G. M.; Sutton, L. E. *J. Chem. Soc.* **1960**, 3367-3371.

186. Morey, S.; Weigmann, H.-J.; Rosenfeld, A. *Chem. Phys. Lett.* **1985**, *115*, 201-204.

187. Niizuma, S.; Kawata, H. *Bull. Chem. Soc. Jap.* **1993**, *66*, 1627-1632.

188. Miyashita, Y.; Niizuma, S.; Kokubun, H.; Koizumi, M. *Bull. Chem. Soc. Jap.* **1973**, *46*, 3373-3377.

189. Fushimi, K.; Kikuchi, K.; Kokubun, H. *J. Photochem.* **1976**, *5*, 457-468.

190. Ortica, F.; Scaiano, J. C.; Pohlers, G. *Chem. Mater.* **1999**, *12*, 414-420.

191. Thompson, L. F.; Willson, C. G.; Bowden, M., J. *Introduction to Microlithography*, 2nd ed.; American Chemical Society: Washington, DC, 1994, pp 527.

192. Shirai, M.; Wakinaka, S.; Ishida, H.; Tsunooka, M.; Tanaka, M. *J. Polym. Sci., Part C: Polym. Lett.* **1986**, *24*, 119-124.

193. Gassman, P. G.; Campbell, G. A. *J. Chem. Soc.: Chem. Comm.* **1971**, 1437-1438.

194. Cadogan, J. I. G.; Rowley, A. G. *J. Chem. Soc., Perkin Trans. 1* **1975**, 1069-1071.

195. Kasal, P. H. *J. Am. Chem. Soc.* **1992**, *114*, 2875-2883.

196. Iwahama, T.; Sakaguchi, S.; Ishii, Y. *J. Chem. Soc., Chem. Comm.* **1999**, 727-728.

197. Rychnovsky, S. D.; Vaidynanathan, R. *J. Org. Chem.* **1999**, *64*, 310-612.

198. Edafiogho, I. O.; Scott, K. R.; Moore, J. A.; Farrar, V. A. *J. Med. Chem.* **1991**, *34*, 387-392.

199. Moore, W. M.; Hammond, G. S.; Foss, R. P. *J. Am. Chem. Soc.* **1961**, *83*, 2789-2794.

200. Inbar, S.; Linschitz, H.; Cohen, S. G. *J. Am. Chem. Soc.* **1981**, *103*, 1048-1054.

201. Johnston, L. J.; Lougnot, D. J.; Wintgens, V.; Scaiano, J. C. *J. Am. Chem. Soc.* **1988**, *110*, 518-524.

202. White, R. C.; Selvam, T.; Ihmels, H.; Adam, W. *J. Photochem. Photobiol. A. Chem.* **1999**, *122*, 7-10.

203. Yoon, U. C.; Oh, S. W.; Lee, S. M.; Cho, S. J.; Gamlin, J.; Mariano, P. S. *J. Org. Chem.* **1999**, *64*, 4411-4418.

204. Griffiths, P. G.; Moad, G.; Rizzardo, E.; Solomon, D. H. *Aust. J. Chem.* **1983**, *36*, 397-401.

205. Reid, D., A.; Bottle, S. E.; Micallef, A. S. *J. Chem. Soc., Chem. Comm.* **1998**, *17*, 1907-1908.

206. Pine, S. H.; Shen, G. S.; Hoang, H. *Synthesis* **1991**, 165.

207. Green, S.; Fox, M. A. *J. Phys. Chem.* **1995**, *99*, 14752-14757.

208. Itoh, Y.; Gouki, M.; Goshima, T.; Hachimori, A.; Kojima, M.; Karatsu, T. *J. Photochem. Photobiol. A.* **1998**, *117*, 91-98.

209. Ciriano, M. V.; Korth, H.-G.; van Scheppingen, W. B.; Mulder, P. *J. Am. Chem. Soc.* **1999**, *121*, 6375-6381.

210. Engel, P. S.; Duan, S.; Arhancet, G. G. *J. Org. Chem.* **1997**, *62*, 3537-3541.

211. Grimaldi, S.; Finet, J.-P.; Zeghdaoui, A.; Tordo, P.; Benoit, D.; Gnanou, Y.; Fountanille, M.; Nicol, P.; Pierson, J.-F. *Polym. Prepr.* **1997**, *38*, 651-653.

212. Fukuda, T.; Tsujii, Y.; Miyamoto, T. *Polym. Prepr.* **1997**, *38*, 723-724.

213. Thijs, L.; Gupta, S. N.; Neckers, D. C. *J. Org. Chem.* **1979**, *44*, 4123-4128.

214. Morlino, E. A.; Bohorquez, M. D.; Neckers, D. C.; Rodgers, M. A. J. *J. Am. Chem. Soc.* **1991**, *113*, 3599-3601.

215. Perrin, D. D.; Armarego, W. L. F. *Purification of Laboratory Chemicals*, 3rd ed.; Pergamon Press: New York, 1988, pp 391.

216. Scaiano, J. C. *J. Am. Chem. Soc.* **1980**, *102*, 7747-7753.

217. Scaiano, J. C.; Tanner, M.; Weir, D. *J. Am. Chem. Soc.* **1985**, *107*, 4396-4403.

218. Turro, N. J.; Kraeutler, B.; Anderson, D. R. *J. Am. Chem. Soc.* **1979**, *101*, 7435-7437.

219. Robbins, W. K.; Eastman, R. H. *J. Am. Chem. Soc.* **1970**, *92*, 6076-6077.

220. Turro, N. J.; Anderson, D. R.; Chow, M.-F.; Chung, C.-J.; Kraeutler, B. *J. Am. Chem. Soc.* **1981**, *103*, 3892-3896.

221. Baum, E. J.; Wan, J. K. S.; Pitts, J. N. J. *J. Am. Chem. Soc.* **1966**, *88*, 2652-2659.

222. Stewart, J. J. P. Semiempirical Molecular Orbital Methods. In *Reviews in Computational Chemistry I*; Lipkowitz, K. B., Boyd, D. B., Eds.; VCH:, 1990; 45-81.

223. Young, R. J.; Lovell, P. A. *Introduction to Polymers*, 2nd ed.; Chapman and Hall: New York, 1991, pp 443.

8. Final Comments and Future Directions

8.1 Final Comments

The work presented in this thesis all relates to reactions occurring in the living free radical polymerization (LFRP) process. While each chapter has dealt with various elements of thermal or photochemical LFRP, they all relate to provide a deeper understanding of this polymerization process. Ultimately, the knowledge expressed in this thesis can be used to design unimolecular initiators capable of promoting LFRP of any monomer either thermally or photochemically.

The kinetic and thermodynamic investigation of a series of unimolecular initiators has provided insight into the successful nitroxide mediated polymerization of styrene and the failure of acrylate type monomers. The trapping rate constants for the propagating carbon centered radical in the acrylates systems is considerably faster than the phenylethyl radical in styrene polymerization. Complementary to this difference between the two systems is the BDE for the C-O bond, which is expected to be higher. These two differences suggest a shift in the equilibrium between "dormant" and "active" species present during polymerization, where very few propagating radicals are formed in the case of acrylate polymerization. The overall observed results are low molecular weight polymers with broad molecular weight distributions. The poor living polymerization of acrylates was found to be compounded by the formation of disproportionation products. These were found to be suppressed when a nitroxide containing bulky substituents in the 2 and 6 positions was used. These groups are responsible for increasing the height of the rotational barrier required for correct overlap for a four center elimination. A nitroxide with bulky groups promoted living free radical polymerization of acrylates by suppressing the formation of disproportionation products.

Other important findings stem from the photophysical and photochemical properties of LFRP initiators. Excitation of selective chromophores was found to promote energy transfer to an alkoxyamine covalently bonded to the donor. Under suitable conditions, i.e. no energy dissipating steps and high efficiency of triplet formation, the energy transferred induced C-O bond homolysis generating the two radicals capable of sustaining living polymerization. The orientation of the donor (chromophore) and acceptor (alkoxyamine) were found to be important. Only oligomers could be photochemically formed with an orientation of head-to-head, while head-to-tail orientation led to photoinduced living polymerization of acrylates. Intramolecular hydrogen abstraction, change

in triplet character, low triplet quantum yields, and non-radiative energy dissipation were found to be responsible for decreasing the efficiency of desired homolytic C-O bond fragmentation.

8.2 Future Directions

The results presented in this thesis are by no means the end of research in this area. Many avenues for further research are still possible. A few possibilities for future exploration based upon the work presented here follows and are divided into their appropriate section for easy of reference.

8.2.1 Photoinitiators

i) Triplet based photoinitiators containing a rigid frame work between the donor chromophore and the acceptor alkoxyamine would be suitable photoliving initiators for LFRP. An ideal chromophore being investigated as an initiator is 4-methyl-xanthone whose triplet is a π,π^* character and cannot undergo the energy wastage steps of hydrogen abstraction encountered with benzophenone based chromophores as energy donors.

ii) An alternative to triplet initiators are singlet based photoinitiators. Preliminary work has shown that the photophysical properties of pyrene as a singlet sensitizer containing a covalently linked alkoxyamine possess the desirable properties for photoliving polymerization.

iii) Triplet states that do not undergo rapid intramolecular processes would be suitable photoinitiators for LFRP. However, they must posses a high triplet quantum yield and ensure high efficiency of C-O bond homolysis.

8.2.2 Thermal Initiators

Work involving the synthesis of organometallic based LFRP initiators is yet another possibility for future research. This would involve the incorporation of Group IV metals capped with nitroxide of the general structure Ph_3X-T, where X = Metal and T = TEMPO. The trapping rate constants of the organometallic radicals by TEMPO and semi-empirical calculations suggest these structures would be ideal candidates for thermal LFRP initiators. This gives rise to polymers with metal containing termini and could subsequently be modified leading to different polymer architectures.

8.2.2.1 Biphasic

i) The salt of 4-carboxy-TEMPO can be used as an alternate nitroxide for the polymerization of acrylates under biphasic conditions. Its concentration can be controlled by buffering the pH of the reaction conditions ultimately leading to LFRP polymerization in aqueous solutions. A water based biphasic approach would be welcomed by industry for environmental reasons.

ii) Fluorine containing nitroxides would also prove beneficial for biphasic polymerization. This requires the use of a fluorous phase not miscible with the bulk phase which could easily be separated and recycled for industrial purposes. This will also prove to be an attractive industrial application for LFRP. Also, the change in electronic factors with the incorporation of fluorine groups on the nitroxide would influence the BDE in a favorable manner allowing for the living polymerization of many monomers not previously possible.

8.2.2.2 Incorporation of Steric Factors

The incorporation of bulky groups at the 2 and 6 positions of the nitroxide would be favorable for the living polymerization of aliphatic monomers. The bulky groups introduce steric elements that suppress the reaction leading to disproportionation products with aliphatic monomers. In turn, this leads to controlled polymerization and aliphatic polymers with living properties.

8.2.2.3 New Generation of Nitroxides

The new generation of nitroxides containing a hydrogen adjacent to the nitroxide function appears to promote living polymerization of monomers not previously supporting LFRP. Nitroxides containing electron donating or withdrawing groups can be synthesized that allow fine tuning of the labile C-O bond. Also, the kinetics of the coupling reaction can also be influenced by incorporating other groups. These factors combined would lead to the living polymerization of many monomers not previously capable of sustaining LFRP.

8.3 Claims to Original Research

Many areas of LFRP have been examined during the course of this thesis including kinetic and thermodynamic analyses. The investigation done for this thesis contributes to the understanding of the fundamental processes occurring in nitroxide mediated LFRP. This knowledge was also been used for the design of new initiators potentially capable of promoting LFRP.

i) The BDE for the C-O bond of alkoxyamines typically used in LFRP were found to be ca. 30 kcal/mol and dependent upon the structure of the subsequently generated carbon centered radical. The bond energy is independent of the nitroxide structure. The BDE of homolytic cleavage of the N-O bond of the same alkoxyamines was found to be approximately 45 kcal/mol.

ii) Trapping rate constants of carbon centered radicals with nitroxides were found to be influenced by the structures of the carbon centered radical and not the nitroxide. Benzylic type radicals exhibited rate constants in the order of 10^8 M^{-1} s^{-1} while propionate radicals were faster, ~10^9 M^{-1} s^{-1}.

iii) Organometallic radicals possessed trapping kinetics similar to their carbon center analogue initiators. Semi-empirical calculations compounded with kinetic investigation suggest this class of initiators to be suitable candidates for LFRP.

iv) The formation of disproportionation products during the LFRP were found to be generated from a four center concerted elimination. Incorporation of stereoelectronic factors into either the nitroxide or the monomer were found to suppress the formation of these products. The bulky nitroxide substituents in the 2 and 6 positions suppress of observed disproportionation products leading to LFRP of acrylate monomers.

v) The use of a second medium, not miscible with the bulk monomer, was found to promote nitroxide mediated controlled polymerization of acrylates.

vi) Photoacoustic calorimetry studies involving homolytic bond breaking processes could be examined with a series of non-homologous solvents leading to isolation of the volume contributions.

vii) Photoliving polymerization was possible through the use of a benzophenone chromophore with a covalenty linked alkoxyamine group.

viii) Energy transfer from triplet donors to alkoxyamine acceptors was found to lead to C-O bond homolysis. The efficiency of this process was found to depend on the triplet energy, type of triplet states, and the presence of other energy competing processes.

ix) Homolytic C-Br bond cleavage was observed to occur upon direct excitation of a benzophenone chromophore. The efficiency of photoacid generation not previously measured was determined through the use of a dye and was found to depend on the structural position of the bond to be cleaved.

x) The photodecomposition pathways of the LFRP initiators were found to be wavelength dependent. Shorter wavelengths promoted the homolytic N-O and C-O bond cleavages and the formation of disproportionation products while longer wavelengths induce only detectable C-O bond cleavage.

xi) The thermal decomposition pathway of a benzoin based LFRP initiator could be controlled through the use of additives giving either a radical or ionic mechanism.

8.4 Publications Resulting From Research Presented in This Thesis

1. Skene, W. G., S. T. Belt, T. J. Connolly, P. Hahn and J. C. Scaiano. (1998). Decomposition Kinetics, Arrhenius Parameters, and Bond Dissociation Energies for Alkoxyamines of Relevance in "Living" Free Radical Polymerization. *Macromolecules.* **31**, 9103-9105.

2. Skene, W. G. (1998). Final report for PAC studies done at the Max-Planck-Institut für Strahlenchemie, Germany under the auspices of a DAAD scholarship.

3. Skene, W. G., T. J. Connolly and J. C. Scaiano. (1999). The Thermolysis and Photochemistry of Hybrid Initiators for "Living" Free Radical Polymerization. *Tetrahedron Lett.* **40**, 7297-7302.

4. Skene, W. G., T. J. Connolly and J. C. Scaiano. (2000). Trapping of Photogenerated Group IV Radicals by TEMPO: Potential New Organometallic Initiators for Persistent Free Radical Polymerization. *Int. J. Chem. Kinet.* **32**, 238-244.

5. Skene, W. G. and J. C. Scaiano. (2000). Photoinduced TEMPO Release from a Living Free Radical Polymerization Initiator. *Polym. Prepr.* **41**, 163-164.

6. Skene, W. G., J. C. Scaiano and G. P. A. Yap. (2000). A 'Penultimate' Initiator for Living Free Radical Polymerization. *Polym. Prepr.* **41**, 119-120.

7. Skene, W. G., J. C. Scaiano and G. P. A. Yap. (2000). An Improved Mimetic Compound for Styrene "Living" Free Radical Polymerization. An Initiator Containing the "Penultimate" Unit. *Macromolecules*. **33**, 3536-3542.

8. Skene, W. G., J. C. Scaiano, N. A. Listigovers, P. E. Kazmaier and M. K. Georges. (2000). Rate Constants For The Trapping of Various Carbon Centered Radicals by Nitroxides: Unimolecular Initiators for Living Free Radical Polymerization. *Macromolecules*. **33**, 5065-5072.

9. Skene, W. G. and J. C. Scaiano. (2000). A New Class of Photochemical Initiators for Living Free Radical Polymerization. Manuscript in preparation.

10. Skene, W. G., I. Piletic and J. C. Scaiano. (2000). The Use of Biphasic Media For Living Free Radical Polymerizatoin of Acrylates. Manuscript in preparation.

11. Skene, W. G. and J. C. Scaiano. (2000). Kinetics of Nitroxides Trapping Reactions with Oxygen Centered Radicals. Manuscript in preparation.

12. Skene, W. G. and J. C. Scaiano. (2000). The Photochemistry and Photophysics of Nitroxide Containing Benzoylbenzoate Esters for Living Free Radical Polymerization. Manuscript in preparation.

13. Skene, W. G. and J. C. Scaiano. (2000). A New Initiator for Acrylate Living Free Radical Polymerization. Manuscript in preparation.

14. Skene, W. G. and J. C. Scaiano. (2000). Quantum Yields Of Photodecomposition and Bond Dissociation Enthalpies Of Living Free Radical Polymer Initiators. Manuscript in preparation.

15. Skene, W. G., A. Martin and J. C. Scaiano. (2000). The Photochemistry and Photophysics of TEMPO containing Benzophenone Initiators for Living Free Radical Polymerization. Manuscript in preparation.